Algorithm Optimization of non-DMSO Cryopreservation Protocols to Improve Mesenchymal Stem Cell Post-Thaw Function

A Dissertation
SUBMITTED TO THE FACULTY OF
UNIVERSITY OF MINNESOTA
BY

Kathryn Lindsay Pollock

IN PARTIAL FULFILLMENT OF THE REQUIREMENTS
FOR THE DEGREE OF
DOCTOR OF PHILOSOPHY

Allison Hubel, Ph.D., Advisor

September 2016

Parts of this dissertation have been published previously:

Pollock K, Budenske JW, McKenna DH, Dosa PI, Hubel A. Algorithm-driven optimization of cryopreservation protocols for transfusion model cell types including Jurkat cells and mesenchymal stem cells. *J Tissue Eng Reg Med*, Published online May **2016**, doi: 10.1002/term.2175

Pollock K, Sumstad D, Kadidlo D, McKenna DH, Hubel A. Clinical mesenchymal stem cell products experience functional changes in response to freezing. *Cytotherapy* **2015**; 17(1): 38-45

Sharma RR, **Pollock K**, Hubel A, McKenna DH. Mesenchymal Stem/Stromal Cells: A Review of Clinical Applications and Manufacturing Practices. *Transfusion* **2014**; 54 (5): 1418-1437

Parts of this dissertation will be published in the future:

Pollock K*, Yu G*, Moller-Trane R, Koran M, Dosa PI, McKenna DH, Hubel A. Combinations of osmolytes including monosaccharides, disaccharides, and sugar alcohols act in concert during cryopreservation to improve mesenchymal stromal cell survival. Submitted July **2016**. *In Review*.
*These authors contributed equally. Yu G performed all Raman experiments.

Pollock K, Samsonraj RM, Stumbras A, McKenna DH, Dosa PI, van Wijnen A, Hubel A. Mesenchymal stem cell post-thaw cell function is maintained or improved by freezing with algorithm optimized non-DMSO solutions. *In preparation*

Acknowledgements

My first thanks go to Allison Hubel, my advisor throughout this project. Thank you for giving me the opportunity to learn about stem cells, algorithms, and cryobiology and for being a wonderful mentor and role model. I would also like to thank my other mentors, co-collaborators, and committee members Peter Dosa, David McKenna, Brenda Ogle, and Jonathan Sachs. Your combined contributions to guide the direction of my research and your excellent feedback have made this work much stronger.

Thanks are also due to the funding sources that supported me personally (3M science and technology fellowship, DDF fellowship, Hematology workforce training grant), and the funding sources for the projects included in this dissertation (ITDD grant, PACT funding, and the National Institutes of Health grant R21 EB016247-01A1).

My collaborators have been amazing, and much of this work would not be possible without their guidance and assistance. I would like to thank Ralph Moller-Trane for his statistics expertise and contributions to this work (included here in Chapter 5). Additionally, I would like to thank Andre van Wijnen and his post-doctoral student Rebekah Samsonraj, who have been instrumental in guiding and performing RNA qRT-PCR and DNA hydroxymethylation experiments at their Mayo facilities (included here in Chapter 8). Darin Sumstad was an invaluable resource for bone marrow isolation and culture, and the experiments described in Chapter 4 performed at the Molecular and Cellular Therapeutics facility (MCT) would not have been possible without him. A

thank-you also goes out to the Institute for Therapeutics discovery and development (ITDD) for allowing us to use their high-throughput liquid handling equipment and to the Bischof lab for allowing us to use their plate-reader.

My lab mates have not only helped me with experiments, they have made my time in graduate school much more enjoyable. Thank you to PhD student Guanglin Yu for designing and performing Raman experiments at Char-Fac (included in Chapter 6), to Masters student Sri Mushnoori for performing DSC experiments in the Macosko lab (included in Chapter 6), and to Masters student Aron Stumbras for his work on flow cytometry performed with the University Flow Cytometry Resource (included in Chapter 8) I have also enjoyed working with other past and present Hubel lab PhD students including Michael DiVito and Mian Wang.

I have had the pleasure of mentoring several masters and undergraduate students during my time in graduate school. Thank you to masters students Chi Tran, Marissa Koran, and Emily Vance for their research contributions and assistance. A BIG shoutout goes to my two undergraduate rock-stars Joe Budenske and Elizabeth Moy, as well as all of my other undergraduates for their assistance including: Jane Danstrom, Caitlin Fermoyle, Laura Billiar, Tijen Petersen, Nathan Jeurgens, Matt Osten, Luke Albares, and Jeremy Boedeker.

The mentorship I received in high school and college from amazing female role models has helped drive me forward in STEM. Thank you to Kimberly Anderson at the University of Kentucky for allowing a high-school researcher with no experience to work in your lab and to Morgan Abney, an incredible graduate student mentor who encouraged me to keep learning and keep trying even when I made mistakes. A huge thank you also goes to Pam Kreeger at the University of Wisconsin, who helped me develop a wide range of bench skills and gave me the opportunity to work independently on my own project as an undergraduate researcher. It has been an honor to work with all of you and I can only hope to inspire future researchers one day as much as you have inspired me.

I owe a huge amount of thanks to my tremendously supportive network of family and friends. There are not enough pages here to express my gratitude for all the meals, hangouts, phone calls, and well wishes sent my way, but please know that I appreciate each and every one of you. Big thank-you's go to Laura Zitella and Kerianne Steucke, roommates extraordinaire, and Randy Weyer, my boogly constant, for keeping me sane throughout grad school. Last but not least, thank you to my father, Dan Pollock. Your overwhelming support and unwavering confidence in me for everything I've ever tried has made it possible to push the limits of my potential. I wouldn't be where I am today without you.

Dedication

This thesis is dedicated to Kay Pollock.

I love you. I miss you.

I wish you could be here for all the good stuff.

Abstract

Mesenchymal stem cells (MSCs) are a common transfusion cell therapy that have been used in over 300 clinical trials to treat over 2000 patients with diseases ranging from Crohn's disease to heart failure. These cells are frequently cryopreserved to better coordinate the timing of cell administration with patient care regimes and to accommodate transport of samples between different sites of collection, processing, and administration. However, cryopreservation with DMSO (the current gold standard) can result in poor cell function post-thaw and adverse reactions upon infusion.

We hypothesize that non-DMSO cryopreservative molecules, including sugars, sugar alcohols, amino acids, and other small molecule additives, can be used in combination to protect cell viability and function post-thaw. This research demonstrates that some combinations of non-DMSO cryopreservatives preserve cell functionality better than others, and these effects are dependent not on osmotic or physical changes in solution, but on biological changes that affect the cell during the freezing process. We observe that there is likely a sweet spot concentration combination that produces maximum recovery for each combination of molecules, and demonstrate that an evolutionary algorithm can be used to identify optimized combinations of molecules that yield high cell recovery post-thaw. Additionally, we demonstrate that these novel solutions maintain MSC functionality when evaluated using surface markers, attachment, proliferation, actin alignment, RNA expression, and DNA hydroxymethylation. These advances in cryopreservation can improve cell therapy, and ultimately patient care.

Table of Contents

List of Tables

List of Figures

Abbreviations and Symbols

7-AAD	7-amino-actinomycin D
AO	Acridine orange
AT	Adipose tissue
BIC	Bayesian Information Criterion
BM	Bone marrow
CCM	Complete culture medium
cDNA	Complementary DNA (reverse transcription product)
cGMP	Clinical Grade Manufacturing Product
CRF	Controlled rate freezer
CRM	Confocal Raman microscopy
CT	Cycle threshold
DAPI	4',6-diamidino-2-phenylindole
DC	Dendritic cell
diH_20	Deionized water
DMSO	Dimethyl Sulfoxide
DNA	Deoxyribonucleic acid
DPBS	Dulbeccos phosphate buffered saline
DSC	Differential scanning calorimetry
FBS	Fetal bovine serum
FDA	Food and Drug Administration
FFT	Fast Fourier transform
GGC	Glucose/Glycerol/Creatine
GMC	Glucose/Mannitol/Creatine
H9MSC	H9 embryonic derived MSC
HBSS	Hanks buffered salt solution
HCl	Hydrochloric acid
HEPES	4-(2- hydroxyethyl)-1-piperazineethanesulfonic acid

HLA	Human leukocyte antigen
HSA	Human serum albumin
IDO	Indoleamine 2,3-dioxygenase
IL	Interleukin
ITDD	Institute for therapeutics discovery and development
LME	Linear mixed effects
MHC	Major Histocompatibiliity complex
MNC	Mononuclear cell
MSC	Mesenchymal Stem cell
NaOH	Sodium Hydroxide
NK	Natural Killer cell
NO	Nitric Oxide
PCR	Polymerase chain reaction
PGE2	Prostaglandin
PI	Propidium iodide
RNA	Ribonucleic acid
SD	Standard Deviation
SEGA	Sucrose/Ethylene Glycol/Alanine/Taurine/Ectoine
SEM	Standard error of the mean
SGC	Sucrose/Glycerol/Creatine
SGI	Sucrose/Glycerol/Isoleucine
SMC	Sucrose/Mannitol/Creatine
SSC	Saline Sodium Citrate
t-BHP	tert-butyl hydroperoxide
TGE	Trehalose/Glycerol/Ectoine
UCB	Umbilical cord blood
αMEM	Alpha modified eagles medium
βgal	β-galactosidase

Units

°C	Degrees celsius
°C/min	Degrees celsius/min (cooling rate)
cm^2	Centimeters square (area)
Da	Daltons
ex/em	Excitation/Emission
g	Grams
hr	Hours
cm^{-1}	Inverse centimeters (frequency)
µg	Micrograms
µL	Microliters
µM	Micromolar
mg	Milligrams
mL	Milliliters
mm	Millimeters
mM	Millimolar
mOsm	MilliOsmolar
mW	MilliWatts
min	Minutes
nm	Nanometers
s	Seconds
xg	Times gravity

Chapter 1

Introduction

1.1 Motivation

Mesenchymal stem cells (MSCs) are currently being investigated as a therapeutic treatment for a growing number of diseases due to their unique ability to independently home to sites of injury, differentiate, secrete bioactive molecules, and immuno-modulate the host environment[1]. To date, more than 600 clinical trials involve the use of MSCs [2] and more than 2000 patients have been safely treated for a variety of conditions that use MSC traits to fill a missing niche, ranging from bone and muscle regeneration/maintenance to immuno-modulation for immune disorders such as graft vs. host and crohn's disease [3]. In addition, MSCs can be easily harvested from adult tissues (most commonly bone marrow and adipose tissue), and as such are an ethically superior alternative to embryonic stem cells for cell therapy.

In attempts to increase the availability of this promising treatment, freshly isolated and expanded MSCs can be cryopreserved and stored in low temperature cell banks[4]. Cryopreserved samples can be batch processed, allowing for more efficient use of resources at cell therapy processing facilities by reducing staff required for culture maintenance, culture costs, and risk of contamination. Bio-banks of cryo samples can be tracked easily with barcodes and require minimal human intervention, as temperature and liquid nitrogen levels can be monitored with automated instruments and alarms. At liquid nitrogen temperatures, cells are stable for long periods of time [5, 6] and can be

transported to sites of administration using liquid nitrogen charged dry shippers or dry ice.

However, to survive freezing, cell samples must be combined with cryopreservatives to draw water out of and limit ice crystal formation within cells[7]. Dimethyl sulfoxide (DMSO) has become the gold standard cryopreservative used for cell freezing in the last 50 years. However, DMSO is systemically toxic in humans and can result in side effects ranging from mild (such as nausea and vomiting) to severe (including cardiovascular and respiratory complications) when transfused in even trace amounts with thawed cells [8]. As some treatments require multiple infusions of cryopreserved cells, non-toxic cryopreservative alternatives to DMSO are desirable. Aside from these negative systemic side effects, it has also been suggested that current freezing with DMSO produces sub-optimal functioning post-thaw stem cell products[9, 10]. As the cell therapy industry expands, it will be important to identify alternative methods of freezing cell types whose functions are sensitive to cryopreservation in DMSO.

A non-DMSO cryopreservative solution with biologically non-toxic solution components could improve cell function post-thaw and make cell therapy accessible to more patients, as non-DMSO solutions would likely require less post-thaw cell processing to be administered as a safe, functional product.

1.2 Hypothesis and Aims

This research proposes to eliminate DMSO for the cryopreservation of MSCs, and hypothesizes that a combination of non-DMSO cryopreservative agents will act in concert to maintain cellular viability and function throughout the freezing process. This hypothesis produced the following aims:

Aim 1 – Identify combinations of solution components likely to result in high post-thaw cell recovery, and establish potential mechanisms of cryo-protection for these combinations.

Aim 1.1 –Identify solution combinations most likely to result in high post-thaw cell recovery.

Candidate solutions that include compounds from several cryoprotective categories will be screened in Chapter 5 to identify compositions that maximize recovery in cells after undergoing freezing and thawing.

Aim 1.2 – Identify mechanisms of cryoprotection for multicomponent solutions.

In Chapter 6, solutions containing components identified as promising in Aim 1.1 will be combined with cells and evaluated to determine the mechanisms by which they protect cells during cryopreservation.

Aim 2 - Establish and validate differential evolution algorithm for predictive optimization of solution components, concentrations, and freezing rates.

In Chapter 7, a MATLAB algorithm based on the Storn and Price differential evolution algorithm[11] will be validated for subsequent application to MSC functional cryopreservative optimization in Aim 3.

Aim 3 – Iterate algorithm to optimize cryopreservation solutions for MSCs, and confirm optimized solutions maintain cellular function post-thaw.

In Chapter 8, MSC freezing solutions will be optimized using the algorithm for functional attachment post-thaw, and subsequently analyzed for additional functionality metrics.

In addressing these specific aims, we will determine whether it is possible to optimize non-DMSO cryopreservation of MSCs using an evolutionary algorithm, and establish whether the cells resultant from freezing in these multicomponent solutions display functional behavior that is maintained or improved compared to DMSO freezing. The outcomes of this work will assist us in understanding and improving MSC freezing, contributing to the long-term goal of increasing the number of patients who are successfully treated with transfused stem cell products.

Chapter 2

Background

2.1 Mesenchymal Stem Cells

Much of the text, figures, and tables in this section have previously appeared in the publication below, included here with copyright permission from John Wiley and Sons:

Sharma RR, **Pollock K**, Hubel A, McKenna DH. Mesenchymal Stem/Stromal Cells: A Review of Clinical Applications and Manufacturing Practices. *Transfusion* **2014**; 54 (5): 1418-1437

MSCs were isolated in 1968 by Friedenstein et al[12], who characterized them as adherent fibroblast-like cells in the bone marrow (BM) capable of differentiating into bone. MSCs have since been isolated from various other tissues including adipose tissue (AT)[13] and umbilical cord blood (UCB)[14]. However, source tissue can influence isolated MSC behavior, and several laboratories have used different strategies to identify, isolate, and culture MSCs to obtain optimal properties for indication-specific applications.[15–17]

The minimal criteria required to define MSCs were defined by Dominici et al in 2006[18], and can be summarized as follows:

1. MSCs must be adherent to plastic under standard tissue culture conditions;

2. MSCs must have positive expression of certain cell surface markers such as CD73, CD90, and CD105, and negative expression of other markers including CD45, CD34, CD14, CD11b, CD79α, or CD19 and HLA-DR surface molecules;

3. MSCs must be capable of differentiating into osteoblasts, adipocytes, and chondroblasts under defined *in vitro* conditions.

Based on current literature[1, 19], MSCs are believed to exert their therapeutic effects by several mechanisms including:

1. Homing to sites of inflammation after tissue injury;

2. Differentiation into multi-lineage cell types;

3. Secretion of bioactive molecules capable of stimulating recovery of injured cells and inhibiting inflammation;

4. Ability to immunomodulate the host environment (and non-immunogenicity)

These four potential modes of therapeutic efficacy have been demonstrated in various preclinical animal model studies[20]. The first clinical trial in humans using culture-expanded MSCs was carried out in 1995; in this study, 15 hemato-oncology patients received injections of autologous (BM-MSCs) cells as part of a safety and feasibility study[21]. Since then, the use of MSCs has been further explored. In October 2012, the clinical trials database displayed 218 clinical trials using MSCs for a wide range of therapeutic applications internationally, and this number has since grown to 607 trials as of September 2016[2]. An analysis of the studies underway in October 2012 reveals that most trials were in Phase I (safety studies, n = 42), Phase II (proof of efficacy, n = 57), or combined Phases I and II studies (n = 105). A much smaller number of trials were in Phase III (comparison to gold standard, n = 8) or combined Phases II and III (n = 6). The

disease conditions, phase, and enrollment of trials are listed in Table 1 and their sources are summarized in Figure 1.

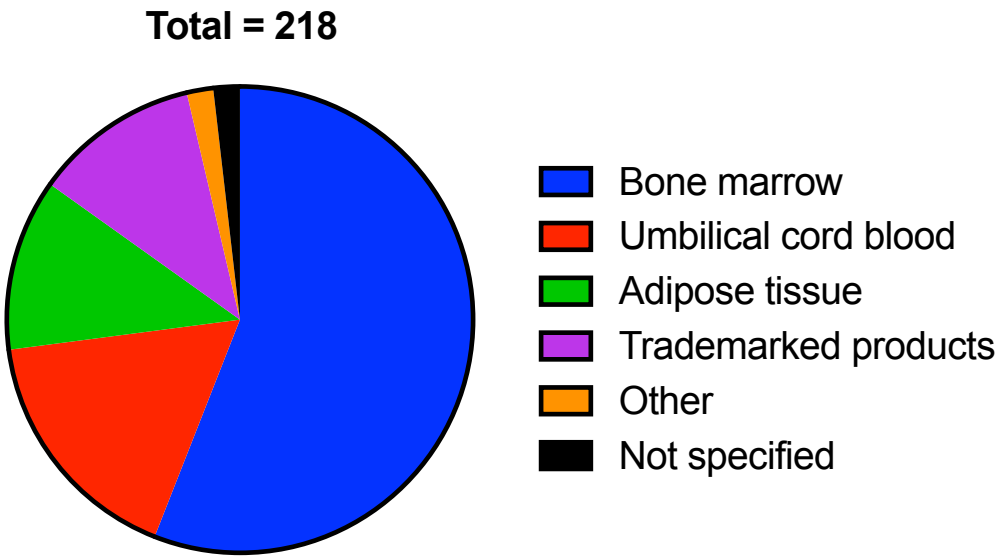

Figure 1: Distribution of sources for MSCs in Table 1.

Encouraging results from these clinical trials have increased research into MSC therapy for a variety of clinical disorders including: bone and cartilage disorders, bone neoplasms, hematologic disorders, diabetes, liver diseases, cardiovascular disorders, gastrointestinal diseases, autoimmune or skin disorders, lung diseases, neuromuscular diseases, limb ischemia, and renal diseases.

Table 1: Status and enrollment of MSC clinical trials as of October 22, 2012.

TABLE 1. Current status and enrollment of MSC clinical trials*

Targeted condition	Phases, number of studies [targeted enrollment]				
	I	I/II	II	II/III	III
Bone/cartilage disorders					
Bone cysts	1 [6]	1 [10]			
Bone neoplasms				1 [50]	
Cartilage defect	1 [50]	2 [38]	1 [100]		
Degenerative osteoarthritis		2 [30]		1 [25]	
Distraction osteogenesis	1 [6]				
Fractures	2 [16]	1 [24]	1 [40]		
Ligament injury		1 [24]	1 [10]		
Meniscectomy		2 [110]			
Osteoarthritis	5 [42]	2 [45]	4 [222]		1 [104]
Osteodysplasia	1 [8]				
Osteogenesis imperfecta	1 [9]				
Osteonecrosis	1 [21]	2 [39]	1 [10]		
Osteoporosis			1 [290]		
Pseudoarthrosis			1 [50]		
Spinal fusion		1 [62]			
Hematologic disorders					
Aplastic anemia		2 [60]	1 [30]		
BMT	1 [125]	3 [40]	3 [125]		
GVHD	2 [59]	6 [130]	6 [286]	1 [100]	1 [240]
Myelodysplastic syndrome			1 [30]		
Diabetes					
Type 1	1 [24]	5 [168]	1 [60]	1 [80]	
Type 2	1 [24]	3 [170]			
Liver diseases					
Autoimmune hepatitis		1 [100]			
Cirrhosis	3 [29]	7 [715]	5 [266]		
Hypercholesterolemia	1 [1]				
Liver failure		2 [228]	1 [120]		
Liver transplant		1 [40]	1 [60]		
Primary biliary cirrhosis		1 [100]			
Cardiovascular diseases					
Dilated cardiomyopathy		2 [66]	2 [80]		
Heart failure		3 [172]	4 [160]		
Myocardial infarction	1 [53]	2 [45]	2 [380]	1 [80]	2 [165]
Myocardial ischemia	2 [144]	3 [89]	1 [60]		
Gastrointestinal diseases					
Crohn's disease		3 [56]	1 [10]		4 [696]
Fistula in ano		1 [10]	1 [40]		
Ulcerative colitis		1 [50]			
Autoimmune or skin disorders					
Burns		1 [20]			
Epidermolysis bullosa			1 [75]		
HIV		1 [36]			
SLE		1 [20]			
Rheumatoid arthritis		2 [203]			
Sjogren's disease		1 [20]			
Systemic sclerosis		1 [20]			
Lung diseases					
Bronchopulmonary dysplasia	3 [28]				
COPD			1 [62]		
Emphysema	1 [10]				
Idiopathic pulmonary fibrosis	1 [8]				
Neuromuscular diseases					
ALS	1 [25]	1 [24]	1 [30]		
Alzheimer's	1 [9]	1 [30]			
Brain injury		1 [2]			
Cerebellar ataxia		1 [8]	1 [20]		
Disc disease		3 [55]			
Hereditary ataxia		1 [20]			
ICSOL hemorrhage		1 [20]			
Limbus insufficiency		1 [30]			
Multiple sclerosis	1 [24]	5 [103]	1 [16]		
Multiple sclerosis and NMO		1 [20]			
Multiple system atrophy			1 [27]		
Parkinson's disease		1 [20]			
Retinitis pigmentosa	1 [10]				
Romberg's disease			1 [5]		
Spinal cord injury	4 [53]	2 [100]	2 [90]	1 [32]	
Stroke	1 [30]	3 [203]	3 [100]		
Muscular dystrophy		1 [15]			
Neomyogenesis		1 [30]			
Limb ischemia					
Diabetic foot	1 [40]		1 [30]		
Limb ischemia		9 [245]	2 [176]		
Renal diseases					
Kidney injury	1 [9]		1 [200]		
Kidney transplant		3 [41]			
Lupus nephritis		1 [20]	1 [25]		
Miscellaneous					
Endometriosis	1 [60]				
Prostate cancer		1 [31]			
Total: 218 [9757]	42 [923]	105 [3957]	57 [3285]	6 [367]	8 [1225]

* The data were searched on the website of ClinicalTrials.gov (http://www.clinicaltrials.gov) on October 22, 2012. The following key words including "mesenchymal stem cells," "mesenchymal stromal cells," "multi-potent stromal cells," "multi-potent progenitor cells," "BM stromal cells," and "connective tissue progenitor" were used.

ALS = amyotrophic lateral sclerosis; COPD = chronic obstructive pulmonary disease; HIV = human immunodeficiency virus; ICSOL = intracranial space–occupying lesion; NMO = neuromyelitis optica; SLE = systemic lupus erythematosus.

2.1.1 Immunomodulatory effects of MSCs

MSCs have unique immunologic characteristics, which promote their survival and growth in allogeneic or xenogeneic environments[22, 23]. They express low levels of major histocompatibility complex (MHC) Class I antigens and do not express MHC Class II antigens or costimulatory molecules such as CD40, CD80, and CD86[24]. These characteristics protect them from alloreactive natural killer (NK) cell–mediated lysis[25]. In addition, human MSCs express HLA-G, a non-classical MHC Class I antigen, which may prevent an immune response against MSCs (as shown by blocking experiments), although its expression seems to decrease in culture[26]. Culture conditions may also affect MSC immunogenicity due to internalization of protein molecules in the culture medium[27]. However, patients receiving treatment with allogeneic human MSCs do not show anti-allogeneic MSC antibody production or T-cell priming[28].

MSCs act on both the adaptive and the innate immune systems by suppressing T cells[27], suppressing dendritic cell maturation[29, 30], reducing B-cell activation and proliferation[31, 32], inhibiting proliferation and cytotoxicity of NK cells[33], and promoting the generation of regulatory T cells via an interleukin (IL)-10 mechanism[34, 35]. Secretion of prostaglandins and growth factors such as vascular endothelial growth factor, keratinocyte growth factor, and hepatocyte growth factor are also believed to influence immunomodulation and repair of various tissues[36]. When influenced by inflammatory cytokines, MSCs are capable of migrating to inflamed tissues and modulating the local inflammatory reactions at two levels via their effects on both innate and adaptive immunity[34, 37]. One level occurs locally via the secretion of mediators

that inhibit proliferation of immune cells in the vicinity of MSCs, while the other induces a systemic response (either an anti-inflammatory Th-2 immune activation or the generation of regulatory T-cells). In addition, MSCs may recruit and support growth of local autologous stem cells within injured tissues, promoting cell survival and tissue repair[38]. Figure 2 summarizes the current known cell–cell interactions of MSCs with the immune system.

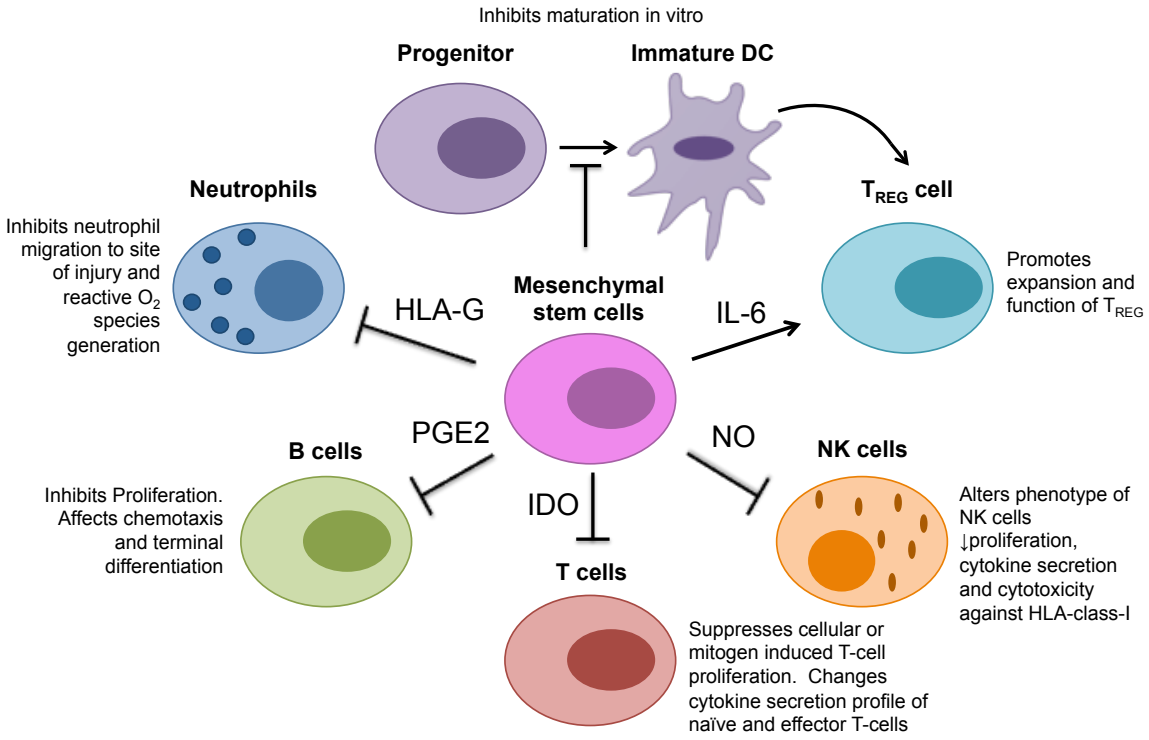

Figure 2: MSC cell-cell interactions After activation, mesenchymal stem cells secrete soluble mediators – such as nitric oxide (NO), prostaglandin (PGE2), indoleamine 2,3-dioxygenase (IDO), IL-6, and human leukocyte antigen (HLA)-G. Production of these mediators regulates the proliferation and function of a variety of immune cells as well as the induction of regulatory T (TREG) cells either directly or indirectly through the generation of immature dendritic cells (DC). NK, natural killer.

2.1.2 MSC homing, engraftment, and differentiation.

MSCs selectively home to sites of tissue injury and/or inflammation after systemic administration[37]. Once located at an inflammation site, MSCs can exert local functional effects in the resident tissue[37, 38]. Cell migration is dependent upon paracrine signaling from injured cells and local immune cells which release growth factors and chemokines [39]. *In vitro* migration assays suggest that MSC migration is specifically influenced by growth factors including platelet-derived growth factor (PDGF), insulin-like growth factor-1 (IGF-1), and chemokines such as CCR2, CCR3, CCR4, or CCL5 [40].

MSCs can differentiate into mesodermal lineages such as bone, cartilage, adipocytes, and connective stromal cells[41]. It has been suggested that MSCs may also be capable of differentiating into endodermal lineage cells (e.g., hepatocytes)[42–44]. However, these results come from *in vitro* experiments, and the complex microenvironment of local tissue may alter how engrafted MSCs differentiate *in vivo*[45]. Based on current literature, engrafted MSCs appear to be capable of differentiating into at least three types of cells *in vivo* due to local tissue signaling:

1. Tissue-specific cells necessary for repair. For example, cardiomyocytes, smooth muscle cells, and vascular endothelial cells when engrafted in cardiac tissue[46–48].

2. Function-relative cells necessary for optimum growth and proliferation in local tissue. For example, in BM after stem cell transplantation[49].

3. Regulatory cells, which contribute to tissue repair and regeneration via trophic and immunomodulatory mechanisms[50].

There are currently several hypotheses to explain differentiation initiation for MSCs. Dennis et al [51] suggest a role for storage genes in MSCs that can adjust differentiation fate when exposed to different conditions. Phinney and Prockop[38] propose that MSCs are "equipped with motor proteins and a proteolytic arsenal that enables them to interact with and respond to signals from the extracellular matrix and differentiate into unique structures such as muscle, bone, cartilage, or other connective tissues".

The trophic effects of MSCs have also been implicated as significant in tissue regeneration[52, 53]. After engraftment, MSCs secrete a number of trophic molecules that include soluble extracellular matrix glycoproteins (collagen types I and II, osteopontin), cytokines (transforming growth factor [TGF]-β, IL-10, IL-6), and growth factors (vascular endothelial growth factor, hepatocyte growth factor, keratinocyte growth factor)[50]. These trophic molecules promote cell–cell connections[54], reduce inflammation, apoptosis, and fibrosis of damaged tissues, and can stimulate tissue cell regeneration.

2.2 Mechanics of Cell Freezing and Damage

If cells are not frozen properly, large distortions in the cellular system (such as membrane deformation) can occur due to ice crystal formation[55, 56]. Free water exists both inside the cell in the cytoplasm and in the surrounding extracellular fluid. Ice solidifies

anisotropically during the freezing process and rejects cells and proteins from the solid phase. This ice formation (both extracellular and intracellular) can result in undesirable mechanical stresses on the membrane and cytoskeleton. Solutes in the freezing media help to suppress the freezing temperature of water, resulting in more control over ice nucleation and formation of small extracellular ice crystals, which helps limit damage to cells. Freezing in these systems is stochastic, and controlling ice nucleation using a controlled rate freezer has been shown to result in higher cell viability for MSCs than other freezing methods, such as vitrification (high cooling rate, low volumes of cryoprotectant, no ice crystal formation)[57].

Intrinsic factors of different cell types and interaction with cryoprotectants help to determine cellular recovery after freezing[58]. Optimal cooling rates vary with different systems of cells and cryoprotectants[7]. In most systems, slow freezing rates (less than 10°C/min in the linear phase) induce extracellular ice formation, which concentrates cryoprotectants in the extracellular fluid and increases the osmotic gradient across cell membranes to draw free water out of cells. This osmotic dehydration at slow cooling rates[59] helps to limit intracellular ice formation that can result in cell injury[7, 60] before total solidification takes place.

Increasing concentrations of cryoprotectants can destabilize the plasma membrane of cells by inducing chemical, electrical, and ionic stresses[61]. However, as temperature decreases so do the metabolism of the cell and the kinetics of all reactions, mitigating

damage as the system cools. Samples must be cooled and stored at temperatures below the threshold of activity at which degradative processes occur in order to maintain maximum cellular viability and function over time[62]; typically this is achieved by storage in liquid nitrogen or liquid vapor phase nitrogen at a temperature of -196°C. Thawing of cells after storage is typically performed as quickly as possible by agitating cells in a 37°C water bath until just-thawed[63].

Cells can be damaged at any of the five steps in the freezing process: sample preparation, freezing, storage, thawing, and analysis. Cryoprotectants, controlled freezing, and rapid thawing help mitigate damage that occurs in the freezing and thawing phases where cells are undergoing the greatest changes. However, death and damage still result due to freezing[64], suggesting that current methods are suboptimal[9] as they can result in variably poor performing post-thaw products[10].

Some forms of cellular damage result in cell death, which can be observed immediately post-thaw using membrane integrity fluorescent stains. Determining latent damage present in viable cells post-thaw is less straightforward. Thawed cells may still test positive for viability during the early stages of apoptosis, resulting in poorer than expected post-thaw function of the cell sample as a whole. Membrane and cytoskeletal damage may also be present in cells post-thaw. Localized bulging (blebbing) of the plasma membrane is characteristic of stress[65] and is observed during both apoptosis[66], and under freezing stresses[67]. Rupture of the cell membrane and changes in actin distribution can also result from freezing[68].

2.3 Dimethyl Sulfoxide (DMSO) Cryopreservation

Dimethyl Sulfoxide (DMSO) was first identified as an effective cryopreservative in 1959 by Lovelock and Bishop[69], and has since become the standard cryopreservative used for cell freezing in the last 50 years. However, the mechanisms of DMSO cell stabilization during freezing are not fully understood. DMSO is a small (78 Da) amphiphilic molecule, which makes it highly membrane permeable and allows for efficient osmotic equilibration across the cell membrane during freezing and thawing. It is also believed to act as a stabilizer during freezing by binding just inside in the head group region of the cell membrane, increasing spacing between phospholipids, thinning the membrane, and decreasing membrane rigidity[70]. This allows cells to adjust and accommodate rather than rupture when confronted with external mechanical stimuli (such as ice crystals), and reduces the energy cost required to form pores[70, 71]. However, DMSO is systemically toxic. Although many treatment protocols call for washing of thawed cell products to reduce DMSO content before transfusion (which can cause cell losses during centrifugation and aspiration steps), DMSO can induce side effects such as nausea, vomiting, and cardiovascular and respiratory complications when transfused in even trace amounts with thawed cells[8, 72]. As some treatments require multiple infusions of cryopreserved cells, non-toxic cryopreservative alternatives to DMSO are desirable and will become necessary as transfusion cell therapy advances.

In addition to DMSO's negative systemic side effects, it has also been suggested that current freezing with DMSO produces sub-optimal functioning post-thaw stem cell

products[9, 73]. Specifically, mesenchymal stem cells have demonstrated diminished indoleamine deoxygenase activity [10], altered cytoskeletal function [74], and impaired immunomodulatory properties [75] after DMSO freezing. Other studies have shown that natural killer cells used for immunotherapies may also exhibit diminished post-thaw function after DMSO cryopreservation [76].

These decreases in function are accompanied by changes in gene expression caused by epigenetic alterations. DMSO increases the mRNA level of the *de novo* DNA methyltransferase Dnmt3a accompanied by hyper- or hypo-methylation of many genetic loci [77] making it unsuitable for use with reprogrammed cells of high therapeutic value, such as induced pluripotent stem cells or cells derived from them. Epigenetic changes in cells including increased DNA hydroxymethylation[78] have also been linked to DMSO. Clearly, development of alternative methods of preserving cells to eliminate DMSO and improve post-thaw function is desirable.

2.4 Non-DMSO Cryopreservatives

Any molecule cocktails selected to replace DMSO should additively create an environment similar to the stabilizing environment that DMSO is able to provide. DMSO mechanisms of protection during freezing dictate that at a minimum, new non-DMSO solutions should be able to draw water out of cells to regulate the osmotic environment during freezing, and stabilize the membrane of the cell to promote thinning and transient pore formation. Additionally, components should be selected to stabilize areas of the cell

that DMSO has not shown evidence of protecting, including the cytoskeleton and intracellular protein conformations.

Organisms in nature provide insight into possible non-toxic alternatives for cell stabilization[79]. Extremophile bacteria produce and accumulate amino acid polymers[80] and other non-toxic compounds such as ectoine[81] to prevent osmotic dehydration at high salt concentrations, and plants accumulate sugars, polyols (sugar alcohols), and amino acids under osmotic stress without affecting cellular metabolism [82, 83].

Several well-researched molecules fall into these categories and exhibit different mechanisms of cryoprotection including osmoprotection, protein hydration, and membrane stabilization. Sugars, specifically trehalose, have been studied extensively for the osmoprotective effects they exert and have shown moderate cryoprotectivity at appropriate concentrations [84–86]. Polyols (such as glycerol) have been used as cryoprotectants for proteins, functionally stabilizing protein structure by maintaining hydrogen bonding in protein-bound water[87, 88]. To address membrane stability, amino acids have been utilized for liposomal cryopreservation[89, 90], and ampholytic amino acid polymers have demonstrated cryoprotection and result in cellular recoveries similar to DMSO[91, 92]. Evidence from several groups indicates that the use of multiple cryoprotectants from different families above, such as trehalose and proline[90], and trehalose and glycerol[93] exhibit improved cellular survival than either cryopreservative

alone, suggesting additive[87] stabilizing effects are possible when multiple cryopreservatives are used[94]. However, the concentrations of these cryoprotectants dictate whether they will be stabilizing or destabilizing[95, 96] and concentrations that result in stabilization optimums may differ when cryoprotectants are combined.

2.5 Cryopreservation Optimization

2.5.1 Previous factorial cryopreservation optimization attempts

Many groups in the field of cryobiology have attempted to optimize cryopreservation of a variety of cell types. Most commonly, factorial protocol optimization is used to empirically determine optimums by varying a limited range of conditions. Different aspects of the cryopreservation process can be altered to identify optimums, including: cryoprotectant identity, cryoprotectant concentration, rate of addition and removal of cryoprotectant, pre-freeze incubation time, pre-freeze incubation temperature, hold temperature, nucleation temperature, cooling rate, single vs. multistep cooling, storage temperature, and thawing rate. For example, Conrad et al[97] evaluated a total of 8 different factorial combinations to determine how changes in concentration of trehalose, borate and pH affect recovery of *Lactobacillus acidophilus* freeze dried products. Dijkstra-Tiekstra et al[98] studied a total of 32 different factorial combinations to determine the effects of precooling, changes in DMSO concentration, freezing rate, and storage condition on hematopoietic progenitor cell quality. Dong et al[99] looked at 64 total factorial combinations capturing differences in pre-cooling, cryoprotectants, cooling, and thawing conditions to optimize rhesus monkey sperm cryopreservation.

Freimark et al[100] assessed a total of 36 different factorial combinations of cryoprotectants, equilibration period, and cooling rate to optimize Mesenchymal stem cell cryopreservation. Kearney et al[101]evaluated a total of 36 factorial combinations of different cryoprotectants, permeation times, and cooling rates to optimize murine skin cell cryopreservation. Ting et al[102]studied a total of 16 factorial combinations of different vitrification solutions, incubation times, and polymer additions to optimize macaque ovarian tissue vitrification, as well as a total of 48 factorial combinations[103] of different vitrification solutions, concentrations, and post-thaw sugar dilutions to optimize vitrification of pre-antral macaque ovarian follicles. At most, these factorial optimization schemes looked at 2-6 different values for 2-6 different variables, limiting the total conditions tested in each of these studies to a manageable experimental size.

2.5.2 Differential Evolution Algorithm

In order to increase the number of potential combinations that can be tested while avoiding factorial testing of all possible combinations within a given system, a more systematic optimization approach can be employed. The differential evolution algorithm was developed by Storn and Price[11], and was used recently by Tsutsui et al[104] to optimize growth medium composition for embryonic stem cells. When applied to solution optimization problems, the algorithm utilizes an objective (cost) function that models the problem as a maximization task. For the cryopreservation applications described in this work, vectors containing information regarding the viability of cells frozen and thawed (dependent variable to be maximized) and the solutions in which they

are frozen (independent variables) populate the cost function. The cost function is filled with discrete data vectors, and as such is non-linear and non-differentiable. Solving requires the use of a stochastic direct search method, which generates variations by taking the difference between two existing vectors and perturbing a third vector with the result. After producing a vector variation, the algorithm makes a decision (based on the existing data points in the cost function) whether or not to accept the new vector by using the greedy criterion, and only accepts the result if it increases the value of the cost function. To avoid local maxima, parallel searches are run simultaneously. This allows for faster and smoother convergence to a global maximum when compared to optimization algorithms that utilize probability distribution functions.

It would take thousands of trials to determine the best concentration set of non-DMSO cryoprotectants for MSC freezing if every possible combination in large parameter ranges were tested. The differential evolution algorithm will assist in identifying interactions between non-DMSO cryoprotectants, and in selecting new combinations and concentrations to test experimentally.

Chapter 3

Methods

3.1 Materials and Equipment

Table 2 lists all equipment described in the following methods section, along with manufacturer information and physical location where the equipment was used. All products are from the USA unless otherwise indicated

Table 2: Equipment.

Chapter(s)	Material	Details	Location used	Manufacturer/location
4-8	Controlled rate freezer	Planer series III Kryo 10	UMN Hubel lab	Sunberry-on-Thames Middlesex, UK
5,7	Biomek FX-96 liquid handler		UMN HTSS/ITDD	Beckman Coulter Indianapolis, IN
5,7	Synergy HT multi-mode Biomek plate reader		UMN Bischof lab	Biotek Winooski, VT
5,7	WellPro 96 liquid handler	Model 3000	UMN HTSS/ITDD	ProGroup Instrument Corporation Alton, IL
6	100X air objective	NA 0.90	UMN CharFac	Nikon Instruments Melville, NY
6	Differential scanning calorimeter	TA DSC Q1000	UMN Macosko Lab	TA Instruments New Castle, DE
6	Osmometer	Osmette ™	UMN Hubel lab	Precision systems Natick, MA
6	Witec confocal RAMAN system		UMN CharFac	WITec Ulm, Germany
8	CFX384 Real-Time PCR detection system		Mayo van Wijnen lab	Bio-Rad Hercules, CA
8	ChemiDoc ™ Touch Imaging System		Mayo van Wijnen lab	Bio-Rad Hercules, CA
8	Flow cytometer	LSRII	UMN UFCR	BD Biosciences San Jose, CA
8	Zeiss Axioplan 2 with 20x objective		UMN UIC	Carl Zeiss Microscopy Maple Grove, MN

Table 3 lists all materials described in the following methods section, along with associated abbreviations and manufacturer information. All products are from the USA unless otherwise indicated

Table 3: Materials.

Chapter(s)	Material	Details	Abbrev	Manufacturer/location
4	4-(2-hydroxyethyl)-1-piperazineethanesulfonic acid		HEPES	Life Technologies Carlsbad, CA
4	7-amino-actinomycin D		7-AAD	BD Biosciences San Jose, CA
4	Alpha-Modified Eagles Medium		αMEM	Invitrogen Grand Island, NY
4	Annexin V/PI			BD Biosciences San Jose, CA
4	Bone marrow	MSC source	BM-MSC	Lonza Walkersville, MD
4	CD45			BD Biosciences San Jose, CA
4	CD90			BD Biosciences San Jose, CA
4	Dimethyl Sulfoxide		DMSO	Bioniche Pharma Belleville, ON, Canada
4	Dulbecco's Phosphate Buffered Saline		DPBS	Invitrogen Grand Island, NY
4	Fetal bovine serum			Hyclone - Thermo Scientific Waltham, MA
4	Ficoll Paque Premium	Density gradient centrifugation	Ficoll	GE Healthcare Pittsburgh, PA
4	Glutamax	200mM/L		Invitrogen Grand Island, NY
4	Hanks balanced salt solution	No phenol red, calcium, or magnesium	HBSS	Lonza Walkersville, MD
4	Human Serum Albumin	25%	HAS	Baxter Deerfield, IL
4	Plasmalyte A			Baxter Deerfield, IL
4	t-Flasks	Tissue culture treated		Corning Corning, NY
4	TrypLE Select			Invitrogen Grand Island, NY
4,8	Beta-glo assay			Promega Madison, WI
4,8	Tert-butyl hydroperoxide	100mM	t-BHP	Sigma St. Louis, MO
4-8	Acridine Orange		AO	Life Technologies Carlsbad, CA
4-8	Cryovials			Nunc/Nalge Thermo Scientific Waltham, MA
4-8	Neubauer hemocytometer			Hausser Scientific Horsham, PA
4-8	Propidium Iodide		PI	Life Technologies Carlsbad CA
5	Arabitol	A3506		Sigma St. Louis, MO
5	Erythritol	E7500		Sigma St. Louis, MO
5	Inositol	I5125		Sigma St. Louis, MO
5	Ribitol (Adonitol)	A5502		Sigma St. Louis, MO

Chapter(s)	Material	Details	Abbrev	Manufacturer/location
5	Sorbitol	S1876		Sigma St. Louis, MO
5	Valine	V0500		Sigma St. Louis, MO
5	Xylitol	X3375		Sigma St. Louis, MO
5,6,8	Creatine	C0780		Sigma St. Louis, MO
5,6,8	Mannitol	M4125		Sigma St. Louis, MO
5,7	Alanine	A7469		Sigma St. Louis, MO
5,7	Biomek tips			Fisher Scientific Pittsburgh, PA
5,7	Black walled 96-well plates			Corning Corning, NY
5,7	Calcein AM			Fisher Scientific Pittsburgh, PA
5,7	Ectoine	81619		Fluka analytical - Sigma St. Louis, MO
5,7	Taurine	T0625		Sigma St. Louis, MO
5,7	WellPro tips			Fisher Scientific Pittsburgh, PA
5-7	Trehalose	T5251		Sigma St. Louis, MO
5,8	Isoleucine	I2752		Sigma St. Louis, MO
5-8	Alpha modified eagles medium base	with Glutamine	αMEM	Life Technologies Carlsbad, CA
5-8	Dimethyl Sulfoxide	BP231-1	DMSO	Fisher Scientific Pittsburgh, PA
5-8	Fetal bovine serum	Qualified	FBS	Life Technologies Carlsbad, CA
5-8	Glycerol (Glycerin)	NDC 0395-1031-16		Humco Austin, TX
5-8	H9 embryonic stem cell derived MSCs		H9 MSCs	Hematti Lab Madison, WI
5-8	Non-essential amino acids		NEAA	Life Technologies Carlsbad, CA
5-8	Normasol-R™	ph 7.4	Normasol	Hospira Lake Forest, IL
5-8	Porcine gelatin			Thermo Fisher Scientific Waltham, MA
5-8	Sucrose	S5-3		Fisher Scientific Pittsburgh, PA
5-8	Trypsin	0.05%		Gibco - Thermo Fisher Waltham, MA
6	Glucose (Dextrose)	4908		Mallinckrodt St Louis, MO
6	Kapton tape			Dupont Wilmington, DE
6	Mica			TED PELLA Redding, CA

Chapter(s)	Material	Details	Abbrev	Manufacturer/location
7	Jurkat cells		Jurkats	ATCC TIB-1522 Manassas, VA
7	Molded silicone round well covers			Laboratory supply distributers Melville, NJ
7	RPMI 1640	High glucose		Life Technologies Carlsbad, CA
8	6-well plates			Corning Corning, NY
8	Alcian blue			Fisher Scientific Pittsburgh, PA
8	Alizarin red			Fisher Scientific Pittsburgh, PA
8	anti-5hmC	39770		Active Motif Carlsbad, CA
8	Bio-Dot ® microfiltration apparatus			Bio-Rad Hercules, CA
8	Formaldehyde	37%, F1635		Sigma St. Louis, MO
8	miRNeasy Mini Kit			Qiagen Germantown, MD
8	mouse IgG1 anti-human CD105	clone 166707 PE conjugated	CD105	R&D systems Minneapolis, MN
8	mouse IgG1 anti-human CD45	clone HI30 BV421 conjugated	CD45	BD Biosciences San Jose, CA
8	mouse IgG1 anti-human CD73	clone ad2 APC conjugated	CD73	BD Biosciences San Jose, CA
8	mouse IgG1 anti-human CD90	clone 5E10 FITC conjugated	CD90	Invitrogen Grand Island, NY
8	NanoDrop ® 2000			Thermo Fisher Scientific Waltham, MA
8	Nitrocellulose membranes			Bio-Rad Hercules, CA
8	Paraformaldehyde	32%, 15714		Fisher Scientific Pittsburgh, PA
8	Phalloidin			Thermo Fisher Life Technologies Carlsbad, CA
8	Prolong gold anti-fade reagent+DAPI			Invitrogen Grand Island, NY
8	Qiagen Dneasy Blood & Tissue Kit			Qiagen Germantown, MD
8	Qiazol			Qiagen Germantown, MD
8	QuantiTect SYBR Green PCR Kit			Qiagen Germantown, MD
8	Stem-Pro chondrogenesis and osteogenesis medium			Thermo Fisher Scientific Waltham, MA
8	SuperScript III First-Strand Synthesis System			Invitrogen Grand Island, NY
8	SuperSignal West Femto Maximum Sensitivity Substrate kit			Thermo Fisher Scientific Waltham, MA
8	Triton x-100	T8787		Sigma St. Louis, MO

3.2: Cell culture

3.2.1 Bone marrow isolation, plating, and culture

The MSCs used for Chapter 4 were isolated from bone marrow (BM) that was shipped overnight on ice from Lonza. Mononuclear cells (MNCs) were isolated from the bone marrow using Ficoll density gradient centrifugation and separation. On initial receipt, the 10mL bone marrow sample was diluted with 10mL of 0.9% saline. In a 50mL conical tube, this dilute marrow cell suspension was carefully layered over 15mL of Ficoll. The resulting layered suspension was centrifuged at 300xg for 25 min at room temperature with no brake. The cell layer was collected and was then washed with 50mL of HBSS and centrifuged at 300xg for 5 min. A second wash was performed using the same procedure described above. The supernatant was discarded after both washes.

The MNCs isolated with this method were resuspended in BM-MSC complete culture medium (MSC CCM) composed of αMEM base, 16.5% FBS, and 1% Glutamax. Cells were seeded at a density of 1.0-1.5 x 10^5cells/cm^2 in appropriately sized tissue culture treated t-flasks at a media depth of 1.6 mm. Cells were cultured in a 5% CO_2, 37°C incubator.

Media changes were performed every 2-4 days until cells reached the desired 70-80% confluence between days 8-12. When cells reached the desired confluence, they were passaged. BM-MSCs were washed with Dulbecco's phosphate-buffered saline, removed from the culture surface with TrypLE select, diluted with MSC CCM to quench the action of TrypLE select and centrifuged.

3.2.2 Jurkat cell culture

The lymphoblastoid cells used in this study (Jurkats) were cultured in medium composed of high-glucose RPMI 1640 and 10% fetal bovine serum. Jurkat cells were cultured to maintain cell density within $1 \times 10^5 – 3 \times 10^6$ cells/mL.

3.2.3 H9 MSC cell culture

H9 embryonic stem cell derived MSCs (H9-MSCs) were obtained from Dr. Brenda Ogle and from Dr. Peimann Hematti's lab at the University of Wisconsin[105]. These cells have shown similar phenotypic expression to BM-MSCs, and exhibit appropriate migration and homing behavior in *in-vivo* mouse models[106]. Media used with H9 MSCs was composed of αMEM base, 10% FBS, and 1% non-essential amino acids. Culture flasks were coated with 0.01% porcine gelatin for a minimum of 2 hours before H9 MSC seeding. H9 MSCs were seeded in gelatin-coated flasks at a density of approximately 2500 cells/cm^2. Cells were split using 0.05% trypsin when they reached 70% confluence and were used for experiments only from passages 8 to 12.

3.3: Freezing

3.3.1 Vial freezing of BM-MSCs

At each passage harvest, 1-10x10^6 cells were frozen down in a total volume of 1mL per cryovial. Cells were harvested, washed in DPBS and resuspended in 5% human serum albumin (HSA) to a concentration of 2-20x10^6 cells/mL (2x the desired freezing concentration). The cells were combined stepwise with an equal volume of 2x freezing media composed of 60% Plasmalyte A, 20% HSA, and 20% Dimethylsulfoxide (DMSO).

The final concentration of DMSO was 10% by volume. Cells were frozen in a controlled rate freezer with the use of the following protocol:

1) Wait at 0.0°C (place sample in freezer at this step)
2) Wait at chamber = 0.0°C until sample = 1.0°C.
3) Ramp -1°C/min until sample = -12°C.
4) Ramp -20°C/min until chamber = -60°C.
5) Ramp +15°C/min until chamber = -18°C.
6) Ramp -1°C/min until sample = -60°C.
7) Ramp -3°C/min until sample = -100°C.
8) End.

After completion of the freezing protocol, cell vials were removed from the controlled-rate freezer (with the use of insulated gloves) and transferred quickly (<30 seconds) to liquid nitrogen storage to minimize transient warming of the sample. Samples were stored in liquid nitrogen for 30-45 days before being thawed for post-thaw analysis.

3.3.2 96-well plate freezing of Jurkats and H9-MSCs

In both screening and DE algorithm experiments, cells were frozen in 96-well plates to limit the number of cells and volumes of reagent necessary, and to increase the number of samples that could be tested at one time. Solutions were made at 2× their final concentration in distilled water (diH_2O). Cells were centrifuged and supernatant was

aspirated before cells were suspended in Normasol-R™. Cells were combined 1:1 with 2× solutions, using a single-step addition in clear-bottomed black 96-well plates to produce a 1× concentration of cryoprotectant solution with a total volume of 50 µl and a cell concentration of ~300, 000 cells/well (~6 million cells/mL). Actual seeding counts were confirmed by manual acridine orange/propidium iodide (AO/PI) counts of the cell stock added to each plate. As a control, wells of 10% DMSO solution were also included on each plate to normalize results between all experiments. All samples were run in triplicate wells on each plate. The plates were sealed with molded silicone round well covers to prevent desiccation during freezing and storage. The plates were placed in a rack in a controlled-rate freezer, and frozen using the profile below using a Planar Series III Kryo 10 controlled rate freezer:

1 Starting temperature 20°C

2 -10°C/min to 0°C

3 Hold at 0°C for 15min

4 -1°C/min to -8°C

5 -50°C/min to -45°C

6 +15°C/min to -12°C

7 –0.5, -1, -3, -5 or -10°C/min to-100°C (as dictated by the DE algorithm)

The rapid cooling and rewarming in steps 5 and 6 are included to promote ice crystal nucleation outside the cell before slow cooling proceeds, discouraging stochastic ice formation within the cells. A temperature of -8°C was selected for this step, as a

conservative temperature at which all possible solution compositions should have exceeded their freezing point (based on their predicted osmolarity) to ensure that this ice nucleation step would be successful.

In order to validate this freezing format, freezing profiles (temperature versus time) were measured at center, edge, and corner wells of a 96 well plate to determine if freezing rate differences between locations on a plate were likely to alter cellular behavior. A 96 well plate was loaded with 50 µl of cell culture media and covered with a silicone plate sealer. Thermocouple probes were placed in 3 wells of the plate: a center well, a column edge

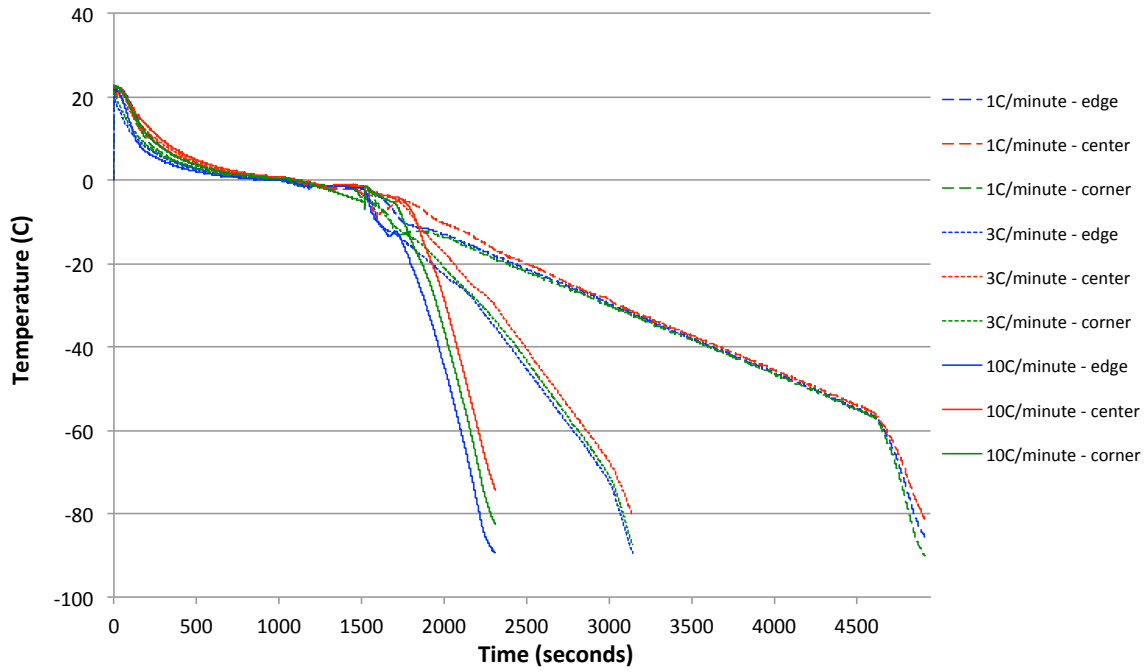

Figure 3: Freezing profiles in a 96-well plate. Corner, edge, and center well freezing profiles on a 96-well plate were measured during programmed freezing routines with linear freezing rates of 1°C/min, 3°C/min, and 10°C/min. Well to well differences were largest for the 10°C/min freezing profile and differed most between edge and center. Location freezing rate variations were not large enough to indicate problematic gradients exist.

well, and a corner well. Temperatures experienced by each of the thermocouples were recorded with Labview acquisition software, and monitored as the plate was frozen three separate times in a controlled rate freezer at linear freeze rates of 1°C/minute, 3°C/minute, and 10°C/minute according to the same protocol described earlier in this section (shown in Figure 3).

The freezing behavior observed at different locations on the plate differed most between the center and the edge of the plate. Higher cooling rates resulted in increasing variation between different plate locations. For cooling between -12°C to -40°C, the 1°C/minute cooling program resulted in a 0.94 ± 0.0036°C/minute cooling rate and the 10°C/minute cooling program resulted in a 2.52 ± 0.0532°C/minute cooling rate, a 15 fold increase in standard deviation. However, the standard deviations observed even for the 10°C/minute cooling program were less than 2% of the total rate, indicating that freezing rate variations across the plate are acceptable.

To confirm that this freezing rate uniformity correlated to cell survival uniformity, a 96 well plate of cells suspended in 10% DMSO in media was frozen and thawed to confirm that cellular recovery was not affected by well location. Calcein AM fluorescence, representative of the number of live cells present in each well, was uniform across the plate with no large differences between the edges of the readable area of the plate or the center (shown in Figure 4).

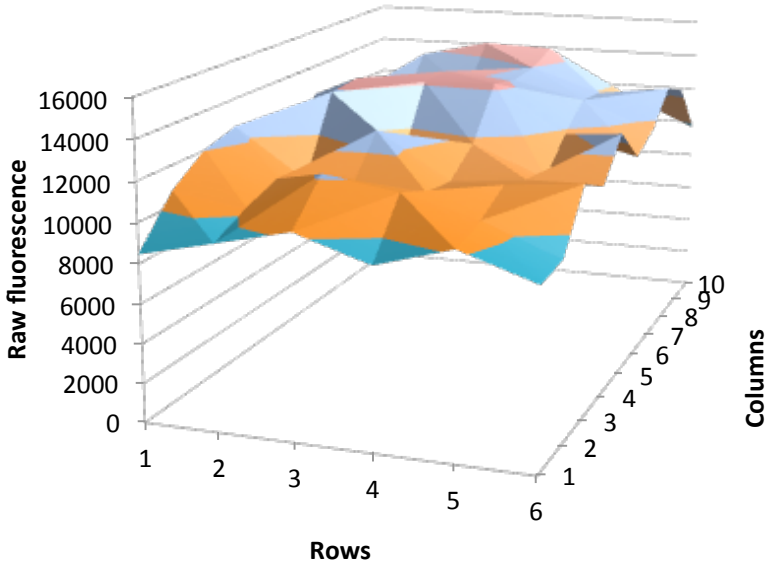

Figure 4: 96 well plate profile of cells frozen in 10% DMSO.
Fluorescence results correlate directly to cell content. Roughly uniform fluorescence profile across the plate indicates that cells experience similar recovery in all wells.

3.3.3 Vial freezing of Jurkats and H9-MSCs

Solutions were prepared at 2x the final freezing concentration and added stepwise to cells in Normasol-R® at a 1:1 final volume ratio in a Nalgene freezing vial. Control cells in media were similarly combined stepwise with DMSO at a 1:1 final volume ratio (final concentration of 10% DMSO). Each of these vials was incubated at room temperature for 0, 1, or 2 hours. Vials were frozen using the same freezing protocol as plates (detailed in section 3.3.2) on a Planar Series III Kryo 10 controlled rate freezer.

3.4: Thawing

Both 96-well plate and vial samples were thawed using a 37°C water bath. Vials were submerged in a 37°C bath (to just under cap level) and agitated until only a small ice crystal was present.

Plates were also thawed using a 37°C water bath. Briefly, the plates were submerged to half their height and agitated for 1 min. At t = 1 min, they were removed from the bath and the silicone cover was removed to observe the samples as they thawed. The plates were returned to the 37°C water bath and again submerged to half their height. When opaque samples became transparent (~1 min after being returned to the water bath) the plates were removed for immediate addition of viability dye. Thermocouple probe analysis of the freezing and thawing rate in different wells of a 96-well plate showed that no significant difference existed in the temperature profiles of the wells tested in these experiments.

3.5: Viability testing

3.5.1 Acridine Orange/Propidium Iodide manual counting

Cells were tested for viability using acridine orange (AO) and propidium iodide (PI). The final working solution with concentrations of 20mM/ L AO and 20mg/mL PI in DPBS was combined with cells in a 1:2-1:20 dilution. At least 100 cells were counted in a Neubauer hemocytometer under fluorescence. Under these conditions, viable live cells fluoresced green as the result of AO binding to nucleic acids through intercalation. Conversely, membrane impermeant PI caused only dead cells to fluoresce red. Sample viability percentage was calculated by dividing the number of live cells by the number of total cells (live + dead) and multiplying by 100.

3.5.2 Plate reader viability testing

After the 96-well plates were thawed, a dye composed of calcein AM (ex/em = 494/520 nm) and PI (ex/ em = 535/617 nm) was added to each well and the wells were covered to protect against light and placed in a 37°C incubator for 30 min to allow the live cells to cleave calcein AM; the latter was used for these experiments instead of acridine orange (which has multiple fluorescent peaks, one of which overlaps with the peak for propidium iodide), as it has narrow excitation/emission peaks that do not interfere with the peaks for propidium iodide. The plates were then analyzed for fluorescence on a plate reader, using existing filter sets with excitation/emission wavelengths of 485/528 nm to measure calcein fluorescence and 530/590 nm to measure PI fluorescence. Raw fluorescence values were used to calculate the number of live and dead cells present in each well, by correlating to a control curve of unfrozen cells generated using serial dilution of known live and dead (killed using heat shock at 60°C for 15 min) cell counts. The live cell recovery was calculated by dividing the number of live cells present in thawed samples (calcein AM plate reader fluorescence) by the number of live cells seeded pre-freeze (AO/PI counts visually observed on a hemocytometer for the seeded cell stock). To normalize results between different plates and different cooling rates, these raw recoveries were divided by a control well containing 10% DMSO on the same plate (to normalize for stochastic variations in freezing experienced by the plate as a whole), then multiplied by a standard DMSO recovery at each cooling rate to give the 'scaled raw recovery'. After each experimental generation, the DMSO recovery for each cooling rate was averaged with all DMSO recoveries at that cooling rate from previous generations to

calculate the DMSO standard recovery for that cooling rate, and the scaled recovery for all data from all generations was recalculated at the conclusion of each generation, based on these new standards, before reiteration through the algorithm. The final DMSO standard recoveries for Jurkat cells at each cooling rate are listed in Table 12. The differences in DMSO recovery between cooling rates were noticeable and, although not statistically significantly different, consistently fell in the same order relative to one another at each generation, which is why simply scaling to the DMSO recovery on each plate without correcting for the cooling rate would give an incomplete picture of experimental recovery.

3.6: Senescence testing

Senescence in cells is associated with an inflammatory secretome, which can cause undesirable results for immunotherapies. Cells were tested for senescence using the Beta-glo assay, which measures lysosomal β-galactosidase expression associated with senescence in cells. In contrast to the conventional, absorbance-based Miller method, this assay is well-suited for high-throughput screening and has been used in this context for other organisms [107, 108]. Cells were centrifuged at 300xg for 5 min and resuspended with 25mM 4-(2- hydroxyethyl)-1-piperazineethanesulfonic acid (HEPES) in 0.9% NaCl. In white-walled flat- bottom 96-well plates, 100mL of Beta-glo assay was added to 100mL of cell solution in each well. The plates were allowed to incubate for 30 min at room temperature and were subsequently read for luminescence on a plate reader for studies described in Chapter 4.

In Chapter 8, thawed samples described in section 3.4 were re-suspended in 4mL of media and 1mL was added to each of four gelatin-coated 6-well plates. After 2 hours or 24 hours, plates were washed with PBS and two plates were analyzed at a time, one for proliferation as described in section 3.14 below, and one for senescence. For the senescent plate, 1mL of Beta-glo luminescent dye was added, to the other, 1mL of 1μM calcein-am dye was added. Beta-glo plates were incubated at room temperature for 30 min, while calcein-am plates were incubated at 37°C for 30 min. Plates were analyzed using a BioTek plate reader for luminescence (Beta-glo plate) and fluorescence (485ex/528em, calcein am plate) respectively. A relative measure of senescence is reported in Chapter 8 by dividing the base-corrected luminescence (approximation of total senescent character) per well by the base-corrected fluorescence (approximation of total cells per well).

A population of MSCs was forced into senescence by treatment with 100mM tert-butyl hydro peroxide (t-BHP) 1 hr/day for 5-7 days. After each treatment, cells were washed with DPBS and fresh media was replaced. This senescent positive control population was seeded in a 96-well plate and serially diluted to produce a control curve for Chapter 4, or into 6-well plates for Chapter 8. The linear best-fit line of this curve was used to calculate the percentage of β -galactosidase expressed by experimental populations compared with fully senescent populations of the same size for Chapter 4, and was used as a positive control reference for Chapter 8.

3.7: Flow cytometry

Flow cytometry can be used to confirm appropriate cell surface marker expression. Flow cytometry was performed on an LSRII at low flow rate with the fine adjust knob five turns from max. At least 15,000 events were recorded for each sample gating for forward and side scatter cell population as well as with a negative unstained control and a Jurkat CD45 positive control to gate fluorescent graphs. Cells were suspended to a concentration of $1x10^6$ cells/mL in media and stained with a panel of antibodies for 30 min at 4°C. Viability was assessed using a standard 7-amino-actinomycin D (7-AAD) test. MSC samples were also characterized for cell surface phenotype. Specifically, cells were stained for the presence of CD45 and CD90 as markers for cells surface phenotype in Chapter 4, in addition to CD73 and CD105 in Chapter 8. The acceptance criteria included that MSCs were >85% CD45 negative, and >85% CD73, CD90, and CD105 positive. Apoptosis was assessed using AnnexinV/PI staining; early apoptotic cells stain positive for AnnexinV only, while necrotic cells stain positive for both AnnexinV and PI.

3.8: Karyotyping

Samples were sent to an external facility for karyotyping. G-banded karyotype analysis was performed on 20 metaphase cells to rule out the presence of any numerical or structural chromosomal abnormality. If one cell tested abnormal, additional cells were analyzed to rule out the presence of a clonal abnormality. Documented benign heritable heteromorphisms, such as 9 small-p small-h, were not considered abnormalities. Pre-culture samples of marrow were available for comparison.

3.9: Liquid handling

Liquid handling robots were used to perform plate transfers for cell freezing experiments involving 3-component solutions. These experiments were performed on WellPro (row and column transfers) and Biomek liquid handlers (full plate transfers) at the Institute for Therapeutics Discovery and Development (ITDD).

3.9.1 WellPro serial dilutions for Chapter 7

A dual serial dilution performed by the WellPro 96 creates a 6x6 matrix with a full array of combinations of solution components 1 and 2. A 4x final concentration of component 1 was loaded in the top wells of a 96-well plate, and Normasol blank was loaded in the remaining wells. The WellPro serially diluted the concentrated top well down the plate vertically. Subsequently, additional 4x final concentration of component 2 was loaded on the left hand side of the plate, in addition to an equal volume of Normasol blank in the remaining wells (diluting both component 1 and component 2 by a factor of two across the whole plate). The WellPro serially diluted this left to right across the plate horizontally. The final result was a 6x6 matrix of component 1 and component 2. This plate was transferred to the Biomek liquid handler for subsequent plate transfers.

3.9.2 Biomek plate transfers for Chapter 7

Figure 5 shows an outline of the tip and plate layout for the transfer described in this section.

Figure 5: Biomek plate transfer layout.

Cells were suspended in a 2x final concentration of component 3 or Normasol for blank. These solutions were loaded into separate 96-well plates in the same 6x6 locations as the serial dilution of components 1 and 2 from the WellPro. The Biomek was programmed to transfer cells diluted in 2x component 3 to the level 5 plate, and cells in Normasol to each of 5 remaining target plates. Cells in component 3 were then serially diluted across the Normasol plates. An equal volume of the 6x6 array of component 1 and 2 from the well pro serial dilution above was added to each of the plates, producing a full array of components and concentrations for a single 3 component solution.

3.9.3 Plate transfers for Chapter 5

In order to test many different solution components together, a single intermediate concentration of each component was selected for testing. Each of 8 plates were individually loaded with different sugar alcohols, in addition to a 9th plate that was loaded with an equal amount of Normasol. An additive plate was prepared with a different additive in each column, including a column of Normasol. These 10 plates were organized on the Biomek for plate transfers along with another plate containing cells suspended in a 2x concentration of sugar. Plate transfers were performed to add additives and cells/sugar to each of the sugar alcohol plates. Cells in DMSO were added to an empty column of each plate to act as a plate-to-plate control comparison.

3.10: Raman

Guanglin Yu performed all confocal Raman microscopy experiments.

Confocal Raman Microspectroscopy (CRM) measurements were conducted using a Witec Confocal Raman Microscope System Alpha 300R with a UHTS300 spectrometer and DV401 CCD detector with 600/mm grating. The WITec spectrometer was calibrated with a Mercury-argon lamp. A wavelength of 532 nm Nd:YAG laser powered at 10 mW was used as an excitation source. The laser was transmitted to the microscopy in a singer fiber. A 100X air objective was used for focusing the 532-nm excitation laser to the sample. Samples were frozen using a controlled temperature stage described in more detail elsewhere[59].

3.10.1 Raman measurement of frozen MSC cells

MSC cells were detached from the flask and washed with DPBS solution before being suspended in experimental solutions. Roughly 1 μL of cell suspension was placed on an aluminum sheet, covered with a piece of mica and sealed with Kapton tape, to prevent evaporation/sublimation during each experiment. Cell suspensions were cooled to -6^{o}C at which point the sample was seeded by a nitrogen-cooled needle. Subsequently, the solution was cooled down at 3^{o}C/min to -50^{o}C. Ten Raman images of 30 μm x 30 μm were collected.

3.10.2 Raman image/spectral analysis

Spectrums at each pixel were analyzed using characteristic wavenumbers of common intracellular and extracellular materials (Table 4), and were integrated with background subtraction to result in an image. Spectra for the osmolytes used in the investigation overlapped with each other, so a broad peak centered at 850 cm^{-1} was used to generate Raman images for all osmolytes. Data analysis was performed by Windows-based Project FOUR software plus version 4.0.

Table 4: Peak assignments for molecules of interest detected using Raman spectroscopy.

Component	Frequency used for this study cm^{-1}	Ref.
Ice	3120 (O-H stretching)	[59]
Amide I	1659 (C=O stretching)	[109]
Glycerol	851 (C-C stretching)	[110]
Sorbitol	878 (C-C=O stretching)	[111]
Glucose	840 (C-C stretching)	[112]
Sucrose	836 (C-C stretching)	[112]
Creatine	840 (C-N torsion)	[113]

3.11: Differential Scanning Calorimetry

Differential scanning calorimetry was performed on a TA Differential Scanning Calorimeter (DSC) Q1000. Experimental solutions without cells were frozen to -150°C using the following protocol:

1. Set starting temperature to 20°C
2. Cool to -150°C at 10°C/min
3. Hold for 3 min at -150°C
4. Warm to 20°C at 10°C/min

3.12: Osmolarity testing

Osmolarity of solutions was measured using an Osmette ™ osmometer (Precision Systems) for each solution and all measurements were repeated in triplicate.

3.13: Algorithm iteration

The DE algorithm used in this study was developed from strategy 2 (DE/local-to-best/1, which balances robustness and convergence) by Storn and Price [11] and was coded in MATLAB by modifying existing open source Storn and Price MATLAB code to accept discrete parameters, and output information about the test population and emergent population after each iteration. The DE algorithm utilizes stochastic direct search and independently perturbs population vectors to identify a global maximum within the user-defined parameter space. Briefly, the DE algorithm randomly generates an initial

population (generation 0) that spans the entire parameter space. This population is composed of a given number of solutions expressed as vectors (a set of numbers). The number of different solution components being tested defines how many slots the population vectors have. Experimentally, these vectors correspond either to the different levels of solute in a solution or to different cooling rates. Cells are frozen at DE algorithm-dictated cooling rates with solutions made from these vector specifications, and the resulting experimental live cell recoveries (or other success metric) are iterated back into the DE algorithm.

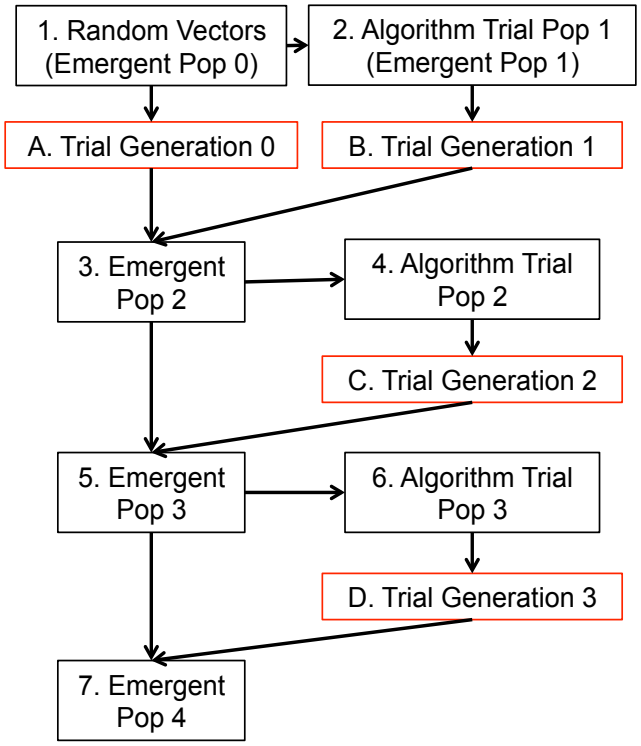

Figure 6: DE algorithm flowchart. Black boxes represent DE algorithm steps and red boxes represent experimental steps. The DE algorithm produces a population in gen 0 that randomly spans the parameter space, and a trial population (gen 1) that is based on mutation of gen 0. These are both experimentally tested by the user and the live cell recovery results are input into the DE algorithm, producing an emergent population which is further mutated and iterated in subsequent experiments. As the algorithm converges, an optimum solution can be identified .

The DE algorithm utilizes this experimental information to modify the existing population vectors, and predicts solutions that may result in more favorable live cell recovery. Briefly, the algorithm mutates existing vectors to generate new test vectors, and performs head-to-head comparisons of the resulting experimental live cell recovery of each of the population slots. The best value from this comparison (either the original or the new mutant vector) is stored in an emergent population. This mutation/comparison process is repeated for all subsequent generations (**Figure 6**) and results an emergent population that changes less and less as the algorithm converges. The final emergent population contains a set of solutions that have all been independently optimized using stochastic direct search, and includes the best possible compositions for freezing cells within the defined parameter space. Convergence can be measured by observing an increase in cumulative best member live cell recovery, a decrease in the number of improved solutions within the emergent population after each generation, or by the generational average, which captures both metrics.

3.14: Attachment and proliferation

Cell attachment of samples post-thaw was measured using a fluorescent plate reader. Aspirated samples from the thawing section above were re-suspended in 2mL of media and split to seed 1mL in each of two gelatin coated 6-well plates. After 2 hours or 24 hours, these paired plates were washed with PBS and 1μM calcein AM dye was added, then analyzed for fluorescence on a plate reader. Raw fluorescence values were used to calculate the number of live cells present in each well by correlating to a control curve of

serially diluted unfrozen cells seeded at known densities. The live cell attachment was calculated by dividing the number of live cells present in 2-hour plated samples (calcein am plate reader fluorescence) by the number of live cells seeded pre-freeze (AO/PI counts).

3.15: Actin staining and fiber alignment analysis

After thawing, centrifugation and aspiration, cells were re-suspended in 1mL of media and plated in gelatin coated 6-well plates containing a cover slip. After 2 hours, wells were washed with PBS, treated with 3.7% Formaldehyde to fix cells, then 0.1% Triton x-100 to permeabilize the cell membranes, followed by addition of 250μM phalloidin for 20 minutes. Cover slips were removed from wells, inverted, and mounted on glass slides using prolong gold anti-fade reagent with DAPI. Slides were imaged using a Zeiss Axioplan 2 scope with 20x objective. A minimum of 5 fields of view were captured for each slide, and MATLAB edge detect analysis[114](a more computationally efficient alternative to FFT[115]) was used to isolate and analyze fiber orientation in 30 individual cells total from 5+ fields of view for each sample. Triplicate biological samples were analyzed and results were averaged for 90 total cells from each sample.

3.16: Multi-lineage differentiation

Cells (both fresh and after freezing in experimental solutions or DMSO) were plated according to the Stem-Pro chondrogenesis and osteogenesis protocols for differentiation.

3.16.1 Chondrogenesis

Cells were suspended in MSC CCM at $1.6x10^7$ cells/mL, and 5µl droplets were seeded to form micromass cultures for chondrogenesis. After 2 hrs, pre-warmed chondrogenesis media was added to the micromass cultures. Chondrogenesis media was changed every 3 days for 14-21 days. At 14-21 days post-seeding, cells were fixed with 4% paraformaldehyde for 10 min. Cells were washed 3 times in PBS, then stained using 1% Alcian Blue solution in HCl for 1hr with gentle agitation. Samples were washed with 0.1M HCl, and subsequently imaged for analysis.

3.16.2 Osteogenesis

Cells were suspended in MSC CCM and seeded at $5x10^3$ cells/cm^2. After 4 hrs, cultures were washed with PBS, and pre-warmed osteogenesis media was added. Osteogenesis media was changed every 3 days for 14-21 days. At 14-21 days post-seeding, cells were fixed with 4% paraformaldehyde for 10 min. Cells were washed 3 times in PBS, then stained using 2% Alizarin red solution at pH 4.2 for 1hr with gentle agitation. Samples were washed with diH_20, and subsequently imaged for analysis.

3.17: DNA hydroxymethylation

3.17.1 DNA isolation and quantification

After PBS washing and centrifugation, pellets of fresh and thawed samples were flash frozen in liquid nitrogen, then transferred to -80°C (dry ice transport) for further DNA isolation and processing. Genomic DNA was isolated using QIAGEN DNeasy Blood & Tissue Kit according to the manufacturer's protocol. The purified DNA was quantified using a NanoDrop® 2000. The purity of the DNA was verified by the A260/A280 ratio, and all samples were ~1.8.

3.17.2 DNA hydroxymethylation by dot blotting

DNA samples were prepared by diluting total DNA to final concentrations of 2 µg, 1 µg, 0.5 µg, and 0.25 µg with 0.1M NaOH. The samples were denatured at 95°C for 10 min and cooled quickly on an ice bath followed by neutralization with ammonium acetate. Loading sample volumes of 400 µl were prepared by adding equal volumes of 0.1 M NaOH and 2M ammonium acetate to the denatured DNA. Nitrocellulose membranes were pre-wet in distilled water and placed on a Bio-Dot® Microfiltration Apparatus and assembled as per the manufacturer's recommendations. Vacuum was applied and the screws re-tightened to hold the apparatus together. The membrane was rehydrated with 0.1 M NaOH and prepared for sample application. With the vacuum off, 400 µl of denatured DNA was added for each sample. All other wells were filled with the same volume of distilled water to obtain homogenous filtration. Gentle vacuum was applied to pull samples through the filter, followed by the addition of 400 µl of 0.1M NaOH to all

wells. The vacuum was applied again until all wells were empty. The apparatus was disassembled followed by membrane rinsing with 2x Saline Sodium Citrate (SSC) buffer. After air-drying, the membrane was blocked with 5% skimmed milk in PBS for 1 hour. The membranes were washed three times with PBS and incubated with anti-5hmC overnight. The next day, the membrane was washed three times with PBS and incubated with anti-rabbit secondary antibody. The blots were washed and developed using the SuperSignal West Femto Maximum Sensitivity Substrate kit by auto-exposure settings on the ChemiDoc™ Touch Imaging System. Data were quantified by densitometry and analyzed using Image Lab software by applying background subtraction and approximation for linearity across the multiple dilutions of DNA seeded.

3.18: Gene expression analysis by real time quantitative PCR

Pellets of thawed samples described above were re-suspended in Qiazol and transferred to -80C (dry ice transport) for further RNA isolation and processing. RNA was isolated using the miRNeasy Mini Kit as per the manufacturer's protocol for cultured cells and cell pellets. The purified RNA was quantified using NanoDrop® 2000 to determine concentration, and 800ng of RNA was used for reverse transcription to make cDNA using SuperScript III First-Strand Synthesis System. The cDNA was diluted to a concentration of 4 ng/µl and real-time qPCR was performed with 10 ng cDNA per 10 µl reaction with QuantiTect SYBR Green PCR Kit on a CFX384 Real-Time PCR detection system. The list of genes tested and their primer sequences are provided in Table 5 Melt

curves were analyzed using the comparative CT method[116] with GAPDH as an internal control gene.

Table 5: PCR primers.

Gene	Name	Function	Primer	Sequence (5'->3')	NM reference ID
HGF	Hepatocyte growth factor	immunomodulation, antiapoptosis	Forward	CACGAACACAGCTTTTTGCC	NM_001010934
			Reverse	GGGGGAATAGAATGGCCCAC	
VEGF	Vascular endothelial growth factor	angiogenesis, antiapoptosis	Forward	ACTCGCGTTGCAAGATGTG	NM_001025369.2
			Reverse	GGACTGTTCTGTCGATGGTGA	
FGF2	Fibroblast growth factor	support of progenitor cells, angiogenesis, antiapoptosis	Forward	GCTGTACTGCAAAAACGGGG	NM_002006.4
			Reverse	CCGTAACACATTTAGAAGCCAGT	
TWIST1	twist-basic helix-loop-helix transcription factor 1	mesoderm related marker	Forward	GCCGGAGACCTAGATGTCATT	NM_000474.3
			Reverse	CCCACGCCCTGTTTCTTTGA	
TWIST2	twist-basic helix-loop-helix transcription factor 2	mesoderm related marker	Forward	CAGAGCGACGAGATGGACAA	NM_057179.2
			Reverse	ATTCAGAATCTCCTCCTGGCG	
MSX2	MSH homeobox 2	osteogenic regulator	Forward	CCGCCAAGACATATGAGCCC	NM_002449.4
			Reverse	GTTCTGCCTCCTGCAGTCTT	
CXCL12	CXC motif chemokine ligand 12	chemoattraction	Forward	AGATTGTAGCCCGGCTGAAG	NM_000609.6
			Reverse	CAGGCCCTTCCCTAACACTG	
GAL	Galanin and GMAP protopeptide	osmotic regulation and water balance	Forward	CCTGACGCTAAGAGCTTCGT	NM_002305
			Reverse	GGAAGGGAAAGACAGCCTCC	
BCL2	b-cell cll/lymphoma 2	anti-apoptotic	Forward	GGAGGCTGGGATGCCTTTGT	NM_000633.2
			Reverse	CAGCCTGCAGCTTTGTTTCAT	
EGR1	early growth response 1	differentiation, mitogenesis, stress	Forward	ACCCCTCTGTCTACTATTAAGGC	NM_001964
			Reverse	TGGGACTGGTAGCTGGTATTG	
NFE2L2	erythroid like nuclear factor	antioxidant transcription regulator	Forward	TCAGCGACGGAAAGAGTATGA	NM_001145412.3
			Reverse	CCACTGGTTTCTGACTGGATGT	
AKT1	AKT serine threonine kinase	survival	Forward	ATGGCGCTGAGATTGTGTCA	NM_005163
			Reverse	CCCGGTACACCACGTTCTTC	
CD106 (VCAM1)	Vascular cell adhesion molecule 1	cell adhesion/signal transduction	Forward	TGTTTGCAGCTTCTCAAGCTTTT	NM_001078.3
			Reverse	GATGTGGTCCCCTCATTCGT	
CD54 (ICAM1)	Intracellular adhesion molecule 1	cell adhesion	Forward	AGCCCAAGTTGTTGGGCATA	NM_000201
			Reverse	GGAGTCCAGTACACGGTGAG	

3.19: Statistical Analysis

At a minimum, technical triplicates of all experimental samples were performed. Where noted, technical triplicates of biological replicates were performed. Samples were compared using a students paired t-test with a 95% confidence interval. Significance markers indicate $p < 0.05$. Error bars are specified in each figure as standard deviation or standard error of the mean. Ralph Moller-Trane performed the more complex linear mixed effects statistical analysis presented in Chapter 5.

Chapter 4

Clinical Mesenchymal Stem Cell Products Experience Functional Changes in Response to Freezing in DMSO

Much of the text and figures in this chapter have previously appeared in the publication below, included here with copyright permission from Elsevier.

Pollock K, Sumstad D, Kadidlo D, McKenna DH, Hubel A. Clinical mesenchymal stem cell products experience functional changes in response to freezing. *Cytotherapy* **2015**; 17(1): 38-45

4.1 Introduction

Development of MSC- based therapies requires standardization of methods of culture and cryopreservation. MSCs are typically cultured *ex vivo* and expanded to a sufficient cell number before patient administration. Uniform, optimized methods of cell expansion have not been developed, and media composition (basal media, serum and additional supplements), seeding density, expansion vessel and *in vitro* population doublings can vary considerably among investigators.

Ex vivo culture of cells has been associated with changes in cell phenotype [117, 118] One such change observed in MSCs is the development of a senescent phenotype [119]. Senescent cells exhibit an inflammatory secretome [120], and, as such, may cause undesirable results in immunomodulatory therapies. *Ex vivo* culture of cells can also influence freezing response. Both hematopoietic progenitors and lymphocytes exhibited changes in subzero water transport and intracellular ice formation tendencies after *ex-vivo* culture [121, 122], which in turn can influence freezing response. Francois et al. [10]

quantified diminished response for indoleamine 2,3-dioxygenase (critical to immunomodulatory cell function) for frozen and thawed MSCs when compared with fresh non-frozen cells. A recent study by Moll et al. [123] also showed that cryopreserved MSCs had reduced immunomodulatory and blood regulatory properties immediately after thaw.

These temporal and freezing-induced changes in cell behavior can lead to confounding outcomes for clinical studies with the use of cryopreserved MSCs. One investigator hypothesized that poor post-thaw MSC function may have been responsible for the failure of a recent clinical trial [73]. The objective of this chapter was to determine the influence of *ex vivo* cell expansion on phenotype of MSCs at harvest and the response of resulting phenotypes to freezing and thawing. This information will help to clarify the influence of culture conditions on the biological characteristics of MSC products and identify potential shifts in composition or behavior resulting from the freezing process.

4.2 Methods

The MSCs used in this chapter were isolated from bone marrow (obtained from Lonza) using ficoll gradient separation and seeded in tissue culture flasks according to the methods described in section 3.2.1. Volume, cell count and viability of samples were recorded immediately upon arrival, and again after MNC isolation along with flow cytometry testing for the negative marker CD45 and positive marker CD90.

At 24 hr and 48 hr after seeding, non-adherent cells were removed by media change. In these culture conditions, only MSCs from the mononuclear cell population were surface adherent. Cell enumeration and characteristics (doubling time, viability, senescence and apoptosis) taken on and after the first harvest reflect only MSC characteristics. At 70-80% desired confluence, cells were harvested, re-suspended in MSC CCM and analyzed for viability, senescence and apoptosis. Half of the remaining cells not used for assays were seeded in new flasks at densities of 40-50 cells/cm^2, and the rest were frozen down at each passage according to the procedure outlined in section 3.3.1. A total of 6 passages were performed, which corresponds to approximately 35-40 population doublings in healthy cells.

Frozen vials were thawed according to the procedure outlined in section 3.4.1. A portion of these cells was analyzed immediately for viability and senescence. Remaining cells were plated and analyzed for viability and senescence after 48 h.

Cells were measured for viability using AO/PI according to the procedure outlined in section 3.5.1. Cells were tested for senescence using the beta-glo assay from Promega according to the procedure outlined in section 3.6. Flow cytometry was performed to assess viability, cell surface phenotype and apoptosis of MSC samples according to the procedures outlined in section 3.7.

In this chapter, error bars represent standard deviations of triplicate measurements. A Student's t-test was used to compare populations, and P values reported are considered significant at $P < 0.05$. Triplicate β-galactosidase measurements for senescence were

compared between individual passages, whereas individual data points for passage viability, recovery and apoptosis were pooled for all passages and compared between samples.

4.3 Results

4.3.1 Characterization pre-culture

Each initial marrow sample from Lonza had high viability (98% ± 2%). However, samples varied widely in initial concentration and total cell number. Initial samples had average concentrations of $2.40x10^7 \pm 1.28x10^7$ cells/mL with total cell counts of $3.27x10^8 \pm 1.85x10^8$.

Initial samples underwent density gradient centrifugation to isolate MNCs. Total MNC counts averaged $1.24x10^8 \pm 7.24x10^7$ total cells. The MNC populations (Table 6) constituted similar proportions of their respective initial bone marrow population (38% ± 4%), and had similar viability (98% ± 1%). Senescence was low in the MNC population of all samples, with an average of 0.62% ± 0.63%. It is interesting to note that sample 2 had the lowest viability and total cell count before and after centrifugation and exhibited the highest senescence percentage.

Table 6: Patient data and initial mononuclear cell characterization.

Sample	Patient age, years	Patient sex	Total isolated MNCs	Fraction of initial population	MNC viability (AO/PI)	MNC β-galactosidase (senescence)
1	36	M	9.55×10^7	34%	99%	0.00%
2	41	F	6.98×10^7	41%	97%	1.27%
3	29	F	2.06×10^8	39%	99%	0.60%
Average			1.24×10^8	38%	98%	0.62%
Standard deviation			7.24×10^7	4%	1%	0.63%

4.3.2 Characterization of in vitro expansion cultures

MSCs were isolated from the MNC population obtained after density gradient isolation through attachment to the culture surface. Flow cytometry performed on MSC populations confirmed appropriate expression for all markers in all samples at each passage (Table 7). Population doublings were set to zero for passage 1.

Table 7: Pre-freeze MSC characterization at each passage.

		Surface marker characterization, %		Viability, %		Apoptosis, %	
Sample	Passage	CD45	CD90	AO/PI	7-AAD	AnnexinV+/PI−	Karyotype results
1	P1	1.80	99.55	99	93	9.54	Normal
	P2	0.33	99.76	99	90	3.73	Normal
	P3	0.12	99.85	99	83	2.00	Normal
	P4	0.21	99.41	98	77	6.54	Normal
	P5	0.55	99.14	97	80	5.03	Duplication of chromosome 17 in 6%
	P6	0.24	98.67	93	77	3.94	Duplication of chromosome 17 in 6%
2	P1	2.09	98.92	94	90	2.74	Normal
	P2	0.42	99.84	99	81	1.41	Normal
	P3	0.47	99.47	92	83	2.31	Normal
	P4	0.74	99.58	95	80	3.68	Normal
	P5	0.52	90.16	88	34	21.61	–
3	P1	9.72	92.63	94	92	0.89	Normal
	P2	0.19	99.88	98	86	2.71	Normal
	P3	0.22	99.81	97	91	1.61	Normal
	P4	1.31	99.95	96	91	1.55	Normal
	P5	0.22	99.67	96	85	5.67	Normal
	P6	0.24	97.35	93	93	2.83	Normal

Further population doublings were calculated on the basis of cells seeded and harvested on each subsequent passage. Population doublings were consistent over time (as shown by a constant slope in Figure 7A) for samples 1 and 3. Both had relatively constant rates of doubling, undergoing approximately 0.7 population doublings per day for the duration of their culture through passage 6. Sample 2 exhibited slowing growth at passage 3, and population doublings plateaued in passages 4 and 5 at around 19.5, just over half of the total doublings in samples 1 and 3. Passage 6 of sample 2 could not be performed because of sample growth arrest.

Viability for each sample remained high as culture time and population doublings increased when measured by both AO/PI and 7AAD (Table 7). Samples 1 and 3 showed viabilities of >70% through 35+ population doublings, with a consistent gradual decrease in viability over time. Sample 2 exhibited a more rapid drop in viability as population doublings increased, with a final viability in passage 5 below threshold viability criteria for lot release when measured with the 7-AAD assay.

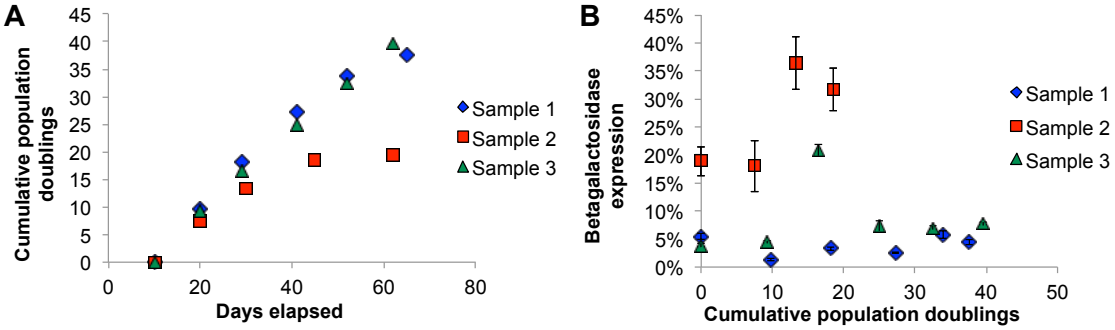

Figure 7: Pre-freeze MSC population doublings and β-galactosidase percentage. (A) Population doublings over time. Samples 1 and 3 show robust growth; sample 2 exhibits growth arrest beginning in passage 3. (B) β-Galactosidase expression percentage indicative of senescence in population for MSCs in ex vivo culture. β-Galactosidase expression tended to increase over time in all samples. Sample 2 had significantly higher values ($P < 0.05$) at each passage than did samples 1 and 3. Error bars represent standard deviations of triplicate β-galactosidase measurements.

The β -galactosidase percentage (used as a measure of total population senescence) tended to increase over time (Figure 7B). Other than the reading for sample 3 in P3 (20.8%), the β -galactosidase percentages for samples 1 and 3 remained low (below 10%) and slowly increased over time after the first passage. Sample 2 displayed a trending increase in β -galactosidase over time with final values in P4 of >30%. Sample 2 values were also significantly higher ($P < 0.05$) than either of the other samples. Samples 1 and

3 did not have significantly different values ($P > 0.05$). β -Galactosidase testing could not be performed on P5 of sample 2 because of low cell recovery at harvest.

Karyotyping performed on these initial samples showed no mutations in any passage of samples 2 and 3. Sample 1 presented with duplication on the long arm of chromosome 17 in 6% of cells in P5 and P6. Karyotyping could not be performed on P5 of sample 2 because of low cell recovery at harvest.

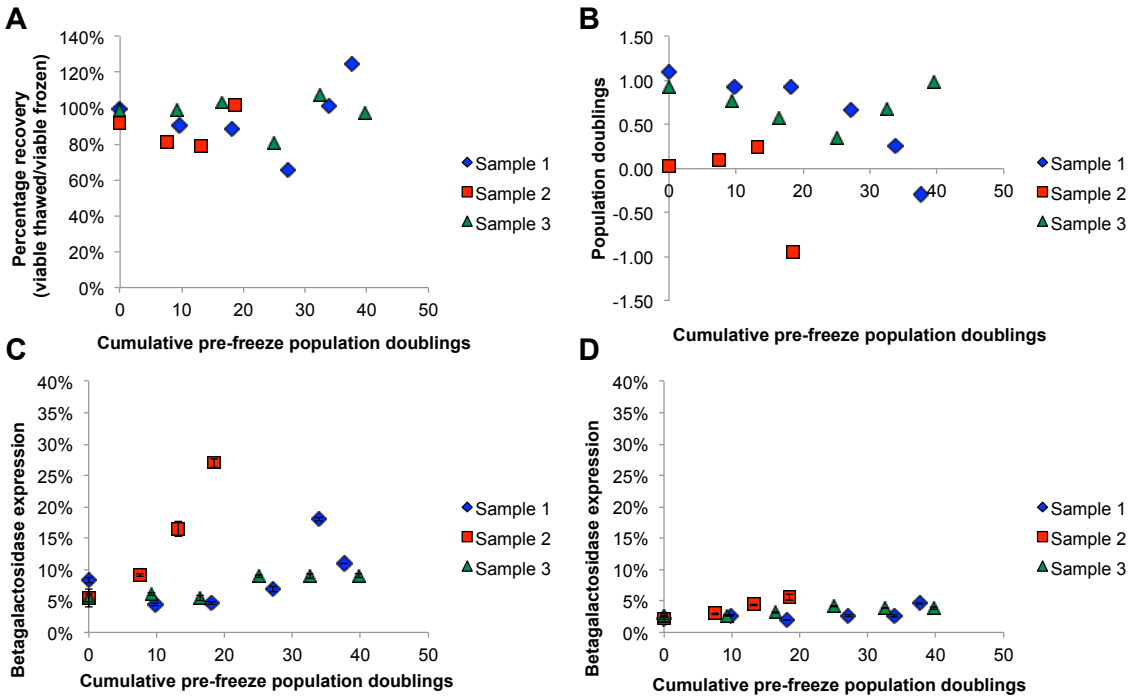

Figure 8: Post-thaw MSC recovery and β-galactosidase characterization. (A) Recovery of MSCs post-thaw. Recovery = (viable cells pre freeze)/(viable cells post-thaw) * 100 and is used to account for cellular losses during freezing. Recovery does not vary significantly between samples and was consistently high (>80% for almost all samples). (B) Population doublings in thawed cells after 48 h in culture. Sample 2 had low to no population doublings in every passage, with P4 showing cellular losses (negative doublings). Growth in samples 1 and 3 was higher in early-passage samples and declined with increasing passage number. (C) Immediate pre-freeze β-galactosidase expression. Sample 2 had significantly higher initial post-thaw expression than did samples 1 and 3. Trends observed in post-thaw samples matched those seen in pre-freeze data and were significantly higher in samples 1 and 3 ($P < 0.05$) when compared with pre-freeze values. (D) 48 hour post-thaw β-galactosidase expression. Expression values dropped significantly ($P < 0.05$) after 48 h in culture for all samples when compared with immediate post-thaw values.

Apoptosis results for pre-freeze cells were low, with <10% of cells testing positive for apoptosis in all passages of all samples except for P5 of sample 2 (Table 7). There was not compelling evidence of an increase in apoptotic percentage over time in culture for the number of samples tested.

4.3.3 Post-thaw characterization

Total cell counts as well as viability, senescence and apoptosis measurements were taken immediately on thawing and after 48 h in culture after thaw. Immediate post-thaw recovery was calculated by dividing the total number of viable cells post-thaw by the total number of viable cells pre-freeze in each frozen passage. Recovery was similar for all samples and passages (**Figure 8**A), with no obvious trending as a function of pre-freeze population doublings. The majority of the data points fell between 80-100% recovery.

Although there was no visible trending in the initial recovery of cells post-thaw, after 48 hr of culture the population doublings tended to decrease with increasing pre-freeze passage number in all 3 samples (**Figure 8**B). Samples 1 and 3 had greater population doubling than sample 2, with a significant difference between samples 2 and 3 ($P < 0.05$). Sample 2 had very little growth in its first 3 passages post-thaw in addition to a decrease in cell number in P4 (as evidenced by the negative population doubling). In contrast, samples 1 and 3 showed almost a full population doubling in thawed samples from P1, which decreased as passage number increased. Sample 3 exhibited an increase in population doublings in P5 and P6.

Every passage of samples 1 and 3 (except sample 3 P3) had a significant ($P < 0.05$)

senescent enrichment after thaw when individual passages were compared before freeze and after thaw (**Figure 8**C). Sample 2 had a significant decrease in its senescent fraction of cells in P1 and P3 but showed the same trends as pre-freeze populations of increasing senescence with increasing population doublings. These senescent percentages dropped significantly ($P < 0.05$) for each sample and passage at 48 h after thaw compared with immediate post-thaw percentages (**Figure 8**D).

4.4 Discussion

The wide variation in cell behavior observed among the 3 separate samples characterized in this study is likely a result of sample quality differences and donor-to-donor variability [124, 125]. Variability on initial receipt could result from differences in donor age, hemodilution of the sample or variability in shipping time or temperature. The older age of the donor of sample 2 (41 years old) could explain the initial lower cell counts and expression of higher levels of senescence in culture. In the future, quality control metrics such as total cell count, viability and senescence measured on whole marrow could be used to screen samples on initial receipt.

Flow cytometry performed on the MSCs confirmed that the cells used in the study expressed the cell surface phenotype consistent with MSCs (CD45 [<15%] and CD90 [>85%]) in all passages of each sample. This appropriate expression indicates that MSCs were successfully isolated in this study, and the results presented are representative of MSC freezing behavior. Karyotyping abnormalities were low, with only 6% of cells in

sample 1 showing duplication in the long arm of chromosome 17 in passages 5 and 6. The limited chromosomal abnormality observed is consistent with the literature [126]. Because of the similar post-thaw behavior observed in samples 1 and 3, the chromosomal abnormalities present do not appear to affect proliferative post-thaw sample behavior.

Population doublings are a metric for assessing cellular health. Previous research by Bertolo et al. [127] has proposed the use of *in vitro* expansion scores for grading cells intended for transfusion. Cellular age has also been proposed as a metric for grading MSCs [128]. Growth kinetics for sample 2 were relatively normal initially (i.e., rates were the same as other samples for the first 2 passages), but even these early passages had growth arrest post-thaw. Samples that have this type of growth arrest should not be used as transfusion products but can go undetected with current selection criteria. This latent growth behavior may explain the poor performance of some cellular transfusion products *in vivo*. It is important to develop screening criteria to identify sub-standard products such as sample 2 before transfusion, as growth arrest may not be observed or predicted before administration with current techniques.

Pre-freeze viability remained high among all samples at all passages (well above the 70% viability selection criterion for infusion) and did not predict cellular vigor or proliferative potential. Pre-freeze apoptosis also did not appear to be correlated with post-thaw behavior. However, pre-freeze senescence increased over time in all samples, and senescence β-galactosidase values were significantly higher in sample 2 both pre-freeze and immediately post-thaw. Senescence may provide a valuable metric for sample screening in the future; even in early passages with normal population doublings and

viability, sample 2 (which had poor post-thaw cellular performance even at early passages) had significantly higher senescence than other populations. We suggest that future studies be performed to evaluate introducing pre-freeze senescence as additional lot selection criteria for BM-MSCs intended for clinical use. Additional studies with a larger sample size are necessary to determine whether pre-freeze senescence is statistically indicative of poor post-thaw function, and, if so, establish a maximum acceptable senescence threshold for pre-freeze populations.

Several groups have previously analyzed MSC response to cryopreservation. Bruder et al. [129] showed that cryopreserved MSC samples grown for extended passages in culture have growth kinetics and ATPase activity similar to that in unfrozen cells. Mamidi et al. [130] showed that multiple rounds of cryopreservation did not functionally alter MSCs when compared with MSCs that had undergone cryopreservation only once. Dariolli et al. [131] performed experiments to analyze porcine MSCs by measuring growth kinetics, senescence and ability to respond to chemical cues. This previously published work as a whole suggests that cryopreservation does not alter the growth or differential behavior of cells. However, freezing can induce changes in MSC phenotype and proliferation, which has also been shown by Francois et al. [10] and Moll et al. [123].

In post-thaw populations, recovery was high for all cellular products, with most showing 80-100% recoveries independent of sample or passage number. However, when cells were cultured for 48 hr post-thaw, differences in cellular population doublings became more apparent. If researchers or clinicians look solely at immediate post-thaw recovery and viability, this potential for growth arrest may not be observed.

Senescence immediately post-thaw was consistent with the trends seen in pre-freeze populations. There was a significant enrichment of senescent cells in the post-thaw populations of samples 1 and 3 and a significant decrease in several passages of sample 2.

4.5 Conclusion

The studies in this chapter show that high pre-freeze MSC senescence appears to correlate with poor post-thaw performance. To maximize the future success of clinical trials involving frozen MSC samples, future studies with larger sample size should be performed to statistically evaluate the effects of freezing and storage on the regenerative and immunomodulatory properties of MSCs. A better understanding of cell behavior in response to freezing may improve lot selection criteria and enhance the effectiveness of transfused MSCs.

However, the differences in these samples indicate that donor variability may play a large role in sample behavior, and make it difficult to draw conclusions about cell freezing response without significantly higher sample sizes. Future studies described in subsequent chapters utilized culture cell lines to make batch-to-batch comparisons possible for large scale screening (Chapter 5) and iterative optimization experiments (Chapter 7, 8).

Chapter 5

Screening and Statistical Analysis of non-DMSO Cryopreservation Combinations

5.1 Introduction

We have identified potential groups of cryopreservatives (Sugars, Sugar Alcohols, Additives), which might together replicate the cryopreservative function of DMSO, but it is important to determine which combinations have the highest probability of high recovery before optimizing their concentrations in solution. In addition to solution composition, cooling rate also needs to be considered, as cooling rate may alter the effectiveness of different combinations.

5.2 Methods

A combination of 1-3 solution components in Table 8 below (no more than one from each column) and cells were combined using the Biomek liquid handler as described in section 3.9.3 above. These combinations were tested with H9 MSCs at 4 different cooling rates: 1, 3, 5, and 10°C/min.

Table 8: Components tested.

Sugar	Sugar Alcohol	Additive
Sucrose	Arabitol	Alanine
Trehalose	Erythritol	Creatine
	Glycerol	Ectoine
	Inositol	Isoleucine
	Mannitol	Proline
	Ribitol	Taurine
	Sorbitol	Valine
	Xylitol	

After this large dataset was collected, it was sent to Ralph Moller-Trane who performed linear mixed effects (LME) modeling to assess the importance of the four explanatory variables of interest (Sugar, Rate, Additive and Alcohol), without neglecting the variation between each batch and between each plate within the batches.

The LME model was defined as:

$$y_i = x_i\beta + z_i\gamma + \varepsilon_i$$

Where y_i is the i'th outcome of the response, X_i represents the corresponding values of the covariates, β is a vector for fixed effects, γ is a vector for random effects normally distributed with mean 0, Z_i is the design matrix for the random effects, and ε_i is the error term, normally distributed with mean 0.

Backward elimination based on the Bayesian Information Criterion (BIC) was performed to select the most fitting model. The initial model included all variables and second order interactions as well as two random variables to account for batch effect and effect of each plate within the batch:

$$y_i = x_{i,Sugar}\beta_{Sugar} + x_{i,Rate}\beta_{Rate} + x_{i,Alcohol}\beta_{Alcohol} + x_{i,Additive}\beta_{Additive} + x_{i,SugarXRate}\beta_{SugarXRate} + x_{i,SugarXAdditive}\beta_{SugarXAdditive} + x_{i,SugarXAlcohol}\beta_{SugarXAlcohol} + x_{i,RateXAdditive}\beta_{RateXAdditive} + x_{i,RateXAlcohol}\beta_{RateXAlcohol} + x_{i,AdditiveXAlcohol}\beta_{AdditiveXAlcohol} + z_{i,Batch}\gamma_{Batch} + z_{i,Plate}\gamma_{Plate} + \varepsilon_i$$

where x's are the covariates, β's are the corresponding fixed effects, z's are covariates for the random effects, $\gamma_{Batch} \sim N(0,\sigma_{Batch})$ is the random batch effect variable, $\gamma_{Plate} \sim N(0,\sigma_{Plate})$ is the random plate effect variable, and $\varepsilon_i \sim N(0,\sigma_{\varepsilon})$ is the error term.

The models were fitted using the lmer function from the R package lme4. Elimination of terms from the model was made using the step function from the lmerTest R. Table 9

Table 9: Anova table with results of step function application to the full model.

	Sum Sq	Mean Sq	NumDF	DenDF	F.value	elim.num	Pr(>F)
Rate:Alcohol	0.019	0.00077	24	28.5	1.3	1	2.8e-01
Sugar	0.786	0.39300	2	2160.0	639.0	kept	0.0e+00
Rate	0.014	0.00483	3	3.8	7.8	kept	4.2e-02
Alcohol	0.025	0.00315	8	53.9	5.1	kept	8.9e-05
Additive	0.164	0.02346	7	3091.2	38.1	kept	0.0e+00
Sugar:Rate	0.059	0.00989	6	2136.3	16.1	kept	0.0e+00
Sugar:Alcohol	0.058	0.00363	16	2117.5	5.9	kept	8.2e-13
Sugar:Additive	0.064	0.00456	14	3091.2	7.4	kept	1.8e-15
Rate:Additive	0.065	0.00311	21	3091.2	5.1	kept	4.3e-13
Alcohol:Additive	0.137	0.00244	56	3091.2	4.0	kept	0.0e+00

shows the resulting ANOVA table, and only the interaction between Rate and Alcohol was dropped.

Even after dropping the Rate:Alcohol term, the residuals of this model were still large and correlated strongly with the fitted values. To combat this phenomenon, the model was refit to the square root of the recovery values; square root transformation was chosen instead of a logarithmic transformation because the dataset included recovery rates of 0. Figure 9 shows that this transformation improved the model, giving smaller residuals and reduced correlation with fitted values, and tightening up the qq-plot which compares the probability distribution of the actual data residuals to the theoretical values predicted by the model.

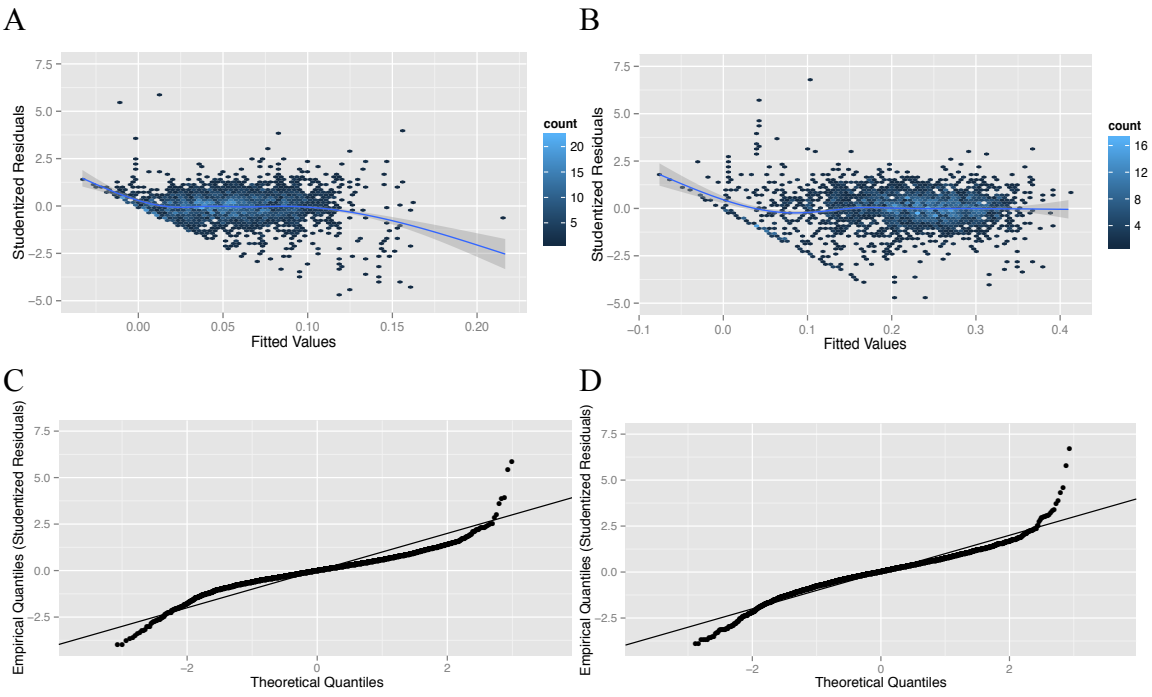

Figure 9: Studentized residuals plotted against fitted values. (A) Residuals vs. fitted values of original recovery values. (B) Residuals vs. fitted values of square root transformed recovery values. (C) QQ-plot of original recovery values vs. model. (D) QQ-plot of square root transformed recovery values vs. model.

5.3 Results

The model used bootstrapping to predict the value of the recovery for each combination of rate, sugar, alcohol, and additive. Figure 10 and Figure 11 show the models predictions and confidence intervals for each different combination.

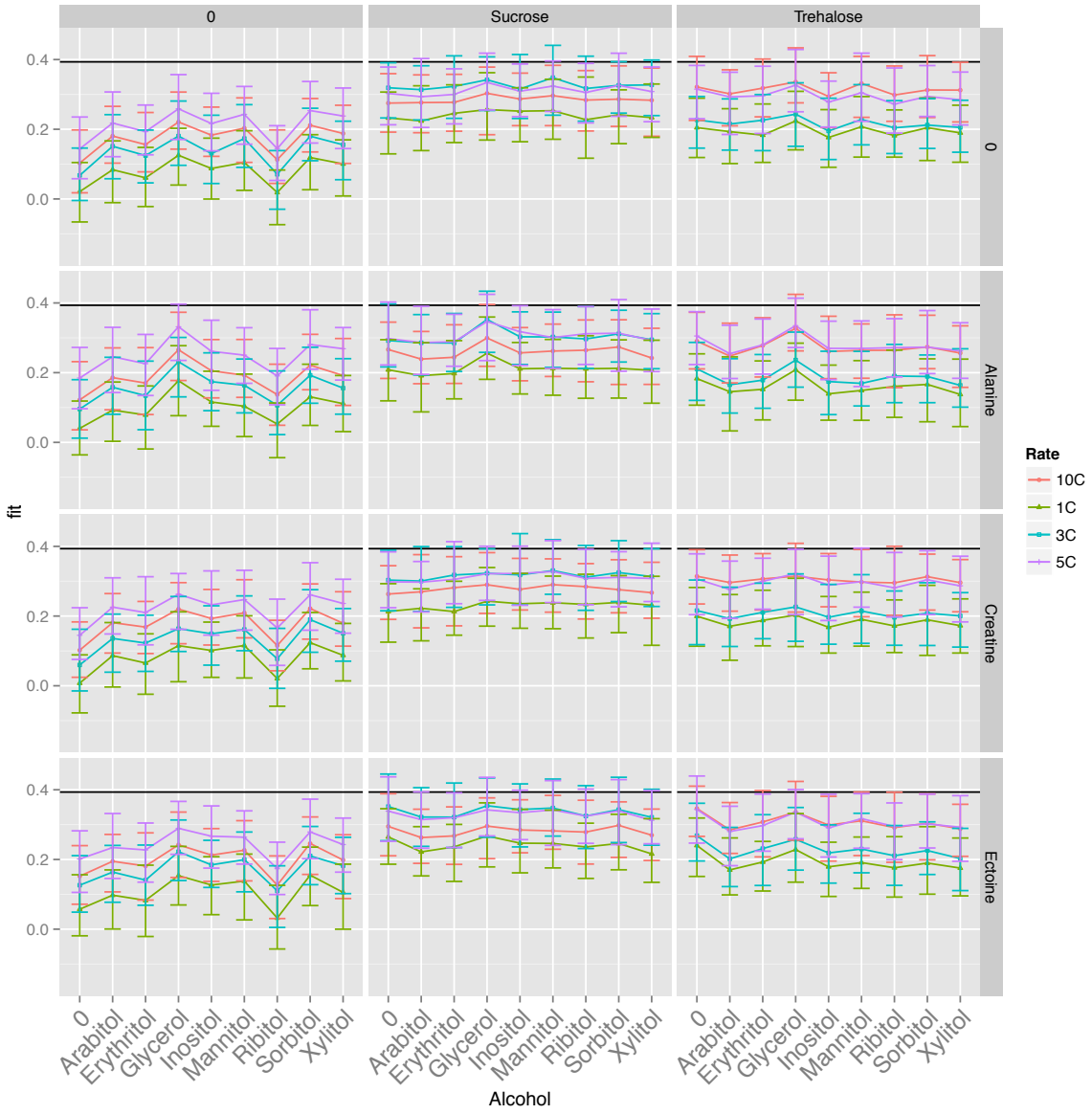

Figure 10: Predictions and confidence intervals for: 0, Alanine, Creatine, Ectoine.

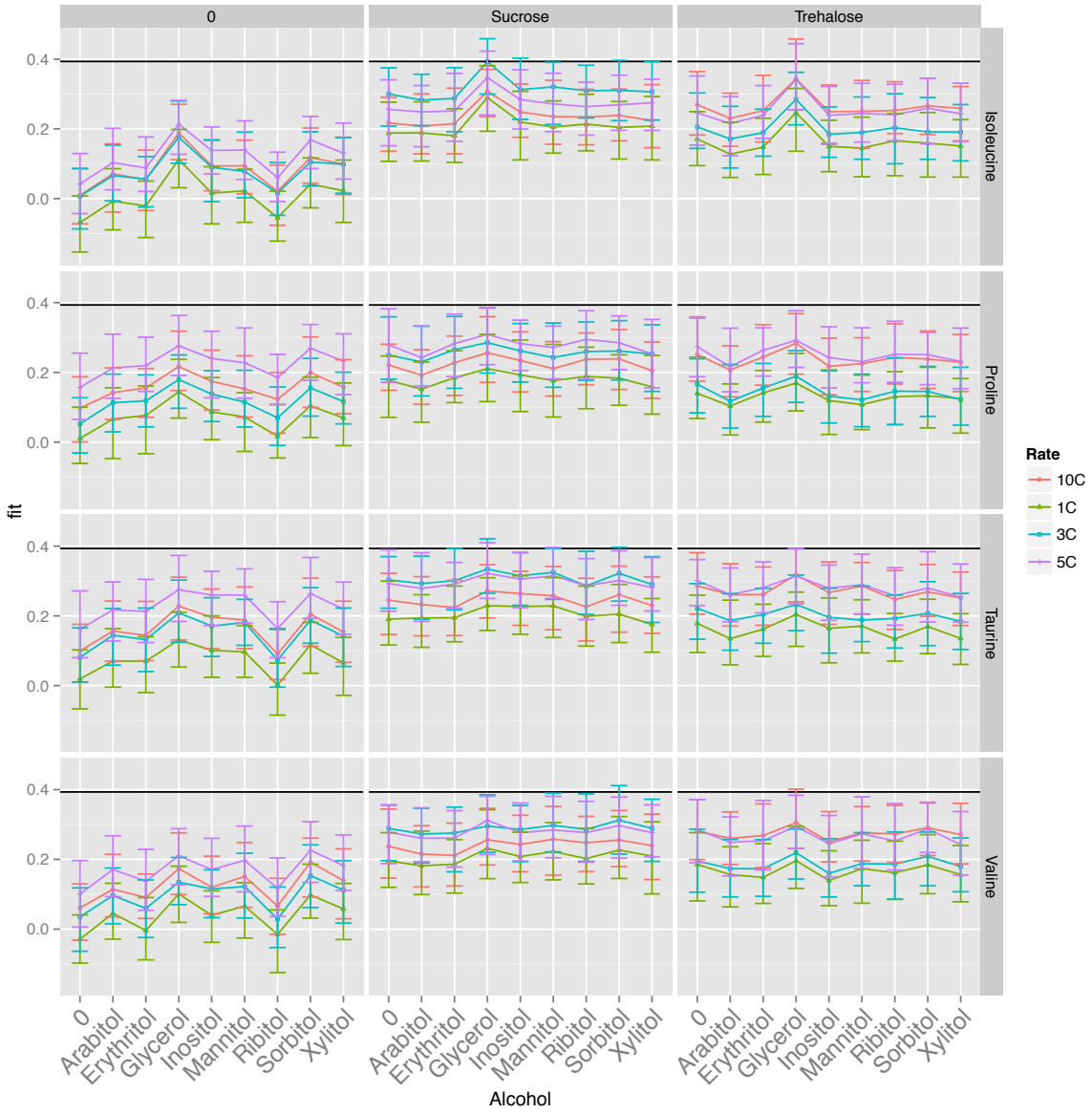

Figure 11: Predictions and confidence intervals for: Isoleucine, Proline, Taurine, and Valine.

There were 76 combinations for which the confidence interval contained the highest predicted recovery rate. A contingency table (Table 10) of rate vs. sugar shows that most of these 76 combinations contained sucrose and were frozen at 3°C or 5°C/min.

Table 10 Rate vs. Sugar contingency table

	0	Sucrose	Trehalose
10C	0	1	14
1C	0	0	0
3C	0	30	0
5C	1	23	7

Further evaluation of a contingency table of additives vs. alcohols within the 3°C/min sucrose dataset (Table 11) shows that some alcohols and additives occur more frequently in these high performing solutions than others.

Table 11: Additive vs. Alcohol contingency table for 3°C/min Sucrose.

	0	Arabitol	Erythritol	Glycerol	Inositol	Mannitol	Ribitol	Sorbitol	Xylitol	Sum
0	0	0	1	1	1	1	1	1	1	7
Alanine	1	0	0	1	0	0	0	0	0	2
Creatine	0	1	1	0	1	1	1	1	0	6
Ectoine	1	1	1	1	1	1	1	1	1	9
Isoleucine	0	0	0	1	1	0	0	1	0	3
Proline	0	0	0	0	0	0	0	0	0	0
Taurine	0	0	0	1	0	0	0	1	0	2
Valine	0	0	0	0	0	0	0	1	0	1
Sum	2	2	3	5	4	3	3	6	2	30

5.4 Discussion

The best selection of sugar, alcohol, and additive is still unclear as there is massive overlap in recovery performance of the different combinations. However, this analysis makes it easier to rule out low performing solution components that negatively impact recovery, and rationally select high performing combinations for further study.

It is clear from both the predictions and contingency tables above that inclusion of sucrose and trehalose improves recovery vs. no-sugar solutions. Combinations including sucrose accounted for 53 of the 76 top performing combinations, and all of these

occurred at cooling rates of 3°C/min and 5°C/min. This unbalanced distribution of optimums suggests that the selection of sugar and cooling rate has a high impact on the recovery of a given solution.

The contingency comparison of sugars and sugar alcohols within the sucrose 3°C/min group (Table 11) shows a more even distribution of optimum solutions among the different components than the sugar/cooling rate contingency table. This suggests that selection of alcohol and additive make less of a difference if a high performing sugar and cooling rate have already been selected.

Observing the last row and last column of Table 11, we see the total number of times each alcohol and additive is present. The additives proline and valine are present 0 and 1 times, respectively, while the additives ectoine, creatine, and isoleucine are present 9, 6, and 3 times, respectively. Based on this information, using proline or valine as the additive seems to decrease the expected recovery rate while using ectoine, creatine, or isoleucine as the additive seems to increase recovery. The alcohols sorbitol, glycerol, and mannitol are present 6, 5, and 3 times respectively, while the alcohols ribitol and xylitol are present 2 times each. This suggests that using sorbitol, glycerol, or mannitol is expected to increase the recovery, while using ribitol or xylitol may decrease recovery.

5.5 Conclusion

The screening and analysis in this chapter showed that selection of cooling rate and sugar in solution appears to predict solution recovery more strongly than either alcohol or

additive. Additionally, multicomponent solutions exhibited higher recovery than single component solutions. Due to the high performance of sucrose at 3°C/min, this cooling rate was selected for future use in Chapters 6 and 8. Based on the selection of 3°C/min as the only cooling rate, the favorable multicomponent combinations of Sucrose/Glycerol/Creatine (SGC), Sucrose/Mannitol/Creatine (SMC), and Sucrose/Glycerol/Isoleucine (SGI) were selected for future analysis and concentration optimization.

Chapter 6

Combinatorial Effects of Incubation, Osmolarity, and Solution Composition on Mesenchymal Stem Cell Survival During Freezing

Much of the text and figures in this chapter will appear in a future publication:

Pollock K*, Yu G*, Moller-Trane R, Koran M, Dosa PI, McKenna DH, Hubel A. Combinations of osmolytes acting in concert to improve post-thaw viability of mesenchymal stem cells. **2016**. *In Review*.

*These authors contributed equally. Yu G performed all Raman experiments.

6.1 Introduction

There is demand for non-DMSO cryoprotective agents that maintain cell viability without causing systemic toxicity or poor post-thaw function. Single molecule replacement of DMSO has been explored, but results have been sub-optimal. Multi-component solutions have also been explored, and work in the previous chapter as well as factorial experiments by other groups to identify favorable combinations and freezing protocols have shown increased success [99, 100]

The focus of this chapter involves expanding our understanding of multicomponent osmolyte solutions and their ability to preserve cell viability during freezing. The study characterizes interactions between solutes using surface plots to describe how concentrations of multiple components contribute to recovery. Differences in single cell

response to freezing using different experimental parameters (incubation time, composition) were captured using low temperature Raman spectroscopy. These studies help expand our understanding of these solutions and the manner by which they enhance post-thaw recovery.

6.2 Methods

H9-MSCs were cultured according to the methods described in section 3.2.3. Freezing and thawing of samples were carried out according to sections 3.3.3 and 3.4 respectively, followed by viability and recovery analysis according to sections 3.5.1. Physical testing of solutions at their final freezing concentration was performed using a differential scanning calorimeter according to section 3.11 and an osmometer according to section 3.12. Confocal Raman spectroscopy was performed on samples according to section 3.10. Statistical analysis represents technical triplicates of biological replicates, with error bars representing standard error of the mean. Two-tailed t-tests were considered significant with $p<0.05$.

6.3 Results

6.3.1 Permeation/partitioning of solute

Several of the osmolytes studied here are large (> ~300 Da) and, as a result, may take longer to enter the cell than smaller solutes traditionally used like DMSO (78 Da). Other large molecules including trehalose are known to have very limited penetration[132]. In order to determine the proper incubation time for the cells in the multicomponent

osmolyte solutions, solutions of SMC (sucrose = 150mM, mannitol = 125mM, creatine = 12.5mM) and SGC (sucrose = 150mM, glycerol = 2.5%, creatine = 12.5mM) were incubated with cells at room temperature in Normasol ® for 0 min, 30 min, 1 hour, 2 hours, or 4 hours before undergoing freezing at 3°C/min (**Figure 12**A). Live cell recovery increased and experienced a maximum at 1 hour for SGC samples, and 2 hours for SMC samples. Longer incubation times (4h) decreased the viability. As expected, incubation times of more than 30 minutes resulted in a decrease in viability for cells in DMSO.

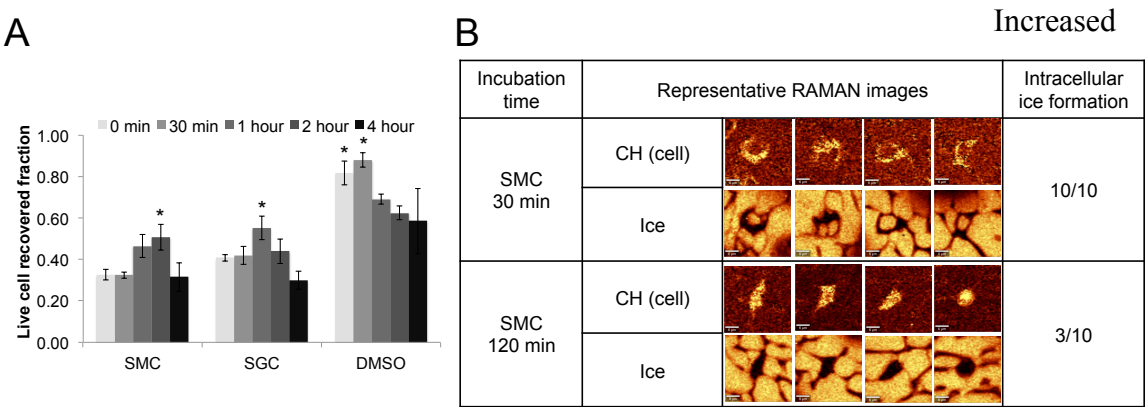

Figure 12: Recovery reaches a maximum with appropriate incubation time for slow penetrating components (A) Fraction of live cells recovered for DMSO-free solutions SMC and SGC and DMSO solutions as a function of incubation time prior to freezing at 3°C/min; (B) Raman images obtained of MSCs frozen at 3°C/min in SMC solution after 30 and 120 minutes of incubation prior to freezing. Raman images are rendered for both –CH and ice.

incubation times have a profound influence on cell response to freezing as imaged using Raman spectroscopy (**Figure 12**B). MSCs were incubated for 30 and 120 minutes in the same SMC composition described above, frozen to -50°C and imaged using low temperature Raman spectroscopy. Cells incubated for 30 minutes exhibited large internal ice crystals for 10/10 of the cells imaged. In contrast, cells incubated for 120 minutes exhibited ice in only 3/10 cells imaged. The formation of ice inside the cell is considered

to be a damaging event, and the ice formation observed here is consistent with the poorer post-thaw viability observed in **Figure 12**A for cells incubated only 30 mins.

Influence of osmolarity and composition

The range of solution compositions studied is important. It is common for cryopreservation solutions to contain high concentrations of cryoprotective agents and therefore exhibit high solution osmolarity. For example, a 10% DMSO solution has an osmolarity of ~1400 mOsm. MSCs suspended in different combinations of sucrose, mannitol and creatine (SMC), and sucrose, glycerol and creatine (SGC) were frozen at 3^{o}C/min, thawed and post-thaw recovery measured. The post-thaw recovery of SGC and SMC were plotted as a function of total osmolarity for a range of different tested compositions (Figure 13). For SMC solutions, the range of solution osmolarities is low (< 500 mOsm) and there is a weak negative correlation between osmolarity and post-

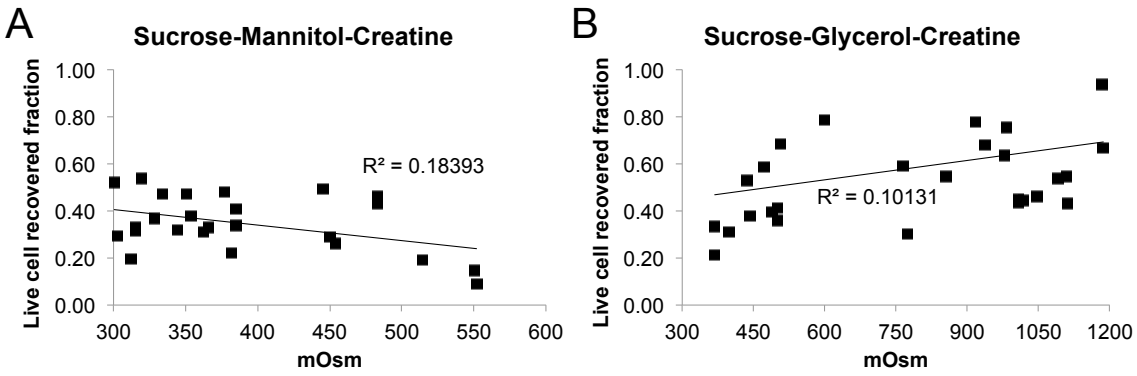

Figure 13: Post thaw recovery of MSCs cryopreserved in SGC and SMC as a function of total solution osmolarity. Linear best fit is given with correlation coefficient. (A) Recovery of cells has slight negative correlation for different osmolarity sucrose-mannitol-creatine solutions. (B) Recovery of cells has slight positive correlation for different osmolarity sucrose-glycerol-creatine solutions.

thaw recovery of MSCs (Figure 13A). In contrast, SGC solutions were evaluated over a higher range of osmolarities (< 1200 mOsm) and exhibited a weak positive correlation

with the compositions tested (Figure 13B). These weak correlations suggest that higher solution concentration does not necessarily correlate to higher levels of post-thaw recovery.

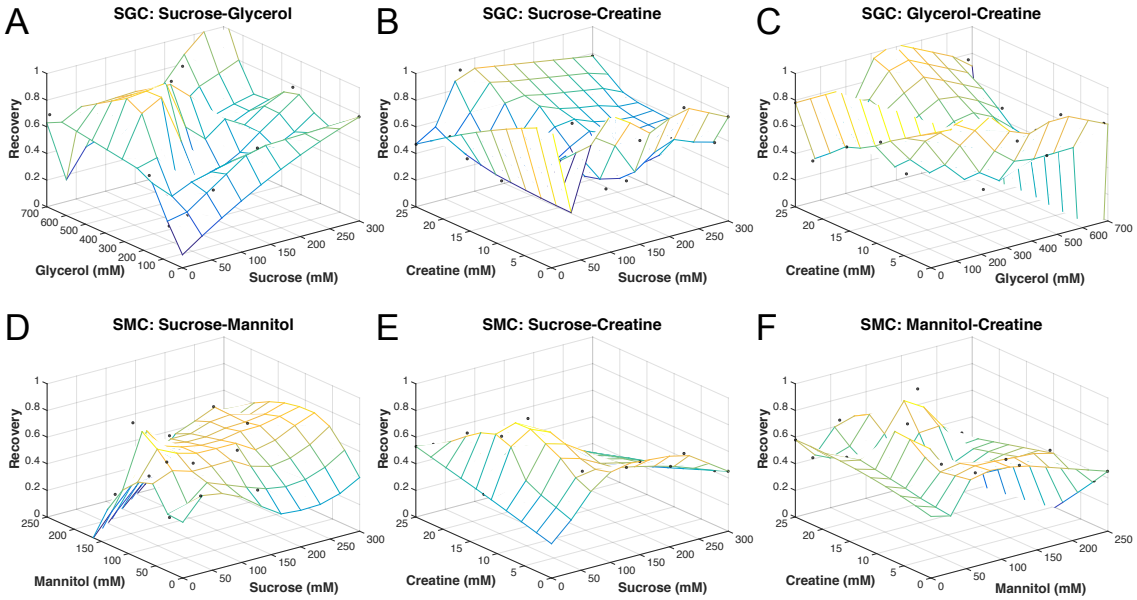

Figure 14: Scattered interpolant meshgrid plots. Plots show recovery vs. two of three components for SGC (A,B,C) and SMC (D,E,F) solutions.

For the same 3-component solution compositions used in Figure 13, MATLAB was used to generate scattered interpolant plots that mapped the post-thaw recovery measured as a function of solution composition for two of the three components present in solution using 20-25 experimental points (recovery was averaged for vectors with same values for the 2 components being plotted). As described previously, the post-thaw recovery varied significantly with composition for solutions containing the same three components (Figure 14). It is noteworthy that the variation in the fraction of recovered cells post-thaw exhibited an inverted "U" shaped behavior. For example, the relationship between sucrose and creatine exhibits a maximum cell recovery for concentrations ~150 mOsm of

sucrose (Figure 14B,E). The fraction of recovered cells diminishes for concentrations above and below that optimum. Similar behavior is observed in Figure 14D where the optimum concentration of mannitol ~150 mOsm and the fraction of recovered cells increases with increasing sucrose concentration to the highest concentration tested (300 mOsm).

In order to understand differences in freezing response for different combinations of the same three osmolytes, freezing studies using two different compositions of SGC (SGC-A and SGC-B) were repeated (**Figure 15**). MSCs were frozen under the same conditions (total osmolarity and 3°C/min cooling rate) and imaged using low temperature Raman confocal microscopy. Cells frozen in SGC-B exhibited ice inside the cells for 10/10 cells

Solution	Composition	Ice	Osmolytes 780-920cm^{-1}	CH(cell)	Intracellular ice formation
SGC-A	150mM Sucrose 684mM Glycerol 25mM Creatine	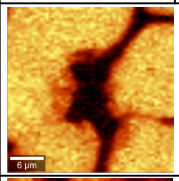	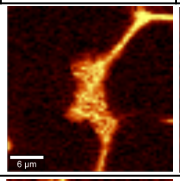	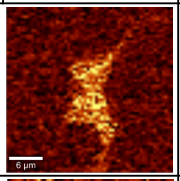	3/10
SGC-B	300mM Sucrose 684mM Glycerol 12.5mM Creatine	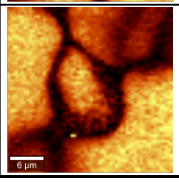	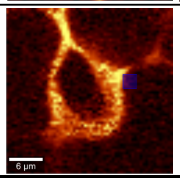	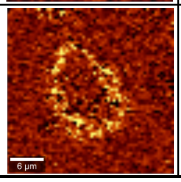	10/10

Figure 15: Low temperature Raman microscopy of MSCs cryopreserved at 3°C/min in SGC with two different compositions. Images are rendered on ice, osmolyte mixture and –CH. The fraction of cells with ice is described for 10 cells measured.

imaged and the formation of ice inside the cell is known to be damaging[61]. Contrastingly, fewer cells cryopreserved in SGC-A exhibited intracellular ice formation (3/10 cells imaged). Post-thaw recovery trends (average of biological replicates ± SEM,

n=4) for cells frozen in SGC-A (0.82 ± 0.07) and SGC-B (0.71 ± 0.05) using conventional controlled rate freezing were consistent with the ice formation trends observed using Raman, in that SGC-A had higher recovery and fewer cells with ice crystal formation than SGC-B.

Solidification behavior

It is common to formulate cryopreservation solutions to result in full or partial vitrification (see [133] for review). The next phase of the investigation involved characterizing the solidification behavior of the solutions tested. SMC solutions with similar osmolarity and significantly different ($p<0.05$) recovery (recovery ± SEM, n = 4; SMC-A = 0.73±0.03, SMC-B = 0.62±0.02) were seeded for ice crystal nucleation at -6^{o}C, cryopreserved without cells (solution only) at 3^{o}C/min and imaged using Raman microscopy. Representative images are given in Figure 16A. There is little difference in the macroscopic solidification patterns observed between the two solutions imaged (in spite of the significant difference in post-thaw viability observed between the two solutions). There is also no statistical difference in the area of ice crystals between the two solutions. As a control, a DPBS solution was seeded at 0°C, cryopreserved at 3°C/min and imaged using Raman microscopy. Only very small amount of solution was incorporated into ice and hydrohalite could be found in the narrow solution gap based on Raman spectra.

A

Solution	Composition	Ice	Ice crystal Area (μm^2)
SMC-A	0mM sucrose 125mM mannitol 50mM creatine	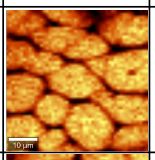	163.3±66.8 N = 40
SMC-B	60mM sucrose 50mM mannitol 37.5mM creatine	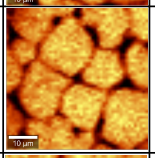	184.0±54.5 N = 40
DPBS	8.007g NaCl 0.202g KCl 0.204g KH_2PO_4 1.15g Na_2HPO_4	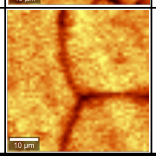	N/A

B

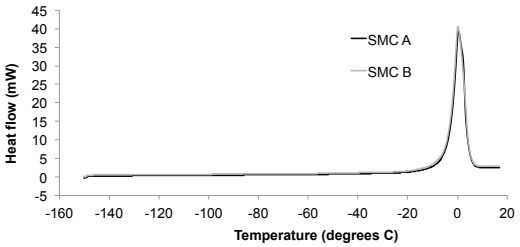

Figure 16: Physical behavior of multicomponent solutions associated with different recovery. (A) Low temperature Raman spectroscopy of two SMC solutions at -50°C. Two different compositions with similar osmolarity were studied: one associated with high recovery (SMC-A) and the other associated with lower recovery (SMC-B) (B) DSC thermograph for the same SMC solutions during warming. The melting curves are almost identical and display a large exotherm associated with melting of the solution, and no glass formation is observed for either solution.

Additional studies were performed using DSC to determine whether the different compositions exhibited differences in glass forming tendency (Figure 16B). No change in the melting curves was observed for either pair, and no signs of full or partial vitrification of the solutions were observed using DSC.

Component substitution

There has been considerable interest in the use of sugars (specifically trehalose) for the preservation of cells[132]. The next phase of the investigation involved determining whether the structure of the sugar has a significant influence on post-thaw recovery. Specifically, a monosaccharide, glucose, was substituted for sucrose at the same concentration (solution compositions: SMC (sugar = 150mM, mannitol = 125mM,

creatine = 12.5mM), SGC (sugar = 150mM, glycerol = 2.5%, creatine = 12.5mM)). When a monosaccharide is substituted for a disaccharide for both of the solution compositions tested, the post-thaw recovery of MSCs is reduced and those differences are statistically significant (Figure 17A). Cells in SMC and GMC were cryopreserved and imaged using Raman spectroscopy. For cells cryopreserved in SMC, Raman images demonstrated that a small fraction of the cells exhibited ice during freezing (4/10) when compared to cells cryopreserved in a solution containing GMC exhibited ice inside the cell during freezing (6/10) (Figure 17B). Images of the cell freezing response are consistent with the controlled rate freezing experiments described in Figure 17A.

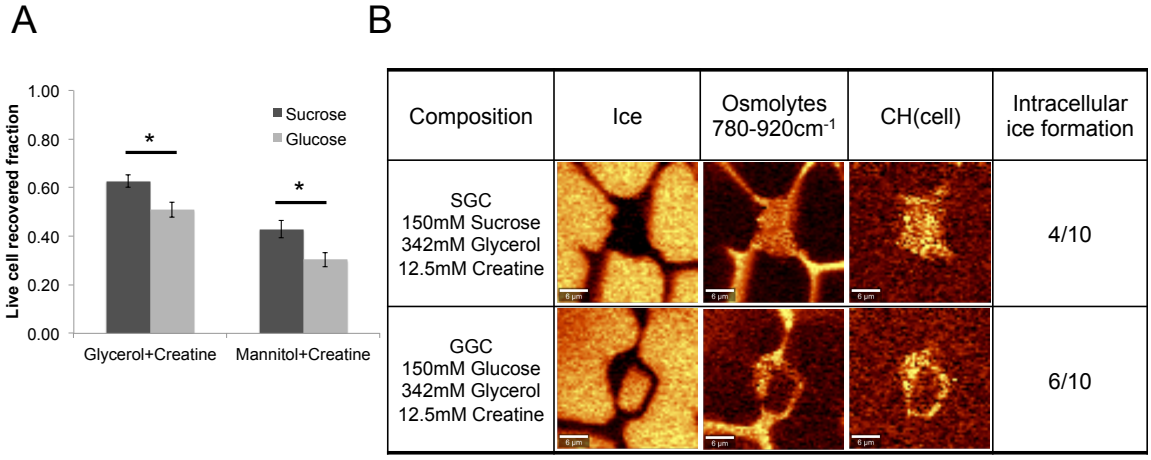

Figure 17: Sugar substitution results in different recovery and ice formation behavior. (A) post thaw recovery of MSCs cryopreserved in glycerol+creatine and mannitol+creatine solutions with either sucrose or glucose (n=9, error bars represent standard error of the mean) (B) Low temperature Raman microscopy of MSCs cryopreserved at 3°C/min in SGC and GGC concentrations listed. Images are rendered on ice, osmolyte mixture and –CH. The fraction of cells with ice is consistent with cell recovery described in (A).

6.4 Discussion

6.4.1 Permeation/partitioning of solutes

Conventional cryoprotective agents (DMSO and glycerol) have small molecular weights

(78 and 92 Da respectively) and permeate the cell in a matter of minutes (see [134] for review). Little has been done to characterize the uptake of osmolytes with the exception of trehalose [135], which appears to penetrate poorly into the cell. The results of this investigation suggest that longer incubation times may be needed for cells frozen with non-DMSO cryoprotectants to allow for penetration of larger components and elicit maximum cell recovery. Raman measurement of mannitol indicated that permeation for this molecule takes ~90 mins (data not shown), which is consistent with the results of this study. The observation that post-thaw recovery increases and the prevalence of ice inside the cell decreases with increasing incubation time also suggests that the presence of osmolytes inside the cell is needed for protection. This observation is consistent with previous studies of the protective effect of trehalose [136], which demonstrated a similar outcome.

6.4.2 Influence of osmolarity and composition

It has been postulated that one mechanism of action for cryoprotective agents results from a colligative effect [137]. Specifically, higher concentrations of cryoprotectants reduce concentrations of damaging solutes and thereby protect the cell. In contrast, the outcome of this investigation suggests that there is little relationship between total osmolarity of the solution and post-thaw recovery for multi-osmolyte solutions (Figure 13). Similarly, the solidification behavior of the solutions (crystallization patterns and DSC thermograms) for the different compositions tested does not exhibit significant differences from one SGC or SMC composition to the other.

Based on the results in Figure 13, osmolarity alone is not enough to predict cell recovery. Additionally, as shown in Figure 16, there was no change in the physical solution behavior at these low osmolarity solution concentrations below -30°C. There is no eutectic peak indicating that a glass transition occurred in any of the samples at these concentrations (it would be expected around -80°C if it existed). Because this physical change is absent, we hypothesize that the mechanism of protection for these solutions is biological. This suggests that there is a biological 'sweet spot' solution composition that results in maximum cell recovery.

One reason these solution compositions may be successful could be the result of their interactions to stabilize proteins within the cell. Osmolytes are well known for stabilizing protein folding by providing a thermodynamically unfavorable environment for denatured proteins [138], including during cryopreservation[139] Additionally, mixtures of two different osmolyte monomers have been found to have better stabilization effects than that of a single type of monomer at the same molar concentrations [140]. Thus, literature supports the possibility that different osmolytes could stabilize different proteins and different parts of the cell to result in increased viability. Within mixtures of osmolytes, each osmolyte exerts independent protein stabilization effects[141]. This effect is due to the low binding affinity between osmolytes and proteins, resulting in neither competition nor cooperation between osmolytes[141]. Therefore, the activity of each osmolyte should be considered individually without cooperation between them.

Different combinations of osmolytes may also stabilize the cell membrane. Both surface and internal membranes are main areas of injury regardless of cooling rate[7]. Normal cells have a layer of water surrounding the cell surface, which helps maintain surface protein folding[55]. During freezing the concentration of liquid water is decreased, which can lead to destabilization of these proteins [55]. Combined with observations that membrane proteins are denatured and lost post-thaw [55], stabilization of proteins in the membrane is very important to the success of cryopreservation. Meryman proposed that conformational stability of surface macromolecules depends on the interactions of solute and water at the cell surface [55], and osmolytes themselves have been postulated to replace water in the cell membrane during freezing[142]. Osmolytes also play a role in preferential exclusion, which has been associated with protein stabilization caused by increases in surface tension due to sugars and amino acids present in solution [143]. In the solutions used in this study, each component could differ in location (intracellular or extracellular), the macromolecules it stabilizes, and the surface area it stabilizes. These differences could help to protect multiple critical structures, thus decreasing the cumulative damage to the cell.

It is well established in literature that larger sugar osmolytes provide better stabilization [96, 140, 144], due to their increased polar contact area [140]. Sugars can provide stabilization by replacing water surrounding membranes during dehydration [139, 140]. The trend observed for improved disaccharide behavior may be due insertion between the

phospholipid heads of the lipid membrane, creating more space than monosaccharides for additional binding [144]. Binding of sugars to membranes can increase the rigidity of the membrane, which provides greater resistance to disruption [144]. Cells dehydrate at slow cooling rates, making stabilization with osmolytes important. During thawing, changes in the protein environment could induce denaturing, but osmolytes, including sugars, can assist with stabilization. This can reduce damage to membrane proteins, as well as internal proteins.

In a study that supplemented cryopreservation media with monosaccharides or disaccharides during freezing of boar sperm, glucose was found to be the most effective of the monosaccharides in maintaining post-thaw sperm quality[145]. Gomez et al found that disaccharides containing the same monomers with different links had similar results [145]. Additionally, disaccharides are known for being better stabilizers than monosaccharides [145][140], and this is supported by the results presented herein Figure 17.

6.5 Conclusion

As the field of cryobiology expands to include new applications that require non-toxic alternatives to DMSO, it is important to understand the role of multicomponent solutions in preserving cell function. In this chapter, we demonstrate that incubation time must be

sufficient for penetration of components, concentration of components (not total osmolarity) determines recovery, and molecular substitution results in changes in recovery. We hypothesize that these differences are biological, as we have found no evidence of physical changes in ice crystal formation between these solutions. Ultimately, these observations increase our understanding of multicomponent solution behavior, and move the field closer to clinically acceptable DMSO alternatives for cryopreservation of MSCs and other cryo-sensitive cell types.

Because we hypothesize that differences in concentration of components and not total osmolarity determines recovery, it is important to identify the concentrations of components in solution that result in optimum recovery. Factorial optimization limits the number of experimental conditions that can be tested, and in Chapter 7, we validate that an algorithm can be used to optimize solution concentrations with significantly fewer experiments than traditional factorial strategies.

Chapter 7

Algorithm-Driven Optimization of Cryopreservation Protocols for Transfusion Model Cell Types Including Jurkats and Mesenchymal Stem Cells

Much of the text and figures in this chapter have previously appeared in the publication below, included here with copyright permission from John Wiley & Sons Ltd:

Pollock K, Budenske JW, McKenna DH, Dosa PI, Hubel A. Algorithm-driven optimization of cryopreservation protocols for transfusion model cell types including Jurkat cells and mesenchymal stem cells. *J Tissue Eng Reg Med*, Published online May **2016**, doi: 10.1002/term.2175

7.1 Introduction

Survival for many cell types is strongly influenced by cooling rate, with a narrow range of cooling rates over which post-thaw survival is optimal [56]. Freezing solution composition also influences cell survival [7], and changing the composition of the cryopreservation solution may change the cooling rate at which optimum survival is observed. Cryopreservation protocols are most often determined empirically by changing the composition and cooling rate until the desired outcome is obtained [97–101]. This process is typically expensive, time-consuming and may not result in an optimized protocol.

A variety of strategies can be used to optimize processes with multiple inputs (composition of the freezing solution and cooling rate) and outputs (recovery and viability). The objective of this chapter was to validate the use of the differential

evolution (DE) algorithm [11] to optimize compositions and cooling rates for cryopreservation solutions. Other investigators have successfully used DE for other applications, including Tsutsui et al. [104], who used this approach to optimize the formulation of embryonic stem cell media. In the experiments described here, DE is applied to determine optimum DMSO-free cryopreservation solution formulations for different cell types (lymphoblasts and mesenchymal stem cells). The approach was also used to optimize composition and cooling rate simultaneously. The methods involved have been adapted to a high-throughput format: small numbers of cells are used and a small number of experiments are required for optimization. This type of approach will transform the development and optimization of freezing protocols by reducing the number of cells and experiments required, thus accelerating optimization over a multiparameter space.

7.2 Methods

Culture of Jurkats and Mesenchymal Stem Cells was performed according to sections 3.2.2 and section 3.2.3 respectively.

The algorithm was operated according to the procedures outlined in 3.12. For these experiments, the generation size was set to either 18 or 27, the crossover set to 1 and the weight set to 0.85. The concentration of each component was allowed to vary discretely between 0 and the maxima that were identified from the literature or dictated by solubility limits. The concentrations used for each discrete level are listed in Table 12.

Table 12 Discrete concentration levels and cooling rates used for each component in the DE algorithm

Component	Level 0 (0)	Level 1 (1/100)	Level 2 (1/50)	Level 3 (1/10)	Level 4 (1/2)	Level 5 (1)
Trehalose (mM)	0	3	6	30	150	300
Glycerol (%)	0	0.1	0.2	1	5	10
Ectoine (%)	0	0.01	0.02	0.1	0.5	1
Sucrose (mM)	0	3	6	30	150	300
Ethylene glycol (mM)	0	3	6	30	150	300
Alanine (mM)	0	3	6	30	150	300
Taurine (mM)	0	0.5	1	5	25	50
Cooling rate (different scaling) (°C/min)	0	0.5	1	3	5	10
DMSO standard recovery ± standard deviation. (for cooling rates in same column above)	0	0.09 ± 0.03	0.13 ± 0.03	0.12 ± 0.04	0.12 ± 0.04	0.09 ± 0.01

Cells were frozen in 96 well plates according to section 3.3.2 for all results in this section except for Figure 22, in which cells were frozen in vials according to section 3.3.3. All samples were thawed according to section 3.4, and analyzed for viability according to section 3.5.2 for plates and 3.5.1 for vials. To evaluate whether the optimum identified by the algorithm was the optimum of the system, liquid handling experiments according to sections 3.9.1 and 3.9.2 were performed to fully characterize the parameter space at a single cooling rate. Error bars represent standard deviations (SDs) of a minimum of nine sample measurements, taken from experiments performed in batches of three to six over a minimum of 3 different days. Statistical significance was determined using Student's t-test, with a significance level of $p = 0.05$.

7.3 Results

7.3.1 Optimizing a solution composition for a given cooling rate

The first phase of this study involved using the DE algorithm to optimize a three-component cryopreservation solution used at a single cooling rate (1°C/min). Three components, trehalose, glycerol and ectoine (TGE), were selected to comprise the freezing medium used for the preservation of Jurkat cells (a hematopoietic model cell type) based on prescreening of multiple non-DMSO components. For this single cooling-

rate study, the DE algorithm was programmed to output 18 vector solutions/generation, with weight = 0.85 and crossover =1. Jurkat cells cryopreserved in 10% DMSO at a cooling rate of 1°C/min were used as a control. For each generation of solutions tested, the scaled raw recovery of the best solution increased or remained constant (Figure 18A), while the number of solutions that demonstrated improved recovery tended to decrease for each generation (Figure 18B).

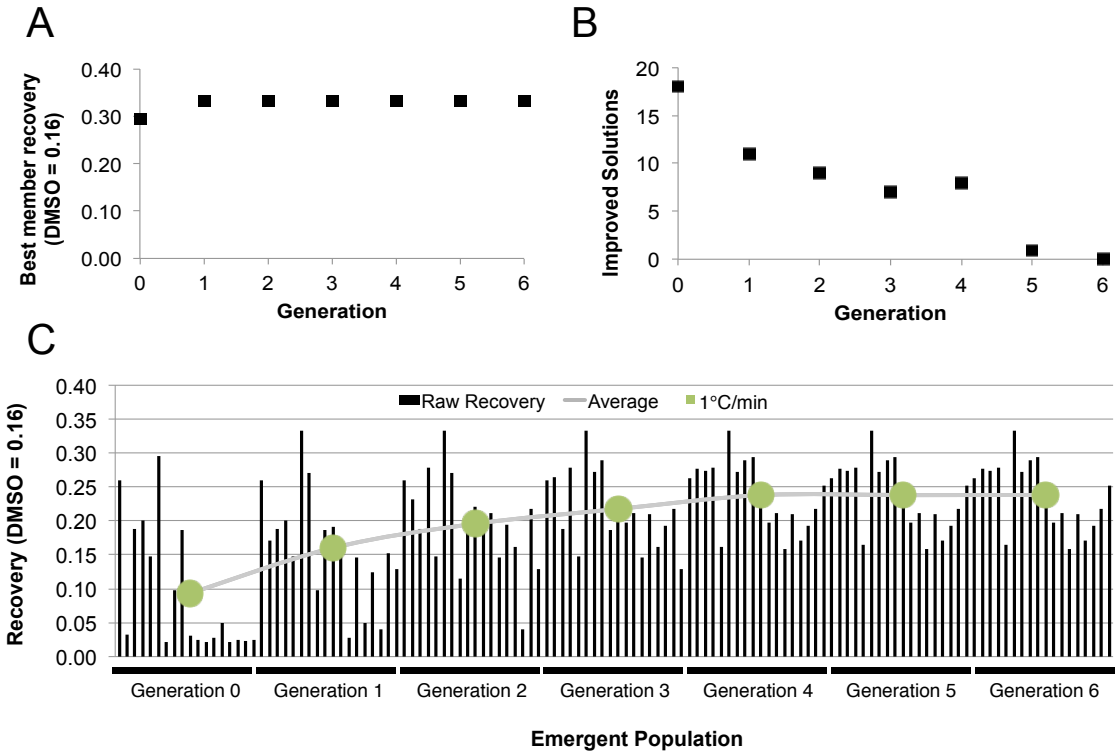

Figure 18: Trehalose, glycerol, ectoine 1°C/min DE algorithm results for Jurkat cells. (A) Cumulative best member solution; recovery associated with the best solution increases and plateaus as the algorithm converges. (B) Number of improved solutions/generation; the number of improved solutions in each generation decreases and reaches zero when the algorithm has converged. (C) Emergent population with the generational average overlaid: the emergent population improves and eventually stops changing as the DE algorithm converges; this is reflected in the generational average, which increases and begins to plateau as the algorithm converges. The optimum composition identified by this run of the algorithm was 150mM trehalose, 10% glycerol, 0.1% ectoine for Jurkat cells frozen at 1°C/min.

These results together (Figure 18C) indicate that the DE algorithm converged after six generations (e.g. seven freezing experiments) to an optimum solution composition of 150mM trehalose, 10% glycerol and 0.1% TGE (Figure 18). The recovery of Jurkat cells frozen in the TGE solution was 32%, almost twice as high as the recovery of the control (16% = highest observed recovery in 10% DMSO at 1°C/min).

7.3.2 Optimizing both composition and cooling rate

Cooling rate influences cell survival [56] and optimal cooling rate varies with the composition of the freezing medium and the cell type being frozen [146]. Therefore, the optimal TGE solution composition identified for Jurkat cells at a constant cooling rate of 1°C/min may not be the optimum composition at other cooling rates, and thus may not produce the highest recovery possible. To optimize both composition and cooling rate in this study, the DE algorithm was programmed to output 27 vector solutions/generation with weight = 0.85 and crossover =1, using cooling rate as an additional optimization variable. Solutions were separated into categories based on their DE algorithm defined cooling rate, and were frozen in batches at these cooling rates (0, 0.5, 1, 3, 5 and 10°C/min). The results were normalized and scaled raw recovery is reported, allowing results from all cooling rates and all generations to be compared directly.

As with previous generations, the best member scaled raw recovery increased or remained constant with increasing iterations (Figure 19A) and the number of improved solutions within each generation tended to decrease (Figure 19B). The number of solutions frozen at given cooling rates is described by pie charts overlaid at the average

recovery of each generation in Figure 19C.

These pie charts show that the DE algorithm quickly identifies poor recovery in solutions frozen at 0°C/min (no freezing, recovery = 0) and 0.5°C/min and eliminates these rates after 2 generations. In early generations, the majority of solutions with high recovery used cooling rates of 5 and 10°C/min. However, a spike in the number of 1°C/min solutions occurs in generation 4 after the DE algorithm identifies the same high recovery 1°C/min composition from the constant cooling rate study described in Figure 18 above.

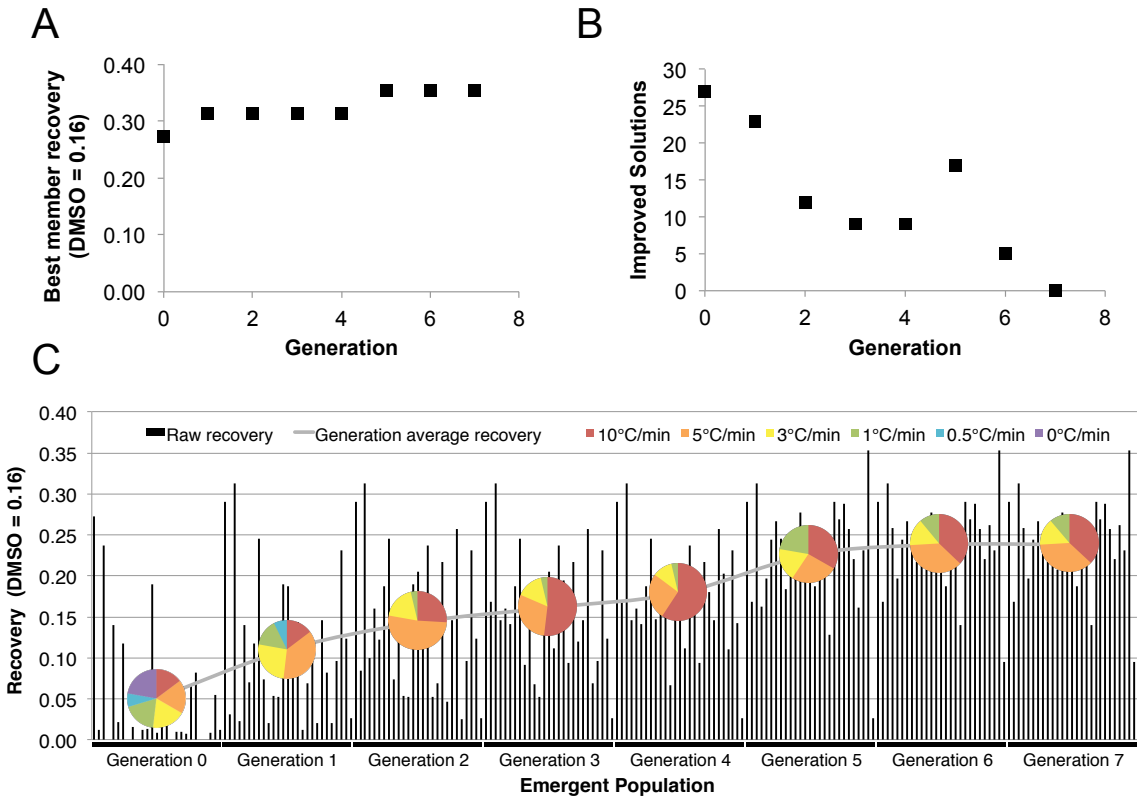

Figure 19: Trehalose, glycerol, ectoine cooling-rate DE algorithm results for Jurkat cells. (A) Cumulative best member solution; this increases and plateaus as the DE algorithm converges. (B) Number of improved solutions/generation; this decreases until it reaches zero as the DE algorithm converges. (C) Emergent population with the generational average overlaid: pie charts at each average show the cooling rate distribution within each generation. The optimum composition identified by this run of the DE algorithm was 300 mM trehalose, 10% glycerol, 0.01% ectoine at 10°C/min cooling.

Ultimately, at convergence, this DE algorithm run identified that a TGE solution containing 300mM trehalose, 10% glycerol, 0.01% ectoine at a cooling rate of 10°C/min resulted in optimum cell recovery for Jurkat cells (35% recovery in TGE at 10°C/min vs. 16% = highest observed recovery in 10% DMSO at 1°C/min). The DE algorithm converged after seven generations (or eight freezing experiments).

7.3.3 Confirmation of the optimum using high-throughput screening over the range of concentrations tested

High-throughput screening of solution compositions was used to confirm that the DE algorithm converged on the true optimum solution composition for a given cooling rate and component concentrations. Samples were frozen and thawed at 10°C/min. Serial dilutions of glycerol and ectoine were combined with dilutions of trehalose and cells suspended in Normasol-R™ in 96-well plates. The final concentrations in each well were equal to the full factorial array of concentrations used in the DE algorithm. The results from each well were normalized to a DMSO control included on each plate. This experiment was repeated in triplicate and the recovery results from each individual composition were averaged and are plotted in Figure 20(SDs were typically <5%). This study confirmed that a composition of 300mM trehalose, 10% glycerol, 0.01% ectoine resulted in the highest recovery for the array tested, indicating that the DE algorithm correctly identified the optimum of the system at 10°C/min.

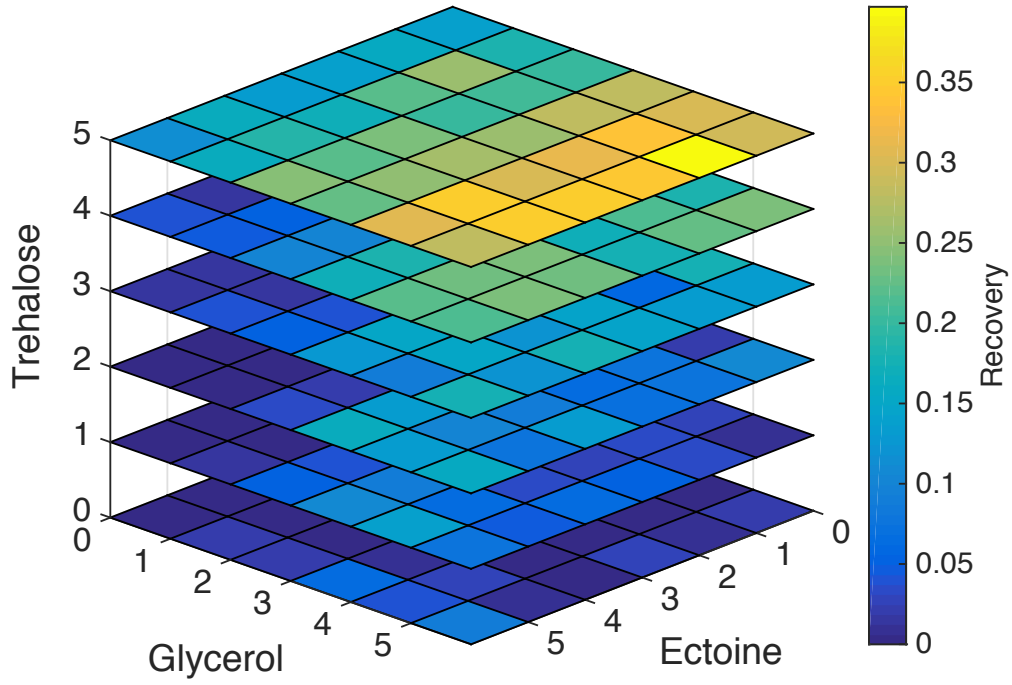

Figure 20: High-throughput concentration study confirmation of Jurkat DE algorithm results. Shades corresponding to recovery values are plotted in squares corresponding to solution compositions within the algorithm parameter space. This concentration study, performed at 10°C/min, identified the solution composition associated with maximum recovery to be 300mM trehalose, 10% glycerol and 0.01% ectoine (corresponds to the points 5-trehalose, 5-glycerol, 1-ectoine in the heat map above). This composition is the same as the composition identified by the DE algorithm, confirming that it is indeed the optimum within the parameter space at 10°C/min.

7.4.1 DE algorithm can be applied to different cell types, using different compositions and different numbers of solution components

The previous studies describe a three-component TGE solution tested with Jurkat cells. To show that the DE algorithm is capable of converging to freezing solution compositions using different solution components and different cell types, a five-component combination of sucrose, ethylene glycol, alanine, taurine and ectoine (SEGA) was tested with mesenchymal stem cells at DE algorithm-defined concentrations and cooling rates. These components were selected based on pre-screening experiments performed to identify combinations with high potential recovery. The DE algorithm was

programmed to output 27 vector solutions/generation with weight = 0.85 and crossover =1. Experimental testing and result normalization were similar to the methods described above.

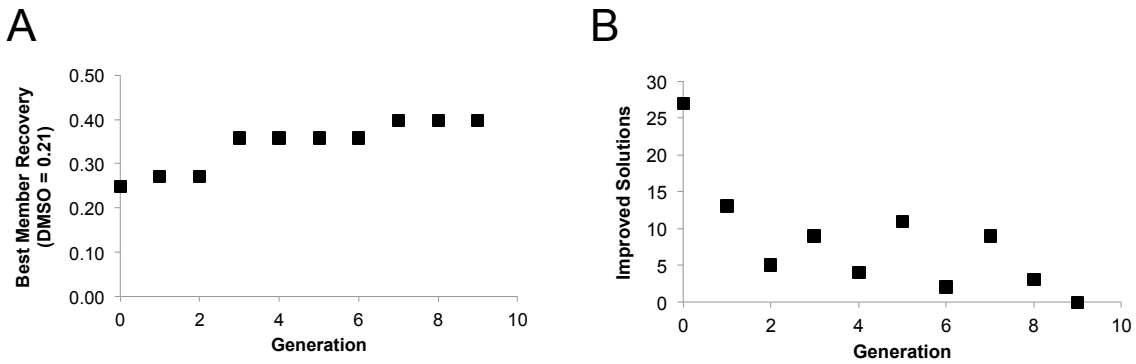

Figure 21: Sucrose, ethylene glycol, alanine, taurine, ectoine cooling-rate algorithm results for MSCs. (A)Cumulative best member solution; this increases and plateaus as the DE algorithm converges. (B) Number of improved solutions/generation; this decreases until it reaches zero as the DE algorithm converges. The optimum composition identified by this run of the DE algorithm included 300 mM ethylene glycol, 1 mM taurine, 1% ectoine with a 1°C/min cooling rate.

As with previous experiments, the cumulative best member composition increased and the number of improved solutions decreased with each generation. At convergence, this run of the DE algorithm identified that a SEGA solution of 300mM ethylene glycol, 1mM taurine and 1% ectoine resulted in optimum cell recovery for MSCs (40% recovery at 1°C/min vs. 21% recovery in 10% DMSO at 1°C/min). Total convergence occurred after nine generations (10 freezing experiments), as evidenced by the increase and plateau of the best member recovery (Figure 21A) and the decrease in the number of improved solutions/generation (Figure 21B). It is noteworthy that two of the components tested (sucrose and alanine) were not present in the final solution formulation, indicating that the presence of these additives did not improve post-thaw survival at this cooling rate.

3.5. Convergence results obtained for 96-well studies scale to larger volumes and are unique to the cell type being frozen

Freezing experiments were performed in 1mL vials to determine whether the results with low volumes and small cell numbers in 96-well studies were reproducible when using larger, more clinically relevant volumes.

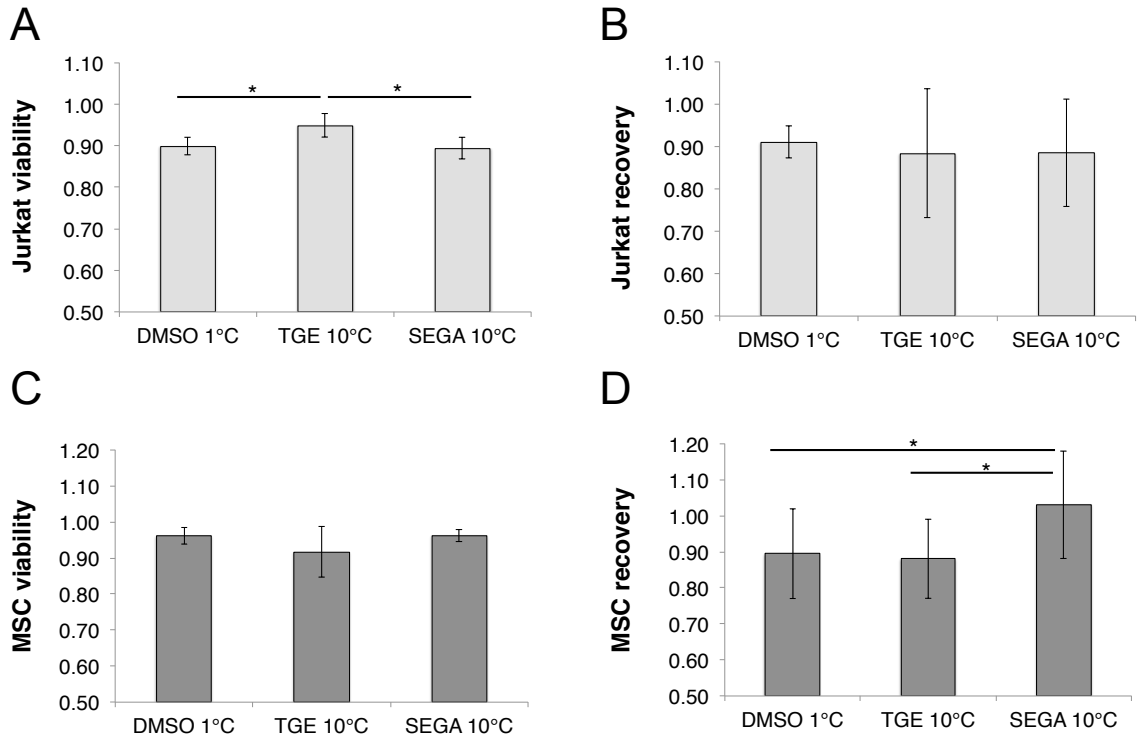

Figure 22: Scale-up viability and recovery of Jurkat cells (A, B) and mesenchymal stem cells (C, D) frozen in DE algorithm-optimized solutions. Each cell type was frozen at 10°C/min in a TGE solution optimized for Jurkat cells (TGE 10°C) and a SEGA solution optimized for MSCs (MSC 10°C). Results were compared to cells frozen in DMSO at 1°C/min (DMSO 1°C), as it represents the current gold standard for both cell types. Jurkat cells performed well in both the SEGA 10°C and TGE 10°C solutions, and Jurkat cell viability was significantly higher in TGE 10°C than both SEGA 10°C and the DMSO 1°C control (A). MSCs also performed well in both SEGA 10°C and TGE 10°C solutions, and had significantly higher recovery in the SEGA 10°C solution than both TGE 10°C and the DMSO 1°C control (D). Significance markers indicate $p < 0.05$.

DE algorithm solutions that resulted in maximum recovery were identified for both Jurkat cells and MSCs at 10°C/min. These solutions are identified as TGE 10°C (300mM trehalose, 10% glycerol and 0.01% ectoine at 10°C/min optimized as above for Jurkat cells) and SEGA 10°C (150mM sucrose, 300mM ethylene glycol, 30mM alanine, 0.5mM taurine and 0.02% ectoine at 10°C/min optimized for MSCs). These solutions were combined with cells, frozen, thawed and analyzed for viability. A minimum of nine samples was analyzed for each solution (batches of three or more on at least 3 different days). These were compared to solutions of cells in 10% DMSO frozen at 1°C/min (the gold standard for both cell types, labeled DMSO 1°C).

The TGE 10°C solution resulted in significantly higher viability than SEGA 10°C and the DMSO 1°C control (Figure 22A; DMSO 1°C = 0.90 ± 0.02; TGE 10°C = 0.95 ± 0.03; SEGA 10°C = 0.89 ± 0.03; $p < 0.05$) for Jurkat cells. Recovery was high across the board (> 88%) but not statistically significantly different for any of the solutions tested with Jurkat cells (Figure 22B; DMSO 1°C = 0.91 ± 0.04; TGE 10°C = 0.88 ± 0.15; SEGA 10°C = 0.88 ± 0.13; $p < 0.05$). Conversely, MSC viability testing showed no statistically significant differences between solutions (Figure 22C; DMSO 1°C = 0.96 ± 0.02; TGE 10°C = 0.92 ± 0.07; SEGA 10°C = 0.96 ± 0.02; $p < 0.05$), while the SEGA 10°C solution produced significantly higher recovery than either TGE 10°C or DMSO 1°C (Figure 22D; DMSO 1°C = 0.90 ± 0.12; TGE 10°C = 0.88 ± 0.11; SEGA 10°C = 1.03 ± 0.15; $p < 0.05$). This indicates that optimization results for individual cell types are unique and can result in significantly higher viability (Figure 22A) or recovery (Figure 22D). However, both TGE and SEGA solutions produced acceptable viability and recovery in cell types

for which they were not optimized, indicating that DE algorithm-optimized solutions may be used to freeze multiple cell types successfully. Follow-up studies currently being performed suggest that cells frozen with these solutions proliferate post-thaw at rates similar to cells frozen in DMSO.

Figure 22 also shows that DE algorithm optimization results are scalable. Although the improvement in recovery for optimized solutions in comparison to DMSO is smaller in vial studies than in 96-well studies, this result is expected because of the limited difference that is possible when recovery and viability are high. Cumulatively, these results support DE algorithm testing of small volumes of cells and solutions, as optimized solutions produce high viability and recovery at larger volumes.

7.4 Discussion

Current methods of optimizing cryopreservation solutions most often use empirical methods, by testing a given composition and cooling rate and measuring post-thaw recovery [97, 99–101, 147]. Our studies show that optimization of freezing solutions can be performed using a DE algorithm. The DE algorithm can be used for different cell types and can concurrently optimize both solution composition and cooling rate.

The three variables examined in this study (cryoprotectants, cryoprotectant concentration and cooling rate) represent only a subset of the variables that can be considered when optimizing a cryopreservation protocol. In the future, rate of addition and removal of cryoprotectants, temperature of nucleation, incubation time, hold temperature, single vs. multistep cooling, storage temperature and thawing rate are all parameters that could be

incorporated into this type of algorithm optimization.

The use of DE to optimize over a multiparametric space has been used in a wide variety of fields. Recently, Tsutsui et al. [148] used this approach to optimize a defined medium for the culture of human embryonic stem cells.

The investigation described above utilizes DE as part of an innovative method to optimize both cooling rate and composition for the cryopreservation of therapeutic cell types. This DE algorithm used a total of seven to nine experiments to optimize a three- or five-component solution. The DE algorithm as implemented rapidly optimized both solution composition and cooling rate with <200 unique experimental points; without the aid of the DE algorithm, ~7000 unique experimental data points would have been required to optimize the compositions tested above. Best member solutions increased and the number of improved solution compositions steadily decreased with advancing generation, consistent with convergence of the DE algorithm. Convergence to a local optimum was confirmed by high-throughput studies using the same components and the same range of concentrations as the DE algorithm. The data here suggest that the DE algorithm can reliably optimize at least six parameters at a time (Figure 21 shows that the DE algorithm optimized five solute concentrations and a cooling rate) and more parameters could theoretically be added if the population size within each generation is increased and the number of generations tested is increased to ensure that convergence is achieved.

The ability to cryopreserve cells in a 96-well format enabled the testing of generations with a large number of solutions (18–27). Freezing of cells in 96-well format has been used to improve the post-thaw recovery of anchorage-dependent cells [149]. Cells cryopreserved in a 96-well format are also available commercially and used for drug screening and other applications. In this study, post-thaw recovery of cells frozen in DMSO was lower for cells frozen in 96-well plates vs. vials. The same was true for cells frozen in DMSO-free solutions. One possible explanation for this reduced viability is the slower warming rates observed for plates vs. vials; 96-well plates had an average sample warming rate of 1.30°C/s (-196°C to 0°C in 150 s), while vials had an average sample warming rate of 1.63°C/s (-196°C to 0°C in 120 s). A second possible explanation for the reduction in recovery observed in 96-well plates could be due to the extended post-thaw incubation time for cells in 96-well plates. Cells in 96-well plates were subject to an additional 30 min of incubation post-thaw in 0.5× cryopreservation solutions after viability dye was added (allowing it time to be metabolized by live cells), while 1mL vials were assessed for recovery immediately using AO/PI. However, the recovery trends observed in 96-well plates were scalable to larger volumes, in that the differences in viability and recovery between experimental solutions and DMSO were comparable. Cumulatively, these results support DE algorithm testing of small volumes of cells and solutions, as optimized solutions produced high viability and recovery at larger, more clinically relevant volumes. Additional metrics of cryopreservation success, such as attachment, proliferation, alignment, gene expression, etc., could easily be incorporated as the input of the algorithm, rather than using recovery.

Preservation of Jurkat cells and MSCs is principally performed using 10% DMSO and a cooling rate of 1°C/min. A limited number of studies have examined vitrification of MSCs [57, 150] and the use of polymers to replace DMSO [92]. This investigation describes novel formulations in which solutions with multiple components are known to preserve cell viability. Glycerol is used for the cryopreservation of red blood cells [151] and was the first cryoprotective agent discovered[152]. Similarly, trehalose has been shown to be an effective cryoprotective agent [153]. What makes this investigation noteworthy is that the combination of two or more cryoprotectants is effective and that effectiveness is not necessarily observed at the highest concentrations tested. Additionally, these multi-component compositions result in cell viability and recovery significantly higher than 10% DMSO, which is an important step forward towards DMSO-free cryopreservation. Additional studies will be needed to characterize the methods of action for these multicomponent solutions. These studies are enabled by the development and implementation of the DE algorithm, which permits optimization of a multicomponent solution in a rational, accelerated fashion.

7.5 Conclusion

This chapter validates the DE algorithm and confirms that the optimums identified by the algorithm are indeed the optimums of the system. However, the iterations described in here optimized cell recovery only, and do not address cell functionality. In the next chapter, the algorithm will be applied to optimize a metric of cell functionality, and subsequent measures of cell health will be evaluated.

Chapter 8

Mesenchymal Stem Cell Post-Thaw Function is Maintained or Improved by Freezing with Algorithm Optimized non-DMSO Solutions

The text and figures in this chapter will appear in a future publication:

Pollock K, Samsonraj RM, Stumbras A, McKenna DH, Dosa PI, van Wijnen A, Hubel A. Mesenchymal stem cell post-thaw cell function is maintained or improved by freezing with algorithm optimized non-DMSO solutions. *In Preparation* **2016**.

8.1 Introduction

Assessment of cellular function post-thaw for MSCs is often limited to the minimal criteria defined by Dominici et al[154]. Previous work has been performed to define other minimal potency criteria[155], but there is not consensus within the field regarding functional characterization metrics[156] due to the limited understanding of the specific therapeutic mechanisms of action of these cells *in vivo*[157].

MSCs have known immunomodulatory behavior *in vivo*[52, 158, 159], and cryopreservation with DMSO has been associated with functional changes in cells, including reduced suppression of t-cell proliferation caused by changes in the indoleamine 2,3 deoxygenase signaling cascade[10, 160–162]. In addition, cryopreservation in DMSO has been associated with reduced engraftment, and has been correlated to a disruption of the actin cytoskeleton[67, 68, 74], and to rapid clearance via

a blood mediated inflammatory reaction after systemic delivery to patients[75]. DMSO has also been implicated in epigenetic changes in cells[77, 78]. These post-thaw functional alterations may be to blame for the failure of a recent phase 3 clinical trial using cryopreserved MSCs [73], and highlight the need for improved cryopreservation methods that are free of DMSO and maintain MSC viability and functionality post-thaw. The work that follows describes optimization of non-DMSO cryopreservative solutions for functionality, and subsequent relevant analysis of MSC functional metrics based on previously identified cryopreservation issues detailed above. These functional metrics include attachment, actin alignment, RNA expression, and DNA hydroxymethylation.

8.2 Methods

Culture, freezing, and thawing of cells was performed according to the same methods referenced in Chapter 6. Algorithm optimization was performed with cells in vials according to section 3.13, using cell attachment as a functional return metric. Optimized solutions identified by algorithm iteration were frozen with cells and analyzed post-thaw for attachment and proliferation according to section 3.14, senescence according to section 3.6, flow cytometry according to section 3.7, actin alignment according to section 3.15, multi-lineage differentiation according to section 3.16, DNA hydroxymethylation according to section 3.17, and gene expression according to section 3.18. Rebekah Samsonraj helped design primers, helped perform qRT-PCR, and performed DNA hydroxymethylation dot blotting.

8.3 Results

8.3.1 Algorithm optimization

Algorithm optimization was performed for three different combinations of sugars, sugar alcohols, and small molecule additives and identified concentrations of components in solution which, when combined with cells, resulted in maximum cell attachment at 2 hours post-thaw/seeding. Figure 23 shows a representative generational progression of the algorithm for a solution of sucrose/glycerol/isoleucine (SGI).

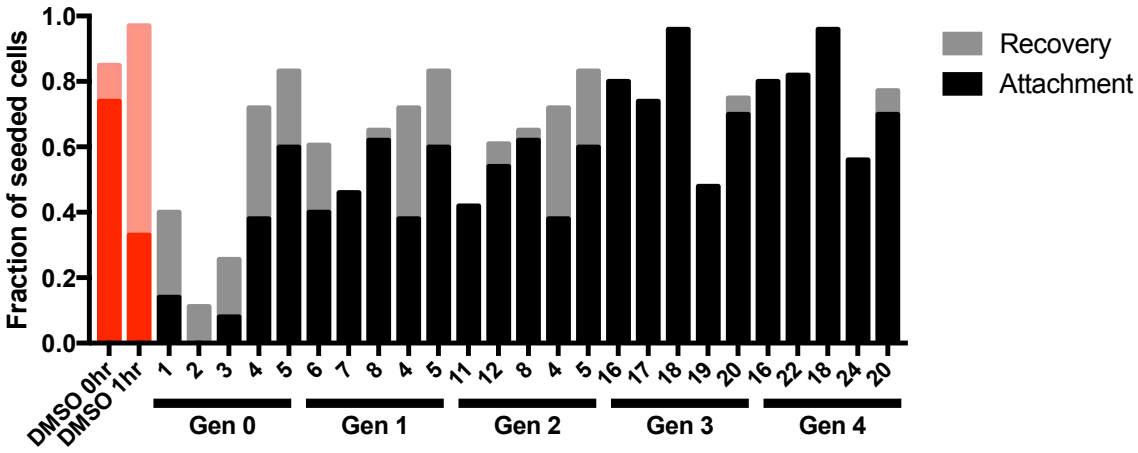

Figure 23: Recovery and attachment of cells during algorithm optimization of SGI solution.

Over multiple generations, the recovery of live cells increases, and the percentage of those recovered cells that are able to attach to a surface also increases. The optimums identified for three separate iterations of the algorithm using different components in solution are listed in Table 13.

Table 13: Optimized solution compositions.

Solution (vector)	Sugar	Sugar alcohol	Additive
SGC (025)	Sucrose (0mM)	Glycerol (1.25%)	Creatine (25mM)
SGI (151)	Sucrose (30mM)	Glycerol (5%)	Isoleucine (7.5mM)
SMC (322)	Sucrose (150mM)	Mannitol (62.5mM)	Creatine (6.25mM)

The optimum solution formulations listed in Table 13 were combined with cells and tested for attachment and recovery using statistical triplicates of biological replicates. Figure 24 shows that samples frozen in experimental solutions have different attachment and recovery behavior. High performing combinations, such as SGI, display recovery and attachment that is not statistically different ($p>0.05$) from fresh cells and DMSO 0hr incubation frozen samples. Other experimental combinations including SGC and SMC

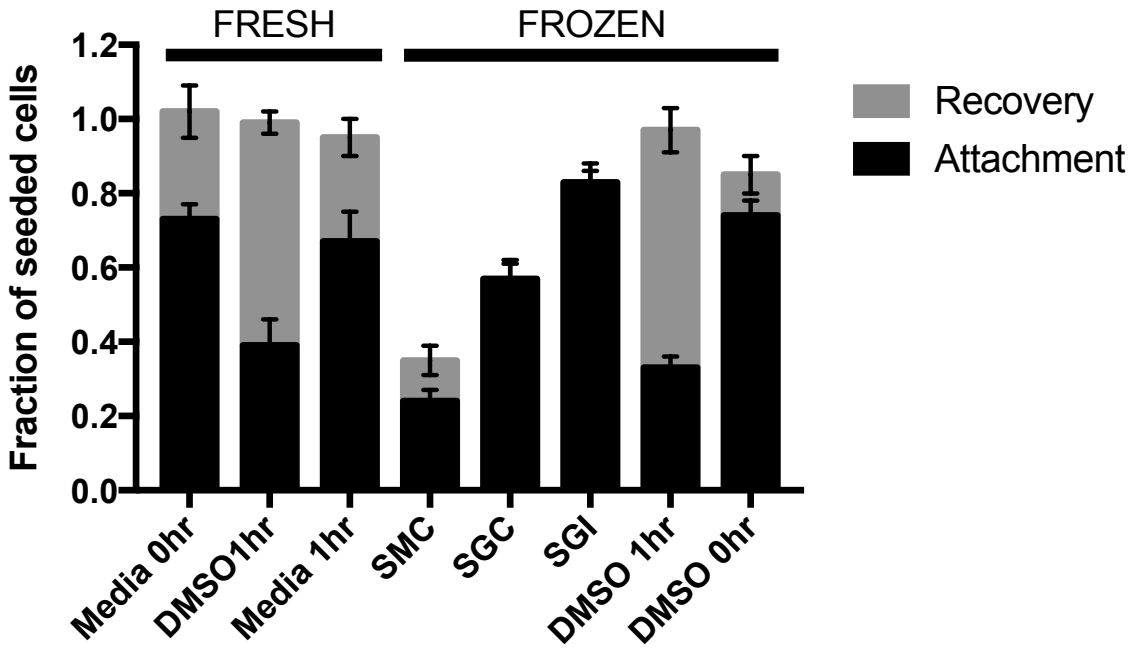

Figure 24: Optimized solution performance. Algorithm optimized solutions were combined with cells and assessed for recovery and attachment at 2hrs post thaw.

displayed significantly worse recovery ($p<0.05$) compared to fresh samples, but had attachment values that approached their total recovery.

Conversely, extended pre-freeze DMSO incubation did not reduce cell recovery, but significantly reduced the attachment of cells. This diminished attachment behavior appears to correlate with increasing pre-freeze DMSO incubation time (Figure 25) and this diminished attachment potential is still present in cells incubated with DMSO that do not undergo freezing (Figure 24).

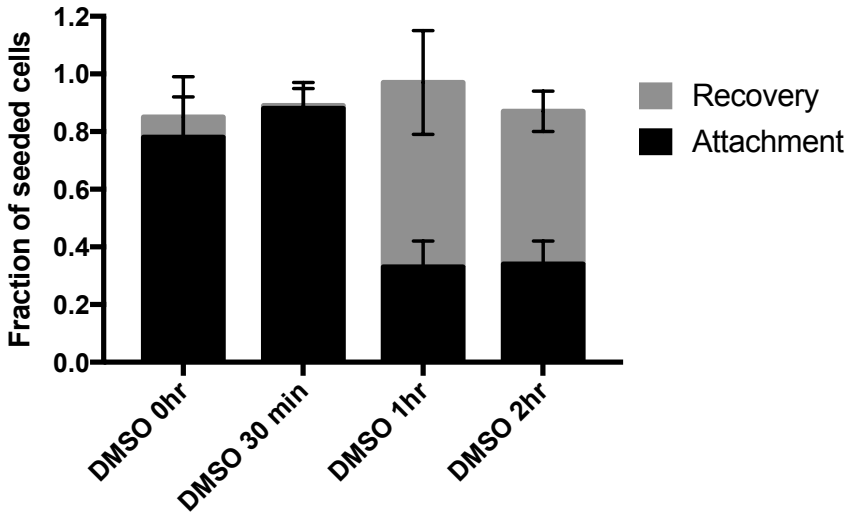

Figure 25: DMSO recovery and attachment as a function of pre-freeze incubation time.

8.3.2 MSC characterization

Both fresh and frozen H9 MSCs showed normal expression of positive (CD73, CD90, CD105) and negative (CD45) markers, summarized in Table 14 below, and were within the release thresholds for clinical samples. Freezing with DMSO and with experimental solutions did not change the expression of these markers significantly.

Table 14 MSC surface marker expression

	Fresh	SMC	SGC	SGI	DMSO 0Hr
CD105 (+)	99.9%	99.9%	99.8%	99.6%	99.6%
CD90 (+)	99.9%	99.9%	99.8%	99.6%	99.6%
CD73 (+)	99.8%	99.8%	99.6%	99.7%	99.9%
CD45 (-)	<1%	<1%	<1%	<1%	<1%

Cells displayed normal multi-lineage differentiation in all samples, as shown in Figure 26. Micromass cultures treated with chondrogenic differentiation media all showed characteristic blue color after staining with Alcian blue, indicating that these cultures accumulated proteoglycans appropriately. Cell monolayers treated with osteogenic differentiation media all showed characteristic red color after staining with Alizarin red, indicating these cultures accumulated calcium deposits appropriately.

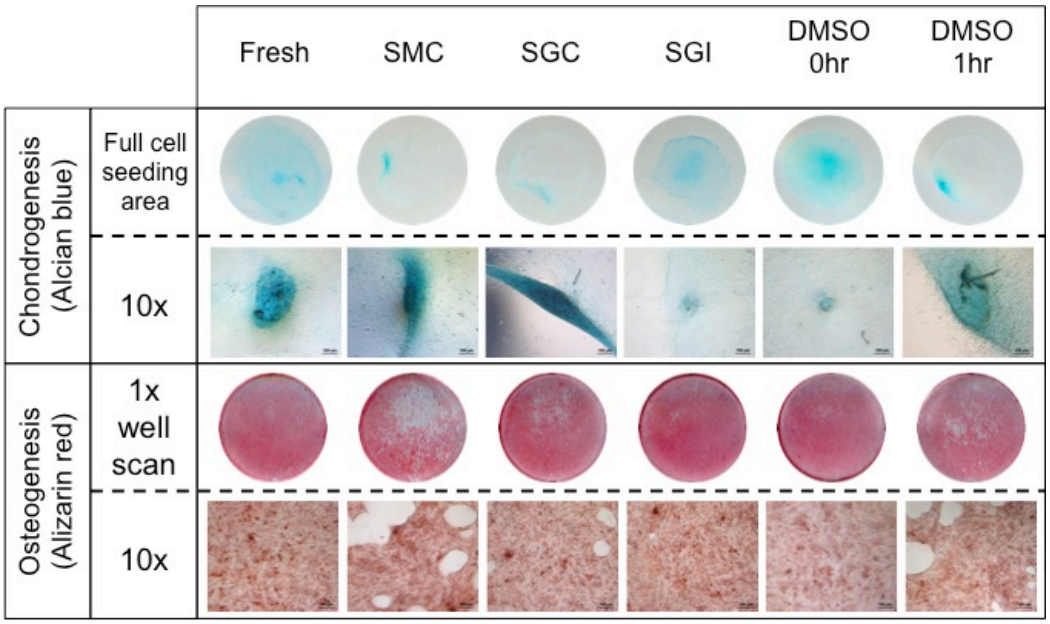

Figure 26 Multilineage differentiation staining of MSCs. Error bars in 10X images = 100μm

Analysis of proliferation (Figure 27) showed that proliferative capacity was maintained in SGI samples and was similar to both fresh and DMSO frozen samples, but was slightly reduced in SMC and SGC samples based on the reduced slope of their growth curves between 2hrs and 24hrs.

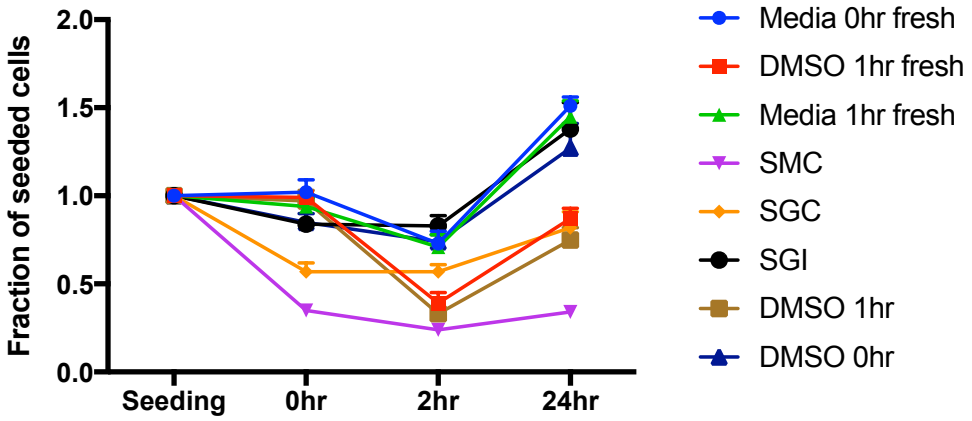

Figure 27: Proliferation of MSCs. Total cells were calculated from hemocytometer counts before freezing (seeding) and immediately after freezing (0hr), as well as from plate reader fluorescence values at 2hrs and 24hrs after thawing and plating. Values were normalized to initial seeding counts.

Senescence (Figure 28) did not vary significantly between samples. There were slight differences in senescence per cell at 2hrs, and these differences were reduced after 24hrs.

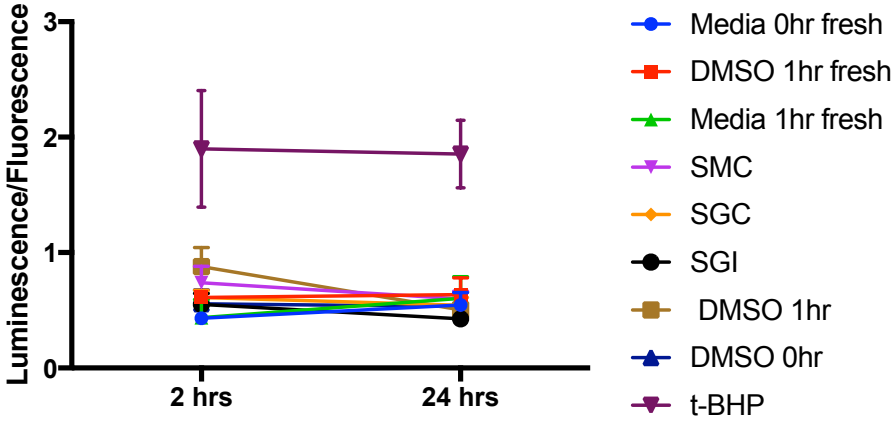

Figure 28: Senescence of MSCs. Beta-glo luminescence values and calcein fluorescence values from two identical plates were used to calculate luminescence/fluorescence, representing relative senescence per cell.

All samples showed significantly lower senescence than the positive control t-BHP treated cells.

8.3.3 Actin alignment analysis

MSCs cryopreserved in DMSO have demonstrated reduced engraftment, and this has been correlated to a disruption of the actin cytoskeleton[67, 68, 74]. Actin alignment in fresh low passage MSCs tends to be unidirectional (Figure 29A), with a majority of fibers oriented in a single direction along the axis of the cell as it undergoes extension. Visually, experimentally frozen cells (Figure 29B) more closely resemble fresh cells, while DMSO frozen cells (Figure 29C) have disrupted actin alignment.

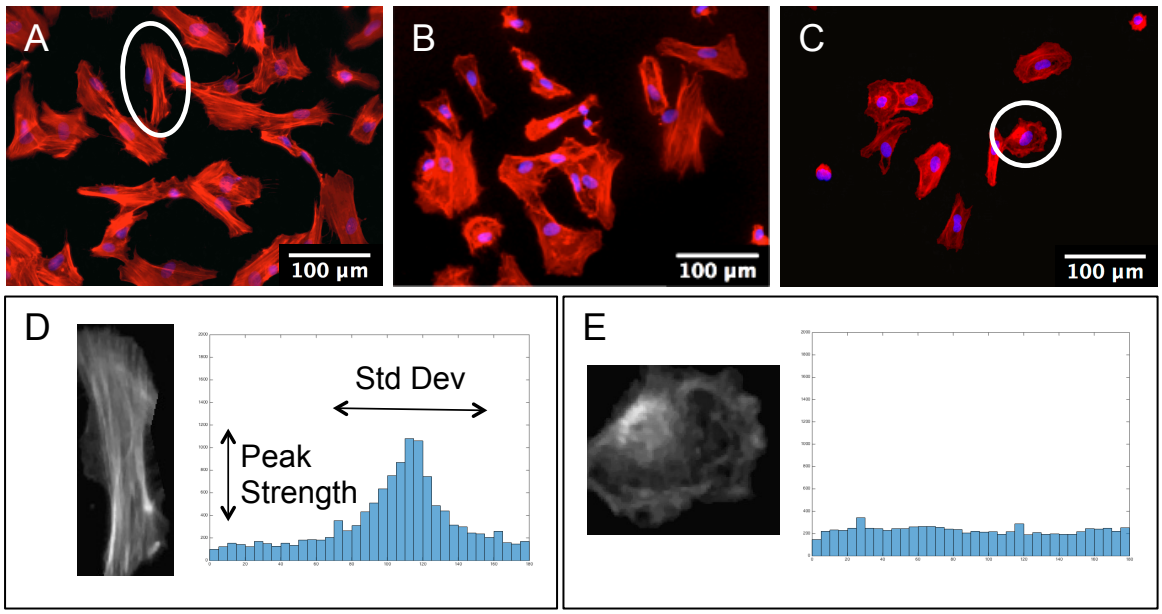

Figure 29: Actin images and representative histograms. Actin images represent (A) Fresh cells, (B) SGI frozen cells, and (C) DMSO 1hr frozen cells. Representative images from a (D) highly aligned cell from image A and a (E) poorly aligned cell from image C show that binned fiber alignment angle histograms for highly aligned cells have lower standard deviation and higher peak strength than fiber alignment angle histograms for poorly aligned cells.

A quantitative analysis of fiber alignment was performed for fresh and frozen samples by isolating fibers in Matlab, and binning each fiber alignment angle into a histogram. For highly aligned cells, this fiber alignment histogram has a clear peak (Figure 29D), while poorly aligned cells have no discernable peak (Figure 29E) with comparatively lower standard deviation and peak strength (peak strength = highest/lowest binned histogram value).

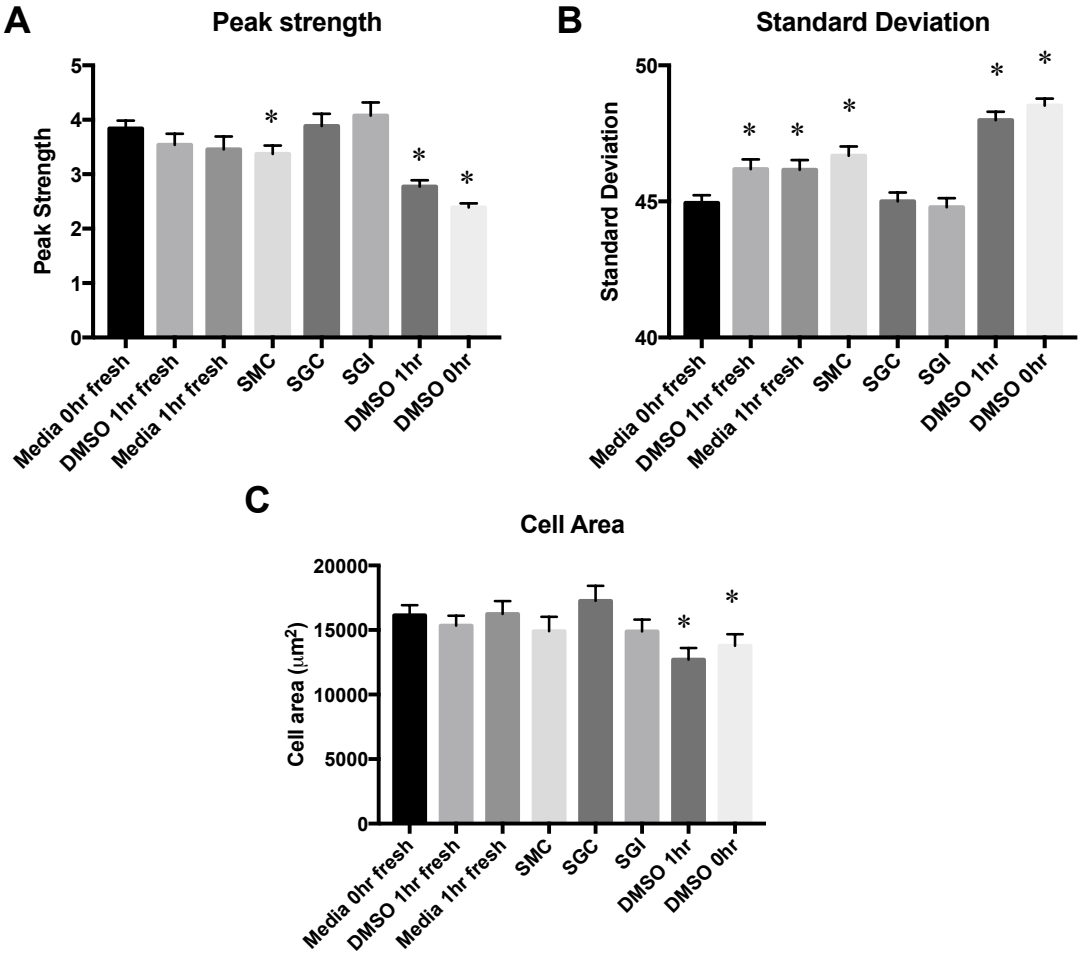

Figure 30: Quantitative actin alignment histogram analyses. (A) Peak strength (histogram highest bar/lowest bar). (B) Standard deviation. (C) Cell size.

The average peak strength (Figure 30A) and standard deviation (Figure 30B) for 90 individual cells were not statistically different between SMC, SGC, SGI samples and fresh samples, but were significantly worse for SMC and DMSO frozen samples regardless of incubation time. Additionally, the average cell size (Figure 30C) was significantly reduced for DMSO frozen cells compared to fresh samples, while and experimentally frozen samples were not significantly different from fresh.

8.3.4 qRT-PCR- Gene expression analysis

H9-MSCs subjected to different freezing approaches were assayed immediately post-thaw for the expression of genes related to trophic factor secretion such as HGF, VEGF, FGF-2, CXCL12 (SDF-1α), mesodermal lineage markers TWIST1, TWIST2 (DERMO1), MSX2, anti-apoptotic marker BCL-2, surface markers for cell adhesion such as CD106 and CD54, the osmotic regulator marker GAL-1, and stress-response markers such as EGR1 and NFE2L2 (NRF2). The gene expression data for these genes is summarized in Figure 32. These data show that the levels of HGF, an anti-scarring and anti-apoptotic factor, showed no differences between different freezing treatments and, as expected, the fresh media 0hr control showed the highest level of HGF expression. Similarly, different freezing conditions did not appear to have any marked effects in the expression of VEGF or FGF-2. In particular, FGF-2 levels were maintained at the same levels in all groups of H9 MSCs.

In a similar fashion, the expression levels of the mesodermal gene TWIST1 showed no significant variation between groups. On the other hand, the expression of TWIST2 was

elevated in almost all of the frozen groups (SMC, SGI, and DMSO freezing for 1 hour) except for SGC, which presented TWIST2 transcript levels comparable to fresh samples. Likewise, when comparing fresh and frozen samples, MSX2 levels were upregulated in all the frozen groups with no significant differences between freezing treatments.

H9-MSCs in fresh media showed no upregulation in CXCL12 gene expression. However, for frozen SMC and DMSO 1hr conditions, the levels were significantly higher. On the other hand, SGC did not affect CXCL12 expression and showed levels similar to that of fresh/unfrozen cells.

SMC, SGC and SGI treatments showed comparably high levels of GAL expression immediately post-thaw. Likewise, the expression of BCL-2, an apoptotic marker, showed a similar pattern in which frozen sample groups displayed higher BCL-2 expression than fresh cells.

The gene expression levels of MSC surface markers CD106 and CD54 for VCAM1 and ICAM1 were also evaluated. Both markers were present in H9-MSCs frozen with SMC, SGC and SGI, suggesting that the MSC adhesion molecule phenotype was not negatively altered for non-DMSO freezing conditions.

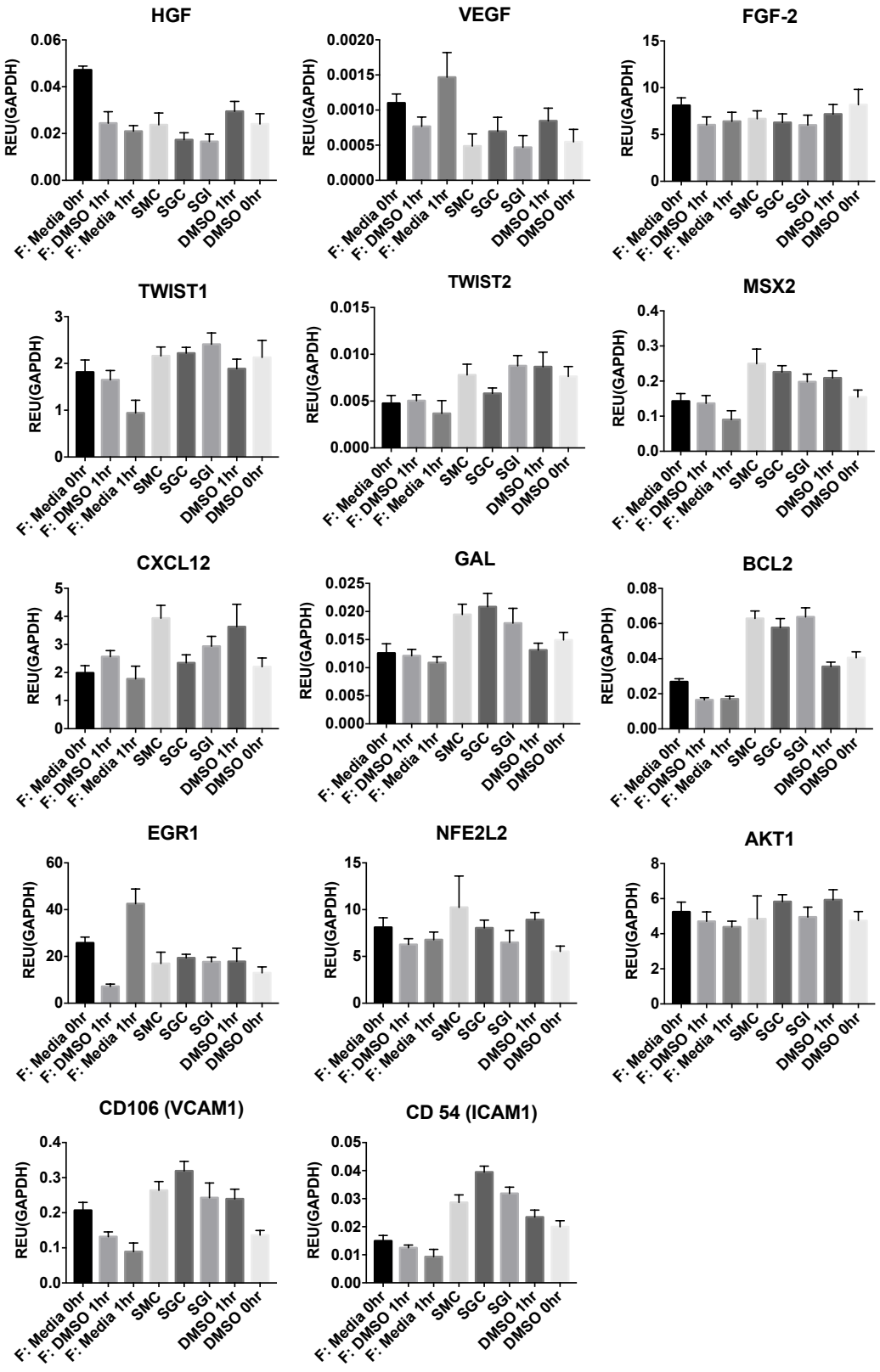

Figure 31: Gene expression profiles for H9 MSCs immediately post-thaw.

This study also included the assessment of stress-response genes such as EGR1 and NFE2L2. Intriguingly, EGR1 levels were highly expressed in the fresh media 1hr group and were significantly lower in the fresh 1hr DMSO incubated samples and in all frozen groups. The expression of NFE2L2 was uniformly similar among all the treatment groups and was not affected by different freezing methods.

8.3.5 Epigenetics - DNA hydroxymethylation

Visual inspection of DNA hydroxymethylation dot blotting (Figure 33A) shows that as predicted, the control fresh media 0hr incubation state displays the lightest staining and thus the lowest degree of hydroxymethylation. The darkest dots appear for SMC and DMSO 1hr (fresh and frozen) incubated samples. This indicates that extended incubation in these solutions causes increases in DNA hydroxymethylation, and that these epigenetic changes may be responsible for some of the negative functional behavior observed for these conditions.

Quantification of these dot-blots (Figure 33B) shows that only SMC frozen samples exhibit statistically significantly higher DNA hydroxymethylation than fresh media 0hr control cells ($p<0.05$). None of the other samples showed hydroxymethylation significantly higher than fresh controls.

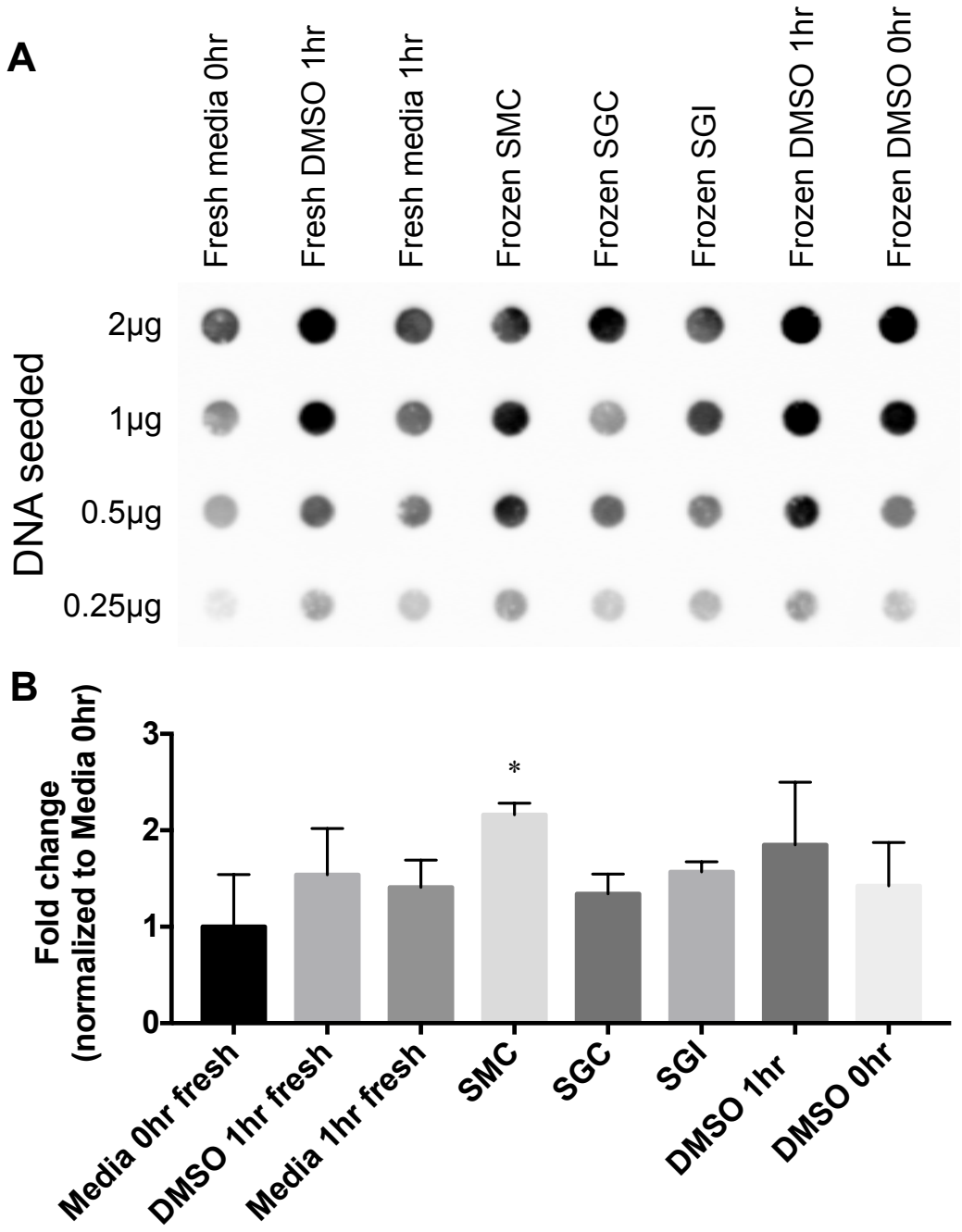

Figure 32: Dot blotting for DNA hydroxymethylation. (A) Representative dot blot of one of the three biological triplicates performed. Darker dots indicate greater DNA hydroxymethylation. (B) Quantified DNA hydroxymethylation results, scaled for dilution linearity within each biological replicate, normalized to Media 0hr fresh, and averaged for three biological replicates. SMC was the only sample significantly different from Media 0hr fresh ($p<0.05$).

8.4 Discussion

MSCs are known to exhibit impaired function after cryopreservation in DMSO, and systematic algorithm optimization of non-DMSO freezing solutions may result in more functional post-thaw cell products. Care must be taken to rationally select a return metric for the algorithm that optimizes crucial post-thaw cellular potency characteristics. In this case, cryopreserved MSCs have shown impaired homing and engraftment potential[163] that may be related to cytoskeletal structural problems[74], and selecting attachment as a return metric ensures that the optimized solution will at least partially promote healthy cytoskeletal assembly and function. This chapter confirms that functionality metrics such as attachment can be used for algorithm iteration as opposed to recovery, the metric used in Chapter 7. Using this strategy, both attachment and recovery improved with increasing generations, and resulted in more functional post thaw cells as confirmed by the additional functionality testing performed in this chapter.

The attachment and recovery of cells frozen in optimized SGI solutions were similar to the attachment and recovery observed for fresh and DMSO 0hr frozen samples. Recovery was lower in SMC and SGC samples, indicating that the maximum recovery possible differs for optimized solutions containing different components. However, the differences between attachment and recovery were low for all experimental solutions, whereas samples incubated with DMSO for at least 1 hour exhibited a significant reduction in attached cells. This indicates that total recovery observed post-thaw for

experimental solutions may better reflect their functional capacity vs. DMSO incubated cells.

Cells were evaluated for well-accepted minimal characterization criteria[18] post-thaw to determine if freezing in experimental solutions altered fundamental aspects of cellular identity. Cell surface marker expression and differentiation did not differ markedly between any fresh or frozen samples. Additionally, proliferation was not substantially reduced in cells frozen in experimental vs. fresh cells. The doubling rate was slightly lower in SMC and SGC samples between 2 and 24 hours post-thaw, and this may be reflective of the poor recovery (and increased dead cells present) in those samples post-thaw. These dead cells may release cytokines, or other cellular stress products that negatively impact proliferation. Cumulatively, these results are consistent with work by other groups that shows cryopreservation does not negatively impact MSC surface marker expression, differentiation, or proliferation [129–131, 164].

Senescence was not significantly different between frozen and fresh samples, and all conditions were significantly lower than a positive control induced for senescence via t-BHP treatment. Elevated senescence in some samples at 2hrs post-thaw followed by a reduction at 24 hours may indicate a transient stress response. This phenomenon could be explained by a reversal of the senescent state or a drowning out/reduction of the senescent signal due to proliferation of non-senescent cells in the population, and is

similar to the senescence trends observed in cells immediately and 48 hours post-thaw in Chapter 4.

Poor actin alignment/assembly is a known problem associated with MSC freezing in DMSO, and is suspected to correlate with poor homing and engraftment of these cells post-thaw[123]. An analysis of actin alignment in both fresh and frozen cells shows that DMSO incubation, and not freezing in general, may be responsible for this altered cytoskeletal behavior. The reduced peak strength and standard deviation of binned actin fiber alignment angle in DMSO frozen samples may also play a role in the differences in cell area observed in these cells. Reduced actin alignment can result in reduced cellular extension, leading to reduced cell area. This altered cellular morphology may also influence gene expression, affecting functional behavior downstream of that expression.

The genes analyzed in qRT-PCR were selected from recent literature summarizing functionality and potency recommendations including a recent ISCT review[165], and previous work by Samsonraj et al[155]. This panel included genes for growth factors, adhesion molecules, transcription factors, chemokines, and stress genes. All genes were compared to a GAPDH internal control, and the additional AKT1 internal housekeeping control confirms that the total amount of seeded RNA was similar for all samples. Trophic factors such as HGF, VEGF, and FGF-2, which share anti-apoptotic properties, did not show significant differences between frozen samples. HGF, an important proliferation and migration regulating molecule[166], exhibited reduced expression in all

samples compared to a fresh 0hr control. This implies that cellular challenges including room temperature incubation and freezing may reduce proliferative cell fitness. However, this phenomenon was observed in all frozen samples, indicating that experimentally frozen cells are no worse than DMSO frozen cells in this regard. Additionally, FGF-2 did not show differences between fresh or frozen samples. Based on this data, experimentally frozen cells do not show a reduction in angiogenic or anti-apoptotic fitness *in vitro* immediately post-thaw compared to currently available alternatives such as DMSO.

Comparatively, mesodermal lineage markers TWIST-1, TWIST-2, and MSX-2 exhibit upregulated expression in frozen samples compared to fresh. Similar to the trophic genes above, these differences are consistent between experimental and DMSO freezing, indicating that experimental solutions did not have detrimental effects on mesodermal marker expression compared to current DMSO freezing. These gene expression effects may be transient, as differentiation potential was maintained in all samples post-thaw as evidenced by the differentiation results presented in Figure 26.

The chemokine CXCL12 (SDF-1α) is secreted by MSCs in response to tissue injury and/or inflammation. For frozen SMC and DMSO 1hr conditions, the levels of CXCL12 were significantly higher, suggesting that SMC and DMSO treatments may create an adverse inflammatory environment *in vitro,* which the MSCs respond to by preparing to secrete CXCL12. It is interesting to note that CXCL12 expression for SMC freezing was

higher than for 0hr DMSO freezing, indicating that SMC freezing may have stronger negative effects on MSCs than current DMSO freezing protocols, contraindicating its use as a replacement for DMSO. However, other stress response genes EGFR1 and NFE2L2 were similar or reduced for all frozen samples compared to fresh media 0hr controls, indicating that experimental freezing did not significantly alter the stress state of the cell.

The GAL (galanin) gene plays a role in osmotic regulation in cells and was found to be upregulated in MSCs subjected to experimental freezing conditions. Expression of the anti-apoptotic marker BCL-2, and cell surface adhesion molecules CD106(VCAM1) and CD54 (ICAM1) showed similar trends. These patterns are a promising indication that transcription of genes responsible for protecting different areas of the cell (including osmotic regulation, apoptosis and cell adhesion) during freezing is upregulated for experimental solutions, but not for DMSO. The differences in expression of the cell surface adhesion molecules observed here may also help explain the downstream attachment and actin alignment differences observed between experimentally and DMSO frozen cells.

DNA hydroxymethylation results indicated that as expected, fresh media 0hr control cells had the lowest levels of epigenetic alteration. The only sample that exhibited significantly higher hydroxymethylation than the fresh 0hr control was SMC, although both 1hr incubated fresh and frozen DMSO samples had visibly darker dot blots than SGC and SGI samples in all three biological replicates. Because the darkness trends for

all other samples remained consistent vs. fresh media 0hr controls, the large error bars present are likely due to the semi-quantitative nature of the assay and subsequent analysis.

8.5 Conclusion

This chapter shows that algorithm can be iterated for functionality metrics including attachment. Cells frozen in algorithm optimized solutions exhibited similar post-thaw minimal functionality criteria, including cell surface marker expression, differentiation, and proliferation. Senescence was not markedly different between fresh and frozen samples post-thaw, and was significantly lower than positive control t-BHP treated samples. Experimentally frozen cells exhibited significantly better attachment than 1hr incubated DMSO fresh and frozen cells, and significantly better actin alignment according to peak strength and standard deviation analysis of fiber angle distribution histograms. Fresh and experimentally frozen cells were also significantly larger than DMSO frozen cells. RNA expression of most genes was not significantly different between frozen samples, but was upregulated in experimental samples for cell adhesion surface markers (CD106, CD54), osmotic regulation (GAL), and anti-apoptosis (BCL-2) genes. DNA hydroxymethylation results showed no significant differences between samples apart from SMC, which was significantly higher than the fresh media 0hr control.

This chapter confirms that non-DMSO experimental solutions can be used to freeze cells effectively to preserve recovery, and results in maintenance or improvement of post-thaw function compared to DMSO frozen samples.

Chapter 9

Conclusions/Future Work

9.1 Conclusions

The replacement of DMSO as a cryoprotective is a necessary future step for some transfusion therapies. This research proposed to eliminate DMSO for the cryopreservation of MSCs, and to fulfill this goal we hypothesized that:

A combination of non-DMSO cryopreservative agents will act in concert to maintain cellular viability and function throughout the freezing process.

We confirmed this hypothesis by fulfilling the following aims in Chapters 5-8.

Aim 1 – Identify combinations of solution components likely to result in high post-thaw cell recovery, and establish potential mechanisms of cryo-protection for these combinations.

Aim 1.1 –Identify solution combinations most likely to result in high post-thaw cell recovery.

In Chapter 5, candidate solutions that included compounds from several cryoprotective categories were screened to identify compositions that maximized recovery in cells after undergoing freezing and thawing. This chapter directly tested the hypothesis that combinations of compounds are capable of protecting cells during cryopreservation by comparing 1, 2, and 3 component solutions. Constant concentrations of components

from each molecule family were incubated with cells and subsequently frozen in 96 well plates at different cooling rates. Thawed cells in these solutions were evaluated for recovery and analyzed statistically to determine which combinations maximized cellular viability and recovery post-thaw. Findings from this chapter include that selection of cooling rate and sugar in solution appears to predict solution recovery more strongly than either alcohol or additive. Additionally, 2 and 3 components outperformed single component solutions across the board, especially when they included a sugar. Due to the high performance of sucrose at 3°C/min, this cooling rate was selected for future use in Chapters 6 and 8. The experiments presented in Chapter 5 fulfill Aim 1.1.

Aim 1.2 – Identify mechanisms of cryoprotection for multicomponent solutions

In Chapter 6, solutions containing Sucrose/Glycerol/Creatine and Sucrose/Mannitol/Creatine (components identified as promising combinations in Chapter 5/Aim 1.1) were combined with cells and evaluated to determine the mechanisms by which they protect cells during cryopreservation. Incubation time, osmolarity, component distribution in the frozen state, physical changes during freezing, and component specificity were evaluated to determine which elements of solution behavior are important to consider when performing optimization. Important findings from Chapter 6 include that incubation time must be sufficient for penetration of all components included in solution to maximize recovery, concentration of components (not total osmolarity) determines recovery, and molecular substitution of monosaccharides to replace disaccharides results in a reduction in recovery. We hypothesize that these differences are biological, as we have found no evidence of physical changes in ice crystal formation

between different solutions with similar osmolarity. Ultimately, these observations increase our understanding of multicomponent solution behavior, and fulfill Aim 1.2.

Aim 2 - Establish and validate differential evolution algorithm for predictive optimization of solution components, concentrations, and freezing rates.

In Chapter 7, we validated that the DE algorithm could be used to optimize 3-5 component solutions, with or without including cooling rate as an optimization variable. High throughput 96-well plate experiments were performed using MSCs and Jurkats as a model cell type, and recovery was iterated to the algorithm as the return metric for the cost function. Optimized solution concentrations were converged upon within 6-9 generations, and confirm that optimums can be identified using a DE algorithm with significantly fewer experiments than traditional factorial strategies. High throughput liquid handling experiments were performed to screen all potential combinations at a single cooling rate, and verify that the optimum identified by the algorithm was indeed the optimum of the system. These experiments validated that the algorithm can be used for predictive optimization of cryopreservation solutions, and fulfill Aim 2.

Aim 3 – Iterate algorithm to optimize cryopreservation solutions for MSCs, and confirm optimized solutions maintain cellular function post-thaw.

In Chapter 8, MSCs were optimized for attachment (a functional metric) in solutions of SMC, SGC, and SGI. The optimized solution compositions resulting from algorithm

iteration were frozen with cells and evaluated for additional post-thaw functionality metrics including attachment, proliferation, senescence, cell surface marker expression, multi-lineage differentiation capacity, cytoskeletal alteration, changes in RNA expression, and epigenetic changes. These functional characteristics were compared between cells frozen in experimental solutions, fresh cells, non-frozen cells incubated with DMSO, and cells frozen with traditional 10% DMSO. These comparisons were used to determine if freezing, DMSO incubation, or a combination of the two is responsible for the current changes observed in functionality for DMSO frozen cells.

Important findings from Chapter 8 include that experimentally frozen cells exhibited significantly better attachment than 1hr incubated DMSO fresh and frozen cells, and significantly better actin alignment according to analysis of fiber angle distribution histograms. Additionally, RNA expression was upregulated in experimental samples for cell adhesion surface markers, osmotic regulation, and anti-apoptosis genes. Other functional characterization metrics showed little difference between experimental and DMSO frozen samples. Chapter 8 experiments fulfill Aim 3.

In addressing these specific aims, we have found that it is possible to optimize non-DMSO cryopreservation of MSCs using an evolutionary algorithm, and that the cells resultant from freezing in multicomponent solutions display functional behavior that is maintained or improved compared to DMSO freezing. However, additional testing is necessary to validate these solutions as replacements for DMSO in cell therapy cryopreservation.

9.2 Future Work

Before the results of this research can be translated into clinical cell therapies, additional *in vitro*, *in vivo*, and clinical studies should be performed to validate the functionality and effectiveness of cells frozen in these solutions. Additionally, this optimization platform and strategy can be applied to other applications.

9.2.1 Validation and clinical application of current therapies

The research described in chapters 5-8 was performed using H9 MSCs, a clonal culture cell line of embryonic stem cell derived Mesenchymal stem cells. This decision was made due to the high variability in behavior between MSC samples from other sources, as shown in Chapter 4. H9 MSCs were selected for optimization experiments to eliminate this variability and make batch-to-batch comparisons possible. However, it is important to evaluate whether cryopreservation results from H9 MSC experiments are translatable to clinical sources of MSCs that would be used for patient cell therapy. Work is currently underway in the Hubel lab to characterize the response of Bone marrow derived MSCs to freezing in solutions optimized for H9-MSCs, and these cells are being evaluated for the same post-thaw functionality characteristics described in Chapter 8.

The work here comprises single cell type studies. In order to better evaluate the physiological fitness of MSCs cryopreserved in experimental solutions, additional multi cell-type studies should be performed. MSCs are known to modulate the immune system by inhibiting t-cell proliferation, and there are established assays to evaluate MSC

inhibition of t-cell proliferation *in vitro*. Briefly, cryopreserved and control MSCs can be co-cultured with different ratios of peripheral blood mononuclear cells (PBMCs, t-cells) to determine the level of proliferation inhibition that results[10]. MSCs with higher fitness can more effectively inhibit t-cell proliferation.

The experimental solutions optimized in Chapter 8 showed significant improvements in actin alignment and increases in cell surface adhesion molecule expression compared to cells frozen in DMSO. In order to determine if these *in vitro* characteristics correlate to *in vivo* improvements, murine studies should be performed to evaluate the migration and engraftment potential of these cells in an animal model. Mouse models have been used previously by other groups to evaluate the bio distribution of DMSO frozen cells[74]. Briefly, human MSCs with varying fitness (fresh, experimentally frozen, or DMSO frozen conditions) would be injected into mice intravenously via the tail vein. If migration and engraftment fitness are high, the cells should be capable of engrafting into the mouse lung tissue, and if fitness is low, human cells will be cleared from the system after failing to engraft. After 24 hours, lung tissue from the sacrificed mice can be processed to quantify the level of human DNA present, and thus determine the relative success of engraftment for various freezing conditions.

If these co-culture and *in vivo* studies show that the experimental freezing solutions we've optimized in Chapter 8 display sufficient fitness, continued clinical translation might be indicated. Solution components used in Chapter 8 are available as cGMP

products, and the concentrations present in Chapter 8 solutions are at or below the concentrations listed by the FDA for non-active ingredients in currently approved products. The Dietz research group at Mayo hospital has identified groups of patients with advanced Crohn's disease and fistulas that are not eligible to receive current DMSO cryopreserved MSC treatments due to the negative DMSO interactions predicted to occur upon transfusion. This group represents a patient population that would benefit from compassionate care studies using cells cryopreserved in our non-DMSO solutions, as they have exhausted other treatment options.

9.2.2 Alternative application of optimization strategy

Thus far, we have utilized the DE algorithm to optimize 3-5 component solutions. We have limited the composition of solutions to include a single sugar, a single sugar alcohol, and 1-3 small molecule additives. The components that have undergone screening are summarized in Chapter 4 (Table 8), and represent a limited selection of molecules from each of these categories. In the future, additional molecules from each of these categories should be screened, and different combinations of these molecules should also be evaluated. For example, we have seen enhanced effectiveness in solutions that contain high levels of sugar alcohols, and it would be interesting to see whether solutions that include multiple sugar alcohols in solution exhibit improvements in freezing performance.

We have applied the DE optimization algorithm to a limited number of cell types, including Jurkats, a model lymphocyte suspension cell, and H9 MSCs. Now that the algorithm platform is well established, it would be straightforward to apply algorithm optimization to other cryo-sensitive cell types. Other cell types including cardiomyocytes, t-cells, natural killer cells, and iPS cells display high levels of cell death or impaired post-thaw cell function following cryopreservation with DMSO. Algorithm optimization of non-DMSO solutions or DMSO containing solutions may produce cells with improved post-thaw recovery or fitness.

The experiments performed in this work and experiments performed in the future will improve our understanding of cell responses during the cryopreservation process. Superior solutions identified through optimization can improve the fitness of cryopreserved cells, improve the quality and availability of treatments, and ultimately, improve patient care.

Bibliography

1. Wang S, Qu X, Zhao R, et al. Clinical applications of mesenchymal stem cells. **J. HEMATOL. ONCOL.** 2012;5(1):19. Available at: http://jhoonline.biomedcentral.com/articles/10.1186/1756-8722-5-19. Accessed August 1, 2016.
2. Anon. Search of: mesenchymal stem cells - List Results - ClinicalTrials.gov. **CLINICALTRIALS.GOV** . Available at: https://clinicaltrials.gov/ct2/results?term=mesenchymal+stem+cells&Search=Search. Accessed September 3, 2016.
3. Sharma RR, Pollock K, Hubel A, et al. Mesenchymal stem or stromal cells: a review of clinical applications and manufacturing practices. **TRANSFUSION** 2014;54(5):1418–1437. Available at: http://doi.wiley.com/10.1111/trf.12421. Accessed May 27, 2016.
4. Hubel A. Advancing the preservation of cellular therapy products. **TRANSFUSION** 2011;51(SUPPL. 4).
5. Pruksananonda K, Rungsiwiwut R, Numchaisrika P, et al. Eighteen-Year Cryopreservation Does Not Negatively Affect the Pluripotency of Human Embryos: Evidence from Embryonic Stem Cell Derivation. **BIORES. OPEN ACCESS** 2012;1(4):166–173. Available at: http://online.liebertpub.com/doi/abs/10.1089/biores.2012.0242. Accessed September 3, 2016.
6. Shen J, Huang Y, Xu S, et al. Effectiveness of human mesenchymal stem cells derived from bone marrow cryopreserved for 23–25years. **CRYOBIOLOGY** 2012;64(3):167–175.
7. Mazur P. Freezing of living cells: mechanisms and implications. **AM. J. PHYSIOL. CELL. PHYSIOL.** 1984;247(3):C125–142. Available at: http://ajpcell.physiology.org/content/247/3/C125.
8. Windrum P, Morris TCM, Drake MB, et al. Variation in dimethyl sulfoxide use in stem cell transplantation: a survey of EBMT centres. **BONE MARROW TRANSPLANT.** 2005;36(7):601–603. Available at: http://www.nature.com/doifinder/10.1038/sj.bmt.1705100. Accessed August 1, 2016.
9. Carvalho KAT, Cury CC, Oliveira L, et al. Evaluation of Bone Marrow Mesenchymal Stem Cell Standard Cryopreservation Procedure Efficiency. **TRANSPLANT. PROC.** 2008;40(3):839–841.
10. François M, Copland IB, Yuan S, et al. Cryopreserved mesenchymal stromal cells display impaired immunosuppressive properties as a result of heat-shock response and impaired interferon-γ licensing. **CYTOTHERAPY** 2012.
11. Storn R, Price K. Differential Evolution -- A Simple and Efficient Heuristic for global Optimization over Continuous Spaces. **J. GLOB. OPTIM.** 1997;11(4):341–359. Available at: http://dx.doi.org/10.1023/A:1008202821328.
12. Friedenstein AJ, Petrakova K V, Kurolesova AI, et al. Heterotopic of bone marrow. Analysis of precursor cells for osteogenic and hematopoietic tissues. **TRANSPLANTATION** 1968;6(2):230–47. Available at: http://www.ncbi.nlm.nih.gov/pubmed/5654088. Accessed September 3, 2016.
13. Zuk PA, Zhu M, Ashjian P, et al. Human adipose tissue is a source of multipotent stem cells. **MOL. BIOL. CELL** 2002;13(12):4279–95. Available at: http://www.ncbi.nlm.nih.gov/pubmed/12475952. Accessed September 3, 2016.
14. Anker PS In 't, Scherjon SA, Kleijburg-van der Keur C, et al. Isolation of mesenchymal stem cells of fetal or maternal origin from human placenta. **STEM CELLS** 2004;22(7):1338–45. Available at: http://www.ncbi.nlm.nih.gov/pubmed/15579651. Accessed September 3, 2016.
15. Wagner W, Wein F, Seckinger A, et al. Comparative characteristics of mesenchymal stem cells from

human bone marrow, adipose tissue, and umbilical cord blood. **EXP. HEMATOL.** 2005;33(11):1402–16. Available at: http://www.ncbi.nlm.nih.gov/pubmed/16263424. Accessed September 3, 2016.

16. Kern S, Eichler H, Stoeve J, et al. Comparative analysis of mesenchymal stem cells from bone marrow, umbilical cord blood, or adipose tissue. **STEM CELLS** 2006;24(5):1294–301. Available at: http://www.ncbi.nlm.nih.gov/pubmed/16410387. Accessed September 3, 2016.
17. Bochev I, Elmadjian G, Kyurkchiev D, et al. Mesenchymal stem cells from human bone marrow or adipose tissue differently modulate mitogen-stimulated B-cell immunoglobulin production in vitro. **CELL BIOL. INT.** 2008;32(4):384–93. Available at: http://www.ncbi.nlm.nih.gov/pubmed/18262807. Accessed September 3, 2016.
18. Dominici M, Blanc K Le, Mueller I, et al. Minimal criteria for defining multipotent mesenchymal stromal cells. The International Society for Cellular Therapy position statement. **CYTOTHERAPY** 2006;8(4):315–7. Available at: http://www.sciencedirect.com/science/article/pii/S1465324906708817.
19. Bieback K, Kinzebach S, Karagianni M. Translating research into clinical scale manufacturing of mesenchymal stromal cells. **STEM CELLS INT.** 2011;2010:193519. Available at: http://www.ncbi.nlm.nih.gov/pubmed/21318154. Accessed August 23, 2016.
20. Otto WR, Wright NA. Mesenchymal stem cells: from experiment to clinic. **FIBROGENESIS TISSUE REPAIR** 2011;4:20. Available at: http://www.ncbi.nlm.nih.gov/pubmed/21902837. Accessed September 3, 2016.
21. Lazarus HM, Haynesworth SE, Gerson SL, et al. Ex vivo expansion and subsequent infusion of human bone marrow-derived stromal progenitor cells (mesenchymal progenitor cells): implications for therapeutic use. **BONE MARROW TRANSPLANT.** 1995;16(4):557–64. Available at: http://www.ncbi.nlm.nih.gov/pubmed/8528172. Accessed September 3, 2016.
22. Liechty KW, MacKenzie TC, Shaaban AF, et al. Human mesenchymal stem cells engraft and demonstrate site-specific differentiation after in utero transplantation in sheep. **NAT. MED.** 2000;6(11):1282–6. Available at: http://www.ncbi.nlm.nih.gov/pubmed/11062543. Accessed September 3, 2016.
23. Popp FC, Eggenhofer E, Renner P, et al. Mesenchymal stem cells can induce long-term acceptance of solid organ allografts in synergy with low-dose mycophenolate. **TRANSPL. IMMUNOL.** 2008;20(1-2):55–60. Available at: http://www.ncbi.nlm.nih.gov/pubmed/18762258. Accessed September 3, 2016.
24. Tse WT, Pendleton JD, Beyer WM, et al. Suppression of allogeneic T-cell proliferation by human marrow stromal cells: implications in transplantation. **TRANSPLANTATION** 2003;75(3):389–97. Available at: http://www.ncbi.nlm.nih.gov/pubmed/12589164. Accessed September 3, 2016.
25. Sotiropoulou PA, Perez SA, Gritzapis AD, et al. Interactions between human mesenchymal stem cells and natural killer cells. **STEM CELLS** 2006;24(1):74–85. Available at: http://www.ncbi.nlm.nih.gov/pubmed/16099998. Accessed September 3, 2016.
26. Nasef A, Mathieu N, Chapel A, et al. Immunosuppressive effects of mesenchymal stem cells: involvement of HLA-G. **TRANSPLANTATION** 2007;84(2):231–7. Available at: http://www.ncbi.nlm.nih.gov/pubmed/17667815. Accessed September 3, 2016.
27. Sundin M, Ringdén O, Sundberg B, et al. No alloantibodies against mesenchymal stromal cells, but presence of anti-fetal calf serum antibodies, after transplantation in allogeneic hematopoietic stem cell recipients. **HAEMATOLOGICA** 2007;92(9):1208–15. Available at: http://www.ncbi.nlm.nih.gov/pubmed/17666368. Accessed September 3, 2016.

28. Nicola M Di, Carlo-Stella C, Magni M, et al. Human bone marrow stromal cells suppress T-lymphocyte proliferation induced by cellular or nonspecific mitogenic stimuli. **BLOOD** 2002;99(10):3838–43. Available at: http://www.ncbi.nlm.nih.gov/pubmed/11986244. Accessed September 3, 2016.
29. Zhang W, Ge W, Li C, et al. Effects of mesenchymal stem cells on differentiation, maturation, and function of human monocyte-derived dendritic cells. **STEM CELLS DEV.** 2004;13(3):263–71. Available at: http://www.ncbi.nlm.nih.gov/pubmed/15186722. Accessed September 3, 2016.
30. Zhang B, Liu R, Shi D, et al. Mesenchymal stem cells induce mature dendritic cells into a novel Jagged-2-dependent regulatory dendritic cell population. **BLOOD** 2009;113(1):46–57. Available at: http://www.ncbi.nlm.nih.gov/pubmed/18832657. Accessed September 3, 2016.
31. Corcione A, Benvenuto F, Ferretti E, et al. Human mesenchymal stem cells modulate B-cell functions. **BLOOD** 2006;107(1):367–72. Available at: http://www.ncbi.nlm.nih.gov/pubmed/16141348. Accessed September 3, 2016.
32. Asari S, Itakura S, Ferreri K, et al. Mesenchymal stem cells suppress B-cell terminal differentiation. **EXP. HEMATOL.** 2009;37(5):604–15. Available at: http://www.ncbi.nlm.nih.gov/pubmed/19375651. Accessed September 3, 2016.
33. Spaggiari GM, Capobianco A, Becchetti S, et al. Mesenchymal stem cell-natural killer cell interactions: evidence that activated NK cells are capable of killing MSCs, whereas MSCs can inhibit IL-2-induced NK-cell proliferation. **BLOOD** 2006;107(4):1484–90. Available at: http://www.ncbi.nlm.nih.gov/pubmed/16239427. Accessed September 3, 2016.
34. Aggarwal S, Pittenger MF. Human mesenchymal stem cells modulate allogeneic immune cell responses. **BLOOD** 2005;105(4):1815–22. Available at: http://www.ncbi.nlm.nih.gov/pubmed/15494428. Accessed August 1, 2016.
35. English K, Ryan JM, Tobin L, et al. Cell contact, prostaglandin E(2) and transforming growth factor beta 1 play non-redundant roles in human mesenchymal stem cell induction of CD4+CD25(High) forkhead box P3+ regulatory T cells. **CLIN. EXP. IMMUNOL.** 2009;156(1):149–60. Available at: http://www.ncbi.nlm.nih.gov/pubmed/19210524. Accessed September 3, 2016.
36. Matthay MA, Thompson BT, Read EJ, et al. Therapeutic potential of mesenchymal stem cells for severe acute lung injury. **CHEST** 2010;138(4):965–72. Available at: http://www.ncbi.nlm.nih.gov/pubmed/20923800. Accessed September 3, 2016.
37. Devine SM, Cobbs C, Jennings M, et al. Mesenchymal stem cells distribute to a wide range of tissues following systemic infusion into nonhuman primates. **BLOOD** 2003;101(8):2999–3001. Available at: http://www.ncbi.nlm.nih.gov/pubmed/12480709. Accessed September 3, 2016.
38. Phinney DG, Prockop DJ. Concise review: mesenchymal stem/multipotent stromal cells: the state of transdifferentiation and modes of tissue repair--current views. **STEM CELLS** 2007;25(11):2896–902. Available at: http://www.ncbi.nlm.nih.gov/pubmed/17901396. Accessed September 3, 2016.
39. Spaeth E, Klopp A, Dembinski J, et al. Inflammation and tumor microenvironments: defining the migratory itinerary of mesenchymal stem cells. **GENE THER.** 2008;15(10):730–8. Available at: http://www.ncbi.nlm.nih.gov/pubmed/18401438. Accessed September 3, 2016.
40. Yagi H, Soto-Gutierrez A, Parekkadan B, et al. Mesenchymal stem cells: Mechanisms of immunomodulation and homing. **CELL TRANSPLANT.** 2010;19(6):667–79. Available at: http://www.ncbi.nlm.nih.gov/pubmed/20525442. Accessed September 3, 2016.
41. Pittenger MF, Mackay AM, Beck SC, et al. Multilineage potential of adult human mesenchymal stem cells. **SCIENCE** 1999;284(5411):143–7. Available at: http://www.ncbi.nlm.nih.gov/pubmed/10102814. Accessed September 3, 2016.
42. Jiang Y, Jahagirdar BN, Reinhardt RL, et al. Pluripotency of mesenchymal stem cells derived from

adult marrow. **NATURE** 2002;418(6893):41–9. Available at: http://www.ncbi.nlm.nih.gov/pubmed/12077603. Accessed September 3, 2016.
43. Lee OK, Kuo TK, Chen W-M, et al. Isolation of multipotent mesenchymal stem cells from umbilical cord blood. **BLOOD** 2004;103(5):1669–75. Available at: http://www.ncbi.nlm.nih.gov/pubmed/14576065. Accessed September 3, 2016.
44. Tomita Y, Makino S, Hakuno D, et al. Application of mesenchymal stem cell-derived cardiomyocytes as bio-pacemakers: current status and problems to be solved. **MED. BIOL. ENG. COMPUT.** 2007;45(2):209–20. Available at: http://www.ncbi.nlm.nih.gov/pubmed/17262204. Accessed September 3, 2016.
45. Bianco P, Cao X, Frenette PS, et al. The meaning, the sense and the significance: translating the science of mesenchymal stem cells into medicine. **NAT. MED.** 2013;19(1):35–42. Available at: http://www.ncbi.nlm.nih.gov/pubmed/23296015. Accessed September 3, 2016.
46. Gojo S, Gojo N, Takeda Y, et al. In vivo cardiovasculogenesis by direct injection of isolated adult mesenchymal stem cells. **EXP. CELL RES.** 2003;288(1):51–9. Available at: http://www.ncbi.nlm.nih.gov/pubmed/12878158. Accessed September 3, 2016.
47. Barbash IM, Chouraqui P, Baron J, et al. Systemic delivery of bone marrow-derived mesenchymal stem cells to the infarcted myocardium: feasibility, cell migration, and body distribution. **CIRCULATION** 2003;108(7):863–8. Available at: http://www.ncbi.nlm.nih.gov/pubmed/12900340. Accessed September 3, 2016.
48. Psaltis PJ, Zannettino ACW, Worthley SG, et al. Concise Review: Mesenchymal Stromal Cells: Potential for Cardiovascular Repair.
49. Petrie Aronin CE, Tuan RS. Therapeutic potential of the immunomodulatory activities of adult mesenchymal stem cells. **BIRTH DEFECTS RES. C. EMBRYO TODAY** 2010;90(1):67–74. Available at: http://www.ncbi.nlm.nih.gov/pubmed/20301222. Accessed September 3, 2016.
50. Ankrum J, Karp JM. Mesenchymal stem cell therapy: Two steps forward, one step back. **TRENDS MOL. MED.** 2010;16(5):203–9. Available at: http://www.ncbi.nlm.nih.gov/pubmed/20335067. Accessed September 3, 2016.
51. Dennis JE, Merriam A, Awadallah A, et al. A quadripotential mesenchymal progenitor cell isolated from the marrow of an adult mouse. **J. BONE MINER. RES.** 1999;14(5):700–9. Available at: http://www.ncbi.nlm.nih.gov/pubmed/10320518. Accessed September 3, 2016.
52. Caplan AI, Dennis JE. Mesenchymal stem cells as trophic mediators. **J. CELL. BIOCHEM.** 2006;98(5):1076–1084.
53. Poll D van, Parekkadan B, Cho CH, et al. Mesenchymal stem cell-derived molecules directly modulate hepatocellular death and regeneration in vitro and in vivo. **HEPATOLOGY** 2008;47(5):1634–43. Available at: http://www.ncbi.nlm.nih.gov/pubmed/18395843. Accessed September 3, 2016.
54. Plotnikov EY, Khryapenkova TG, Vasileva AK, et al. Cell-to-cell cross-talk between mesenchymal stem cells and cardiomyocytes in co-culture. **J. CELL. MOL. MED.** 12(5A):1622–31. Available at: http://www.ncbi.nlm.nih.gov/pubmed/18088382. Accessed September 3, 2016.
55. Meryman HT. Freezing injury and its prevention in living cells. **ANNU. REV. BIOPHYS. BIOENG.** 1974;3(237):341–363.
56. Leibo SP, Mazur P. The role of cooling rates in low-temperature preservation. **CRYOBIOLOGY** 1971;8(5):447–452.
57. Todorov P, Hristova E, Konakchieva R, et al. Comparative studies of different cryopreservation methods for mesenchymal stem cells derived from human fetal liver. **CELL BIOL. INT.** 2010;34(5):455–462. Available at: http://doi.wiley.com/10.1042/CBI20090127. Accessed August 1,

2016.
58. Roach KL, King KR, Uygun K, et al. High-throughput single cell arrays as a novel tool in biopreservation. **CRYOBIOLOGY** 2009;58(3):315–321. Available at: http://dx.doi.org/10.1016/j.cryobiol.2009.03.001.
59. Dong J, Malsam J, Bischof JC, et al. Spatial distribution of the state of water in frozen mammalian cells. **BIOPHYS. J.** 2010;99(8):2453–2459.
60. Karlsson JO, Cravalho EG, Borel Rinkes IH, et al. Nucleation and growth of ice crystals inside cultured hepatocytes during freezing in the presence of dimethyl sulfoxide. **BIOPHYS. J.** 1993;65(6):2524–2536. Available at: http://dx.doi.org/10.1016/S0006-3495(93)81319-5.
61. Toner M, Cravalho EG, Karel M. Thermodynamics and kinetics of intracellular ice formation during freezing of biological cells. **J. APPL. PHYS.** 1990;67(3):1582. Available at: http://scitation.aip.org/content/aip/journal/jap/67/3/10.1063/1.345670. Accessed August 1, 2016.
62. CAREY H V., ANDREWS MT, MARTIN SL. Mammalian Hibernation: Cellular and Molecular Responses to Depressed Metabolism and Low Temperature. **PHYSIOL. REV.** 2003;83(4):1153–1181. Available at: http://physrev.physiology.org/content/83/4/1153.abstract.
63. Haack-Sørensen M, Kastrup J. Cryopreservation and Revival of Mesenchymal Stromal Cells. In: ; 2011:161–174. Available at: http://link.springer.com/10.1007/978-1-60761-999-4_13. Accessed August 1, 2016.
64. Baust JM. Molecular Mechanisms of Cellular Demise Associated with Cryopreservation Failure. **CELL PRESERV. TECHNOL.** 2002;1(1):17–31. Available at: http://www.liebertonline.com/doi/abs/10.1089/15383440260073266. Accessed August 1, 2016.
65. Gores GJ, Herman B, Lemasters JJ. Plasma membrane bleb formation and rupture: A common feature of hepatocellular injury. **HEPATOLOGY** 1990;11(4):690–698. Available at: http://doi.wiley.com/10.1002/hep.1840110425. Accessed August 1, 2016.
66. Laster SM, Mackenzie JM. Bleb formation and F-actin distribution during mitosis and tumor necrosis factor-induced apoptosis. **MICROSC. RES. TECH.** 1996;34(3):272–280. Available at: http://doi.wiley.com/10.1002/%28SICI%291097-0029%2819960615%2934%3A3%3C272%3A%3AAID-JEMT10%3E3.0.CO%3B2-J. Accessed August 1, 2016.
67. Ragoonanan V, Hubel A, Aksan A. Cryobiology Response of the cell membrane – cytoskeleton complex to osmotic and freeze / thaw stresses q. **CRYOBIOLOGY** 2010;61(3):335–344. Available at: http://dx.doi.org/10.1016/j.cryobiol.2010.10.160.
68. Ragoonanan V, Less R, Aksan A. Response of the cell membrane–cytoskeleton complex to osmotic and freeze/thaw stresses. Part 2: The link between the state of the membrane–cytoskeleton complex and the cellular damage. **CRYOBIOLOGY** 2013;66(2):96–104.
69. LOVELOCK JE, BISHOP MWH. Prevention of Freezing Damage to Living Cells by Dimethyl Sulphoxide. **NATURE** 1959;183(4672):1394–1395. Available at: http://www.nature.com/doifinder/10.1038/1831394a0. Accessed September 4, 2016.
70. Gurtovenko A a, Anwar J. Modulating the structure and properties of cell membranes: the molecular mechanism of action of dimethyl sulfoxide. **J. PHYS. CHEM. B** 2007;111(35):10453–10460.
71. Notman R, Noro M, O'Malley B, et al. Molecular Basis for Dimethylsulfoxide (DMSO) Action on Lipid Membranes. **J. AM. CHEM. SOC.** 2006;128(43):13982–13983. Available at: http://pubs.acs.org/doi/abs/10.1021/ja063363t. Accessed August 1, 2016.
72. Cox MA, Kastrup J, Hrubiško M. Historical perspectives and the future of adverse reactions associated with haemopoietic stem cells cryopreserved with dimethyl sulfoxide. **CELL TISSUE BANK.**

2012;13(2):203–215. Available at: http://link.springer.com/10.1007/s10561-011-9248-2. Accessed September 4, 2016.
73. Galipeau J. The mesenchymal stromal cells dilemma—does a negative phase III trial of random donor mesenchymal stromal cells in steroid-resistant graft-versus-host disease represent a death knell or a bump in the road? **CYTOTHERAPY** 2013;15(1):2–8.
74. Chinnadurai R, Garcia MA, Sakurai Y, et al. Actin Cytoskeletal Disruption following Cryopreservation Alters the Biodistribution of Human Mesenchymal Stromal Cells In Vivo. **STEM CELL REPORTS** 2014;3(1):60–72.
75. Moll G, Alm JJ, Davies LC, et al. Do cryopreserved mesenchymal stromal cells display impaired immunomodulatory and therapeutic properties? **STEM CELLS** 2014;32(9):2430–2442.
76. Mata MM, Mahmood F, Sowell RT, et al. Effects of cryopreservation on effector cells for antibody dependent cell-mediated cytotoxicity (ADCC) and natural killer (NK) cell activity in 51Cr-release and CD107a assays. **J. IMMUNOL. METHODS** 2014;406:1–9.
77. Iwatani M, Ikegami K, Kremenska Y, et al. Dimethyl Sulfoxide Has an Impact on Epigenetic Profile in Mouse Embryoid Body. **STEM CELLS** 2006;24(11):2549–2556. Available at: http://doi.wiley.com/10.1634/stemcells.2005-0427. Accessed August 1, 2016.
78. Thaler R, Spitzer S, Karlic H, et al. DMSO is a strong inducer of DNA hydroxymethylation in pre-osteoblastic MC3T3-E1 cells. **EPIGENETICS** 2012;7(6):635–651. Available at: http://www.tandfonline.com/doi/abs/10.4161/epi.20163. Accessed August 15, 2016.
79. Khomyakova M, Bükmez Ö, Thomas LK, et al. A methylaspartate cycle in haloarchaea. **SCIENCE** 2011;331(6015):334–7. Available at: http://www.ncbi.nlm.nih.gov/pubmed/21252347. Accessed August 1, 2016.
80. Candela T, Fouet A. Poly-gamma-glutamate in bacteria. **MOL. MICROBIOL.** 2006;60(5):1091–1098. Available at: http://doi.wiley.com/10.1111/j.1365-2958.2006.05179.x. Accessed August 1, 2016.
81. Grein TA, Freimark D, Weber C, et al. Alternatives to dimethylsulfoxide for serum-free cryopreservation of human mesenchymal stem cells. **INT. J. ARTIF. ORGANS** 2010;33(6):370–80. Available at: http://www.ncbi.nlm.nih.gov/pubmed/20669142. Accessed August 1, 2016.
82. Conde A, Chaves MM, Gerós H. Membrane transport, sensing and signaling in plant adaptation to environmental stress. **PLANT CELL PHYSIOL.** 2011;52(9):1583–1602.
83. Chen THH, Murata N. Enhancement of tolerance of abiotic stress by metabolic engineering of betaines and other compatible solutes. **CURR. OPIN. PLANT BIOL.** 2002;5(3):250–257.
84. Buchanan SS, Pyatt DW, Carpenter JF. Preservation of Differentiation and Clonogenic Potential of Human Hematopoietic Stem and Progenitor Cells during Lyophilization and Ambient Storage. Neves NM, ed. **PLOS ONE** 2010;5(9):e12518. Available at: http://dx.plos.org/10.1371/journal.pone.0012518. Accessed August 1, 2016.
85. Sawangwan T, Goedl C, Nidetzky B. Glucosylglycerol and glucosylglycerate as enzyme stabilizers. **BIOTECHNOL. J.** 2010;5(2):187–191.
86. Lynch AL, Chen R, Dominowski PJ, et al. Biopolymer mediated trehalose uptake for enhanced erythrocyte cryosurvival. **BIOMATERIALS** 2010;31(23):6096–6103.
87. Guo F, Friedman JM. Osmolyte-induced perturbations of hydrogen bonding between hydration layer waters: Correlation with protein conformational changes. **J. PHYS. CHEM. B** 2009;113(52):16632–16642.
88. Johnson ME, Malardier-Jugroot C, Head-Gordon T. Effects of co-solvents on peptide hydration water structure and dynamics. **PHYS. CHEM. CHEM. PHYS.** 2010;12(2):393–405.
89. Mohammed AR, Coombes AGA, Perrie Y. Amino acids as cryoprotectants for liposomal delivery

systems. **EUR. J. PHARM. SCI.** 2007;30(5):406–413.
90. Rudolph AS, Crowe JH. Membrane stabilization during freezing: The role of two natural cryoprotectants, trehalose and proline. **CRYOBIOLOGY** 1985;22(4):367–377.
91. Matsumura K, Hyon S-H. Polyampholytes as low toxic efficient cryoprotective agents with antifreeze protein properties. **BIOMATERIALS** 2009;30(27):4842–4849.
92. Matsumura K, Bae JY, Hyon SH. Polyampholytes as Cryoprotective Agents for Mammalian Cell Cryopreservation. **CELL TRANSPLANT.** 2010;19(6):691–699. Available at: http://openurl.ingenta.com/content/xref?genre=article&issn=0963-6897&volume=19&issue=6&spage=691. Accessed August 1, 2016.
93. Cicerone MT, Soles CL. Fast Dynamics and Stabilization of Proteins: Binary Glasses of Trehalose and Glycerol. **BIOPHYS. J.** 2004;86(6):3836–3845.
94. Sasnoor LM, Kale VP, Limaye LS. Prevention of apoptosis as a possible mechanism behind improved cryoprotection of hematopoietic cells by catalase and trehalose. **TRANSPLANTATION** 2005;80(9):1251–1260.
95. Plank C, Zauner W, Wagner E. Application of membrane-active peptides for drug and gene delivery across cellular membranes. **ADV. DRUG DELIV. REV.** 1998;34(1):21–35.
96. Singh LR, Poddar NK, Dar TA, et al. Protein and DNA destabilization by osmolytes: The other side of the coin. **LIFE SCI.** 2011;88(3):117–125.
97. Conrad PB, Miller DP, Cielenski PR, et al. Stabilization and Preservation of Lactobacillus acidophilus in Saccharide Matrices. **CRYOBIOLOGY** 2000;41(1):17–24. Available at: http://linkinghub.elsevier.com/retrieve/pii/S0011224000922600. Accessed August 1, 2016.
98. Dijkstra-Tiekstra MJ, Setroikromo AC, Kraan M, et al. Optimization of the freezing process for hematopoietic progenitor cells: Effect of precooling, initial dimethyl sulfoxide concentration, freezing program, and storage in vapor-phase or liquid nitrogen on in vitro white blood cell quality. **TRANSFUSION** 2014;54(12):3155–3163.
99. Dong Q, Hill D, VandeVoort CA. Interactions among pre-cooling, cryoprotectant, cooling, and thawing for sperm cryopreservation in rhesus monkeys. **CRYOBIOLOGY** 2009;59(3):268–274.
100. Freimark D, Sehl C, Weber C, et al. Systematic parameter optimization of a Me2SO- and serum-free cryopreservation protocol for human mesenchymal stem cells. **CRYOBIOLOGY** 2011;63(2):67–75.
101. Kearney JN, Wheldon LA, Gowland G. Effects of cryobiological variables on the survival of skin using a defined murine model. **CRYOBIOLOGY** 1990;27(2):164–170. Available at: http://linkinghub.elsevier.com/retrieve/pii/001122409090008R. Accessed August 1, 2016.
102. Ting AY, Yeoman RR, Lawson MS, et al. Synthetic polymers improve vitrification outcomes of macaque ovarian tissue as assessed by histological integrity and the in vitro development of secondary follicles. **CRYOBIOLOGY** 2012;65(1):1–11. Available at: http://www.ncbi.nlm.nih.gov/pubmed/22569078. Accessed September 4, 2016.
103. Ting AY, Yeoman RR, Campos JR, et al. Morphological and functional preservation of pre-antral follicles after vitrification of macaque ovarian tissue in a closed system. **HUM. REPROD.** 2013;28(5):1267–1279. Available at: http://humrep.oxfordjournals.org/lookup/doi/10.1093/humrep/det032. Accessed September 4, 2016.
104. Tsutsui H, Valamehr B, Hindoyan A, et al. An optimized small molecule inhibitor cocktail supports long-term maintenance of human embryonic stem cells. **NAT. COMMUN.** 2011;2(1):167. Available at: http://www.mendeley.com/catalog/optimized-small-molecule-inhibitor-cocktail-supports-longterm-maintenance-human-embryonic-stem-cells-2/.
105. Trivedi P, Hematti P. Derivation and immunological characterization of mesenchymal stromal cells

from human embryonic stem cells. **EXP. HEMATOL.** 2008;36(3):350–359.
106. Gruenloh W, Kambal A, Sondergaard C, et al. Characterization and in vivo testing of mesenchymal stem cells derived from human embryonic stem cells. **TISSUE ENG. PART A** 2011;17(11-12):1517–1525.
107. Almeida RA de, Burgess D, Shema R, et al. ASaccharomyces cerevisiae cell-based quantitative β-galactosidase assay compatible with robotic handling and high-throughput screening. **YEAST** 2008;25(1):71–76. Available at: http://doi.wiley.com/10.1002/yea.1570. Accessed August 1, 2016.
108. Jag UR, Zavadil J, Stanley FM. Insulin Acts through FOXO3a to Activate Transcription of Plasminogen Activator Inhibitor Type 1. **HTTP://DX.DOI.ORG/10.1210/ME.2008-0421** 2011.
109. Harkness L, Novikov SM, Beermann J, et al. Identification of abnormal stem cells using Raman spectroscopy. **STEM CELLS DEV.** 2012;21(12):2152–9.
110. Mendelovici E, Frost RL, Kloprogge T. Cryogenic Raman spectroscopy of glycerol. **J. RAMAN SPECTROSC.** 2000;31(12):1121–1126. Available at: http://doi.wiley.com/10.1002/1097-4555%28200012%2931%3A12%3C1121%3A%3AAID-JRS654%3E3.0.CO%3B2-G. Accessed May 26, 2016.
111. Veij M De, Vandenabeele P, Beer T De, et al. Reference database of Raman spectra of pharmaceutical excipients. **J. RAMAN SPECTROSC.** 2009;40(3):297–307.
112. Mathlouthi M, Vinh Luu D. Laser-raman spectra of d-glucose and sucrose in aqueous solution. **CARBOHYDR. RES.** 1980;81(2):203–212.
113. Gangopadhyay D, Sharma P, Singh RK. Temperature dependent Raman and DFT study of creatine. **SPECTROCHIM. ACTA. A. MOL. BIOMOL. SPECTROSC.** 2015;150:9–14.
114. Kemeny SF, Clyne AM. A Simplified Implementation of Edge Detection in. **PUBMED** 2011:156–166.
115. Ayres CE, Jha BS, Meredith H, et al. Measuring fiber alignment in electrospun scaffolds: a user's guide to the 2D fast Fourier transform approach. **J. BIOMATER. SCI. POLYM. ED.** 2008;19(5):603–621. Available at: http://www.tandfonline.com/doi/abs/10.1163/156856208784089643.
116. Schmittgen TD, Livak KJ. Analyzing real-time PCR data by the comparative CT method. **NAT. PROTOC.** 2008;3(6):1101–1108. Available at: http://www.nature.com/doifinder/10.1038/nprot.2008.73.
117. Baxter MA, Wynn RF, Jowitt SN, et al. Study of Telomere Length Reveals Rapid Aging of Human Marrow Stromal Cells following In Vitro Expansion. **STEM CELLS** 2004;22(5):675–682. Available at: http://doi.wiley.com/10.1634/stemcells.22-5-675. Accessed August 1, 2016.
118. Wright LS, Prowse KR, Wallace K, et al. Human progenitor cells isolated from the developing cortex undergo decreased neurogenesis and eventual senescence following expansion in vitro. **EXP. CELL RES.** 2006;312(11):2107–2120.
119. Coppé J-P, Patil CK, Rodier F, et al. A Human-Like Senescence-Associated Secretory Phenotype Is Conserved in Mouse Cells Dependent on Physiological Oxygen. Blagosklonny M V., ed. **PLOS ONE** 2010;5(2):e9188. Available at: http://dx.plos.org/10.1371/journal.pone.0009188. Accessed August 1, 2016.
120. Campisi J, d'Adda di Fagagna F. Cellular senescence: when bad things happen to good cells. **NAT. REV. MOL. CELL BIOL.** 2007;8(9):729–740. Available at: http://www.nature.com/doifinder/10.1038/nrm2233. Accessed August 1, 2016.
121. Hubel A, Darr TB, Norman JA. Freezing characteristics of genetically modified lymphocytes for the treatment of MPS II. **CELL TRANSPLANT.** 1998;8(5):521–30. Available at:

http://www.ncbi.nlm.nih.gov/pubmed/10580346. Accessed August 1, 2016.
122. Hubel A, Norman J, Darr TB. Cryobiophysical Characteristics of Genetically Modified Hematopoietic Progenitor Cells. **CRYOBIOLOGY** 1999;38(2):140–153. Available at: http://linkinghub.elsevier.com/retrieve/pii/S0011224099921570. Accessed August 1, 2016.
123. Moll G, Alm JJ, Davies LC, et al. Do Cryopreserved Mesenchymal Stromal Cells Display Impaired Immunomodulatory and Therapeutic Properties? **STEM CELLS** 2014;32(9):2430–2442. Available at: http://doi.wiley.com/10.1002/stem.1729. Accessed August 1, 2016.
124. Portalska KJ, Groen N, Krenning G, et al. The Effect of Donor Variation and Senescence on Endothelial Differentiation of Human Mesenchymal Stromal Cells. **TISSUE ENG. PART A** 2013;19(21-22):2318–2329. Available at: http://online.liebertpub.com/doi/abs/10.1089/ten.tea.2012.0646. Accessed August 1, 2016.
125. Stolzing A, Jones E, McGonagle D, et al. Age-related changes in human bone marrow-derived mesenchymal stem cells: Consequences for cell therapies. **MECH. AGEING DEV.** 2008;129(3):163–173.
126. Sensebé L, Tarte K, Galipeau J, et al. Limited Acquisition of Chromosomal Aberrations in Human Adult Mesenchymal Stromal Cells. **CELL STEM CELL** 2012;10(1):9–10.
127. Bertolo A, Mehr M, Janner-Jametti T, et al. An *in vitro* expansion score for tissue-engineering applications with human bone marrow-derived mesenchymal stem cells. **J. TISSUE ENG. REGEN. MED.** 2016;10(2):149–161. Available at: http://doi.wiley.com/10.1002/term.1734. Accessed August 1, 2016.
128. Wagner W, Bork S, Lepperdinger G, et al. How to track cellular aging of mesenchymal stromal cells? **AGING (ALBANY. NY).** 2010;2(4):224–30. Available at: http://www.ncbi.nlm.nih.gov/pubmed/20453259. Accessed August 1, 2016.
129. Bruder SP, Jaiswal N, Haynesworth SE. Growth kinetics, self-renewal, and the osteogenic potential of purified human mesenchymal stem cells during extensive subcultivation and following cryopreservation. **J. CELL. BIOCHEM.** 1997;64(2):278–294. Available at: http://doi.wiley.com/10.1002/%28SICI%291097-4644%28199702%2964%3A2%3C278%3A%3AAID-JCB11%3E3.0.CO%3B2-F. Accessed August 1, 2016.
130. Mamidi MK, Nathan KG, Singh G, et al. Comparative cellular and molecular analyses of pooled bone marrow multipotent mesenchymal stromal cells during continuous passaging and after successive cryopreservation. **J. CELL. BIOCHEM.** 2012;113(10):3153–64. Available at: http://www.ncbi.nlm.nih.gov/pubmed/22615164. Accessed August 1, 2016.
131. Dariolli R, Bassaneze V, Nakamuta JS, et al. Porcine Adipose Tissue-Derived Mesenchymal Stem Cells Retain Their Proliferative Characteristics, Senescence, Karyotype and Plasticity after Long-Term Cryopreservation. **PLOS ONE** 2013;8(7).
132. Eroglu A, Russo MJ, Bieganski R, et al. Intracellular trehalose improves the survival of cryopreserved mammalian cells. **NAT. BIOTECHNOL.** 2000;18(2):163–167. Available at: http://www.nature.com/doifinder/10.1038/72608. Accessed August 1, 2016.
133. Fahy GM, Wowk B. Chapter 2 Principles of Cryopreservation by Vitrification. **METHODS MOL. BIOL.** 1007;1257(10):978–1.
134. McGrath J. *Low temperature biotechnology : emerging applications and engineering contributions*. New York NY (345 E. 47th St. New York 10017): ASME; 1988.
135. Abazari A, Meimetis LG, Budin G, et al. Engineered Trehalose Permeable to Mammalian Cells. Singh SR, ed. **PLOS ONE** 2015;10(6):e0130323. Available at:

http://dx.plos.org/10.1371/journal.pone.0130323. Accessed August 1, 2016.
136. Acker JP, Lu X, Young V, et al. Measurement of trehalose loading of mammalian cells porated with a metal-actuated switchable pore. **BIOTECHNOL. BIOENG.** 2003;82(5):525–532. Available at: http://doi.wiley.com/10.1002/bit.10599. Accessed June 29, 2016.
137. Santarius KA, Giersch C. Cryopreservation of spinach chloroplast membranes by low-molecular-weight carbohydrates. **CRYOBIOLOGY** 1983;20(1):90–99. Available at: http://linkinghub.elsevier.com/retrieve/pii/0011224083900639. Accessed June 29, 2016.
138. Arakawa T, Timasheff SN. The stabilization of proteins by osmolytes. **BIOPHYS. J.** 1985;47(3):411–4. Available at: http://www.ncbi.nlm.nih.gov/pubmed/3978211. Accessed May 26, 2016.
139. Crowe JH, Crowe LM, Carpenter JF, et al. Interactions of sugars with membranes. **BBA - REV. BIOMEMBR.** 1988;947(2):367–384.
140. Poddar NK, Ansari ZA, Singh RKB, et al. Effect of monomeric and oligomeric sugar osmolytes on ΔGD, the Gibbs energy of stabilization of the protein at different pH values: Is the sum effect of monosaccharide individually additive in a mixture? **BIOPHYS. CHEM.** 2008;138(3):120–129.
141. Holthauzen LMF, Bolen DW. Mixed osmolytes: The degree to which one osmolyte affects the protein stabilizing ability of another. **PROTEIN SCI.** 2006;16(2):293–298. Available at: http://doi.wiley.com/10.1110/ps.062610407. Accessed May 26, 2016.
142. Goodrich RP, Crowe JH, Crowe LM, et al. Alterations in membrane surfaces induced by attachment of carbohydrates. **BIOCHEMISTRY** 1991;30(21):5313–5318. Available at: http://pubs.acs.org/doi/abs/10.1021/bi00235a026. Accessed June 29, 2016.
143. Arakawa T, Carpenter JF, Kita YA, et al. The basis for toxicity of certain cryoprotectants: A hypothesis. **CRYOBIOLOGY** 1990;27(4):401–415.
144. Strauss G, Hauser H. Stabilization of lipid bilayer vesicles by sucrose during freezing. **PROC. NATL. ACAD. SCI. U. S. A.** 1986;83(8):2422–6. Available at: http://www.ncbi.nlm.nih.gov/pubmed/16593683. Accessed May 26, 2016.
145. Gómez-Fernández J, Gómez-Izquierdo E, Tomás C, et al. Effect of different monosaccharides and disaccharides on boar sperm quality after cryopreservation. **ANIM. REPROD. SCI.** 2012;133(1):109–116.
146. Mazur P. Freezing of living cells: mechanisms and implications. **AM. J. PHYSIOL.** 1984;247(3 Pt 1):C125–42. Available at: http://www.ncbi.nlm.nih.gov/pubmed/6383068. Accessed August 1, 2016.
147. Dijkstra-Tiekstra MJ, Setroikromo AC, Kraan M, et al. Optimization of the freezing process for hematopoietic progenitor cells: effect of precooling, initial dimethyl sulfoxide concentration, freezing program, and storage in vapor-phase or liquid nitrogen on in vitro white blood cell quality. **TRANSFUSION** 2014;54(12):3155–3163. Available at: http://doi.wiley.com/10.1111/trf.12756. Accessed August 1, 2016.
148. Tsutsui H, Valamehr B, Hindoyan A, et al. An optimized small molecule inhibitor cocktail supports long-term maintenance of human embryonic stem cells. **NAT. COMMUN.** 2011;2:167. Available at: http://www.nature.com/doifinder/10.1038/ncomms1165. Accessed August 1, 2016.
149. Katkov II, Kan NG, Cimadamore F, et al. DMSO-Free Programmed Cryopreservation of Fully Dissociated and Adherent Human Induced Pluripotent Stem Cells. **STEM CELLS INT.** 2011;2011:981606.
150. Moon JH, Lee JR, Jee BC, et al. Successful vitrification of human amnion-derived mesenchymal stem cells. **HUM. REPROD.** 2008;23(8):1760–70. Available at: http://www.ncbi.nlm.nih.gov/pubmed/18541648. Accessed August 1, 2016.
151. Valeri CR, Ragno G, Pivacek LE, et al. An Experiment with Glycerol-Frozen Red Blood Cells Stored

at -80C for up to 37 Years. **VOX SANG.** 2000;79(3):168–174. Available at: http://www.karger.com/doi/10.1159/000031236. Accessed August 1, 2016.
152. POLGE C, SMITH AU, PARKES AS. Revival of Spermatozoa after Vitrification and Dehydration at Low Temperatures. **NATURE** 1949;164(4172):666–666. Available at: http://www.nature.com/doifinder/10.1038/164666a0. Accessed August 1, 2016.
153. Crowe JH, Crowe LM. Preservation of mammalian cells—learning nature's tricks. **NAT. BIOTECHNOL.** 2000;18(2):145–146. Available at: http://www.nature.com/doifinder/10.1038/72580. Accessed August 1, 2016.
154. Dominici M, Blanc K Le, Mueller I, et al. Minimal criteria for defining multipotent mesenchymal stromal cells. The International Society for Cellular Therapy position statement. **CYTOTHERAPY** 2006;8(4):315–317. Available at: http://linkinghub.elsevier.com/retrieve/pii/S1465324906708817. Accessed August 1, 2016.
155. Samsonraj RM, Rai B, Sathiyanathan P, et al. Establishing Criteria for Human Mesenchymal Stem Cell Potency. **STEM CELLS** 2015;33(6):1878–1891. Available at: http://doi.wiley.com/10.1002/stem.1982. Accessed June 24, 2016.
156. Bianco P, Robey PG, Simmons PJ. Mesenchymal Stem Cells: Revisiting History, Concepts, and Assays. **CELL STEM CELL** 2008;2(4):313–319.
157. Chagastelles PC, Nardi NB, Camassola M. Biology and applications of mesenchymal stem cells. **SCI. PROG.** 2010;93(2):113–127.
158. Caplan AI, Correa D. The MSC: An injury drugstore. **CELL STEM CELL** 2011;9(1):11–15. Available at: http://dx.doi.org/10.1016/j.stem.2011.06.008.
159. Nauta AJ, Fibbe WE, Friedenstein A, et al. Immunomodulatory properties of mesenchymal stromal cells. **BLOOD** 2007;110(10):3499–506. Available at: http://www.ncbi.nlm.nih.gov/pubmed/17664353. Accessed August 1, 2016.
160. François M, Romieu-Mourez R, Li M, et al. Human MSC Suppression Correlates With Cytokine Induction of Indoleamine 2,3-Dioxygenase and Bystander M2 Macrophage Differentiation. **MOL. THER.** 2012;20(1):187–195. Available at: http://dx.doi.org/10.1038/mt.2011.189/nature06264.
161. Chinnadurai R, Galipeau J. Mini Review Defining mesenchymal stromal cells responsive- ness to IFNγ as a surrogate measure of suppressive potency. 2014;34(4):168–175.
162. Chinnadurai R, Copland IB, Garcia MA, et al. Cryopreserved Mesenchymal Stromal Cells Are Susceptible to T-Cell Mediated Apoptosis Which Is Partly Rescued by IFNγ Licensing. **STEM CELLS** 2016. Available at: http://doi.wiley.com/10.1002/stem.2415. Accessed July 13, 2016.
163. Castelo-Branco MTL, Soares IDP, Lopes D V., et al. Intraperitoneal but Not Intravenous Cryopreserved Mesenchymal Stromal Cells Home to the Inflamed Colon and Ameliorate Experimental Colitis. Allodi S, ed. **PLOS ONE** 2012;7(3):e33360. Available at: http://dx.plos.org/10.1371/journal.pone.0033360. Accessed September 5, 2016.
164. Luetzkendorf J, Nerger K, Hering J, et al. Cryopreservation does not alter main characteristics of Good Manufacturing Process-grade human multipotent mesenchymal stromal cells including immunomodulating potential and lack of malignant transformation. **CYTOTHERAPY** 2015;17(2):186–198. Available at: http://dx.doi.org/10.1016/j.jcyt.2014.10.018.
165. Galipeau J, Krampera M, Barrett J, et al. International Society for Cellular Therapy perspective on immune functional assays for mesenchymal stromal cells as potency release criterion for advanced phase clinical trials. **CYTOTHERAPY** 2015;18:151–159. Available at: http://dx.doi.org/10.1016/j.jcyt.2015.11.008. Accessed June 2, 2016.
166. Forte G, Minieri M, Cossa P, et al. Hepatocyte Growth Factor Effects on Mesenchymal Stem Cells:

Proliferation, Migration, and Differentiation. **STEM CELLS** 2006;24(1):23–33. Available at: http://doi.wiley.com/10.1634/stemcells.2004-0176. Accessed September 5, 2016.

Appendix

A.1 Chapter 7 raw algorithm data

Emergent population data is presented here, including vectors for each solution composition used. Corresponding solution concentrations and cooling rates for each vector are located in Table 12. Cells highlighted in yellow indicate improvement when compared head to head vs the same slot in the previous generation.

A.1.1 Jurkat single cooling rate TGE recovery algorithm raw emergent population data from Figure 18

JURKAT CELLS

Improved solutions	Generation	Emergent population	Recovery	Trehalose	Glycerol	Ectoine
18	0	1	0.259	0	5	4
		2	0.033	2	2	2
		3	0.188	1	3	3
		4	0.201	4	4	3
		5	0.147	2	4	3
		6	0.295	2	5	5
		7	0.021	3	3	3
		8	0.099	1	1	2
		9	0.187	1	5	1
		10	0.031	1	1	1
		11	0.025	2	1	5
		12	0.022	2	1	5
		13	0.027	5	2	0
		14	0.050	1	2	3
		15	0.021	1	3	4
		16	0.025	1	0	1
		17	0.023	1	2	3
		18	0.024	0	1	4
11	1	1	0.259	0	5	4
		20	0.170	2	4	4
		3	0.188	1	3	3
		4	0.201	4	4	3
		5	0.147	2	4	3
		24	0.333	4	5	3
		25	0.271	4	5	5
		8	0.099	1	1	2
		9	0.187	1	5	1
		28	0.191	3	4	2
		29	0.173	0	4	4
		30	0.027	3	3	5
		31	0.146	2	5	3
		14	0.050	1	2	3
		33	0.125	4	4	2
		34	0.040	4	2	4
		35	0.152	2	4	5
		36	0.128	2	4	5
9	2	1	0.259	0	5	4
		38	0.231	2	5	3
		3	0.188	1	3	3
		40	0.278	5	5	4
		5	0.147	2	4	3
		24	0.333	4	5	3
		25	0.271	4	5	5
		44	0.116	4	4	5
		9	0.187	1	5	1
		46	0.221	5	5	0
		47	0.194	0	5	4
		48	0.212	5	5	3
		31	0.146	2	5	3
		50	0.195	2	4	2
		51	0.162	2	5	1
		34	0.040	4	2	4
		53	0.218	5	5	5
		36	0.128	2	4	5

JURKAT CELLS						
Improved solutions	**Generation**	**Emergent population**	**Recovery**	**Trehalose**	**Glycerol**	**Ectoine**
7	3	1	0.259	0	5	4
		56	0.265	3	5	5
		3	0.188	1	3	3
		40	0.278	5	5	4
		5	0.147	2	4	3
		24	0.333	4	5	3
		61	0.272	5	5	2
		62	0.289	5	5	5
		9	0.187	1	5	1
		64	0.231	5	5	1
		65	0.198	1	5	5
		48	0.212	5	5	3
		31	0.146	2	5	3
		68	0.209	5	5	2
		51	0.162	2	5	1
		70	0.194	4	5	4
		53	0.218	5	5	5
		36	0.128	2	4	5
8	4	73	0.263	4	5	5
		74	0.277	3	5	5
		75	0.274	4	5	4
		40	0.278	5	5	4
		77	0.161	2	5	1
		24	0.333	4	5	3
		61	0.272	5	5	2
		62	0.289	5	5	5
		81	0.294	4	5	1
		64	0.231	5	5	1
		65	0.198	1	5	5
		48	0.212	5	5	3
		85	0.159	3	5	3
		68	0.209	5	5	2
		87	0.171	4	5	4
		70	0.194	4	5	4
		53	0.218	5	5	5
		90	0.251	3	5	5

JURKAT CELLS						
Improved solutions	**Generation**	**Emergent population**	**Recovery**	**Trehalose**	**Glycerol**	**Ectoine**
1	5	73	0.263	4	5	5
		74	0.277	3	5	5
		75	0.274	4	5	4
		40	0.278	5	5	4
		95	0.165	4	5	0
		24	0.333	4	5	3
		61	0.272	5	5	2
		62	0.289	5	5	5
		81	0.294	4	5	1
		64	0.231	5	5	1
		65	0.198	1	5	5
		48	0.212	5	5	3
		85	0.159	3	5	3
		68	0.209	5	5	2
		87	0.171	4	5	4
		70	0.194	4	5	4
		53	0.218	5	5	5
		90	0.251	3	5	5
0	6	73	0.263	4	5	5
		74	0.277	3	5	5
		75	0.274	4	5	4
		40	0.278	5	5	4
		95	0.165	4	5	0
		24	0.333	4	5	3
		61	0.272	5	5	2
		62	0.289	5	5	5
		81	0.294	4	5	1
		64	0.231	5	5	1
		65	0.198	1	5	5
		48	0.212	5	5	3
		85	0.159	3	5	3
		68	0.209	5	5	2
		87	0.171	4	5	4
		70	0.194	4	5	4
		53	0.218	5	5	5
		90	0.251	3	5	5

A.1.2 Jurkat multiple cooling rate TGE recovery algorithm raw emergent population data from Figure 19

JURKAT CELLS

Improved solutions	Generation	Emergent population	Recovery	Trehalose	Glycerol	Ectoine	Cooling rate
27	0	1	0.273	4	5	0	5
		2	0.012	3	0	1	3
		3	0.237	5	5	0	5
		4	0.000	5	2	4	0
		5	0.139	2	5	4	5
		6	0.022	3	0	5	5
		7	0.118	4	4	4	2
		8	0.000	3	1	4	0
		9	0.015	1	0	0	4
		10	0.000	4	1	5	0
		11	0.012	2	2	4	4
		12	0.013	1	2	2	3
		13	0.189	4	4	1	4
		14	0.008	3	0	0	2
		15	0.030	5	2	3	1
		16	0.041	4	1	3	4
		17	0.000	5	5	3	0
		18	0.010	0	1	5	1
		19	0.010	4	1	5	2
		20	0.008	1	1	3	2
		21	0.068	2	4	3	3
		22	0.082	5	1	4	4
		23	0.000	2	3	0	0
		24	0.000	3	4	5	0
		25	0.009	3	2	0	2
		26	0.055	0	4	1	3
		27	0.012	0	3	1	3
23	1	28	0.291	5	5	0	5
		29	0.031	3	3	1	4
		30	0.312	5	4	1	5
		31	0.023	5	3	1	1
		5	0.139	2	5	4	5
		33	0.070	5	1	2	3
		7	0.118	4	4	4	2
		35	0.245	5	4	2	4
		36	0.074	3	4	0	4
		37	0.021	2	3	2	3
		38	0.054	2	4	1	4
		39	0.052	0	5	2	3
		13	0.189	4	4	1	4
		41	0.188	5	4	2	2
		42	0.093	2	4	1	2
		43	0.144	5	1	1	5
		44	0.012	4	2	4	1
		45	0.069	2	4	1	3
		46	0.106	2	4	4	3
		47	0.021	3	2	0	4
		48	0.146	4	4	4	3
		22	0.082	5	1	4	4
		50	0.020	3	3	3	2
		51	0.096	3	5	1	3
		52	0.231	5	4	0	4
		53	0.124	3	4	1	4
		54	0.026	1	0	0	4

JURKAT CELLS							
Improved solutions	**Generation**	**Emergent population**	**Recovery**	**Trehalose**	**Glycerol**	**Ectoine**	**Cooling rate**
12	2	28	0.291	5	5	0	5
		56	0.084	5	1	0	4
		30	0.312	5	4	1	5
		58	0.099	5	3	1	4
		59	0.161	5	4	1	4
		60	0.123	5	1	5	5
		61	0.187	5	5	1	4
		35	0.245	5	4	2	4
		36	0.074	3	4	0	4
		64	0.157	5	4	1	4
		38	0.054	2	4	1	4
		39	0.052	0	5	2	3
		13	0.189	4	4	1	4
		68	0.205	2	4	5	5
		69	0.111	5	4	1	2
		70	0.237	5	4	1	5
		71	0.052	5	3	3	3
		45	0.069	2	4	1	3
		73	0.217	5	5	2	5
		74	0.047	3	4	0	4
		48	0.146	4	4	4	3
		76	0.258	5	4	1	5
		77	0.025	4	2	0	4
		51	0.096	3	5	1	3
		52	0.231	5	4	0	4
		53	0.124	3	4	1	4
		54	0.026	1	0	0	4
9	3	28	0.291	5	5	0	5
		83	0.168	5	4	0	5
		30	0.312	5	4	1	5
		85	0.146	4	4	1	5
		59	0.161	5	4	1	4
		87	0.141	5	4	2	3
		61	0.187	5	5	1	4
		35	0.245	5	4	2	4
		90	0.092	5	1	4	5
		91	0.169	5	5	1	5
		92	0.068	3	4	0	4
		39	0.052	0	5	2	3
		13	0.189	4	4	1	4
		68	0.205	2	4	5	5
		69	0.111	5	4	1	2
		70	0.237	5	4	1	5
		98	0.195	5	4	0	5
		99	0.094	3	5	2	5
		73	0.217	5	5	2	5
		101	0.120	5	3	0	5
		48	0.146	4	4	4	3
		76	0.258	5	4	1	5
		104	0.069	5	3	2	5
		51	0.096	3	5	1	3
		52	0.231	5	4	0	4
		53	0.124	3	4	1	4
		54	0.026	1	0	0	4

JURKAT CELLS							
Improved solutions	**Generation**	**Emergent population**	**Recovery**	**Trehalose**	**Glycerol**	**Ectoine**	**Cooling rate**
9	4	28	0.291	5	5	0	5
		83	0.168	5	4	0	5
		30	0.312	5	4	1	5
		85	0.146	4	4	1	5
		59	0.161	5	4	1	4
		87	0.141	5	4	2	3
		61	0.187	5	5	1	4
		35	0.245	5	4	2	4
		117	0.147	5	4	1	4
		118	0.202	5	4	0	5
		119	0.207	5	4	2	5
		120	0.066	0	5	3	5
		121	0.204	4	5	3	5
		68	0.205	2	4	5	5
		69	0.111	5	4	1	2
		70	0.237	5	4	1	5
		98	0.195	5	4	0	5
		99	0.094	3	5	2	5
		73	0.217	5	5	2	5
		128	0.180	4	5	3	3
		48	0.146	4	4	4	3
		76	0.258	5	4	1	5
		131	0.202	5	4	0	5
		132	0.111	4	3	2	5
		52	0.231	5	4	0	4
		134	0.143	5	4	2	4
		54	0.026	1	0	0	4
17	5	28	0.291	5	5	0	5
		83	0.168	5	4	0	5
		30	0.312	5	4	1	5
		139	0.162	3	4	4	3
		140	0.197	4	5	4	2
		141	0.245	5	4	4	4
		142	0.266	4	5	2	3
		35	0.245	5	4	2	4
		144	0.183	4	5	4	2
		145	0.225	4	4	4	3
		119	0.207	5	4	2	5
		147	0.278	4	5	2	5
		148	0.239	4	5	3	4
		68	0.205	2	4	5	5
		150	0.188	4	5	4	2
		70	0.237	5	4	1	5
		152	0.229	4	4	3	4
		153	0.128	3	5	4	2
		154	0.290	4	5	4	3
		155	0.269	5	5	1	4
		156	0.288	4	5	1	3
		76	0.258	5	4	1	5
		158	0.220	4	5	4	2
		159	0.162	3	5	4	2
		52	0.231	5	4	0	4
		161	0.353	5	5	1	5
		54	0.026	1	0	0	4

JURKAT CELLS							
Improved solutions	**Generation**	**Emergent population**	**Recovery**	**Trehalose**	**Glycerol**	**Ectoine**	**Cooling rate**
5	6	28	0.291	5	5	0	5
		83	0.168	5	4	0	5
		30	0.312	5	4	1	5
		166	0.259	5	5	4	4
		140	0.197	4	5	4	2
		141	0.245	5	4	4	4
		142	0.266	4	5	2	3
		35	0.245	5	4	2	4
		171	0.217	4	5	3	4
		145	0.225	4	4	4	3
		119	0.207	5	4	2	5
		147	0.278	4	5	2	5
		148	0.239	4	5	3	4
		176	0.222	5	4	2	4
		150	0.188	4	5	4	2
		70	0.237	5	4	1	5
		152	0.229	4	4	3	4
		180	0.139	4	5	3	5
		154	0.290	4	5	4	3
		155	0.269	5	5	1	4
		156	0.288	4	5	1	3
		76	0.258	5	4	1	5
		158	0.220	4	5	4	2
		186	0.262	5	5	1	4
		52	0.231	5	4	0	4
		161	0.353	5	5	1	5
		54	0.095	4	4	0	5
0	7	28	0.291	5	5	0	5
		83	0.168	5	4	0	5
		30	0.312	5	4	1	5
		166	0.259	5	5	4	4
		140	0.197	4	5	4	2
		141	0.245	5	4	4	4
		142	0.266	4	5	2	3
		35	0.245	5	4	2	4
		171	0.217	4	5	3	4
		145	0.225	4	4	4	3
		119	0.207	5	4	2	5
		147	0.278	4	5	2	5
		148	0.239	4	5	3	4
		176	0.222	5	4	2	4
		150	0.188	4	5	4	2
		70	0.237	5	4	1	5
		152	0.229	4	4	3	4
		180	0.139	4	5	3	5
		154	0.290	4	5	4	3
		155	0.269	5	5	1	4
		156	0.288	4	5	1	3
		76	0.258	5	4	1	5
		158	0.220	4	5	4	2
		186	0.262	5	5	1	4
		52	0.231	5	4	0	4
		161	0.353	5	5	1	5
		54	0.095	4	4	0	5

A.1.3 MSC multiple cooling rates SEGA recovery algorithm raw emergent population data from Figure 21

H9 MESENCHYMAL STEM CELLS

Improved solutions	Generation	Emergent population	Recovery	Sucrose	EG	Alanine	Taurine	Ectoine	Cooling rate
27	0	1	0.2475	4	5	0	5	3	0
		2	0.1197	1	3	5	5	0	5
		3	0.1808	5	2	4	0	2	5
		4	0.2077	4	5	3	0	5	5
		5	0.1643	4	4	4	2	3	1
		6	0.1789	4	0	1	0	0	4
		7	0.1301	4	1	5	0	2	2
		8	0.1801	4	4	1	2	2	3
		9	0.2481	4	4	1	4	3	0
		10	0.0691	0	2	5	2	3	1
		11	0.1365	4	1	3	4	5	5
		12	0.1533	3	0	0	1	5	1
		13	0.1562	4	1	5	2	1	1
		14	0.0734	3	2	2	4	3	3
		15	0.1074	5	1	4	4	2	3
		16	0.1365	0	0	3	4	5	0
		17	0.0749	3	2	0	2	0	4
		18	0.0305	1	3	0	3	1	3
		19	0.1928	4	4	2	0	1	5
		20	0.1005	0	4	3	5	0	2
		21	0.1559	0	5	0	4	4	5
		22	0.0394	0	2	1	4	2	5
		23	0.0951	1	1	0	0	5	3
		24	0.1149	3	0	5	3	2	3
		25	0.0359	2	0	1	0	1	1
		26	0.0756	2	0	5	5	2	2
		27	0.1390	2	5	2	0	4	2
13	1	1	0.2475	4	5	0	5	3	0
		29	0.1409	4	3	1	4	2	2
		30	0.1907	5	5	1	0	2	5
		4	0.2077	4	5	3	0	5	5
		5	0.1643	4	4	4	2	3	1
		6	0.1789	4	0	1	0	0	4
		7	0.1301	4	1	5	0	2	2
		8	0.1801	4	4	1	2	2	3
		9	0.2481	4	4	1	4	3	0
		10	0.0691	0	2	5	2	3	1
		11	0.1365	4	1	3	4	5	5
		39	0.2061	2	3	0	3	3	1
		40	0.2718	4	4	2	1	4	0
		41	0.1568	5	4	0	4	3	5
		42	0.1497	5	4	2	2	1	3
		16	0.1365	0	0	3	4	5	0
		44	0.1825	5	5	0	3	0	3
		45	0.1143	4	3	3	4	4	4
		19	0.1928	4	4	2	0	1	5
		47	0.2539	4	3	1	3	2	1
		21	0.1559	0	5	0	4	4	5
		49	0.1582	3	4	4	5	3	4
		23	0.0951	1	1	0	0	5	3
		51	0.2072	5	2	2	1	4	0
		52	0.0545	2	0	1	0	1	1
		53	0.1645	4	4	1	3	2	3
		27	0.1390	2	5	2	0	4	2

H9 MESENCHYMAL STEM CELLS									
Improved solutions	**Gen**	**Solution #**	**Scaled raw recovery**	**Sucrose**	**EG**	**Alanine**	**Taurine**	**Ectoine**	**Cooling rate**
5	2	1	0.2475	4	5	0	5	3	0
		29	0.1409	4	3	1	4	2	2
		57	0.2177	4	5	4	0	2	4
		4	0.2077	4	5	3	0	5	5
		5	0.1643	4	4	4	2	3	1
		6	0.1789	4	0	1	0	0	4
		7	0.1301	4	1	5	0	2	2
		8	0.1801	4	4	1	2	2	3
		9	0.2481	4	4	1	4	3	0
		10	0.0691	0	2	5	2	3	1
		65	0.1922	2	4	0	3	5	2
		39	0.2061	2	3	0	3	3	1
		40	0.2718	4	4	2	1	4	0
		68	0.1753	5	4	2	2	1	3
		42	0.1497	5	4	2	2	1	3
		16	0.1365	0	0	3	4	5	0
		44	0.1825	5	5	0	3	0	3
		45	0.1143	4	3	3	4	4	4
		19	0.1928	4	4	2	0	1	5
		47	0.2539	4	3	1	3	2	1
		75	0.2076	4	5	0	4	2	2
		76	0.1932	4	5	2	4	5	2
		23	0.0951	1	1	0	0	5	3
		51	0.2072	5	2	2	1	4	0
		52	0.0545	2	0	1	0	1	1
		53	0.1645	4	4	1	3	2	3
		27	0.1390	2	5	2	0	4	2
9	3	1	0.2475	4	5	0	5	3	0
		29	0.1409	4	3	1	4	2	2
		84	0.3575	3	5	2	0	3	4
		4	0.2077	4	5	3	0	5	5
		5	0.1643	4	4	4	2	3	1
		6	0.1789	4	0	1	0	0	4
		88	0.2035	3	4	2	3	4	0
		8	0.1801	4	4	1	2	2	3
		9	0.2481	4	4	1	4	3	0
		91	0.0821	3	3	2	1	4	3
		65	0.1922	2	4	0	3	5	2
		39	0.2061	2	3	0	3	3	1
		40	0.2718	4	4	2	1	4	0
		95	0.1999	4	5	1	0	2	0
		42	0.1497	5	4	2	2	1	3
		16	0.1365	0	0	3	4	5	0
		44	0.1825	5	5	0	3	0	3
		99	0.2742	1	4	0	1	5	1
		100	0.2406	3	4	1	0	2	5
		47	0.2539	4	3	1	3	2	1
		102	0.2410	4	5	0	3	3	1
		76	0.1932	4	5	2	4	5	2
		23	0.0951	1	1	0	0	5	3
		51	0.2072	5	2	2	1	4	0
		106	0.0982	1	1	0	0	4	1
		107	0.3147	3	5	1	1	5	0
		108	0.2190	4	5	0	3	4	1

H9 MESENCHYMAL STEM CELLS									
Improved solutions	**Gen**	**Solution #**	**Scaled raw recovery**	**Sucrose**	**EG**	**Alanine**	**Taurine**	**Ectoine**	**Cooling rate**
		1	0.2475	4	5	0	5	3	0
		29	0.1409	4	3	1	4	2	2
		84	0.3575	3	5	2	0	3	4
		4	0.2077	4	5	3	0	5	5
		113	0.2051	4	5	2	2	3	4
		6	0.1789	4	0	1	0	0	4
		88	0.2035	3	4	2	3	4	0
		8	0.1801	4	4	1	2	2	3
		9	0.2481	4	4	1	4	3	0
		91	0.0821	3	3	2	1	4	3
		65	0.1922	2	4	0	3	5	2
		39	0.2061	2	3	0	3	3	1
		40	0.2718	4	4	2	1	4	0
4	4	122	0.3553	4	5	1	0	2	2
		42	0.1497	5	4	2	2	1	3
		16	0.1365	0	0	3	4	5	0
		44	0.1825	5	5	0	3	0	3
		99	0.2742	1	4	0	1	5	1
		100	0.2406	3	4	1	0	2	5
		128	0.2810	3	5	1	2	3	0
		102	0.2410	4	5	0	3	3	1
		76	0.1932	4	5	2	4	5	2
		23	0.0951	1	1	0	0	5	3
		51	0.2072	5	2	2	1	4	0
		133	0.1820	4	4	0	0	1	4
		107	0.3147	3	5	1	1	5	0
		108	0.2190	4	5	0	3	4	1
		1	0.2475	4	5	0	5	3	0
		137	0.1624	5	5	0	2	2	1
		84	0.3575	3	5	2	0	3	4
		139	0.2188	4	3	3	0	2	2
		113	0.2051	4	5	2	2	3	4
		141	0.2478	4	4	0	0	0	2
		88	0.2035	3	4	2	3	4	0
		143	0.2322	4	5	3	1	2	5
		9	0.2481	4	4	1	4	3	0
		145	0.0895	3	0	2	1	1	4
		146	0.2047	3	5	0	1	4	0
		39	0.2061	2	3	0	3	3	1
		40	0.2718	4	4	2	1	4	0
11	5	122	0.3553	4	5	1	0	2	2
		150	0.2224	5	5	3	1	0	4
		151	0.1566	4	4	2	4	5	0
		44	0.1825	5	5	0	3	0	3
		99	0.2742	1	4	0	1	5	1
		100	0.2406	3	4	1	0	2	5
		128	0.2810	3	5	1	2	3	0
		102	0.2410	4	5	0	3	3	1
		157	0.2257	3	5	2	1	5	1
		23	0.0951	1	1	0	0	5	3
		51	0.2072	5	2	2	1	4	0
		160	0.2316	4	5	0	0	1	3
		107	0.3147	3	5	1	1	5	0
		162	0.2719	5	5	0	2	2	0

H9 MESENCHYMAL STEM CELLS									
Improved solutions	**Gen**	**Solution #**	**Scaled raw recovery**	**Sucrose**	**EG**	**Alanine**	**Taurine**	**Ectoine**	**Cooling rate**
2	6	1	0.2475	4	5	0	5	3	0
		137	0.1624	5	5	0	2	2	1
		84	0.3575	3	5	2	0	3	4
		139	0.2188	4	3	3	0	2	2
		113	0.2051	4	5	2	2	3	4
		141	0.2478	4	4	0	0	0	2
		169	0.2102	1	5	0	2	5	1
		143	0.2322	4	5	3	1	2	5
		9	0.2481	4	4	1	4	3	0
		145	0.0895	3	0	2	1	1	4
		146	0.2047	3	5	0	1	4	0
		39	0.2061	2	3	0	3	3	1
		40	0.2718	4	4	2	1	4	0
		122	0.3553	4	5	1	0	2	2
		150	0.2224	5	5	3	1	0	4
		151	0.1566	4	4	2	4	5	0
		44	0.1825	5	5	0	3	0	3
		180	0.2895	2	5	0	1	5	1
		100	0.2406	3	4	1	0	2	5
		128	0.2810	3	5	1	2	3	0
		102	0.2410	4	5	0	3	3	1
		157	0.2257	3	5	2	1	5	1
		23	0.0951	1	1	0	0	5	3
		51	0.2072	5	2	2	1	4	0
		160	0.2316	4	5	0	0	1	3
		107	0.3147	3	5	1	1	5	0
		162	0.2719	5	5	0	2	2	0
9	7	1	0.2475	4	5	0	5	3	0
		191	0.3738	3	5	0	4	4	0
		84	0.3575	3	5	2	0	3	4
		139	0.2188	4	3	3	0	2	2
		113	0.2051	4	5	2	2	3	4
		141	0.2478	4	4	0	0	0	2
		196	0.3972	0	5	0	2	5	0
		197	0.2793	2	5	2	0	5	4
		9	0.2481	4	4	1	4	3	0
		199	0.1150	1	3	0	1	3	3
		200	0.2898	1	5	0	3	5	0
		201	0.3501	3	5	0	1	4	0
		40	0.2718	4	4	2	1	4	0
		122	0.3553	4	5	1	0	2	2
		150	0.2224	5	5	3	1	0	4
		205	0.2225	2	5	1	2	5	0
		44	0.1825	5	5	0	3	0	3
		180	0.2895	2	5	0	1	5	1
		100	0.2406	3	4	1	0	2	5
		128	0.2810	3	5	1	2	3	0
		102	0.2410	4	5	0	3	3	1
		157	0.2257	3	5	2	1	5	1
		23	0.0951	1	1	0	0	5	3
		213	0.2090	0	5	0	1	5	1
		160	0.2316	4	5	0	0	1	3
		107	0.3147	3	5	1	1	5	0
		216	0.2881	3	5	0	3	5	0

H9 MESENCHYMAL STEM CELLS									
Improved solutions	**Gen**	**Solution #**	**Scaled raw recovery**	**Sucrose**	**EG**	**Alanine**	**Taurine**	**Ectoine**	**Cooling rate**
3	8	217	0.3273	2	5	2	2	5	3
		191	0.3738	3	5	0	4	4	0
		84	0.3575	3	5	2	0	3	4
		139	0.2188	4	3	3	0	2	2
		113	0.2051	4	5	2	2	3	4
		141	0.2478	4	4	0	0	0	2
		196	0.3972	0	5	0	2	5	0
		224	0.2892	0	5	2	1	5	3
		9	0.2481	4	4	1	4	3	0
		199	0.1150	1	3	0	1	3	3
		200	0.2898	1	5	0	3	5	0
		201	0.3501	3	5	0	1	4	0
		40	0.2718	4	4	2	1	4	0
		122	0.3553	4	5	1	0	2	2
		150	0.2224	5	5	3	1	0	4
		205	0.2225	2	5	1	2	5	0
		44	0.1825	5	5	0	3	0	3
		180	0.2895	2	5	0	1	5	1
		100	0.2406	3	4	1	0	2	5
		128	0.2810	3	5	1	2	3	0
		102	0.2410	4	5	0	3	3	1
		157	0.2257	3	5	2	1	5	1
		239	0.1491	1	1	0	0	5	3
		213	0.2090	0	5	0	1	5	1
		160	0.2316	4	5	0	0	1	3
		107	0.3147	3	5	1	1	5	0
		216	0.2881	3	5	0	3	5	0
0	9	217	0.3273	2	5	2	2	5	3
		191	0.3738	3	5	0	4	4	0
		84	0.3575	3	5	2	0	3	4
		139	0.2188	4	3	3	0	2	2
		113	0.2051	4	5	2	2	3	4
		141	0.2478	4	4	0	0	0	2
		196	0.3972	0	5	0	2	5	0
		224	0.2892	0	5	2	1	5	3
		9	0.2481	4	4	1	4	3	0
		199	0.1150	1	3	0	1	3	3
		200	0.2898	1	5	0	3	5	0
		201	0.3501	3	5	0	1	4	0
		40	0.2718	4	4	2	1	4	0
		122	0.3553	4	5	1	0	2	2
		150	0.2224	5	5	3	1	0	4
		205	0.2225	2	5	1	2	5	0
		44	0.1825	5	5	0	3	0	3
		180	0.2895	2	5	0	1	5	1
		100	0.2406	3	4	1	0	2	5
		128	0.2810	3	5	1	2	3	0
		102	0.2410	4	5	0	3	3	1
		157	0.2257	3	5	2	1	5	1
		239	0.1491	1	1	0	0	5	3
		213	0.2090	0	5	0	1	5	1
		160	0.2316	4	5	0	0	1	3
		107	0.3147	3	5	1	1	5	0
		216	0.2881	3	5	0	3	5	0

A.2 Chapter 8 raw algorithm data

A.2.1 MSC single cooling rate SGI attachment algorithm emergent population data from Figure 23

H9 MESENCHYMAL STEM CELLS

Improved solutions	Generation	Emergent population	Sucrose	Glycerol	Isoleucine	Recovered	Attached	Recovered-Attached (corrected to 0 if attached > recovery)
5	0	1	4	0	1	0.40	0.14	0.26
		2	0	0	4	0.11	0.00	0.11
		3	4	1	5	0.26	0.08	0.18
		4	0	2	2	0.72	0.38	0.34
		5	4	4	1	0.83	0.60	0.23
3	1	6	1	3	4	0.61	0.40	0.21
		7	0	2	1	0.46	0.46	0.00
		8	1	4	3	0.65	0.62	0.03
		4	0	2	2	0.72	0.38	0.34
		5	4	4	1	0.83	0.60	0.23
2	2	11	1	3	4	0.42	0.42	0.00
		12	0	3	1	0.61	0.54	0.07
		8	1	4	3	0.65	0.62	0.03
		4	0	2	2	0.72	0.38	0.34
		5	4	4	1	0.83	0.60	0.23
5	3	16	1	3	2	0.63	0.80	0.00
		17	2	4	4	0.63	0.74	0.00
		18	1	5	1	0.54	0.96	0.00
		19	0	2	1	0.47	0.48	0.00
		20	5	5	1	0.75	0.70	0.05
2	4	16	1	3	2	0.70	0.80	0.00
		22	0	4	3	0.45	0.82	0.00
		18	1	5	1	0.52	0.96	0.00
		24	0	2	1	0.51	0.56	0.00
		20	5	5	1	0.77	0.70	0.07

A.3 Chapter 5 screening data

	SUCROSE 1C/min				Replicates							
Combo number	Sugar	Sugar Alcohol	Additive	Average	1	2	3	4	5	6	7	8
0				0.0468	0.0313	0.0446	0.0353	0.0587	0.0855	0.0522	0.0330	0.0359
1	Sucrose			0.0512	0.0572	0.0449	0.0594	0.0594				
2		Glycerol		0.0247	0.0256	0.0229	0.0233	0.0175	0.0229	0.0194	0.0149	0.0168
3		Sorbitol		0.0306	0.0330	0.0228	0.0292	0.0176	0.0249	0.0288	0.0162	0.0176
4		Arabitol		0.0110	0.0247	0.0092	0.0068	0.0128	0.0140	-0.0039	-0.0051	-0.0122
5		Inositol		0.0155	0.0133	0.0120	0.0101	0.0107	0.0120	0.0120	0.0133	0.0230
6		Erythritol		0.0040	0.0008	0.0021	0.0008	-0.0025	-0.0018	0.0002	0.0008	-0.0005
7		Xylitol		0.0094	-0.0002	0.0060	0.0005	0.0060	0.0054	0.0095	0.0005	-0.0002
8		Mannitol		0.0060	0.0002	0.0024	-0.0028	-0.0013	-0.0021	0.0092	0.0002	0.0032
9		Ribitol(adonitol)		0.0594	missing	missing	missing	missing	missing	missing	missing	missing
10			Proline	0.0168	-0.0258							
11			Alanine	0.0037	-0.0183							
12			Isoleucine	0.0048	-0.0134							
13			Creatine	0.0071	-0.0092							
14			Valine	0.0038	-0.0099							
15			Taurine	0.0046	-0.0138							
16			Ectoine	-0.0052	-0.0299							
17	Sucrose	Glycerol		0.0636	0.0799	0.0821	0.0724	0.0687				
18	Sucrose	Sorbitol		0.0497	0.0698	0.0607	0.0570	0.0441				
19	Sucrose	Arabitol		0.0892	0.1319	0.0914	0.0936	0.0959				
20	Sucrose	Inositol		0.0632	0.0735	0.0876	0.0584	0.0735				
21	Sucrose	Erythritol		0.0556	0.0628	0.0609	0.0798	0.0453				
22	Sucrose	Xylitol		0.0621	0.0853	0.0773	0.0662	0.0642				
23	Sucrose	Mannitol		0.0554	0.0805	0.0670	0.0529	0.0515				
24	Sucrose	Ribitol(adonitol)		0.0288	missing	missing	missing	missing				
25	Sucrose		Proline	0.0394	0.0461	0.0297	0.0451	0.0600				
26	Sucrose		Alanine	0.0443	0.0461	0.0467	0.0520	0.0590				
27	Sucrose		Isoleucine	0.0239	0.0324	0.0234	0.0419	-0.0030				
28	Sucrose		Creatine	0.0289	0.0416	0.0337	0.0587	0.0014				
29	Sucrose		Valine	0.0388	0.0200	0.0469	0.0507	0.0695				
30	Sucrose		Taurine	0.0316	0.0539	0.0528	0.0496	-0.0109				
31	Sucrose		Ectoine	0.0739	0.0706	0.0565	0.0528	0.1754				
32		Glycerol	Proline	0.0118	0.0275							
33		Glycerol	Alanine	0.0181	0.0412							
34		Glycerol	Isoleucine	0.0040	0.0202							
35		Glycerol	Creatine	0.0209	0.0285							
36		Glycerol	Valine	0.0175	0.0231							
37		Glycerol	Taurine	0.0132	0.0164							
38		Glycerol	Ectoine	0.0337	0.0566							
39		Sorbitol	Proline	0.0120	0.0121							
40		Sorbitol	Alanine	0.0160	0.0201							
41		Sorbitol	Isoleucine	0.0131	0.0129							
42		Sorbitol	Creatine	0.0225	0.0221							
43		Sorbitol	Valine	0.0103	0.0199							
44		Sorbitol	Taurine	0.0069	0.0116							
45		Sorbitol	Ectoine	0.0149	0.0290							
46		Arabitol	Proline	0.0150	0.0325							
47		Arabitol	Alanine	0.0181	0.0380							
48		Arabitol	Isoleucine	-0.0004	-0.0009							
49		Arabitol	Creatine	0.0101	0.0194							
50		Arabitol	Valine	0.0061	0.0128							
51		Arabitol	Taurine	0.0189	0.0380							
52		Arabitol	Ectoine	0.0088	0.0116							
53		Inositol	Proline	0.0100	0.0194							
54		Inositol	Alanine	0.0163	0.0265							
55		Inositol	Isoleucine	0.0015	-0.0024							
56		Inositol	Creatine	0.0148	0.0200							
57		Inositol	Valine	0.0016	0.0027							
58		Inositol	Taurine	0.0171	0.0343							
59		Inositol	Ectoine	0.0095	0.0188							
60		Erythritol	Proline	-0.0224	-0.0472							
61		Erythritol	Alanine	-0.0010	0.0008							
62		Erythritol	Isoleucine	0.0024	0.0061							
63		Erythritol	Creatine	0.0045	0.0111							
64		Erythritol	Valine	0.0065	0.0038							
65		Erythritol	Taurine	-0.0069	-0.0140							
66		Erythritol	Ectoine	0.0027	0.0021							
67		Xylitol	Proline	0.0085	0.0085							
68		Xylitol	Alanine	0.0102	0.0102							
69		Xylitol	Isoleucine	-0.0002	-0.0002							
70		Xylitol	Creatine	0.0009	0.0009							
71		Xylitol	Valine	0.0015	0.0015							
72		Xylitol	Taurine	-0.0057	-0.0057							
73		Xylitol	Ectoine	-0.0002	-0.0002							
74		Mannitol	Proline	-0.0203	-0.0203							
75		Mannitol	Alanine	-0.0188	-0.0117							
76		Mannitol	Isoleucine	-0.0159	-0.0136							
77		Mannitol	Creatine	-0.0101	-0.0069							
78		Mannitol	Valine	-0.0078	-0.0065							
79		Mannitol	Taurine	-0.0086	-0.0073							
80		Mannitol	Ectoine	0.0024	0.0186							

	SUCROSE 1C/min				Replicates							
Combo number	Sugar	Sugar Alcohol	Additive	Average	1	2	3	4	5	6	7	8
81		Ribitol(adonitol)	Proline	-0.0299	missing							
82		Ribitol(adonitol)	Alanine	0.0799	missing							
83		Ribitol(adonitol)	Isoleucine	0.0821	missing							
84		Ribitol(adonitol)	Creatine	0.0724	missing							
85		Ribitol(adonitol)	Valine	0.0687	missing							
86		Ribitol(adonitol)	Taurine	0.0698	missing							
87		Ribitol(adonitol)	Ectoine	0.0607	missing							
88	Sucrose	Glycerol	Proline	0.0504	0.0659	0.0415	0.0531	0.0344				
89	Sucrose	Glycerol	Alanine	0.0414	0.0422	0.0323	0.0448	0.0437				
90	Sucrose	Glycerol	Isoleucine	0.0668	0.0514	0.0514	0.0453	0.0540				
91	Sucrose	Glycerol	Creatine	0.0598	0.0652	0.0534	0.0419	0.0469				
92	Sucrose	Glycerol	Valine	0.0596	0.0615	0.0611	0.0487	0.0330				
93	Sucrose	Glycerol	Taurine	0.0563	0.0507	0.0642	0.0321	0.0388				
94	Sucrose	Glycerol	Ectoine	0.0630	0.0754	0.0844	0.0374	0.0442				
95	Sucrose	Sorbitol	Proline	0.0487	0.0352	0.0381	0.0456	0.0368				
96	Sucrose	Sorbitol	Alanine	0.0502	0.0397	0.0582	0.0473	0.0473				
97	Sucrose	Sorbitol	Isoleucine	0.0542	0.0427	0.0602	0.0466	0.0482				
98	Sucrose	Sorbitol	Creatine	0.0582	0.0570	0.0604	0.0530	0.0577				
99	Sucrose	Sorbitol	Valine	0.0527	0.0574	0.0474	0.0468	0.0510				
100	Sucrose	Sorbitol	Taurine	0.0544	0.0530	0.0514	0.0315	0.0564				
101	Sucrose	Sorbitol	Ectoine	0.0609	0.0723	0.0615	0.0646	0.0609				
102	Sucrose	Arabitol	Proline	0.0642	0.0714	0.0592	0.0482	0.0570				
103	Sucrose	Arabitol	Alanine	0.0739	0.0869	0.0758	0.0780	0.0515				
104	Sucrose	Arabitol	Isoleucine	0.0549	0.0609	0.0487	0.0575	0.0411				
105	Sucrose	Arabitol	Creatine	0.0837	0.0948	0.0948	0.0948	0.0703				
106	Sucrose	Arabitol	Valine	0.0586	0.0719	0.0400	0.0553	0.0454				
107	Sucrose	Arabitol	Taurine	0.0566	0.0647	0.0581	0.0504	0.0427				
108	Sucrose	Arabitol	Ectoine	0.0642	0.0841	0.0609	0.0664	0.0564				
109	Sucrose	Inositol	Proline	0.0559	0.0818	0.0696	0.0306	0.0460				
110	Sucrose	Inositol	Alanine	0.0607	0.0699	0.0753	0.0463	0.0511				
111	Sucrose	Inositol	Isoleucine	0.0414	0.0484	0.0460	0.0383	0.0329				
112	Sucrose	Inositol	Creatine	0.0704	0.0987	0.0668	0.0565	0.0596				
113	Sucrose	Inositol	Valine	0.0515	0.0523	0.0668	0.0451	0.0416				
114	Sucrose	Inositol	Taurine	0.0592	0.0638	0.0711	0.0596	0.0553				
115	Sucrose	Inositol	Ectoine	0.0700	0.0790	0.0827	0.0790	0.0796				
116	Sucrose	Erythritol	Proline	0.0403	0.0584	0.0336	0.0503	0.0140				
117	Sucrose	Erythritol	Alanine	0.0458	0.0641	0.0367	0.0385	0.0299				
118	Sucrose	Erythritol	Isoleucine	0.0307	0.0358	0.0376	0.0180	0.0162				
119	Sucrose	Erythritol	Creatine	0.0581	0.0808	0.0606	0.0625	0.0401				
120	Sucrose	Erythritol	Valine	0.0433	0.0491	0.0299	0.0503	0.0355				
121	Sucrose	Erythritol	Taurine	0.0442	0.0410	0.0472	0.0460	0.0281				
122	Sucrose	Erythritol	Ectoine	0.0495	0.0534	0.0710	0.0584	0.0324				
123	Sucrose	Xylitol	Proline	0.0348	0.0463	0.0328	0.0450	0.0264				
124	Sucrose	Xylitol	Alanine	0.0509	0.0596	0.0531	0.0629	0.0370				
125	Sucrose	Xylitol	Isoleucine	0.0384	0.0512	0.0551	0.0473	0.0415				
126	Sucrose	Xylitol	Creatine	0.0580	0.0593	0.0554	0.0632	0.0704				
127	Sucrose	Xylitol	Valine	0.0395	0.0444	0.0392	0.0457	0.0347				
128	Sucrose	Xylitol	Taurine	0.0437	0.0402	0.0392	0.0457	0.0347				
129	Sucrose	Xylitol	Ectoine	0.0475	0.0603	0.0583	0.0583	0.0590				
130	Sucrose	Mannitol	Proline	0.0203	0.0491	0.0193	0.0070	0.0063				
131	Sucrose	Mannitol	Alanine	0.0392	0.0526	0.0324	0.0366	0.0276				
132	Sucrose	Mannitol	Isoleucine	0.0336	0.0345	0.0234	0.0331	0.0262				
133	Sucrose	Mannitol	Creatine	0.0440	0.0452	0.0494	0.0286	0.0272				
134	Sucrose	Mannitol	Valine	0.0406	0.0442	0.0400	0.0372	0.0276				
135	Sucrose	Mannitol	Taurine	0.0465	0.0582	0.0631	0.0338	0.0248				
136	Sucrose	Mannitol	Ectoine	0.0516	0.0614	0.0628	0.0473	0.0369				
137	Sucrose	Ribitol(adonitol)	Proline	-0.0109	missing	missing	missing	missing				
138	Sucrose	Ribitol(adonitol)	Alanine	0.0706	missing	missing	missing	missing				
139	Sucrose	Ribitol(adonitol)	Isoleucine	0.0565	missing	missing	missing	missing				
140	Sucrose	Ribitol(adonitol)	Creatine	0.0528	missing	missing	missing	missing				
141	Sucrose	Ribitol(adonitol)	Valine	0.1754	missing	missing	missing	missing				
142	Sucrose	Ribitol(adonitol)	Taurine	0.0275	missing	missing	missing	missing				
143	Sucrose	Ribitol(adonitol)	Ectoine	0.0412	missing	missing	missing	missing				

	SUCROSE 3C/min				Replicates							
Combo number	Sugar	Sugar Alcohol	Additive	Average	1	2	3	4	5	6	7	8
0				-0.0111	-0.0114	-0.0108	-0.0161	-0.0161	-0.0161	-0.0125	-0.0114	0.0052
1	Sucrose			0.0649	0.0842	0.0932	0.0804	0.0829				
2		Glycerol		0.0232	0.0145	0.0333	0.0212	0.0456	0.0356	0.0234	0.0123	0.0389
3		Sorbitol		0.0163	0.0079	0.0092	0.0319	0.0221	0.0279	0.0214	0.0221	0.0201
4		Arabitol		0.0098	0.0093	0.0153	0.0127	0.0084	0.0119	-0.0054	0.0214	0.0275
5		Inositol		0.0105	0.0170	0.0079	0.0133	0.0111	0.0124	0.0156	0.0143	0.0138
6		Erythritol		0.0052	missing	missing	missing	missing	missing	missing	missing	missing
7		Xylitol		0.0316	0.0284	0.0234	0.0209	0.0230	0.0168	0.0247	0.0276	0.0356
8		Mannitol		0.0362	0.0382	0.0205	0.0188	0.0176	0.0264	0.0329	0.0430	0.0353
9		Ribitol(adonitol)		0.0060	0.0096	-0.0043	-0.0049	-0.0049	-0.0105	-0.0030	-0.0049	-0.0036
10			Proline	0.0403	-0.0024							
11			Alanine	0.0030	-0.0086							
12			Isoleucine	0.0088	-0.0158							
13			Creatine	0.0055	-0.0102							
14			Valine	0.0147	-0.0162							
15			Taurine	0.0185	0.0015							
16			Ectoine	0.0181	0.0128							
17	Sucrose	Glycerol		0.1168	0.1278	0.1549	0.1788	0.1102				
18	Sucrose	Sorbitol		0.1007	0.1084	0.1275	0.1182	0.1105				
19	Sucrose	Arabitol		0.0490	0.0819	0.0447	0.0646	0.0456				
20	Sucrose	Inositol		0.0721	0.0942	0.0947	0.0987	0.0638				
21	Sucrose	Erythritol		0.0319	missing	missing	missing	missing				
22	Sucrose	Xylitol		0.0722	0.0918	0.1015	0.0932	0.0524				
23	Sucrose	Mannitol		0.0765	0.0922	0.0696	0.1042	0.0884				
24	Sucrose	Ribitol(adonitol)		0.0659	0.0707	0.0741	0.0815	0.0815				
25	Sucrose		Proline	0.0500	0.0697	0.0552	0.0678	0.0351				
26	Sucrose		Alanine	0.0782	0.0876	0.1188	0.0921	0.0722				
27	Sucrose		Isoleucine	0.0484	0.0646	0.0691	0.0564	0.0426				
28	Sucrose		Creatine	0.0749	0.0957	0.1067	0.0789	0.0777				
29	Sucrose		Valine	0.0521	0.0637	0.0675	0.0599	0.0567				
30	Sucrose		Taurine	0.0733	0.0957	0.1028	0.0892	0.0707				
31	Sucrose		Ectoine	0.0934	0.1126	0.1087	0.1165	0.1172				
32		Glycerol	Proline	0.0051	0.0157							
33		Glycerol	Alanine	0.0352	0.0489							
34		Glycerol	Isoleucine	0.2204	0.4133							
35		Glycerol	Creatine	0.0177	0.0184							
36		Glycerol	Valine	0.0005	-0.0069							
37		Glycerol	Taurine	0.0095	0.0057							
38		Glycerol	Ectoine	0.0161	0.0212							
39		Sorbitol	Proline	0.0357	0.0589							
40		Sorbitol	Alanine	0.0179	0.0201							
41		Sorbitol	Isoleucine	0.0096	0.0050							
42		Sorbitol	Creatine	0.0215	0.0293							
43		Sorbitol	Valine	0.0374	0.0374							
44		Sorbitol	Taurine	0.0414	0.0414							
45		Sorbitol	Ectoine	0.0211	0.0211							
46		Arabitol	Proline	0.0114	0.0114							
47		Arabitol	Alanine	0.0084	0.0084							
48		Arabitol	Isoleucine	-0.0041	-0.0041							
49		Arabitol	Creatine	0.0097	0.0097							
50		Arabitol	Valine	0.0041	0.0041							
51		Arabitol	Taurine	0.0154	0.0024							
52		Arabitol	Ectoine	0.0172	0.0110							
53		Inositol	Proline	0.0101	-0.0008							
54		Inositol	Alanine	0.0181	0.0131							
55		Inositol	Isoleucine	0.0069	-0.0030							
56		Inositol	Creatine	0.0259	0.0272							
57		Inositol	Valine	0.0116	-0.0043							
58		Inositol	Taurine	0.0307	0.0258							
59		Inositol	Ectoine	0.0311	0.0240							
60		Erythritol	Proline	0.0205	missing							
61		Erythritol	Alanine	0.0188	missing							
62		Erythritol	Isoleucine	0.0176	missing							
63		Erythritol	Creatine	0.0264	missing							
64		Erythritol	Valine	0.0329	missing							
65		Erythritol	Taurine	0.0430	missing							
66		Erythritol	Ectoine	0.0353	missing							
67		Xylitol	Proline	0.0214	0.0333							
68		Xylitol	Alanine	0.0146	0.0335							
69		Xylitol	Isoleucine	0.0006	0.0060							
70		Xylitol	Creatine	0.0056	0.0161							
71		Xylitol	Valine	0.0043	0.0190							
72		Xylitol	Taurine	0.0171	0.0373							
73		Xylitol	Ectoine	0.0239	0.0526							
74		Mannitol	Proline	0.0039	0.0115							
75		Mannitol	Alanine	0.0047	0.0118							
76		Mannitol	Isoleucine	-0.0087	-0.0088							
77		Mannitol	Creatine	0.0069	0.0297							
78		Mannitol	Valine	0.0052	0.0205							
79		Mannitol	Taurine	0.0128	0.0418							
80		Mannitol	Ectoine	0.0242	0.0469							

	SUCROSE 3C/min				Replicates							
Combo number	Sugar	Sugar Alcohol	Additive	Average	1	2	3	4	5	6	7	8
81		Ribitol(adonitol)	Proline	-0.0031	-0.0189							
82		Ribitol(adonitol)	Alanine	0.0649	0.0020							
83		Ribitol(adonitol)	Isoleucine	0.0706	-0.0136							
84		Ribitol(adonitol)	Creatine	0.0847	-0.0093							
85		Ribitol(adonitol)	Valine	0.0472	-0.0158							
86		Ribitol(adonitol)	Taurine	0.0565	0.0046							
87		Ribitol(adonitol)	Ectoine	0.0751	0.0227							
88	Sucrose	Glycerol	Proline	0.1043	0.1295	0.1938	0.0598	0.0200				
89	Sucrose	Glycerol	Alanine	0.1477	0.2498	0.1878	0.1307	0.0598				
90	Sucrose	Glycerol	Isoleucine	0.4834	0.7772	0.6676	0.6896	0.2004				
91	Sucrose	Glycerol	Creatine	0.0573	0.0783	0.0461	0.0644	0.0530				
92	Sucrose	Glycerol	Valine	0.0845	0.0461	0.1272	0.1178	0.0667				
93	Sucrose	Glycerol	Taurine	0.1105	0.2028	0.1149	0.0835	0.1055				
94	Sucrose	Glycerol	Ectoine	0.1175	0.1113	0.0593	0.1561	0.1668				
95	Sucrose	Sorbitol	Proline	0.0840	0.0740	0.1017	0.0941	0.0556				
96	Sucrose	Sorbitol	Alanine	0.1043	0.1066	0.1108	0.1066	0.0989				
97	Sucrose	Sorbitol	Isoleucine	0.0822	0.0843	0.0961	0.0899	0.0768				
98	Sucrose	Sorbitol	Creatine	0.1153	0.0909	0.1239	0.1324	0.1140				
99	Sucrose	Sorbitol	Valine	0.1036	0.1077	0.1021	0.1324	0.0723				
100	Sucrose	Sorbitol	Taurine	0.1128	0.1000	0.1063	0.1317	0.1133				
101	Sucrose	Sorbitol	Ectoine	0.1470	0.1471	0.1507	0.1572	0.1328				
102	Sucrose	Arabitol	Proline	0.0151	0.0064	0.0197	-0.0191	-0.0235				
103	Sucrose	Arabitol	Alanine	0.0477	0.0556	0.0259	0.0268	0.0286				
104	Sucrose	Arabitol	Isoleucine	0.0432	0.0461	0.0398	0.0184	0.0184				
105	Sucrose	Arabitol	Creatine	0.0666	0.0911	0.0810	0.0583	0.0501				
106	Sucrose	Arabitol	Valine	0.0464	0.0623	0.0282	0.0255	0.0237				
107	Sucrose	Arabitol	Taurine	0.0459	0.0438	0.0447	0.0331	0.0384				
108	Sucrose	Arabitol	Ectoine	0.0762	0.0842	0.0669	0.0605	0.0651				
109	Sucrose	Inositol	Proline	0.0648	0.0840	0.0870	0.0340	0.0307				
110	Sucrose	Inositol	Alanine	0.0708	0.0682	0.0750	0.0696	0.0706				
111	Sucrose	Inositol	Isoleucine	0.0533	0.0592	0.0530	0.0439	0.0363				
112	Sucrose	Inositol	Creatine	0.0890	0.1037	0.0987	0.0987	0.0623				
113	Sucrose	Inositol	Valine	0.0728	0.0532	0.0858	0.0750	0.0686				
114	Sucrose	Inositol	Taurine	0.0668	0.0503	0.0818	0.0789	0.0532				
115	Sucrose	Inositol	Ectoine	0.0944	0.0619	0.1255	0.1188	0.1107				
116	Sucrose	Erythritol	Proline	0.0678	missing	missing	missing	missing				
117	Sucrose	Erythritol	Alanine	0.0351	missing	missing	missing	missing				
118	Sucrose	Erythritol	Isoleucine	0.0876	missing	missing	missing	missing				
119	Sucrose	Erythritol	Creatine	0.1188	missing	missing	missing	missing				
120	Sucrose	Erythritol	Valine	0.0921	missing	missing	missing	missing				
121	Sucrose	Erythritol	Taurine	0.0722	missing	missing	missing	missing				
122	Sucrose	Erythritol	Ectoine	0.0646	missing	missing	missing	missing				
123	Sucrose	Xylitol	Proline	0.0530	0.0619	0.0561	0.0417	0.0365				
124	Sucrose	Xylitol	Alanine	0.0642	0.0733	0.0715	0.0697	0.0502				
125	Sucrose	Xylitol	Isoleucine	0.0562	0.0670	0.0594	0.0577	0.0541				
126	Sucrose	Xylitol	Creatine	0.0913	0.0852	0.0902	0.0889	0.0966				
127	Sucrose	Xylitol	Valine	0.0696	0.0628	0.0686	0.0583	0.0517				
128	Sucrose	Xylitol	Taurine	0.0701	0.0927	0.0686	0.0583	0.0517				
129	Sucrose	Xylitol	Ectoine	0.0857	0.0923	0.0932	0.0855	0.0800				
130	Sucrose	Mannitol	Proline	0.0557	0.0551	0.0643	0.0404	0.0551				
131	Sucrose	Mannitol	Alanine	0.0785	0.1039	0.0674	0.0761	0.0774				
132	Sucrose	Mannitol	Isoleucine	0.0730	0.0837	0.0588	0.0830	0.0799				
133	Sucrose	Mannitol	Creatine	0.0906	0.0846	0.0721	0.1138	0.1260				
134	Sucrose	Mannitol	Valine	0.0804	0.0551	0.0843	0.0931	0.0737				
135	Sucrose	Mannitol	Taurine	0.0970	0.1083	0.0619	0.1090	0.1032				
136	Sucrose	Mannitol	Ectoine	0.1108	0.1144	0.1029	0.1119	0.1357				
137	Sucrose	Ribitol(adonitol)	Proline	0.0594	0.0550	0.0610	0.0556	0.0550				
138	Sucrose	Ribitol(adonitol)	Alanine	0.0831	0.1069	0.0802	0.0520	0.0640				
139	Sucrose	Ribitol(adonitol)	Isoleucine	0.0636	0.0717	0.0331	0.0550	0.0496				
140	Sucrose	Ribitol(adonitol)	Creatine	0.0869	0.0945	0.0680	0.0775	0.0782				
141	Sucrose	Ribitol(adonitol)	Valine	0.0705	0.0677	0.0596	0.0523	0.0556				
142	Sucrose	Ribitol(adonitol)	Taurine	0.0392	0.0443	0.0490	0.0403	0.0470				
143	Sucrose	Ribitol(adonitol)	Ectoine	0.0631	0.0761	0.0653	0.0580	0.0674				

	SUCROSE 5C/min				Replicates							
Combo number	Sugar	Sugar Alcohol	Additive	Average	1	2	3	4	5	6	7	8
0				0.0207	0.0082	0.0204	0.0248	0.0237	0.0299	0.0207	0.0181	0.0201
1	Sucrose			0.0663	0.0981	0.0583	0.0807	0.0694				
2		Glycerol		0.0645	0.0739	0.0622	0.0715	0.0557	0.0858	0.0810	0.0640	0.0631
3		Sorbitol		0.0407	0.0463	0.0442	0.0345	0.0289	0.0415	0.0447	0.0469	0.0491
4		Arabitol		0.0330	0.0283	0.0277	0.0379	0.0359	0.0275	0.0374	0.0433	0.0383
5		Inositol		0.0411	0.0503	0.0399	0.0506	0.0371	0.0503	0.0428	0.0337	0.0468
6		Erythritol		0.0358	0.0442	0.0469	0.0288	0.0461	0.0298	0.0429	0.0373	0.0260
7		Xylitol		0.0405	0.0382	0.0339	0.0348	0.0342	0.0296	0.0227	0.0336	0.0397
8		Mannitol		0.0633	0.0655	0.0780	0.0668	0.0389	0.0616	0.0663	0.0595	0.0745
9		Ribitol(adonitol)		0.0294	0.0270	0.0299	0.0383	0.0203	0.0295	0.0186	0.0199	0.0001
10			Proline	0.0587	0.0480							
11			Alanine	0.0581	0.0424							
12			Isoleucine	0.0387	0.0153							
13			Creatine	0.0526	0.0337							
14			Valine	0.0386	0.0215							
15			Taurine	0.0682	0.0506							
16			Ectoine	0.0816	0.0822							
17	Sucrose	Glycerol		0.0424	missing	0.0057	0.0634	0.0365				
18	Sucrose	Sorbitol		0.0982	0.1231	0.0875	0.1268	0.0903				
19	Sucrose	Arabitol		0.0708	0.0802	0.0700	0.0844	0.0732				
20	Sucrose	Inositol		0.0846	0.1198	0.0975	0.0799	0.0814				
21	Sucrose	Erythritol		0.0965	0.1191	0.1163	0.1109	0.1019				
22	Sucrose	Xylitol		0.0871	0.1153	0.1012	0.1016	0.0886				
23	Sucrose	Mannitol		0.0705	0.1051	0.0786	0.0701	0.0574				
24	Sucrose	Ribitol(adonitol)		0.0790	0.0891	0.0880	0.0957	0.0776				
25	Sucrose		Proline	0.0572	0.0742	0.0534	0.0523	0.0591				
26	Sucrose		Alanine	0.0813	0.1026	0.0910	0.0887	0.0753				
27	Sucrose		Isoleucine	0.0574	0.0707	0.0664	0.0660	0.0557				
28	Sucrose		Creatine	0.0790	0.1130	0.0689	0.1036	0.0818				
29	Sucrose		Valine	0.0617	0.0724	0.0685	0.0712	0.0586				
30	Sucrose		Taurine	0.0776	0.0861	0.0877	0.0889	0.0893				
31	Sucrose		Ectoine	0.0985	0.1269	0.0936	0.1274	0.1170				
32		Glycerol	Proline	0.0611	0.0848							
33		Glycerol	Alanine	0.0676	0.0920							
34		Glycerol	Isoleucine	0.0324	0.0264							
35		Glycerol	Creatine	0.0782	0.1062							
36		Glycerol	Valine	0.0601	0.0803							
37		Glycerol	Taurine	0.0989	0.1472							
38		Glycerol	Ectoine	0.0769	0.1167							
39		Sorbitol	Proline	0.0494	0.0485							
40		Sorbitol	Alanine	0.0495	0.0562							
41		Sorbitol	Isoleucine	0.0256	0.0176							
42		Sorbitol	Creatine	0.0539	0.0609							
43		Sorbitol	Valine	0.0369	0.0296							
44		Sorbitol	Taurine	0.0559	0.0650							
45		Sorbitol	Ectoine	0.0366	0.0443							
46		Arabitol	Proline	0.0435	0.0409							
47		Arabitol	Alanine	0.0373	0.0449							
48		Arabitol	Isoleucine	0.0285	0.0142							
49		Arabitol	Creatine	0.0383	0.0393							
50		Arabitol	Valine	0.0262	0.0264							
51		Arabitol	Taurine	0.0370	0.0359							
52		Arabitol	Ectoine	0.0426	0.0513							
53		Inositol	Proline	0.0461	0.0574							
54		Inositol	Alanine	0.0545	0.0749							
55		Inositol	Isoleucine	0.0213	0.0130							
56		Inositol	Creatine	0.0526	0.0825							
57		Inositol	Valine	0.0298	0.0260							
58		Inositol	Taurine	0.0655	0.0914							
59		Inositol	Ectoine	0.0783	0.0910							
60		Erythritol	Proline	0.0605	0.0430							
61		Erythritol	Alanine	0.0530	0.0392							
62		Erythritol	Isoleucine	0.0259	0.0130							
63		Erythritol	Creatine	0.0507	0.0399							
64		Erythritol	Valine	0.0416	0.0168							
65		Erythritol	Taurine	0.0622	0.0649							
66		Erythritol	Ectoine	0.0690	0.0635							
67		Xylitol	Proline	0.0368	0.0466							
68		Xylitol	Alanine	0.0419	0.0540							
69		Xylitol	Isoleucine	0.0310	0.0236							
70		Xylitol	Creatine	0.0298	0.0392							
71		Xylitol	Valine	0.0348	0.0402							
72		Xylitol	Taurine	0.0208	0.0230							
73		Xylitol	Ectoine	0.0275	0.0351							
74		Mannitol	Proline	0.0177	0.0353							
75		Mannitol	Alanine	0.0474	0.0468							
76		Mannitol	Isoleucine	0.0258	0.0091							
77		Mannitol	Creatine	0.0450	0.0747							
78		Mannitol	Valine	0.0382	0.0426							
79		Mannitol	Taurine	0.0461	0.0706							
80		Mannitol	Ectoine	0.0513	0.0521							

	SUCROSE 5C/min				Replicates							
Combo number	Sugar	Sugar Alcohol	Additive	Average	1	2	3	4	5	6	7	8
81		Ribitol(adonitol)	Proline	0.0497	0.0172							
82		Ribitol(adonitol)	Alanine	0.0215	0.0215							
83		Ribitol(adonitol)	Isoleucine	0.0072	0.0087							
84		Ribitol(adonitol)	Creatine	0.0448	0.0261							
85		Ribitol(adonitol)	Valine	0.0225	0.0085							
86		Ribitol(adonitol)	Taurine	0.0690	0.0149							
87		Ribitol(adonitol)	Ectoine	0.0653	0.0432							
88	Sucrose	Glycerol	Proline	0.0886	missing	0.1079	0.0266	0.0930				
89	Sucrose	Glycerol	Alanine	0.1190	missing	0.1108	0.1554	0.1193				
90	Sucrose	Glycerol	Isoleucine	0.1015	missing	0.0927	0.1238	0.1093				
91	Sucrose	Glycerol	Creatine	0.1190	missing	0.1253	0.1529	0.1277				
92	Sucrose	Glycerol	Valine	0.1003	missing	0.1084	0.1031	0.1055				
93	Sucrose	Glycerol	Taurine	0.1209	missing	0.1433	0.1433	0.1238				
94	Sucrose	Glycerol	Ectoine	0.1461	missing	0.1545	0.1625	0.1476				
95	Sucrose	Sorbitol	Proline	0.0773	0.0802	0.0602	0.0894	0.0591				
96	Sucrose	Sorbitol	Alanine	0.0883	0.0884	0.0862	0.1074	0.0795				
97	Sucrose	Sorbitol	Isoleucine	0.0788	0.0795	0.0660	0.0959	0.0712				
98	Sucrose	Sorbitol	Creatine	0.1038	0.1098	0.1007	0.0950	0.0942				
99	Sucrose	Sorbitol	Valine	0.0892	0.0878	0.0686	0.1025	0.0707				
100	Sucrose	Sorbitol	Taurine	0.0909	0.0878	0.1000	0.0885	0.0672				
101	Sucrose	Sorbitol	Ectoine	0.0990	0.0987	0.0998	0.1118	0.0827				
102	Sucrose	Arabitol	Proline	0.0698	0.0656	0.0553	0.0533	0.0596				
103	Sucrose	Arabitol	Alanine	0.0722	0.0796	0.0530	0.0633	0.0639				
104	Sucrose	Arabitol	Isoleucine	0.0699	0.0777	0.0537	0.0614	0.0551				
105	Sucrose	Arabitol	Creatine	0.0754	0.0868	0.0711	0.0676	0.0627				
106	Sucrose	Arabitol	Valine	0.0724	0.0649	0.0719	0.0620	0.0580				
107	Sucrose	Arabitol	Taurine	0.0736	0.0919	0.0685	0.0723	0.0564				
108	Sucrose	Arabitol	Ectoine	0.0859	0.0969	0.0831	0.0972	0.0822				
109	Sucrose	Inositol	Proline	0.0740	0.1283	0.0727	0.0521	0.0596				
110	Sucrose	Inositol	Alanine	0.0926	0.1285	0.0941	0.0740	0.0773				
111	Sucrose	Inositol	Isoleucine	0.0726	0.1038	0.0676	0.0538	0.0499				
112	Sucrose	Inositol	Creatine	0.0869	0.0968	0.0926	0.0810	0.0685				
113	Sucrose	Inositol	Valine	0.0759	0.1048	0.0888	0.0587	0.0497				
114	Sucrose	Inositol	Taurine	0.0840	0.1071	0.1101	0.0729	0.0558				
115	Sucrose	Inositol	Ectoine	0.0908	0.1234	0.1086	0.0907	0.0781				
116	Sucrose	Erythritol	Proline	0.0877	0.1136	0.1012	0.0864	0.0851				
117	Sucrose	Erythritol	Alanine	0.0856	0.0976	0.0999	0.0936	0.0777				
118	Sucrose	Erythritol	Isoleucine	0.0837	0.0951	0.0636	0.0744	0.0827				
119	Sucrose	Erythritol	Creatine	0.1033	0.1162	0.0954	0.1070	0.1067				
120	Sucrose	Erythritol	Valine	0.0883	0.0992	0.0887	0.0933	0.0717				
121	Sucrose	Erythritol	Taurine	0.0886	0.1062	0.0868	0.0874	0.0871				
122	Sucrose	Erythritol	Ectoine	0.1065	0.1259	0.1246	0.1019	0.1096				
123	Sucrose	Xylitol	Proline	0.0578	0.0548	0.0544	0.0697	0.0436				
124	Sucrose	Xylitol	Alanine	0.0763	0.0910	0.0818	0.0862	0.0562				
125	Sucrose	Xylitol	Isoleucine	0.0661	0.0715	0.0687	0.0806	0.0538				
126	Sucrose	Xylitol	Creatine	0.0868	0.0896	0.0888	0.0728	0.0697				
127	Sucrose	Xylitol	Valine	0.0762	0.0925	0.0756	0.0792	0.0646				
128	Sucrose	Xylitol	Taurine	0.0796	0.0750	0.0756	0.0792	0.0646				
129	Sucrose	Xylitol	Ectoine	0.0859	0.0878	0.0910	0.1004	0.0683				
130	Sucrose	Mannitol	Proline	0.0457	0.0566	0.0415	0.0363	0.0219				
131	Sucrose	Mannitol	Alanine	0.0791	0.1005	0.0940	0.0666	0.0656				
132	Sucrose	Mannitol	Isoleucine	0.0799	0.0886	0.0934	0.0682	0.0778				
133	Sucrose	Mannitol	Creatine	0.1119	0.1555	0.1379	0.1073	0.1002				
134	Sucrose	Mannitol	Valine	0.0956	0.1275	0.0956	0.0972	0.0714				
135	Sucrose	Mannitol	Taurine	0.1107	0.1432	0.1309	0.0967	0.0951				
136	Sucrose	Mannitol	Ectoine	0.1121	0.1509	0.1062	0.0894	0.1250				
137	Sucrose	Ribitol(adonitol)	Proline	0.0792	0.0823	0.0633	0.0828	0.0784				
138	Sucrose	Ribitol(adonitol)	Alanine	0.1043	0.1102	0.1007	0.0891	0.0946				
139	Sucrose	Ribitol(adonitol)	Isoleucine	0.0799	0.0763	0.0719	0.0877	0.0698				
140	Sucrose	Ribitol(adonitol)	Creatine	0.0996	0.0990	0.1024	0.0869	0.0825				
141	Sucrose	Ribitol(adonitol)	Valine	0.0895	0.0938	0.0806	0.0850	0.0708				
142	Sucrose	Ribitol(adonitol)	Taurine	0.0730	0.0665	0.0828	0.0628	0.0681				
143	Sucrose	Ribitol(adonitol)	Ectoine	0.0963	0.0908	0.1102	0.1024	0.0864				

	SUCROSE 10C/min				Replicates							
Combo number	Sugar	Sugar Alcohol	Additive	Average	1	2	3	4	5	6	7	8
0				0.0107	0.0104	0.0119	0.0138	0.0130	0.0085	0.0126	0.0062	0.0081
1	Sucrose			0.1463	0.1891	0.1803	0.1896	0.1585				
2		Glycerol		0.0558	0.0486	0.0724	0.0526	0.0822	0.0724	0.0497	0.0562	0.0555
3		Sorbitol		0.0590	0.0521	0.0684	0.0654	0.0450	0.0777	0.0669	0.0658	0.0808
4		Arabitol		0.0360	0.0283	0.0248	0.0258	0.0455	0.0501	0.0487	0.0580	0.0303
5		Inositol		0.0494	0.0520	0.0457	0.0446	0.0418	0.0559	0.0443	0.0696	0.0849
6		Erythritol		0.0521	0.0763	0.0718	0.0396	0.0510	0.0466	0.0414	0.0664	0.0678
7		Xylitol		0.0647	0.0628	0.0608	0.0574	0.0386	0.0640	0.0675	0.0010	0.0414
8		Mannitol		0.0896	0.0944	0.0928	0.0800	0.0554	0.0845	0.0924	0.0832	0.0430
9		Ribitol(adonitol)		0.0402	0.0168	0.0194	0.0227	0.0157	0.0349	0.0357	0.0175	0.0099
10			Proline	0.1156	0.0727							
11			Alanine	0.0378	0.0270							
12			Isoleucine	0.0398	0.0072							
13			Creatine	0.0394	0.0263							
14			Valine	0.0445	0.0069							
15			Taurine	0.0440	0.0156							
16			Ectoine	0.0579	0.0661							
17	Sucrose	Glycerol		0.1066	0.1258	0.1306	0.1334	0.0871				
18	Sucrose	Sorbitol		0.0673	0.0840	0.0720	0.0590	0.0662				
19	Sucrose	Arabitol		0.0840	0.1000	0.0939	0.0992	0.0749				
20	Sucrose	Inositol		0.1047	0.1132	0.1198	0.1221	0.0999				
21	Sucrose	Erythritol		0.0787	0.0953	0.0907	0.0775	0.0645				
22	Sucrose	Xylitol		0.0765	0.0662	0.1005	0.0941	0.0767				
23	Sucrose	Mannitol		0.1113	0.1413	0.1559	0.0449	0.1367				
24	Sucrose	Ribitol(adonitol)		0.0983	0.1067	0.1002	0.1067	0.1108				
25	Sucrose		Proline	0.1266	0.1365	0.1577	0.1457	0.1274				
26	Sucrose		Alanine	0.1370	0.1740	0.1278	0.1493	0.1532				
27	Sucrose		Isoleucine	0.0909	0.1352	0.0878	0.1120	0.0911				
28	Sucrose		Creatine	0.1198	0.1495	0.1385	0.1289	0.1575				
29	Sucrose		Valine	0.0969	0.1350	0.1255	0.0992	0.0992				
30	Sucrose		Taurine	0.1024	0.1367	0.1190	0.1072	0.1038				
31	Sucrose		Ectoine	0.1353	0.1843	0.1237	0.1742	0.1442				
32		Glycerol	Proline	0.0702	0.0917							
33		Glycerol	Alanine	0.0930	0.1280							
34		Glycerol	Isoleucine	0.0219	0.0135							
35		Glycerol	Creatine	0.0489	0.0459							
36		Glycerol	Valine	0.0390	0.0323							
37		Glycerol	Taurine	0.0604	0.0762							
38		Glycerol	Ectoine	0.0427	0.0435							
39		Sorbitol	Proline	0.0570	0.0582							
40		Sorbitol	Alanine	0.0586	0.0730							
41		Sorbitol	Isoleucine	0.0446	0.0196							
42		Sorbitol	Creatine	0.0729	0.0608							
43		Sorbitol	Valine	0.0660	0.0557							
44		Sorbitol	Taurine	0.0647	0.0576							
45		Sorbitol	Ectoine	0.0646	0.0895							
46		Arabitol	Proline	0.0387	0.0264							
47		Arabitol	Alanine	0.0373	0.0279							
48		Arabitol	Isoleucine	0.0256	0.0099							
49		Arabitol	Creatine	0.0559	0.0453							
50		Arabitol	Valine	0.0515	0.0352							
51		Arabitol	Taurine	0.0475	0.0321							
52		Arabitol	Ectoine	0.0510	0.0412							
53		Inositol	Proline	0.0573	0.0572							
54		Inositol	Alanine	0.0631	0.0877							
55		Inositol	Isoleucine	0.0339	0.0037							
56		Inositol	Creatine	0.0607	0.0540							
57		Inositol	Valine	0.0037	0.0064							
58		Inositol	Taurine	0.0550	0.0686							
59		Inositol	Ectoine	0.0628	0.0312							
60		Erythritol	Proline	0.0641	0.0355							
61		Erythritol	Alanine	0.0674	0.0549							
62		Erythritol	Isoleucine	0.0313	0.0072							
63		Erythritol	Creatine	0.0592	0.0338							
64		Erythritol	Valine	0.0499	0.0074							
65		Erythritol	Taurine	0.0707	0.0582							
66		Erythritol	Ectoine	0.0428	0.0427							
67		Xylitol	Proline	0.0373	0.0578							
68		Xylitol	Alanine	0.0397	0.0600							
69		Xylitol	Isoleucine	0.0210	0.0192							
70		Xylitol	Creatine	0.0310	0.0462							
71		Xylitol	Valine	0.0390	0.0432							
72		Xylitol	Taurine	0.0275	0.0192							
73		Xylitol	Ectoine	0.0303	0.0430							
74		Mannitol	Proline	0.0466	0.0834							
75		Mannitol	Alanine	0.0846	0.0964							
76		Mannitol	Isoleucine	0.0193	0.0116							
77		Mannitol	Creatine	0.0314	0.0556							
78		Mannitol	Valine	0.0353	0.0442							
79		Mannitol	Taurine	0.0316	0.0564							
80		Mannitol	Ectoine	0.0265	0.0374							

	SUCROSE 10C/min				Replicates							
Combo number	Sugar	Sugar Alcohol	Additive	Average	1	2	3	4	5	6	7	8
81		Ribitol(adonitol)	Proline	0.0430	0.0199							
82		Ribitol(adonitol)	Alanine	0.0775	0.0293							
83		Ribitol(adonitol)	Isoleucine	0.0679	0.0051							
84		Ribitol(adonitol)	Creatine	0.0780	0.0227							
85		Ribitol(adonitol)	Valine	0.0458	0.0046							
86		Ribitol(adonitol)	Taurine	0.0502	0.0164							
87		Ribitol(adonitol)	Ectoine	0.0439	0.0159							
88	Sucrose	Glycerol	Proline	0.0924	0.1184	0.0763	0.0923	0.1160				
89	Sucrose	Glycerol	Alanine	0.0961	0.1031	0.0976	0.0965	0.1172				
90	Sucrose	Glycerol	Isoleucine	0.0952	0.0886	0.0898	0.0967	0.1009				
91	Sucrose	Glycerol	Creatine	0.0999	0.0980	0.1007	0.1011	0.1058				
92	Sucrose	Glycerol	Valine	0.0902	0.0756	0.0793	0.1023	0.0946				
93	Sucrose	Glycerol	Taurine	0.0886	0.0761	0.1040	0.0882	0.0998				
94	Sucrose	Glycerol	Ectoine	0.1104	0.1123	0.1115	0.0959	0.1190				
95	Sucrose	Sorbitol	Proline	0.0514	0.0367	0.0249	0.0319	0.0437				
96	Sucrose	Sorbitol	Alanine	0.0744	0.0649	0.0699	0.0680	0.0471				
97	Sucrose	Sorbitol	Isoleucine	0.0759	0.0803	0.0558	0.0929	0.0505				
98	Sucrose	Sorbitol	Creatine	0.0817	0.0833	0.0670	0.0825	0.0805				
99	Sucrose	Sorbitol	Valine	0.0763	0.0825	0.0825	0.0712	0.0544				
100	Sucrose	Sorbitol	Taurine	0.0740	0.1034	0.0556	0.0701	0.0635				
101	Sucrose	Sorbitol	Ectoine	0.0833	0.1077	0.0858	0.0807	0.0780				
102	Sucrose	Arabitol	Proline	0.0553	0.0617	0.0537	0.0512	0.0437				
103	Sucrose	Arabitol	Alanine	0.0682	0.0686	0.0638	0.0537	0.0544				
104	Sucrose	Arabitol	Isoleucine	0.0649	0.0669	0.0481	0.0557	0.0597				
105	Sucrose	Arabitol	Creatine	0.0789	0.0815	0.0675	0.0793	0.0894				
106	Sucrose	Arabitol	Valine	0.0771	0.0648	0.0496	0.0702	0.0597				
107	Sucrose	Arabitol	Taurine	0.0863	0.0708	0.0682	0.0613	0.0752				
108	Sucrose	Arabitol	Ectoine	0.0785	0.0825	0.0847	0.0881	0.0926				
109	Sucrose	Inositol	Proline	0.0991	0.0836	0.0974	0.0829	0.0948				
110	Sucrose	Inositol	Alanine	0.0961	0.1117	0.0976	0.0871	0.0772				
111	Sucrose	Inositol	Isoleucine	0.0849	0.0799	0.0832	0.0873	0.0740				
112	Sucrose	Inositol	Creatine	0.1107	0.1284	0.0984	0.1245	0.0957				
113	Sucrose	Inositol	Valine	0.0895	0.1021	0.0768	0.0845	0.0735				
114	Sucrose	Inositol	Taurine	0.1051	0.1048	0.0879	0.0976	0.0987				
115	Sucrose	Inositol	Ectoine	0.1262	0.1252	0.1229	0.1186	0.1067				
116	Sucrose	Erythritol	Proline	0.0689	0.0485	0.0507	0.0534	0.0459				
117	Sucrose	Erythritol	Alanine	0.0816	0.0743	0.0649	0.0622	0.0793				
118	Sucrose	Erythritol	Isoleucine	0.0744	0.0510	0.0457	0.0580	0.0431				
119	Sucrose	Erythritol	Creatine	0.0900	0.0804	0.0882	0.0804	0.0732				
120	Sucrose	Erythritol	Valine	0.0740	0.0516	0.0547	0.0521	0.0622				
121	Sucrose	Erythritol	Taurine	0.0805	0.0591	0.0605	0.0645	0.0654				
122	Sucrose	Erythritol	Ectoine	0.0941	0.0730	0.0698	0.0962	0.0962				
123	Sucrose	Xylitol	Proline	0.0485	0.0247	0.0446	0.0404	0.0449				
124	Sucrose	Xylitol	Alanine	0.0656	0.0459	0.0607	0.0495	0.0601				
125	Sucrose	Xylitol	Isoleucine	0.0673	0.0601	0.0696	0.0578	0.0581				
126	Sucrose	Xylitol	Creatine	0.0875	0.0692	0.0867	0.0617	0.0707				
127	Sucrose	Xylitol	Valine	0.0740	0.0551	0.0724	0.0565	0.0477				
128	Sucrose	Xylitol	Taurine	0.0720	0.0544	0.0724	0.0565	0.0477				
129	Sucrose	Xylitol	Ectoine	0.0937	0.0691	0.0908	0.0767	0.0746				
130	Sucrose	Mannitol	Proline	0.1007	0.0846	0.0948	0.0928	0.0961				
131	Sucrose	Mannitol	Alanine	0.1046	0.0905	0.1175	0.0865	0.1032				
132	Sucrose	Mannitol	Isoleucine	0.0981	0.0846	0.1012	0.1062	0.0995				
133	Sucrose	Mannitol	Creatine	0.1021	0.1000	0.1174	0.1074	0.0864				
134	Sucrose	Mannitol	Valine	0.0945	0.0700	0.0865	0.0823	0.0972				
135	Sucrose	Mannitol	Taurine	0.0876	0.0636	0.0912	0.0855	0.0787				
136	Sucrose	Mannitol	Ectoine	0.1028	0.0930	0.1143	0.1108	0.0887				
137	Sucrose	Ribitol(adonitol)	Proline	0.0854	0.0863	0.0635	0.0919	0.0815				
138	Sucrose	Ribitol(adonitol)	Alanine	0.1099	0.0990	0.0802	0.0921	0.0941				
139	Sucrose	Ribitol(adonitol)	Isoleucine	0.0922	0.0839	0.0831	0.0812	0.0891				
140	Sucrose	Ribitol(adonitol)	Creatine	0.1197	0.1120	0.1190	0.0921	0.1010				
141	Sucrose	Ribitol(adonitol)	Valine	0.0956	0.0875	0.0851	0.0744	0.0867				
142	Sucrose	Ribitol(adonitol)	Taurine	0.0765	0.0827	0.0546	0.0725	0.0812				
143	Sucrose	Ribitol(adonitol)	Ectoine	0.0906	0.0857	0.0802	0.0625	0.0965				

	TREHALOSE 1C/min				Replicates							
Combo number	Sugar	Sugar Alcohol	Additive	Average	1	2	3	4	5	6	7	8
0				0.0067	-0.0026	0.0024	0.0054	0.0059	0.0079	0.0110	0.0160	0.0120
1	Trehalose			0.0272	0.0471	0.0394	0.0294	0.0148				
2		Glycerol		0.0101	0.0047	0.0137	0.0137	0.0105	0.0137	0.0098	0.0085	0.0105
3		Sorbitol		0.0083	0.0116	0.0149	0.0067	0.0132	0.0092	0.0083	0.0010	0.0018
4		Arabitol		0.0087	0.0085	0.0093	0.0101	0.0101	0.0093	0.0093	0.0085	0.0022
5		Inositol		0.0006	0.0030	-0.0012	-0.0074	-0.0094	0.0014	0.0019	0.0019	-0.0012
6		Erythritol		0.0069	0.0051	0.0074	0.0040	0.0057	0.0074	0.0057	0.0068	0.0085
7		Xylitol		0.0153	0.0092	0.0136	0.0161	0.0142	0.0117	0.0123	0.0042	0.0092
8		Mannitol		0.0152	0.0136	0.0106	0.0106	0.0136	0.0069	0.0144	0.0159	0.0114
9		Ribitol(adonitol)		0.0027	-0.0022	-0.0022	-0.0027	-0.0018	0.0006	0.0010	0.0024	0.0001
10			Proline	0.0054	-0.0040							
11			Alanine	-0.0018	-0.0083							
12			Isoleucine	0.0044	-0.0049							
13			Creatine	0.0063	-0.0011							
14			Valine	0.0041	-0.0023							
15			Taurine	0.0055	-0.0028							
16			Ectoine	0.0050	0.0002							
17	Trehalose	Glycerol		0.0300	0.0334	0.0400	0.0303	0.0376				
18	Trehalose	Sorbitol		0.0376	0.0564	0.0395	0.0388	0.0426				
19	Trehalose	Arabitol		0.0231	0.0348	0.0274	0.0267	0.0148				
20	Trehalose	Inositol		0.0055	0.0094	0.0133	-0.0039	-0.0063				
21	Trehalose	Erythritol		0.0271	0.0396	0.0280	0.0343	0.0270				
22	Trehalose	Xylitol		0.0440	0.0530	0.0542	0.0501	0.0495				
23	Trehalose	Mannitol		0.0320	0.0426	0.0334	0.0377	0.0370				
24	Trehalose	Ribitol(adonitol)		0.0129	0.0247	0.0129	0.0159	0.0029				
25	Trehalose		Proline	0.0026	0.0159	0.0066	0.0029	-0.0137				
26	Trehalose		Alanine	0.0175	0.0349	0.0249	0.0178	0.0080				
27	Trehalose		Isoleucine	0.0170	0.0230	0.0254	0.0178	0.0103				
28	Trehalose		Creatine	0.0360	0.0401	0.0468	0.0444	0.0391				
29	Trehalose		Valine	0.0238	0.0284	0.0303	0.0223	0.0280				
30	Trehalose		Taurine	0.0280	0.0294	0.0375	0.0337	0.0294				
31	Trehalose		Ectoine	0.0365	0.0447	0.0485	0.0389	0.0413				
32		Glycerol	Proline	0.0041	-0.0011							
33		Glycerol	Alanine	0.0101	0.0118							
34		Glycerol	Isoleucine	0.0034	0.0047							
35		Glycerol	Creatine	0.0082	0.0134							
36		Glycerol	Valine	0.0016	0.0043							
37		Glycerol	Taurine	-0.0033	0.0008							
38		Glycerol	Ectoine	-0.0004	0.0085							
39		Sorbitol	Proline	0.0008	0.0002							
40		Sorbitol	Alanine	0.0105	0.0190							
41		Sorbitol	Isoleucine	-0.0008	-0.0035							
42		Sorbitol	Creatine	0.0060	0.0132							
43		Sorbitol	Valine	0.0037	0.0022							
44		Sorbitol	Taurine	0.0003	-0.0067							
45		Sorbitol	Ectoine	0.0097	0.0153							
46		Arabitol	Proline	0.0022	-0.0014							
47		Arabitol	Alanine	0.0111	0.0149							
48		Arabitol	Isoleucine	0.0010	-0.0038							
49		Arabitol	Creatine	0.0075	0.0081							
50		Arabitol	Valine	0.0057	0.0030							
51		Arabitol	Taurine	0.0029	-0.0034							
52		Arabitol	Ectoine	0.0095	0.0053							
53		Inositol	Proline	-0.0075	-0.0310							
54		Inositol	Alanine	0.0208	0.0273							
55		Inositol	Isoleucine	0.0649	0.1181							
56		Inositol	Creatine	0.0062	0.0001							
57		Inositol	Valine	0.0027	0.0012							
58		Inositol	Taurine	0.0008	-0.0076							
59		Inositol	Ectoine	0.0071	0.0006							
60		Erythritol	Proline	0.0033	-0.0040							
61		Erythritol	Alanine	0.0096	0.0085							
62		Erythritol	Isoleucine	0.0083	0.0029							
63		Erythritol	Creatine	0.0087	0.0104							
64		Erythritol	Valine	0.0091	0.0037							
65		Erythritol	Taurine	0.0140	0.0121							
66		Erythritol	Ectoine	0.0119	0.0124							
67		Xylitol	Proline	0.0068	0.0158							
68		Xylitol	Alanine	0.0082	0.0186							
69		Xylitol	Isoleucine	0.0029	0.0086							
70		Xylitol	Creatine	0.0077	0.0171							
71		Xylitol	Valine	0.0041	0.0076							
72		Xylitol	Taurine	0.0045	0.0080							
73		Xylitol	Ectoine	0.0102	0.0180							
74		Mannitol	Proline	-0.0045	-0.0091							
75		Mannitol	Alanine	0.0026	0.0091							
76		Mannitol	Isoleucine	-0.0083	-0.0084							
77		Mannitol	Creatine	0.0001	0.0050							
78		Mannitol	Valine	-0.0016	-0.0021							
79		Mannitol	Taurine	-0.0018	-0.0013							
80		Mannitol	Ectoine	0.0041	0.0110							

	TREHALOSE 1C/min				Replicates							
Combo number	Sugar	Sugar Alcohol	Additive	Average	1	2	3	4	5	6	7	8
81		Ribitol(adonitol)	Proline	-0.0050	-0.0103							
82		Ribitol(adonitol)	Alanine	0.0191	0.0048							
83		Ribitol(adonitol)	Isoleucine	0.0189	-0.0022							
84		Ribitol(adonitol)	Creatine	0.0166	0.0029							
85		Ribitol(adonitol)	Valine	0.0187	-0.0001							
86		Ribitol(adonitol)	Taurine	0.0294	0.0024							
87		Ribitol(adonitol)	Ectoine	0.0220	0.0045							
88	Trehalose	Glycerol	Proline	0.0334	0.0337	0.0409	0.0234	0.0300				
89	Trehalose	Glycerol	Alanine	0.0413	0.0418	0.0394	0.0486	0.0340				
90	Trehalose	Glycerol	Isoleucine	0.0306	0.0297	0.0327	0.0291	0.0267				
91	Trehalose	Glycerol	Creatine	0.0337	0.0385	0.0288	0.0409	0.0331				
92	Trehalose	Glycerol	Valine	0.0283	0.0324	0.0300	0.0300	0.0222				
93	Trehalose	Glycerol	Taurine	0.0309	0.0343	0.0397	0.0300	0.0355				
94	Trehalose	Glycerol	Ectoine	0.0290	0.0225	0.0449	0.0364	0.0315				
95	Trehalose	Sorbitol	Proline	0.0306	0.0441	0.0365	0.0380	0.0213				
96	Trehalose	Sorbitol	Alanine	0.0399	0.0584	0.0584	0.0537	0.0330				
97	Trehalose	Sorbitol	Isoleucine	0.0317	0.0480	0.0372	0.0395	0.0403				
98	Trehalose	Sorbitol	Creatine	0.0562	0.0595	0.0665	0.0719	0.0434				
99	Trehalose	Sorbitol	Valine	0.0350	0.0395	0.0426	0.0365	0.0281				
100	Trehalose	Sorbitol	Taurine	0.0452	0.0568	0.0445	0.0491	0.0414				
101	Trehalose	Sorbitol	Ectoine	0.0462	0.0591	0.0537	0.0476	0.0437				
102	Trehalose	Arabitol	Proline	0.0166	0.0241	0.0013	0.0035	0.0013				
103	Trehalose	Arabitol	Alanine	0.0243	0.0241	0.0159	0.0159	0.0115				
104	Trehalose	Arabitol	Isoleucine	0.0237	0.0200	0.0193	0.0148	0.0141				
105	Trehalose	Arabitol	Creatine	0.0306	0.0296	0.0237	0.0274	0.0230				
106	Trehalose	Arabitol	Valine	0.0216	0.0215	0.0200	0.0126	0.0112				
107	Trehalose	Arabitol	Taurine	0.0258	0.0304	0.0222	0.0222	0.0207				
108	Trehalose	Arabitol	Ectoine	0.0326	0.0348	0.0296	0.0318	0.0289				
109	Trehalose	Inositol	Proline	-0.0148	-0.0323	-0.0323	-0.0117	-0.0347				
110	Trehalose	Inositol	Alanine	0.0021	0.0111	0.0006	-0.0094	-0.0165				
111	Trehalose	Inositol	Isoleucine	0.0438	0.0046	0.1535	0.0555	-0.0072				
112	Trehalose	Inositol	Creatine	0.0126	0.0213	0.0213	0.0140	-0.0094				
113	Trehalose	Inositol	Valine	0.0154	0.0184	0.0111	0.0237	0.0208				
114	Trehalose	Inositol	Taurine	0.0180	0.0201	0.0220	0.0032	0.0288				
115	Trehalose	Inositol	Ectoine	0.0314	0.0393	0.0252	0.0522	0.0335				
116	Trehalose	Erythritol	Proline	0.0241	0.0346	0.0247	0.0314	0.0267				
117	Trehalose	Erythritol	Alanine	0.0211	0.0328	0.0291	0.0301	0.0270				
118	Trehalose	Erythritol	Isoleucine	0.0208	0.0247	0.0153	0.0143	0.0148				
119	Trehalose	Erythritol	Creatine	0.0295	0.0399	0.0320	0.0241	0.0267				
120	Trehalose	Erythritol	Valine	0.0217	0.0288	0.0210	0.0226	0.0184				
121	Trehalose	Erythritol	Taurine	0.0249	0.0343	0.0275	0.0286	0.0260				
122	Trehalose	Erythritol	Ectoine	0.0347	0.0412	0.0349	0.0380	0.0364				
123	Trehalose	Xylitol	Proline	0.0344	0.0409	0.0344	0.0374	0.0338				
124	Trehalose	Xylitol	Alanine	0.0349	0.0430	0.0382	0.0453	0.0300				
125	Trehalose	Xylitol	Isoleucine	0.0336	0.0430	0.0436	0.0365	0.0347				
126	Trehalose	Xylitol	Creatine	0.0393	0.0376	0.0459	0.0382	0.0347				
127	Trehalose	Xylitol	Valine	0.0340	0.0309	0.0332	0.0332	0.0256				
128	Trehalose	Xylitol	Taurine	0.0323	0.0250	0.0332	0.0332	0.0256				
129	Trehalose	Xylitol	Ectoine	0.0380	0.0409	0.0368	0.0409	0.0321				
130	Trehalose	Mannitol	Proline	0.0181	0.0230	0.0167	0.0119	0.0105				
131	Trehalose	Mannitol	Alanine	0.0240	0.0324	0.0171	0.0212	0.0192				
132	Trehalose	Mannitol	Isoleucine	0.0217	0.0244	0.0153	0.0216	0.0251				
133	Trehalose	Mannitol	Creatine	0.0353	0.0440	0.0320	0.0341	0.0384				
134	Trehalose	Mannitol	Valine	0.0257	0.0286	0.0202	0.0237	0.0265				
135	Trehalose	Mannitol	Taurine	0.0257	0.0240	0.0185	0.0240	0.0247				
136	Trehalose	Mannitol	Ectoine	0.0426	0.0503	0.0447	0.0426	0.0419				
137	Trehalose	Ribitol(adonitol)	Proline	0.0130	0.0170	0.0118	0.0061	0.0005				
138	Trehalose	Ribitol(adonitol)	Alanine	0.0248	0.0288	0.0148	0.0218	0.0139				
139	Trehalose	Ribitol(adonitol)	Isoleucine	0.0222	0.0209	0.0170	0.0135	0.0109				
140	Trehalose	Ribitol(adonitol)	Creatine	0.0301	0.0313	0.0291	0.0308	0.0203				
141	Trehalose	Ribitol(adonitol)	Valine	0.0287	0.0308	0.0264	0.0255	0.0194				
142	Trehalose	Ribitol(adonitol)	Taurine	0.0170	0.0260	0.0203	0.0225	0.0176				
143	Trehalose	Ribitol(adonitol)	Ectoine	0.0291	0.0355	0.0341	0.0337	0.0306				

	TREHALOSE 3C/min				Replicates							
Combo number	Sugar	Sugar Alcohol	Additive	Average	1	2	3	4	5	6	7	8
0				-0.0001	-0.0001	0.0022	0.0008	-0.0058	-0.0077	0.0004	-0.0020	0.0094
1	Trehalose			0.0221	0.0364	0.0287	0.0251	0.0195				
2		Glycerol		0.0565	0.0898	0.0596	0.0497	0.0539	0.0497	0.0554	0.0682	0.0883
3		Sorbitol		0.0349	0.0278	0.0432	0.0528	0.0417	0.0486	0.0296	0.0429	0.0353
4		Arabitol		0.0347	0.0334	0.0389	0.0430	0.0462	0.0389	0.0398	0.0343	0.0375
5		Inositol		0.0268	0.0176	0.0364	0.0440	0.0364	0.0277	0.0262	0.0258	0.0288
6		Erythritol		0.0315	0.0438	0.0258	0.0466	0.0495	0.0290	0.0192	0.0293	0.0307
7		Xylitol		0.0208	0.0237	0.0165	0.0279	0.0225	0.0093	0.0237	0.0117	0.0159
8		Mannitol		0.0331	0.0220	0.0185	0.0378	0.0378	0.0170	0.0428	0.0409	0.0522
9		Ribitol(adonitol)		0.0197	0.0422	0.0124	0.0081	0.0124	0.0063	0.0230	0.0111	0.0371
10			Proline	0.0159	0.0124							
11			Alanine	0.0441	-0.0017							
12			Isoleucine	0.0252	-0.0093							
13			Creatine	0.0274	0.0051							
14			Valine	0.0252	-0.0035							
15			Taurine	0.0491	0.0485							
16			Ectoine	0.0557	0.0560							
17	Trehalose	Glycerol		0.0767	0.0776	0.0754	0.0852	0.0769				
18	Trehalose	Sorbitol		0.0703	0.0697	0.0656	0.0713	0.0566				
19	Trehalose	Arabitol		0.0455	0.0686	0.0481	0.0447	0.0384				
20	Trehalose	Inositol		0.0405	0.0578	0.0400	0.0340	0.0272				
21	Trehalose	Erythritol		0.0647	0.0687	0.0668	0.0710	0.0641				
22	Trehalose	Xylitol		0.0617	0.0667	0.0713	0.0687	0.0602				
23	Trehalose	Mannitol		0.0658	0.0719	0.0741	0.0707	0.0635				
24	Trehalose	Ribitol(adonitol)		0.0698	0.0792	0.0807	0.0843	0.0753				
25	Trehalose		Proline	0.0198	0.0320	0.0132	0.0086	0.0021				
26	Trehalose		Alanine	0.0396	0.0495	0.0480	0.0351	0.0300				
27	Trehalose		Isoleucine	0.0336	0.0407	0.0351	0.0284	0.0305				
28	Trehalose		Creatine	0.0366	0.0501	0.0377	0.0289	0.0274				
29	Trehalose		Valine	0.0434	0.0457	0.0545	0.0348	0.0389				
30	Trehalose		Taurine	0.0367	0.0353	0.0472	0.0302	0.0246				
31	Trehalose		Ectoine	0.0452	0.0587	0.0509	0.0389	0.0384				
32		Glycerol	Proline	0.0286	0.0174							
33		Glycerol	Alanine	0.0269	0.0195							
34		Glycerol	Isoleucine	0.0240	0.0105							
35		Glycerol	Creatine	0.0349	0.0522							
36		Glycerol	Valine	0.0355	0.0345							
37		Glycerol	Taurine	0.0658	0.0876							
38		Glycerol	Ectoine	0.0580	0.0797							
39		Sorbitol	Proline	0.0219	0.0162							
40		Sorbitol	Alanine	0.0374	0.0486							
41		Sorbitol	Isoleucine	0.0183	0.0109							
42		Sorbitol	Creatine	0.0426	0.0563							
43		Sorbitol	Valine	0.0406	0.0374							
44		Sorbitol	Taurine	0.0252	0.0246							
45		Sorbitol	Ectoine	0.0554	0.0643							
46		Arabitol	Proline	0.0438	0.0382							
47		Arabitol	Alanine	0.0408	0.0527							
48		Arabitol	Isoleucine	0.0152	0.0112							
49		Arabitol	Creatine	0.0263	0.0233							
50		Arabitol	Valine	0.0242	0.0176							
51		Arabitol	Taurine	0.0178	0.0118							
52		Arabitol	Ectoine	0.0198	0.0230							
53		Inositol	Proline	0.0281	0.0282							
54		Inositol	Alanine	0.0301	0.0377							
55		Inositol	Isoleucine	0.0086	0.0078							
56		Inositol	Creatine	0.0430	0.0624							
57		Inositol	Valine	0.0116	0.0115							
58		Inositol	Taurine	0.0417	0.0675							
59		Inositol	Ectoine	0.0420	0.0620							
60		Erythritol	Proline	0.0275	0.0365							
61		Erythritol	Alanine	0.0420	0.0463							
62		Erythritol	Isoleucine	0.0245	0.0113							
63		Erythritol	Creatine	0.0294	0.0418							
64		Erythritol	Valine	0.0271	0.0115							
65		Erythritol	Taurine	0.0492	0.0576							
66		Erythritol	Ectoine	0.0530	0.0538							
67		Xylitol	Proline	0.0226	0.0031							
68		Xylitol	Alanine	0.0076	0.0028							
69		Xylitol	Isoleucine	0.0028	-0.0025							
70		Xylitol	Creatine	0.0125	0.0126							
71		Xylitol	Valine	0.0074	0.0084							
72		Xylitol	Taurine	0.0120	0.0010							
73		Xylitol	Ectoine	0.0135	0.0159							
74		Mannitol	Proline	0.0337	0.0302							
75		Mannitol	Alanine	0.0272	0.0420							
76		Mannitol	Isoleucine	0.0025	0.0066							
77		Mannitol	Creatine	0.0194	0.0481							
78		Mannitol	Valine	0.0133	0.0216							
79		Mannitol	Taurine	0.0194	0.0424							
80		Mannitol	Ectoine	0.0517	0.0548							

	TREHALOSE 3C/min				Replicates							
Combo number	Sugar	Sugar Alcohol	Additive	Average	1	2	3	4	5	6	7	8
81		Ribitol(adonitol)	Proline	0.0350	0.0141							
82		Ribitol(adonitol)	Alanine	0.0450	0.0124							
83		Ribitol(adonitol)	Isoleucine	0.0387	0.0021							
84		Ribitol(adonitol)	Creatine	0.0459	0.0066							
85		Ribitol(adonitol)	Valine	0.0394	0.0019							
86		Ribitol(adonitol)	Taurine	0.0479	0.0261							
87		Ribitol(adonitol)	Ectoine	0.0472	0.0288							
88	Trehalose	Glycerol	Proline	0.0405	0.0584	0.0287	0.0243	0.0199				
89	Trehalose	Glycerol	Alanine	0.0640	0.0799	0.0454	0.0648	0.0731				
90	Trehalose	Glycerol	Isoleucine	0.0512	0.0416	0.0424	0.0513	0.0521				
91	Trehalose	Glycerol	Creatine	0.0562	0.0517	0.0592	0.0532	0.0690				
92	Trehalose	Glycerol	Valine	0.0482	0.0465	0.0383	0.0667	0.0450				
93	Trehalose	Glycerol	Taurine	0.0507	0.0562	0.0539	0.0532	0.0517				
94	Trehalose	Glycerol	Ectoine	0.0702	0.0693	0.0708	0.0814	0.0716				
95	Trehalose	Sorbitol	Proline	0.0382	0.0424	0.0380	0.0388	0.0317				
96	Trehalose	Sorbitol	Alanine	0.0530	0.0584	0.0547	0.0596	0.0580				
97	Trehalose	Sorbitol	Isoleucine	0.0452	0.0477	0.0493	0.0533	0.0485				
98	Trehalose	Sorbitol	Creatine	0.0580	0.0606	0.0481	0.0602	0.0525				
99	Trehalose	Sorbitol	Valine	0.0623	0.0668	0.0668	0.0525	0.0586				
100	Trehalose	Sorbitol	Taurine	0.0639	0.0803	0.0584	0.0613	0.0487				
101	Trehalose	Sorbitol	Ectoine	0.0693	0.0744	0.0703	0.0666	0.0711				
102	Trehalose	Arabitol	Proline	0.0374	0.0396	0.0353	0.0238	0.0215				
103	Trehalose	Arabitol	Alanine	0.0524	0.0473	0.0536	0.0449	0.0449				
104	Trehalose	Arabitol	Isoleucine	0.0505	0.0505	0.0490	0.0451	0.0394				
105	Trehalose	Arabitol	Creatine	0.0572	0.0632	0.0553	0.0524	0.0549				
106	Trehalose	Arabitol	Valine	0.0536	0.0553	0.0456	0.0481	0.0471				
107	Trehalose	Arabitol	Taurine	0.0522	0.0500	0.0490	0.0423	0.0456				
108	Trehalose	Arabitol	Ectoine	0.0638	0.0642	0.0726	0.0519	0.0597				
109	Trehalose	Inositol	Proline	0.0311	0.0322	0.0258	0.0188	0.0152				
110	Trehalose	Inositol	Alanine	0.0488	0.0531	0.0426	0.0374	0.0318				
111	Trehalose	Inositol	Isoleucine	0.0503	0.0582	0.0408	0.0392	0.0324				
112	Trehalose	Inositol	Creatine	0.0529	0.0487	0.0638	0.0366	0.0314				
113	Trehalose	Inositol	Valine	0.0462	0.0495	0.0442	0.0310	0.0310				
114	Trehalose	Inositol	Taurine	0.0398	0.0529	0.0384	0.0408	0.0348				
115	Trehalose	Inositol	Ectoine	0.0348	0.0479	0.0438	0.0330	0.0362				
116	Trehalose	Erythritol	Proline	0.0290	0.0345	0.0412	0.0348	0.0260				
117	Trehalose	Erythritol	Alanine	0.0380	0.0492	0.0451	0.0462	0.0473				
118	Trehalose	Erythritol	Isoleucine	0.0422	0.0475	0.0426	0.0367	0.0345				
119	Trehalose	Erythritol	Creatine	0.0516	0.0574	0.0547	0.0472	0.0509				
120	Trehalose	Erythritol	Valine	0.0442	0.0438	0.0472	0.0517	0.0434				
121	Trehalose	Erythritol	Taurine	0.0464	0.0534	0.0557	0.0473	0.0458				
122	Trehalose	Erythritol	Ectoine	0.0548	0.0526	0.0625	0.0507	0.0671				
123	Trehalose	Xylitol	Proline	0.0298	0.0234	0.0285	0.0361	0.0259				
124	Trehalose	Xylitol	Alanine	0.0384	0.0371	0.0396	0.0447	0.0422				
125	Trehalose	Xylitol	Isoleucine	0.0414	0.0486	0.0377	0.0467	0.0435				
126	Trehalose	Xylitol	Creatine	0.0539	0.0628	0.0589	0.0544	0.0435				
127	Trehalose	Xylitol	Valine	0.0415	0.0361	0.0412	0.0476	0.0451				
128	Trehalose	Xylitol	Taurine	0.0402	0.0380	0.0412	0.0476	0.0451				
129	Trehalose	Xylitol	Ectoine	0.0516	0.0521	0.0618	0.0580	0.0586				
130	Trehalose	Mannitol	Proline	0.0402	0.0440	0.0431	0.0341	0.0341				
131	Trehalose	Mannitol	Alanine	0.0478	0.0537	0.0466	0.0396	0.0446				
132	Trehalose	Mannitol	Isoleucine	0.0444	0.0407	0.0543	0.0464	0.0460				
133	Trehalose	Mannitol	Creatine	0.0504	0.0539	0.0597	0.0493	0.0501				
134	Trehalose	Mannitol	Valine	0.0470	0.0639	0.0493	0.0423	0.0440				
135	Trehalose	Mannitol	Taurine	0.0546	0.0624	0.0566	0.0562	0.0504				
136	Trehalose	Mannitol	Ectoine	0.0513	0.0555	0.0564	0.0669	0.0473				
137	Trehalose	Ribitol(adonitol)	Proline	0.0403	0.0465	0.0542	0.0417	0.0347				
138	Trehalose	Ribitol(adonitol)	Alanine	0.0542	0.0553	0.0594	0.0530	0.0445				
139	Trehalose	Ribitol(adonitol)	Isoleucine	0.0576	0.0681	0.0597	0.0516	0.0579				
140	Trehalose	Ribitol(adonitol)	Creatine	0.0632	0.0750	0.0656	0.0712	0.0653				
141	Trehalose	Ribitol(adonitol)	Valine	0.0579	0.0715	0.0688	0.0610	0.0498				
142	Trehalose	Ribitol(adonitol)	Taurine	0.0515	0.0724	0.0621	0.0532	0.0523				
143	Trehalose	Ribitol(adonitol)	Ectoine	0.0559	0.0707	0.0785	0.0553	0.0556				

	TREHALOSE 5C/min				Replicates							
Combo number	Sugar	Sugar Alcohol	Additive	Average	1	2	3	4	5	6	7	8
0				0.0055	-0.0038	0.0047	0.0137	0.0186	0.0047	0.0059	0.0035	-0.0020
1	Trehalose			0.0963	0.1240	0.1199	0.1128	0.1110				
2		Glycerol		0.0658	0.0584	0.0928	0.0656	0.0686	0.0632	0.0680	0.0794	0.0776
3		Sorbitol		0.0686	0.0874	0.0744	0.0790	0.0575	0.0786	0.0719	0.0782	0.0857
4		Arabitol		0.0492	0.0455	0.0620	0.0735	0.0360	0.0698	0.0551	0.0328	0.0620
5		Inositol		0.0604	0.0618	0.0723	0.0778	0.0509	0.0820	0.0654	0.0631	0.0668
6		Erythritol		0.0223	0.0499	0.0383	0.0160	0.0112	0.0144	0.0172	0.0132	0.0424
7		Xylitol		0.0851	0.1224	0.1287	0.1001	0.0339	0.0339	0.0512	0.0877	0.0836
8		Mannitol		0.0702	0.0802	0.0686	0.0482	0.0488	0.0565	0.0638	0.0738	0.0717
9		Ribitol(adonitol)		0.0414	0.0411	0.0441	0.0447	0.0061	0.0318	0.0101	0.0349	0.0472
10			Proline	0.0940	0.0770							
11			Alanine	0.0492	0.0399							
12			Isoleucine	0.0414	-0.0100							
13			Creatine	0.0312	-0.0032							
14			Valine	0.0344	0.0003							
15			Taurine	0.0399	0.0166							
16			Ectoine	0.0558	0.0436							
17	Trehalose	Glycerol		0.1118	0.1140	0.1207	0.1224	0.1224				
18	Trehalose	Sorbitol		0.0898	0.0933	0.0833	0.0926	0.1023				
19	Trehalose	Arabitol		0.0945	0.1025	0.0897	0.0951	0.0978				
20	Trehalose	Inositol		0.1062	0.1354	0.1089	0.1007	0.1115				
21	Trehalose	Erythritol		0.0876	0.1014	0.0692	0.0867	0.1018				
22	Trehalose	Xylitol		0.1017	0.1198	0.1287	0.1097	0.0927				
23	Trehalose	Mannitol		0.0953	0.0901	0.1004	0.1122	0.0955				
24	Trehalose	Ribitol(adonitol)		0.1022	0.1205	0.1071	0.1091	0.1026				
25	Trehalose		Proline	0.0778	0.0845	0.0880	0.0724	0.0662				
26	Trehalose		Alanine	0.0995	0.1048	0.1089	0.0967	0.1013				
27	Trehalose		Isoleucine	0.0715	0.0903	0.0851	0.0707	0.0662				
28	Trehalose		Creatine	0.0927	0.1160	0.1095	0.0926	0.0833				
29	Trehalose		Valine	0.0829	0.0911	0.0894	0.0877	0.0727				
30	Trehalose		Taurine	0.0775	0.0940	0.1004	0.0784	0.0784				
31	Trehalose		Ectoine	0.1011	0.1211	0.1372	0.0946	0.0830				
32		Glycerol	Proline	0.0712	0.0873							
33		Glycerol	Alanine	0.0857	0.1387							
34		Glycerol	Isoleucine	0.0339	0.0059							
35		Glycerol	Creatine	0.0600	0.0581							
36		Glycerol	Valine	0.0709	0.0695							
37		Glycerol	Taurine	0.0747	0.0716							
38		Glycerol	Ectoine	0.0774	0.1038							
39		Sorbitol	Proline	0.0822	0.0823							
40		Sorbitol	Alanine	0.0716	0.0777							
41		Sorbitol	Isoleucine	0.0402	0.0173							
42		Sorbitol	Creatine	0.0777	0.0887							
43		Sorbitol	Valine	0.0608	0.0717							
44		Sorbitol	Taurine	0.0602	0.0821							
45		Sorbitol	Ectoine	0.0495	0.0830							
46		Arabitol	Proline	0.0296	0.0481							
47		Arabitol	Alanine	0.0417	0.0689							
48		Arabitol	Isoleucine	0.0096	0.0020							
49		Arabitol	Creatine	0.0255	0.0377							
50		Arabitol	Valine	0.0424	0.0423							
51		Arabitol	Taurine	0.0851	0.0479							
52		Arabitol	Ectoine	0.0790	0.0293							
53		Inositol	Proline	0.0968	0.0934							
54		Inositol	Alanine	0.0672	0.1005							
55		Inositol	Isoleucine	0.0187	0.0035							
56		Inositol	Creatine	0.0391	0.0271							
57		Inositol	Valine	0.0450	0.0023							
58		Inositol	Taurine	0.0892	0.0948							
59		Inositol	Ectoine	0.0612	0.0422							
60		Erythritol	Proline	0.0392	0.0098							
61		Erythritol	Alanine	0.0482	0.0482							
62		Erythritol	Isoleucine	0.0236	-0.0015							
63		Erythritol	Creatine	0.0510	0.0455							
64		Erythritol	Valine	0.0317	-0.0005							
65		Erythritol	Taurine	0.0672	0.0605							
66		Erythritol	Ectoine	0.0575	0.0432							
67		Xylitol	Proline	0.0715	0.1018							
68		Xylitol	Alanine	0.0896	0.1350							
69		Xylitol	Isoleucine	0.0456	0.0465							
70		Xylitol	Creatine	0.0561	0.1060							
71		Xylitol	Valine	0.0579	0.0840							
72		Xylitol	Taurine	0.0489	0.0877							
73		Xylitol	Ectoine	0.0724	0.1098							
74		Mannitol	Proline	0.0468	0.0464							
75		Mannitol	Alanine	0.0768	0.0765							
76		Mannitol	Isoleucine	0.0276	0.0154							
77		Mannitol	Creatine	0.0320	0.0741							
78		Mannitol	Valine	0.0385	0.0802							
79		Mannitol	Taurine	0.0408	0.0812							
80		Mannitol	Ectoine	0.0557	0.0949							

	TREHALOSE 5C/min				Replicates							
Combo number	Sugar	Sugar Alcohol	Additive	Average	1	2	3	4	5	6	7	8
81		Ribitol(adonitol)	Proline	0.0453	0.0470							
82		Ribitol(adonitol)	Alanine	0.0926	0.0712							
83		Ribitol(adonitol)	Isoleucine	0.0619	0.0031							
84		Ribitol(adonitol)	Creatine	0.0794	0.0364							
85		Ribitol(adonitol)	Valine	0.0602	-0.0021							
86		Ribitol(adonitol)	Taurine	0.0700	0.0467							
87		Ribitol(adonitol)	Ectoine	0.0657	0.0480							
88	Trehalose	Glycerol	Proline	0.0939	0.1041	0.0919	0.0936	0.0875				
89	Trehalose	Glycerol	Alanine	0.1134	0.1128	0.1134	0.1224	0.1162				
90	Trehalose	Glycerol	Isoleucine	0.0903	0.0844	0.0883	0.0861	0.0900				
91	Trehalose	Glycerol	Creatine	0.1036	0.1131	0.1053	0.1047	0.1053				
92	Trehalose	Glycerol	Valine	0.0902	0.0864	0.0908	0.0902	0.0886				
93	Trehalose	Glycerol	Taurine	0.0988	0.1114	0.1008	0.0902	0.0936				
94	Trehalose	Glycerol	Ectoine	0.1168	0.1095	0.1253	0.1123	0.1016				
95	Trehalose	Sorbitol	Proline	0.0635	0.0574	0.0456	0.0559	0.0496				
96	Trehalose	Sorbitol	Alanine	0.0743	0.0778	0.0672	0.0620	0.0639				
97	Trehalose	Sorbitol	Isoleucine	0.0711	0.0607	0.0596	0.0607	0.0629				
98	Trehalose	Sorbitol	Creatine	0.0839	0.0772	0.0788	0.0788	0.0833				
99	Trehalose	Sorbitol	Valine	0.0692	0.0641	0.0727	0.0652	0.0750				
100	Trehalose	Sorbitol	Taurine	0.0657	0.0665	0.0702	0.0527	0.0524				
101	Trehalose	Sorbitol	Ectoine	0.0866	0.0782	0.1009	0.0736	0.0786				
102	Trehalose	Arabitol	Proline	0.0750	0.0548	0.0599	0.0789	0.0618				
103	Trehalose	Arabitol	Alanine	0.0755	0.0673	0.0464	0.0673	0.0677				
104	Trehalose	Arabitol	Isoleucine	0.0665	0.0612	0.0550	0.0531	0.0535				
105	Trehalose	Arabitol	Creatine	0.0758	0.0776	0.0634	0.0720	0.0735				
106	Trehalose	Arabitol	Valine	0.0666	0.0653	0.0642	0.0572	0.0564				
107	Trehalose	Arabitol	Taurine	0.0724	0.0627	0.0649	0.0686	0.0653				
108	Trehalose	Arabitol	Ectoine	0.0917	0.0940	0.0761	0.0894	0.0871				
109	Trehalose	Inositol	Proline	0.0934	0.0927	0.1004	0.0885	0.0897				
110	Trehalose	Inositol	Alanine	0.0974	0.0821	0.0876	0.0996	0.0970				
111	Trehalose	Inositol	Isoleucine	0.0836	0.0785	0.0810	0.0735	0.0781				
112	Trehalose	Inositol	Creatine	0.1067	0.1074	0.1078	0.1030	0.1065				
113	Trehalose	Inositol	Valine	0.0853	0.0775	0.0695	0.0880	0.0889				
114	Trehalose	Inositol	Taurine	0.0863	0.0887	0.0899	0.0916	0.0768				
115	Trehalose	Inositol	Ectoine	0.0973	0.0974	0.0961	0.0974	0.1074				
116	Trehalose	Erythritol	Proline	0.0679	0.0583	0.0549	0.0737	0.0803				
117	Trehalose	Erythritol	Alanine	0.0685	0.0646	0.0704	0.0781	0.0631				
118	Trehalose	Erythritol	Isoleucine	0.0650	0.0717	0.0583	0.0432	0.0470				
119	Trehalose	Erythritol	Creatine	0.0865	0.0713	0.0932	0.0709	0.0881				
120	Trehalose	Erythritol	Valine	0.0603	0.0436	0.0671	0.0474	0.0470				
121	Trehalose	Erythritol	Taurine	0.0685	0.0631	0.0708	0.0551	0.0524				
122	Trehalose	Erythritol	Ectoine	0.0776	0.0638	0.0677	0.0781	0.0883				
123	Trehalose	Xylitol	Proline	0.0724	0.0689	0.0862	0.0671	0.0549				
124	Trehalose	Xylitol	Alanine	0.0786	0.0822	0.0760	0.0847	0.0797				
125	Trehalose	Xylitol	Isoleucine	0.0723	0.0859	0.0772	0.0729	0.0595				
126	Trehalose	Xylitol	Creatine	0.1015	0.1009	0.1109	0.0865	0.0934				
127	Trehalose	Xylitol	Valine	0.0841	0.0887	0.0800	0.0732	0.0689				
128	Trehalose	Xylitol	Taurine	0.0798	0.0843	0.0800	0.0732	0.0689				
129	Trehalose	Xylitol	Ectoine	0.0941	0.1049	0.0862	0.0962	0.0999				
130	Trehalose	Mannitol	Proline	0.0670	0.0651	0.0604	0.0613	0.0571				
131	Trehalose	Mannitol	Alanine	0.0728	0.0711	0.0649	0.0692	0.0696				
132	Trehalose	Mannitol	Isoleucine	0.0681	0.0680	0.0627	0.0590	0.0632				
133	Trehalose	Mannitol	Creatine	0.0805	0.0853	0.0809	0.0916	0.0723				
134	Trehalose	Mannitol	Valine	0.0647	0.0599	0.0590	0.0590	0.0514				
135	Trehalose	Mannitol	Taurine	0.0820	0.0860	0.0763	0.0749	0.0725				
136	Trehalose	Mannitol	Ectoine	0.0943	0.0964	0.1132	0.0974	0.0857				
137	Trehalose	Ribitol(adonitol)	Proline	0.0816	0.1004	0.0685	0.0843	0.0761				
138	Trehalose	Ribitol(adonitol)	Alanine	0.0862	0.0810	0.0761	0.0800	0.0728				
139	Trehalose	Ribitol(adonitol)	Isoleucine	0.0821	0.0642	0.0704	0.0647	0.0742				
140	Trehalose	Ribitol(adonitol)	Creatine	0.0848	0.0968	0.0846	0.0711	0.0769				
141	Trehalose	Ribitol(adonitol)	Valine	0.0667	0.0673	0.0616	0.0588	0.0630				
142	Trehalose	Ribitol(adonitol)	Taurine	0.0713	0.0697	0.0683	0.0644	0.0668				
143	Trehalose	Ribitol(adonitol)	Ectoine	0.1016	0.0887	0.0994	0.0877	0.0936				

	TREHALOSE 10C/min				Replicates							
Combo number	Sugar	Sugar Alcohol	Additive	Average	1	2	3	4	5	6	7	8
0				-0.0167	-0.0260	-0.0098	-0.0117	-0.0174	-0.0184	-0.0203	-0.0165	-0.0203
1	Trehalose			0.0872	0.1454	0.0606	0.1184	0.1232				
2		Glycerol		0.0263	0.0677	0.0197	0.0485	0.0493	0.0091	0.0325	0.0069	0.0204
3		Sorbitol		0.0440	0.0541	0.0541	0.0432	0.0383	0.0545	0.0503	0.0609	0.0586
4		Arabitol		0.0359	0.0380	0.0473	0.0348	0.0435	0.0417	0.0575	0.0380	0.0426
5		Inositol		0.0203	0.0126	0.0242	0.0340	0.0318	0.0215	0.0304	0.0144	0.0300
6		Erythritol		0.0086	0.0278	0.0252	0.0001	0.0179	0.0084	0.0015	0.0190	-0.0021
7		Xylitol		0.0411	0.0350	0.0248	0.0263	0.0248	0.0279	0.0173	0.0324	0.0360
8		Mannitol		0.0484	0.0637	0.0618	0.0521	0.0385	0.0482	0.0405	0.0337	0.0366
9		Ribitol(adonitol)		0.0111	0.0135	-0.0049	-0.0077	0.0052	-0.0086	-0.0086	-0.0017	-0.0054
10			Proline	0.0746	0.0260							
11			Alanine	0.0360	0.0043							
12			Isoleucine	-0.0039	-0.0274							
13			Creatine	0.0127	-0.0231							
14			Valine	0.0059	-0.0375							
15			Taurine	-0.0147	-0.0385							
16			Ectoine	0.0256	0.0187							
17	Trehalose	Glycerol		0.0858	0.1117	0.1178	0.1042	0.0885				
18	Trehalose	Sorbitol		0.0532	0.0675	0.0598	0.0532	0.0649				
19	Trehalose	Arabitol		0.0631	0.0590	0.0657	0.0694	0.0671				
20	Trehalose	Inositol		0.0642	0.0739	0.0704	0.0611	0.0615				
21	Trehalose	Erythritol		0.0764	0.0684	0.0987	0.0796	0.0922				
22	Trehalose	Xylitol		0.0479	0.0347	0.0400	0.0666	0.0597				
23	Trehalose	Mannitol		0.0952	0.0858	0.1075	0.1132	0.1151				
24	Trehalose	Ribitol(adonitol)		0.0630	0.0667	0.0667	0.0709	0.0606				
25	Trehalose		Proline	0.0258	0.0443	-0.0152	0.0093	0.0295				
26	Trehalose		Alanine	0.0604	0.0827	0.0185	0.0705	0.0714				
27	Trehalose		Isoleucine	0.0556	0.0592	0.0360	0.0649	0.0799				
28	Trehalose		Creatine	0.0766	0.0912	0.0518	0.0960	0.0969				
29	Trehalose		Valine	0.0585	0.0813	0.0337	0.0634	0.0794				
30	Trehalose		Taurine	0.0551	0.0719	0.0125	0.0804	0.0672				
31	Trehalose		Ectoine	0.0862	0.1041	0.0513	0.1060	0.1280				
32		Glycerol	Proline	0.0473	0.0371							
33		Glycerol	Alanine	0.0432	0.0485							
34		Glycerol	Isoleucine	0.0173	-0.0080							
35		Glycerol	Creatine	0.0262	0.0397							
36		Glycerol	Valine	0.0240	0.0238							
37		Glycerol	Taurine	0.0344	0.0348							
38		Glycerol	Ectoine	0.0325	0.0333							
39		Sorbitol	Proline	0.0271	0.0327							
40		Sorbitol	Alanine	0.0370	0.0435							
41		Sorbitol	Isoleucine	0.0161	0.0179							
42		Sorbitol	Creatine	0.0373	0.0447							
43		Sorbitol	Valine	0.0317	0.0355							
44		Sorbitol	Taurine	0.0291	0.0329							
45		Sorbitol	Ectoine	0.0228	0.0456							
46		Arabitol	Proline	0.0079	-0.0021							
47		Arabitol	Alanine	0.0207	0.0329							
48		Arabitol	Isoleucine	-0.0030	-0.0075							
49		Arabitol	Creatine	0.0219	0.0249							
50		Arabitol	Valine	0.0081	0.0183							
51		Arabitol	Taurine	0.0262	0.0174							
52		Arabitol	Ectoine	0.0225	0.0201							
53		Inositol	Proline	0.0234	0.0204							
54		Inositol	Alanine	0.0302	0.0356							
55		Inositol	Isoleucine	0.0096	-0.0086							
56		Inositol	Creatine	0.0319	0.0465							
57		Inositol	Valine	0.0130	-0.0064							
58		Inositol	Taurine	0.0306	0.0253							
59		Inositol	Ectoine	0.0569	0.0502							
60		Erythritol	Proline	0.0397	0.0177							
61		Erythritol	Alanine	0.0308	0.0095							
62		Erythritol	Isoleucine	0.0159	-0.0067							
63		Erythritol	Creatine	0.0335	0.0188							
64		Erythritol	Valine	0.0171	-0.0062							
65		Erythritol	Taurine	0.0186	0.0035							
66		Erythritol	Ectoine	0.0326	0.0286							
67		Xylitol	Proline	0.0103	0.0071							
68		Xylitol	Alanine	0.0120	0.0289							
69		Xylitol	Isoleucine	-0.0007	0.0063							
70		Xylitol	Creatine	0.0146	0.0241							
71		Xylitol	Valine	0.0057	0.0200							
72		Xylitol	Taurine	0.0104	0.0294							
73		Xylitol	Ectoine	0.0225	0.0467							
74		Mannitol	Proline	-0.0066	-0.0078							
75		Mannitol	Alanine	0.0303	0.0347							
76		Mannitol	Isoleucine	-0.0098	-0.0239							
77		Mannitol	Creatine	0.0140	0.0555							
78		Mannitol	Valine	0.0169	0.0569							
79		Mannitol	Taurine	0.0058	0.0492							
80		Mannitol	Ectoine	0.0168	0.0721							

	TREHALOSE 10C/min				Replicates							
Combo number	Sugar	Sugar Alcohol	Additive	Average	1	2	3	4	5	6	7	8
81		Ribitol(adonitol)	Proline	0.0123	0.0059							
82		Ribitol(adonitol)	Alanine	0.0673	0.0229							
83		Ribitol(adonitol)	Isoleucine	0.0521	-0.0136							
84		Ribitol(adonitol)	Creatine	0.0476	-0.0091							
85		Ribitol(adonitol)	Valine	0.0380	-0.0125							
86		Ribitol(adonitol)	Taurine	0.0276	-0.0123							
87		Ribitol(adonitol)	Ectoine	0.0312	0.0026							
88	Trehalose	Glycerol	Proline	0.0652	0.0836	0.0725	0.0666	0.0498				
89	Trehalose	Glycerol	Alanine	0.0881	0.1049	0.0840	0.0989	0.0877				
90	Trehalose	Glycerol	Isoleucine	0.0824	0.0974	0.0929	0.0832	0.0795				
91	Trehalose	Glycerol	Creatine	0.0983	0.1227	0.0918	0.1076	0.1038				
92	Trehalose	Glycerol	Valine	0.0866	0.0807	0.1076	0.0926	0.0829				
93	Trehalose	Glycerol	Taurine	0.0778	0.0755	0.0926	0.0836	0.0703				
94	Trehalose	Glycerol	Ectoine	0.1021	0.1117	0.1170	0.1155	0.0922				
95	Trehalose	Sorbitol	Proline	0.0454	0.0425	0.0343	0.0361	0.0439				
96	Trehalose	Sorbitol	Alanine	0.0446	0.0405	0.0363	0.0434	0.0416				
97	Trehalose	Sorbitol	Isoleucine	0.0454	0.0461	0.0428	0.0403	0.0361				
98	Trehalose	Sorbitol	Creatine	0.0533	0.0576	0.0407	0.0468	0.0529				
99	Trehalose	Sorbitol	Valine	0.0601	0.0547	0.0428	0.0475	0.0569				
100	Trehalose	Sorbitol	Taurine	0.0598	0.0596	0.0549	0.0466	0.0581				
101	Trehalose	Sorbitol	Ectoine	0.0660	0.0621	0.0640	0.0611	0.0509				
102	Trehalose	Arabitol	Proline	0.0393	0.0326	0.0485	0.0529	0.0278				
103	Trehalose	Arabitol	Alanine	0.0525	0.0547	0.0655	0.0574	0.0449				
104	Trehalose	Arabitol	Isoleucine	0.0602	0.0603	0.0648	0.0603	0.0487				
105	Trehalose	Arabitol	Creatine	0.0690	0.0762	0.0794	0.0675	0.0621				
106	Trehalose	Arabitol	Valine	0.0590	0.0550	0.0505	0.0585	0.0452				
107	Trehalose	Arabitol	Taurine	0.0716	0.0630	0.0734	0.0639	0.0500				
108	Trehalose	Arabitol	Ectoine	0.0841	0.0707	0.0890	0.0753	0.0721				
109	Trehalose	Inositol	Proline	0.0567	0.0503	0.0403	0.0399	0.0377				
110	Trehalose	Inositol	Alanine	0.0641	0.0630	0.0582	0.0688	0.0639				
111	Trehalose	Inositol	Isoleucine	0.0643	0.0730	0.0545	0.0637	0.0637				
112	Trehalose	Inositol	Creatine	0.0736	0.0809	0.0697	0.0800	0.0666				
113	Trehalose	Inositol	Valine	0.0674	0.0670	0.0764	0.0648	0.0679				
114	Trehalose	Inositol	Taurine	0.0535	0.0471	0.0646	0.0606	0.0510				
115	Trehalose	Inositol	Ectoine	0.0621	0.0733	0.0813	0.0849	0.0863				
116	Trehalose	Erythritol	Proline	0.0459	0.0348	0.0576	0.0546	0.0731				
117	Trehalose	Erythritol	Alanine	0.0513	0.0436	0.0629	0.0596	0.0607				
118	Trehalose	Erythritol	Isoleucine	0.0621	0.0445	0.0709	0.0557	0.0568				
119	Trehalose	Erythritol	Creatine	0.0620	0.0576	0.0776	0.0768	0.0795				
120	Trehalose	Erythritol	Valine	0.0570	0.0412	0.0561	0.0561	0.0609				
121	Trehalose	Erythritol	Taurine	0.0574	0.0414	0.0599	0.0523	0.0621				
122	Trehalose	Erythritol	Ectoine	0.0699	0.0512	0.0872	0.0774	0.0744				
123	Trehalose	Xylitol	Proline	0.0150	0.0053	0.0048	0.0167	0.0124				
124	Trehalose	Xylitol	Alanine	0.0403	0.0299	0.0357	0.0386	0.0328				
125	Trehalose	Xylitol	Isoleucine	0.0400	0.0246	0.0236	0.0420	0.0299				
126	Trehalose	Xylitol	Creatine	0.0565	0.0454	0.0483	0.0547	0.0430				
127	Trehalose	Xylitol	Valine	0.0371	0.0248	0.0325	0.0427	0.0335				
128	Trehalose	Xylitol	Taurine	0.0506	0.0481	0.0325	0.0427	0.0335				
129	Trehalose	Xylitol	Ectoine	0.0651	0.0614	0.0481	0.0708	0.0481				
130	Trehalose	Mannitol	Proline	0.0483	0.0302	0.0302	0.0458	0.0542				
131	Trehalose	Mannitol	Alanine	0.0497	0.0435	0.0620	0.0620	0.0472				
132	Trehalose	Mannitol	Isoleucine	0.0761	0.0727	0.0625	0.0981	0.0840				
133	Trehalose	Mannitol	Creatine	0.0991	0.1199	0.0877	0.0981	0.1104				
134	Trehalose	Mannitol	Valine	0.0665	0.0634	0.0644	0.0458	0.0868				
135	Trehalose	Mannitol	Taurine	0.0516	0.0555	0.0555	0.0863	0.0481				
136	Trehalose	Mannitol	Ectoine	0.0970	0.0943	0.1237	0.1085	0.0783				
137	Trehalose	Ribitol(adonitol)	Proline	0.0411	0.0353	0.0371	0.0357	0.0303				
138	Trehalose	Ribitol(adonitol)	Alanine	0.0630	0.0411	0.0462	0.0627	0.0609				
139	Trehalose	Ribitol(adonitol)	Isoleucine	0.0499	0.0416	0.0581	0.0498	0.0489				
140	Trehalose	Ribitol(adonitol)	Creatine	0.0707	0.0542	0.0593	0.0727	0.0611				
141	Trehalose	Ribitol(adonitol)	Valine	0.0691	0.0569	0.0468	0.0634	0.0500				
142	Trehalose	Ribitol(adonitol)	Taurine	0.0428	0.0455	0.0368	0.0468	0.0478				
143	Trehalose	Ribitol(adonitol)	Ectoine	0.0626	0.0632	0.0674	0.0688	0.0650				

JOHN WILEY AND SONS LICENSE
TERMS AND CONDITIONS

Aug 22, 2016

This Agreement between Kathryn Pollock ("You") and John Wiley and Sons ("John Wiley and Sons") consists of your license details and the terms and conditions provided by John Wiley and Sons and Copyright Clearance Center.

License Number	3934490664720
License date	Aug 22, 2016
Licensed Content Publisher	John Wiley and Sons
Licensed Content Publication	Transfusion
Licensed Content Title	Mesenchymal stem or stromal cells: a review of clinical applications and manufacturing practices
Licensed Content Author	Ratti Ram Sharma,Kathryn Pollock,Allison Hubel,David McKenna
Licensed Content Date	Oct 16, 2013
Licensed Content Pages	20
Type of use	Dissertation/Thesis
Requestor type	Author of this Wiley article
Format	Print and electronic
Portion	Full article
Will you be translating?	No
Title of your thesis / dissertation	Algorithm Optimization of non-DMSO Cryopreservation Solutions to Improve Mesenchymal Stem Cell Post-Thaw Function
Expected completion date	Sep 2016
Expected size (number of pages)	150
Requestor Location	Kathryn Pollock 1380 Terrace Drive Apt #206 SAINT PAUL, MN 55113 United States Attn: Kathryn Pollock
Publisher Tax ID	EU826007151
Billing Type	Invoice
Billing Address	Kathryn Pollock 1380 Terrace Drive Apt #206

Title:	Clinical mesenchymal stromal cell products undergo functional changes in response to freezing
Author:	Kathryn Pollock,Darin Sumstad,Diane Kadidlo,David H. McKenna,Allison Hubel
Publication:	Cytotherapy
Publisher:	Elsevier
Date:	Jan 1, 2015

Order Completed

Thank you for your order.

This Agreement between Kathryn Pollock ("You") and Elsevier ("Elsevier") consists of your order details and the terms and conditions provided by Elsevier and Copyright Clearance Center.

License number	Reference confirmation email for license number
License date	Aug 02, 2016
Licensed Content Publisher	Elsevier
Licensed Content Publication	Cytotherapy
Licensed Content Title	Clinical mesenchymal stromal cell products undergo functional changes in response to freezing
Licensed Content Author	Kathryn Pollock,Darin Sumstad,Diane Kadidlo,David H. McKenna,Allison Hubel
Licensed Content Date	January 2015
Licensed Content Volume	17
Licensed Content Issue	1
Licensed Content Pages	8
Type of Use	reuse in a thesis/dissertation
Portion	full article
Format	both print and electronic
Are you the author of this Elsevier article?	Yes
Will you be translating?	No
Order reference number	
Title of your thesis/dissertation	Algorithm Optimization of non-DMSO Cryopreservation Solutions to Improve Mesenchymal Stem Cell Post-Thaw Function
Expected completion date	Sep 2016
Estimated size (number of pages)	150
Elsevier VAT number	GB 494 6272 12
Requestor Location	Kathryn Pollock 1380 Terrace Drive Apt #206 SAINT PAUL, MN 55113 United States Attn: Kathryn Pollock
Billing Type	Invoice
Billing address	Kathryn Pollock 1380 Terrace Drive Apt #206 SAINT PAUL, MN 55113 United States Attn: Kathryn Pollock
Total	0.00 USD

JOHN WILEY AND SONS LICENSE TERMS AND CONDITIONS

Aug 02, 2016

This Agreement between Kathryn Pollock ("You") and John Wiley and Sons ("John Wiley and Sons") consists of your license details and the terms and conditions provided by John Wiley and Sons and Copyright Clearance Center.

License Number	3920891355353
License date	Aug 02, 2016
Licensed Content Publisher	John Wiley and Sons
Licensed Content Publication	Journal of Tissue Engineering and Regenerative Medicine
Licensed Content Title	Algorithm-driven optimization of cryopreservation protocols for transfusion model cell types including Jurkat cells and mesenchymal stem cells
Licensed Content Author	Kathryn Pollock,Joseph W. Budenske,David H. McKenna,Peter I. Dosa,Allison Hubel
Licensed Content Date	May 27, 2016
Licensed Content Pages	1
Type of use	Dissertation/Thesis
Requestor type	Author of this Wiley article
Format	Print and electronic
Portion	Full article
Will you be translating?	No
Title of your thesis / dissertation	Algorithm Optimization of non-DMSO Cryopreservation Solutions to Improve Mesenchymal Stem Cell Post-Thaw Function
Expected completion date	Sep 2016
Expected size (number of pages)	150
Requestor Location	Kathryn Pollock 1380 Terrace Drive Apt #206 SAINT PAUL, MN 55113 United States Attn: Kathryn Pollock
Publisher Tax ID	EU826007151
Billing Type	Invoice
Billing Address	Kathryn Pollock 1380 Terrace Drive Apt #206 SAINT PAUL, MN 55113 United States Attn: Kathryn Pollock
Total	0.00 USD